Effect of Fuel Content on the Human Perception of Engine Idle Irregularity

Marco Ajovalasit

A thesis submitted for the Degree of Doctor of Philosophy

Department of Mechanical Engineering

The University of Sheffield

October 2005

Summary

This thesis describes a digital signal processing analysis of diesel engine idle vibration in automobiles, and an analysis of the human subjective response to the idle vibration which occurs at the steering wheel. In order to quantify the variations in the diesel idle vibration that can be introduced by the engine technology, the vehicle, and the fuel type, a set of acceleration time histories were measured at the engine block and at the steering wheel for two automobiles equipped with 4-cylinder engines which had different injection systems and which operated under different fuel conditions.

A combination of time domain, frequency domain and time-frequency wavelet-based analysis were used. Both the continuous wavelet transform and the discrete orthogonal wavelet transform were applied to the steering wheel acceleration time histories in order to analyse the statistical variation in terms of both instantaneous variations, and the cycle-to-cycle variations which occur across complete thermodynamic engine cycles. The combination of orthogonal wavelet transform and time-varying auto-covariance analysis, performed across a complete engine thermodynamic cycle, was identified as the most sensitive method for describing the statistical variation in diesel idle vibration.

The second-order engine harmonic H_2 was found to account for most of the vibrational energy at the steering wheel when at idle. Amplitude modulation of the second-order engine harmonic H_2 by the half-order engine harmonic $H_{1/2}$ has been identified as the main characteristic of the steering wheel signature of automobiles at idle. The steering wheel idle vibration produced by different engines and different fuel conditions have therefore been described in terms of the amplitude modulation depth "m" that characterises the idle waveform.

Four psychophysical response tests, determined by the combination of two test protocols and two semantic descriptors, were performed. A model of the growth in the human subjective response to diesel idle vibration has been proposed in which the response scale is a function of the modulation depth parameter "m". The model is defined over two regions of modulation depth. For values of "m" less than 0.2, humans have been found to be unable to distinguish variations in idle modulation. For values of "m" greater than 0.2, the human response grows as a power function with respect to modulation depth. Based on the current findings, suggestions for future research are also provided.

Contents

List of Illustrations

List of Tables

Nomenclature

a	scale dilation parameter $(a > 0)$
$a(t)$	instantaneous acceleration value of a time series [m/s^2]
a_0	reference level of 10^{-6} m/s^2 defined for acceleration (ISO1683, 1983)
$A(t)$	instantaneous amplitude of a time series [m/s^2]
A_0	amplitude of a sinusoidal waveform [m/s^2]
A_{max}	maximum amplitude value of a time series [m/s^2]
A_{min}	minimum amplitude value of a time series [m/s^2]
$a_{in}(f)$	acceleration value at the input reference point [m/s^2]
$a_{out}(f)$	acceleration value at the output reference point [m/s^2]
$a_{r.m.s.}$	acceleration root mean square [m/s^2]
b	time translation parameter
c	Weber fraction
$cA_{j,k}$	approximation coefficient of the discrete wavelet transform
$cD_{j,k}$	detail coefficient of the discrete wavelet transform
CP	cycle period [s]
cSt	centistokes [mm^2/s]
CV_m	coefficient of variation relative to fuel m [%]
CVCA	coefficient of the cycle-to-cycle amplitude variation [%]
CVCF	coefficient of the cycle-to-cycle frequency variation [%]
CVC$_m$	coefficient of the cycle-to-cycle signal statistical variation for fuel m [%]
CVIA	coefficient of variation of the instantaneous amplitude [%]
CVIF	coefficient of variation of the instantaneous frequency [%]
CVI$_m$	coefficient of variation of the instantaneous signal statistics for fuel m [%]
CV$_{CF}$	coefficient of crest factor cycle-to-cycle *intra-fuel* variation
CV$_{Kt.}$	coefficient of kurtosis cycle-to-cycle *intra-fuel* variation
CV$_{r.m.s.}$	coefficient of r.m.s. cycle-to-cycle *intra-fuel* variation
C_{xx}	auto-covariance function [(m/s^2)^2]
C_ψ	admissibility wavelet condition
dB	decibel

E_0	root mean square of a sinusoidal waveform [m/s^2]
f	frequency [Hz]
f_0	center frequency of the base wavelet function [Hz]
f_c	frequency of the carrier waveform [Hz]
$f_{j>k}$	observed frequency of preference of stimulus j over stimulus k
f_k	discrete frequency value [Hz]
f_m	frequency of the modulating waveform [Hz]
f_{max}	upper frequency cutoff value [Hz]
f_{min}	lower frequency cutoff value [Hz]
f_N	Nyquist frequency [Hz]
f_s	sampling frequency [Hz]
F	matrix of the observed frequency of preference
$F(f)$	input force [N]
$F(\omega)$	amplitude of the Fourier transform in the frequency domain
F_C,	engine working cycle repetition frequency [Hz]
F_F	engine firing frequency [Hz]
F_{REV}	rotational frequency of the crankshaft [Hz]
g	acceleration due to gravity
G_{xx}	auto-power spectral density of a time series [(m/s^2)^2/Hz]
G_{xy}	cross-power spectral density of a time series [(m/s^2)^2/Hz]
$H(f)$	transmissibility function
$H_{1/2}$	half-order engine harmonic [Hz]
H_2	second-order engine harmonic [Hz]
H_i	order of the ith harmonic [Hz]
i	$\sqrt{-1}$ imaginary unit
I	Physical intensity of the stimulus
j	number of data in a time series
J	maximum number of levels of the orthogonal wavelet transform
K_t	kurtosis [dimensionless]
L	litre [l]

L_a	acceleration level [dB]
m	modulation depth parameter
m_{th}	modulation depth value at threshold
m^*	relative modulation index, $m - m_{th}$
MSE_K	mean square error of a sample mean [m/s^2]
n	nominal idle speed of the crankshaft [r/min]
n_d	number of averages
$n_{judgements}$	number of judgements for stimulus pair
n_s	number of test stimuli
N	number of data points [samples]
N_s	number of sample records in a time series
p	level of statistical significance
p(x)	probability density function of a time series
$p_{j>k}$	frequency percentage of preference of stimulus j over stimulus k
P	matrix of the frequency percentage of preference
P(x)	probability distribution of a time series
r^2	coefficient of determination
$r(b)$	wavelet ridge
r_{jk}	coefficient of correlation between stimulus j and stimulus k
r.m.s.	root mean square [m/s^2]
rpm	revolution per minute [r/min]
R_{xx}	auto-correlation function [(m/s^2)^2]
$S_1\%$	index of *intra-fuel* variability [%]
$S_2\%$	index of *inter-fuel* variability [%]
S_j	subjective response scale associate to stimuli j
S_k	subjective response scale associate to stimuli k
S_{kew}	skewness [dimensionless]
t	time [s]
T	duration of a time series [s]
$T_{50\%}$	temperature at 50 percent of fuel condensate recovered

T_C	period of one working cycle of the engine [s]
T_F	period between consecutive cylinder firings [s]
T_{REV}	period of one revolution of the crankshaft [s]
T_w	duration of a time interval within a frame-window [s]
$v(f)$	response velocity [m/s]
VDV	vibration dose value [m/s$^{1.75}$]
$w(t)$	window function
W_h	International standard weighting filter for hand-arm vibration (ISO 5349)
W_s	weighting filter for steering wheel hand-arm vibration
$W_\psi(a,b)$	coefficient of the continuous wavelet transform
X	engine block transverse measurement direction
$x(t)$	instantaneous value of a time series [m/s^2]
x'	steering wheel fore-and-aft measurement direction
$\left|x_{j\max}\right|$	modulus of the maximum instantaneous value in a time series [m/s^2]
x_j	instantaneous value of a time series at sample j
$x_{j\max}$	maximum instantaneous value in a time series [m/s^2]
x_k^j	coefficient of the discrete wavelet transform
$\overline{X_k}$	sample mean of K samples [m/s^2]
$\overline{\overline{X}}$	global r.m.s. of the complete time series [m/s^2]
$\overline{\overline{X}}_K$	overall average of sample means [m/s^2]
X_k	amplitude of discrete Fourier transform
X_{th}	stimulus magnitude at threshold
Y	engine block axial measurement direction
y'	steering wheel lateral measurement direction
z_{jk}	normal deviate of the frequency percentage of preference
z'	steering wheel vertical measurement direction
Z	engine block vertical measurement direction
Z	matrix of the normal deviate of the frequency percentage of preference
$Z(f)$	driving point mechanical impedance [N/m s^{-1}]
β	Stevens' power exponent

$\gamma^2(f)$	coherence function
Δt	time resolution [s]
Δt_s	sampling period [s]
Δt_ψ	duration of the wavelet function [s]
Δf	frequency resolution [Hz]
Δf_ψ	frequency bandwidth of the wavelet function [Hz]
ΔI	difference in stimulus intensity
θ	crankshaft angular position [rad degrees]
μ	mean value [m/s^2]
μ_x	mean value of a time series [m/s^2]
μ_x^2	mean square value of a time series [m/s^2]
μ_{IMEP}	mean value of the indicated mean effective pressure
ν_s	instantaneous frequency [Hz]
σ	standard deviation [m/s^2]
σ_{IMEP}	standard deviation of the indicated mean effective pressure
σ_j	standard deviation of the discriminal distribution of stimulus j
σ_k	standard deviation of the discriminal distribution of stimulus k
σ_K	standard deviation of the sample means [m/s^2]
σ_x^2	variance of a time series [m/s^2]
τ	tau-lag displacement [s]
$\phi(t)$	phase of a time series [degrees]
$\phi'(b)$	derivative of the phase
χ^2	Chi-square statistic
Ψ	sensation magnitude
Ψ_o	sensation magnitude at threshold
$\psi(t)$	wavelet function
$\psi_{a,b}(t)$	scaled version of the base wavelet for the continuous wavelet transform
$\psi_{j,k}(t)$	scaled version of the base wavelet for the discrete wavelet transform
ω	angular frequency [s^{-1}]
ω_0	angular center frequency of the base wavelet function [s^{-1}]
$*$	complex conjugate

ANOVA	analysis of variance
ASTM	American Society for Testing and Materials
AVL	Anstalt für Verbrennungskraftmaschinen (Institute for internal combustion engines)
BS	British Standards
C.N.	cetane number
CCV	cycle-to-cycle variation
CF	crest factor
COV_{IMEP}	coefficient of variation of indicated mean effective pressure
CR	category-ratio
CV	coefficient of variation
CWT	continuous wavelet transform
DAT	digital audio tape
DFT	discrete Fourier transform
DI	direct injection
DL	difference threshold
EN	European normative
FA	fast acting receptors
FBP	final boiling point
FFT	fast Fourier transform
HMSO	Highline Medical Services Organization
IBP	initial boiling point
IDI	indirect injection
IMEP	indicated mean effective pressure
ISO	International Organization for Standardization
JND	just noticeable difference
LMS	Leuven Measurement Systems
NP I	non-Pacinian channel type I
NP II	non-Pacinian channel type II
NP III	non-Pacinian channel type III
NVH	noise, vibration and harshness
OWT	orthogonal wavelet transform
P	Pacinian channel
PA	power amplifier

PDF	probability density function
PSD	power spectral density
SA	slowly acting receptors
SAE	society of automotive engineers
SD	standard deviation
STFT	short time Fourier transform
THD	total harmonic distortion
TVA	time-varying auto-covariance
WT	wavelet transform
WVD	Wigner-Ville distribution

Acknowledgments

Chapter 1

Motivations behind the Research

1.1 The problem of Diesel Engine Idle

In city traffic automobiles spend much time operating under idle conditions. Engine idle affects fuel economy, pollutant emissions and human comfort. During city driving automobiles typically consume 30 percent of their fuel while at idle (Jurden, 1995). Decreasing the engine idle speed (600-800 rpm) is considered a means of reducing fuel consumption. However, lower-speed operation degrades the idle stability and increases engine speed oscillations. Even slight fluctuations of engine idle can cause unpleasant vibrations of the vehicle leading to lower customer satisfaction (Hoard and Rehagen, 1997). One of the many challenges facing today's automotive engine designers and fuel manufacturers is the need to perform measurements of human subjective response to idle vibration. A positive human subjective response to idle vibration is one of the often-conflicting requirements which include improved fuel economy (Nishimura and Ishii, 1986; Jurden, 1995), reduced emissions (Ladommatos *et al.*, 1996;

Watanabe and Tahara, 1998), combustion stability (Ando and Motomochi, 1987; Ozdor *et al.*, 1994), noise, vibration and harshness (NVH) quality (Qatu *et al.*, 2002; Stout *et al.*, 2003) and vehicle comfort (Griffin, 1995; Schoeggl and Ramschak, 1997). Studies on idle comfort of passenger cars (Stout *et al.*, 2003) have shown that the overall perception of vehicle quality is mostly correlated to the level of satisfaction a customer has with the vehicle's engine.

The vibration of a reciprocating internal combustion diesel engine is a complex phenomena caused by two main excitatory forces: the unidirectional combustion forces and the multi-directional cyclic forces which are mechanically induced (Priede, 1992; Ozdor *et al.*, 1994; Rahnejat, 1998). The former can be considered as having a random component as well as a periodic component with the combustion cycle, the latter can be considered periodic at idle due to the cyclic operation of the engine, as presented in Figure 1.1.
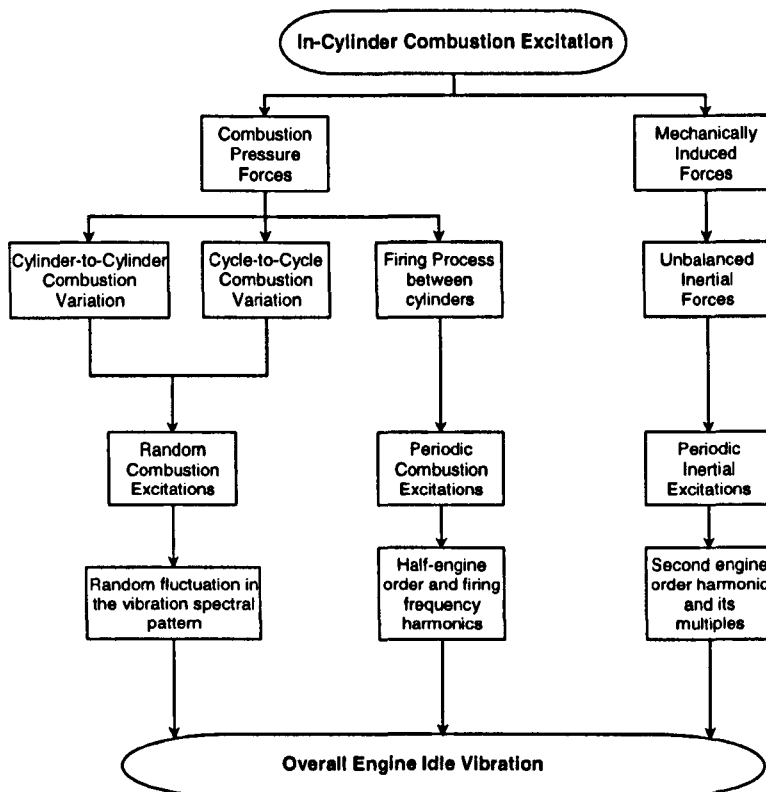
Figure 1.1 Sources of engine idle vibration.

The combustion process in each cylinder acts as the initiating energy source for the vibration of the powertrain system, introducing periodic oscillations at half the rotational frequency of the crankshaft for a 4-stroke engine. For a 4-stroke engine, the half-order component is due to there being only a single power stroke occurring in each cylinder every second crankshaft revolution. The presence of this frequency, and of its higher harmonics (all integer multiples of half-engine order), has been demonstrated by the experimental measurements performed by Dixon et. al. (1994) and by the analytical treatment of the spectral contents of multi-cylinder engines by Rahnejat (1998).

For a 4-cylinder, 4-stroke engine, the firing between consecutive cylinders, even with no cylinder-to-cylinder combustion variation and no cycle-to-cycle variation, is known to produce frequency components at the second engine order (firing frequency) and its higher harmonics (Lichty, 1967; Priede, 1992; Rahnejat, 1998). In addition, unbalanced inertial forces which operate at the engine rotational frequency and at its even-order multiples are mechanically induced by the reciprocating motion of the pistons and of the connecting rods. At low engine speeds the combustion gas forces are greater than the mechanical inertial forces, but at high speeds the opposite is true. In 4-cylinder, 4-stroke engines the first-order inertial forces are normally well balanced by employing balancing masses attached to the crankshaft. Vertically acting second-order imbalance forces and their multiples are, however, more difficult to deal with, normally requiring counter-rotating balancing shafts.

The presence of the firing frequency operating at the second engine order accentuates the effect of the secondary inertial forces since their main spectral content is at the same frequency. Thus the second engine order is the dominant vibration signature for a 4-cylinder, 4 stroke engine (Dixon et al., 1994; Rahnejat, 1998). For an automobile engine which is at idle, the crankshaft rotational speed is typically in the range from 600-840 rpm, corresponding to linear frequencies from 10 to 14 Hz. The firing frequency is thus in the range from 20 to 28 Hz. The half order

harmonic originating from combustion forces in the cylinder is therefore in the range from 5 to 7 Hz, and the corresponding second order linear frequencies are from 20 to 28 Hz.

Superimposed on the periodic oscillation are random fluctuations in the crankshaft angular velocity that are caused by the stochastic nature of the combustion process from cycle-to-cycle (Ozdor et al., 1994; Hinze and Cheng, 1998) and by an unequal distribution of fuel from cylinder-to-cylinder (Ando and Motomochi, 1987; Stout et al., 2003). The unequal combustion forces among cylinders add frequency orders at odd, even and half-order harmonics of the engine speed. Their amplitude and frequency can be highly sensitive to the relative engine torque amplitudes and therefore they can be highly variable from cycle-to-cycle (Shim et al., 1996). Figure 1.2 presents an example of an engine speed waveform during two complete engine cycles for a four-cylinder, four-stroke engine at idle. From Figure 1.2 it can be seen that the engine idle speed is not constant, but is characterised instead by instantaneous crankshaft angular speed fluctuations caused by the combustion process.
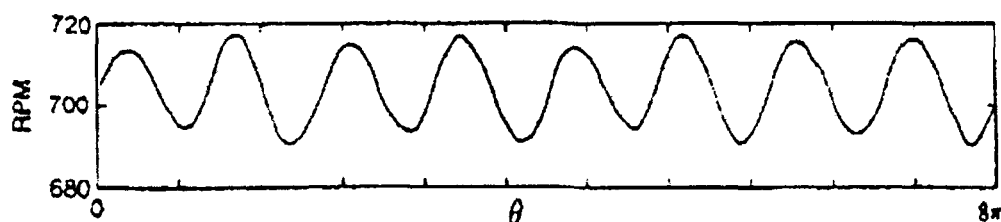
Figure 1.2   Typical waveform of the engine speed, in revolution per minute, during two complete cycles in a four-cylinder, four-stroke engine at idle (reproduced from Shim et al., 1996).

Under idle conditions, the non-stationary character of the combustion process can cause an engine to run "rough" and stall easily (Hinze and Cheng, 1998; Wolf and Portal, 2001; Stout et al., 2003). A more stable diesel engine combustion process can be achieved by means of high pressure injection (Shundoh et al., 1991) and by using different combustion chamber geometries (Yang et al., 1998). The quality and the timing of the combustion process, as well as the vibration levels of the engine structure (Gu et al., 1996), are also affected, however, by the properties of the diesel fuel.

The advantage of a diesel engine is its superior combustion efficiency, which is defined as the amount of work produced by the engine divided by the amount of chemical energy in the fuel that can be released through the combustion process. Compared to gasoline engines, which are about 30% to 33% efficient, diesel engines can achieve combustion efficiencies in excess of 50% (Owen and Coley, 1995). As a result, diesel engines provide better fuel economy than gasoline engines. In addition, in terms of cost, in most European countries the price of diesel fuel is lower than that of gasoline (Ivaldi et al., 2004).

From the viewpoint of a diesel engine manufacturer, the performance characteristics of an engine are determined during its design and development stages (Pavletic *et al.*, 1990). In order to achieve the best engine performance, the design of the fuel injection system is generally finalised based on extensive dynamometer and field testing using a reference fuel of standard characteristics as required by national standards and by fuel quality guide specifications (Owen and Coley, 1995). Several research studies have investigated the effects of the fuel properties which are directly related to engine thermodynamic behaviour (i.e. viscosity, cetane number, heat content, volatility, etc.), and of those characterising the physical properties of the liquid fuel (i.e. homogeneity, cold properties, anticorrosiveness, etc.), on the combustion and emission characteristics of diesel engined automobiles (Nylund, 1997; Kidoguchi *et al.*, 2000; Lee *et al.*, 2004). By adding specific additives to ethanol-based diesel fuels, improvements have been achieved in the combustion irregularity and pollutant emission characteristics (Satgé de Caro *et al.*, 2001).

Unsteady idle vibration can be interpreted by drivers to be a sign of poor engine or fuel performance. Since smooth idle is an important vehicle attribute (Hoard and Rehagen, 1997, Alt *et al.*, 1999, Stout *et al.*, 2003), engine and fuel manufacturers wish to take into account not only the objective measures of performance, but also the driver's subjective response. Measurement of driver subjective response requires, however, a metric which can translate the measurable mechanical (objective) quantities which define human-vehicle interaction into perceived

(subjective) quantities. Such a metric would indicate the likely response of a test jury to questions about the fuel, engine or complete vehicle. Figure 1.3 presents the embedded nature of the idle vibration evaluation process.
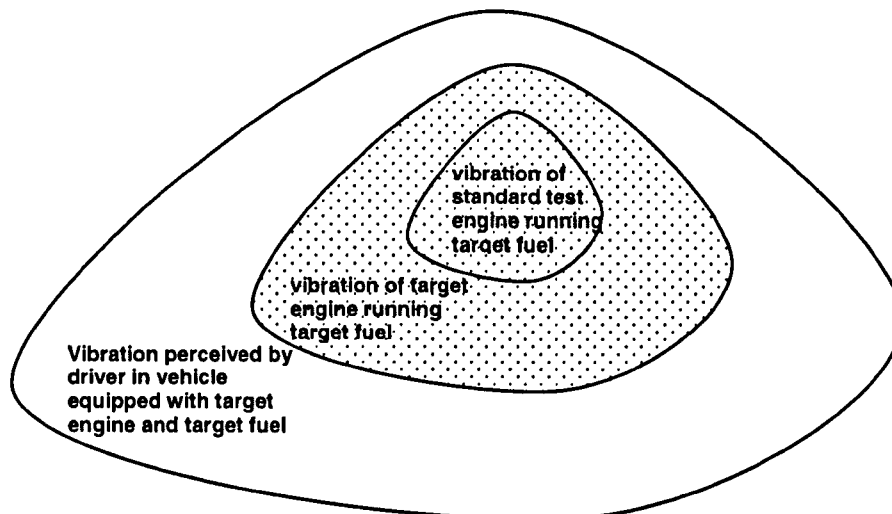
Figure 1.3 Idle evaluation process.

1.2 Quality and Comfort

In the automobile industry there has been in recent years an increased emphasis towards producing high-quality products and providing high-quality services (Hoard and Rehagen, 1997; Meier *et al.*, 1998; Alt *et al.*, 1999, Pflueger and Stuecklschwaiger, 2001). In order to discuss the quality of products and services, it is necessary to define the term "quality". The Oxford dictionary (2000) refers to quality as: "the standard of something when it is compared to other things like it". The Webster dictionary (2004) refers to quality as: "a characteristic property that defines the apparent individual nature of something". Montgomery (1996) defined the same word to mean: "the extent to which products meet the requirements of people who use them". He further distinguished between two types of quality: *quality of design and quality of conformance. Quality of design* reflects the extent to which a product or service possesses an intended feature. For example, an automobile with power steering, a sun roof, or other luxury options would be considered to have better quality of design than a car without these options. *Quality of conformance* reflects instead the extent to which the product or service achieves the intent of its

design. These aspects of quality can be subjectively measured by taking into account the individual's experience (Ljungberg et al., 2004) and satisfaction (Hoard and Rehagen, 1997).

Comfort, instead, is defined by the Oxford dictionary (2000) as: "the state of being physically relaxed and having a pleasant life", whereas the Webster dictionary (2004) refers to comfort as: "contented well-being". Several researchers have conducted interview and questionnaire-based studies to analyse the meaning of the word of comfort. From studies conducted by Metzger (1994) it was found that "comfort describes a quality which persons ascribe to specific objects or situations". Metzger's research suggested that the meaning of the term "comfort" is often associated with well-being, pleasantness, relaxation and convenience rather than with reassurance, luxury, elegance and style. It was also concluded that the meaning of comfort is not mainly dependent on material resources, but rather that it is determinated by subjective needs and benefits. Based on these empirical findings, the term comfort was related to the words "ease" and "efficiency": Ease refers to the degree of relief and relaxation (reduction of physical and psychological strain) to which activities are performed, while efficiency refers to the objective performance data and quality of an object. Also defining comfort in terms of human needs, Krist (1994) proposed a hierarchical model of discomfort sensations based on Maslow's hierarchy of human needs (Maslow, 1954). He assumed that higher needs (i.e. psychological and social) only become conscious if all basic (physiological) ones are satisfied.

The meaning of the word comfort differs according to the object, or the situation, to which it is applied, but all meanings relate to the idea of subjective well-being. Slater (1985) proposed a definition of comfort as "a pleasant state of physiological, psychological and physical harmony between a human being and the environment". Thus comfort may be both mental and physical. Without comfort, Slater (1985) stated, "human existence loses its quality because persons are permanently in an uncomfortable state". According to some ergonomic studies (Pineau, 1982), psychological definitions of comfort refer to a state of well-being under optimal conditions. As

postulated by Pineau (1982), *"comfort cannot be evaluated by the use of purely materialistic and objective criteria, rather it should be analysed psychologically"*.

With respect to the effects of physical motion, Griffin (1990) has stated that *"the study of the relation between vibration and comfort has mainly concerned the extent to which motions are responsible for displeasure, dissatisfaction and discomfort"*. Hertzberg (1972) referred to comfort as an "absence of discomfort".

In recent years vehicle quality and comfort have been gaining in importance as discriminating factors influencing the vehicle development process (Baret *et al.*, 2001). Figure 1.4 presents the criteria of customer satisfaction for different intended sales markets as defined by AVL (Schoeggl and Ramschak, 1997), an automotive sector consulting company.
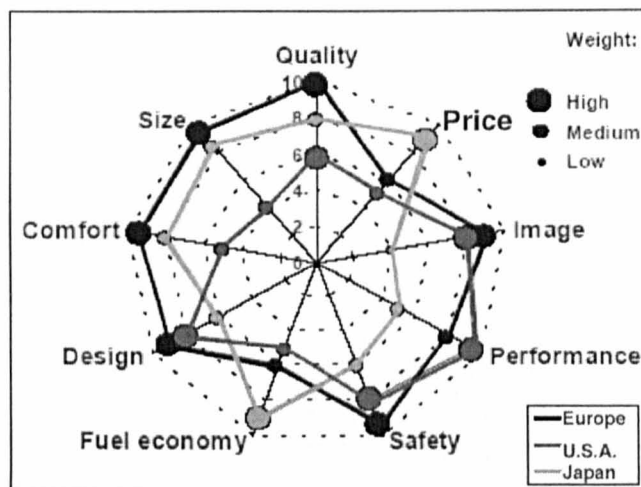
Figure 1.4   Vehicle evaluation criteria for different automobile sales markets (reproduced from Schoeggl and Ramschak, 1997).

Among the criteria are performance, fuel economy and emissions which represent objective quantities, whereas the design, image, comfort and quality represent subjective metrics. Currently, automobile manufacturers usually evaluate vehicle quality by means of subjective assessments performed by their experienced test drivers or by juries of normal drivers (Hoard and Rehagen, 1997; Baret *et al.*, 2001; Pflueger and Stuecklschwaiger, 2001). However, these assessment criteria can be time and cost intensive, limited in repeatability, and do not always

address the real issues affecting customer expectation. As a consequence, for vehicle, vehicle component and fuel manufacturers, it has proved necessary to develop methods for quantifying the human subjective response to vibration in order to gain a more accurate evaluation of the customer's perception of vehicle quality and comfort (Biermayer *et al.*, 2001; Pielemeier *et al.*, 2001; Harrison, 2004).

1.3 The Problem of Steering Wheel Vibration

When investigating what aspects of engine idle vibration are important towards the driver's judgment of fuel or vehicle quality, consideration must be given to the role of the fuel, the engine and the vehicle intermediate mechanical structures which are found between the emission source at the engine and the points of contact with the human body. As shown in Figure 1.5, the points of contact through which the driver perceives engine vibration include the floor panel, the pedals, the gearshift, the seat and the steering wheel (Giacomin and Abrahams, 2000; Baret *et al.*, 2001).
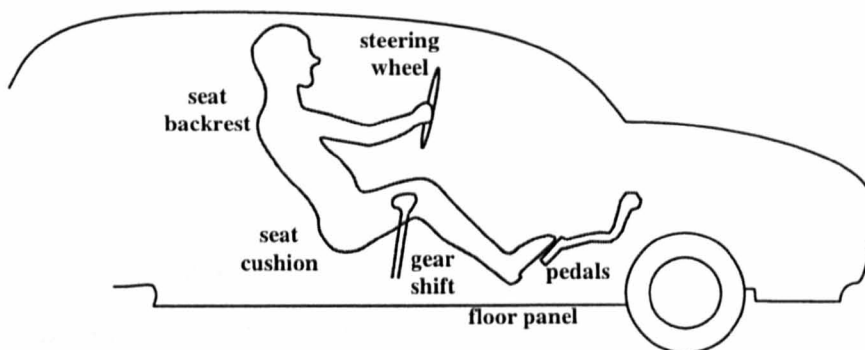
Figure 1.5 Vibrational disturbances acting on the driver.

Considering the research of Takeda (1982) and of Pottinger and Marshall (1986), it can be stated that the vibration transmitted to the driver depends for its characteristics on:

- the nature of the engine (its rotating and reciprocating mechanisms, mass unbalance and firing torque fluctuation);
- the design of the engine mounting system and of the steering column of the vehicle;
- tyre, wheel and drive train design;
- the road surface profile.

Of the car/driver interfaces, the steering wheel (Pak *et al.*, 1991) is the fundamental subsystem in the case of idle vibration due to the great sensitivity of the skin tactile receptors of the hand (Verrillo, 1985; Bolanowski Jr and Gescheider, 1988) and due to the lack of intermediate structures such as shoes and clothing which can act to attenuate vibration stimuli. Under idle conditions the engine can be considered to represent the major source of the vibration that excites the steering system (Bellmann *et al.*, 2000; Demers, 2001). Focusing attention on the steering wheel suggests the importance of the steering system components, which often have important vibrational modes (either the wheel itself or the column assembly) in the frequency range from 20 to 60 Hz (Kim *et al.*, 1985; Pottinger and Marshall, 1986; Fujikawa, 1988; Demers, 2001) thus sometimes coinciding with the engine idling firing frequency (20-28 Hz) (Rahnejat, 1998).

The vibration at the steering wheel (Figure 1.6) is usually measured along the three principal axis of the automobile defined by SAE standard J670e (1974). These are:

- the x - axis which is taken along the fore-and-aft direction of the automobile with the positive direction taken as forwards, i.e. from driver towards front bumper;
- the y - axis which is taken along the lateral direction of the automobile with the positive direction towards the left of the vehicle;
- the z - axis which is taken along the vertical direction of the automobile with the positive direction towards the roof of the vehicle.
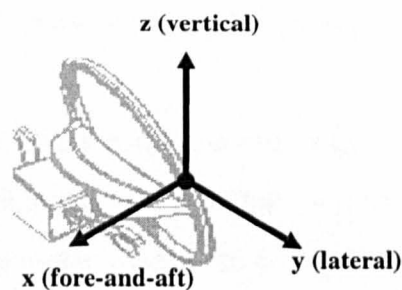
Figure 1.6 Measurement directions for steering wheel vibration.

Vibration measurements performed in automobiles during representative driving conditions have shown that acceleration magnitudes at the steering wheel are often several times greater than at the seat and footrest (Parsons et al., 1982; Bellmann et al., 2000). Figure 1.7 presents an example of the acceleration power spectral densities measured along the three orthogonal directions, for both the seat and the steering wheel, for a mid-sized diesel passenger car when at idle at 910 rpm (Bellmann et al., 2000). It can be seen that the acceleration levels at the steering wheel (Figure 1.7b) are higher than those at the seat position (Figure 1.7a) in the frequency range from 8 to 100 Hz. Research has shown that, for the frequency range 8 to 100 Hz, the vertical and fore-and-aft directions are the directions where most of the vibrational energy is concentrated (Peruzzetto, 1988; Amman et al., 2001; Giacomin et al., 2004).
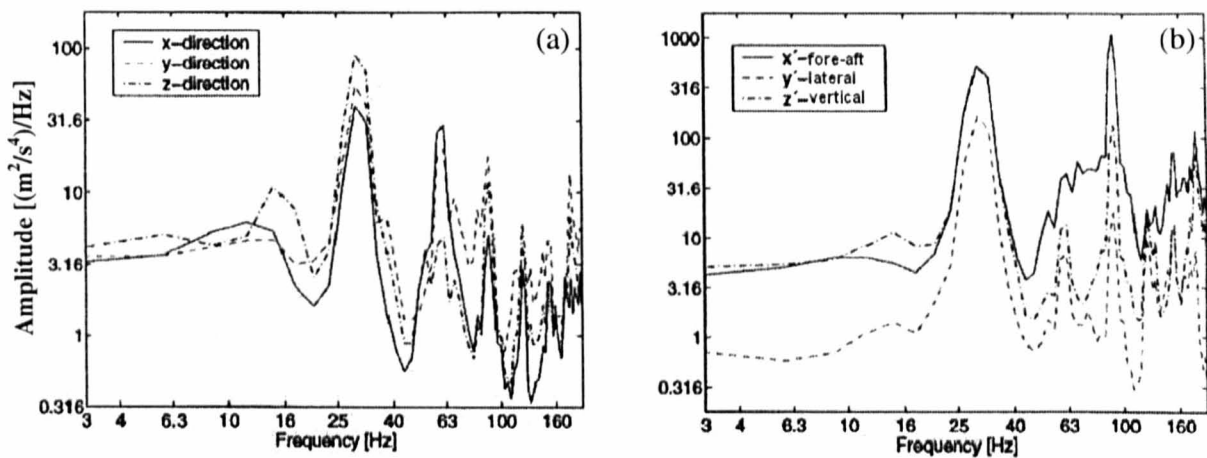
Figure 1.7 Acceleration power spectral densities of a diesel engined automobile at idle at 910 rpm (adapted from Bellmann, 2000).

a) driver's seat rail measured at the right rear mounting bolt;

b) steering wheel measured at the 60° position, with respect to top centre.

For what regards perceived discomfort, research has shown (Peruzzetto, 1988) that the equivalent discomfort ratio (defined as the ratio between hand vibration acceleration magnitude and whole-body vibration acceleration magnitude having the same level of subjective discomfort) can be as high as 7. This suggests that vibration occurring at the hand is likely to be a source of discomfort, annoyance and fatigue. Figure 1.8 presents an example of the steering wheel

acceleration measured for a mid-sized European passenger car while driving at 40 km/h over seven different road surfaces (Giacomin *et al.*, 2004). The figure presents the steering acceleration power spectral densities measured at the 60° position with respect to top centre, along the three orthogonal axes (see Figure 1.6). The figure also presents the average power spectral densities of the data sets. It can be seen that the acceleration levels along the vertical direction are higher than those along either the fore-and-aft or the lateral direction in the frequency range from 8 to 100 Hz for all seven roads considered.
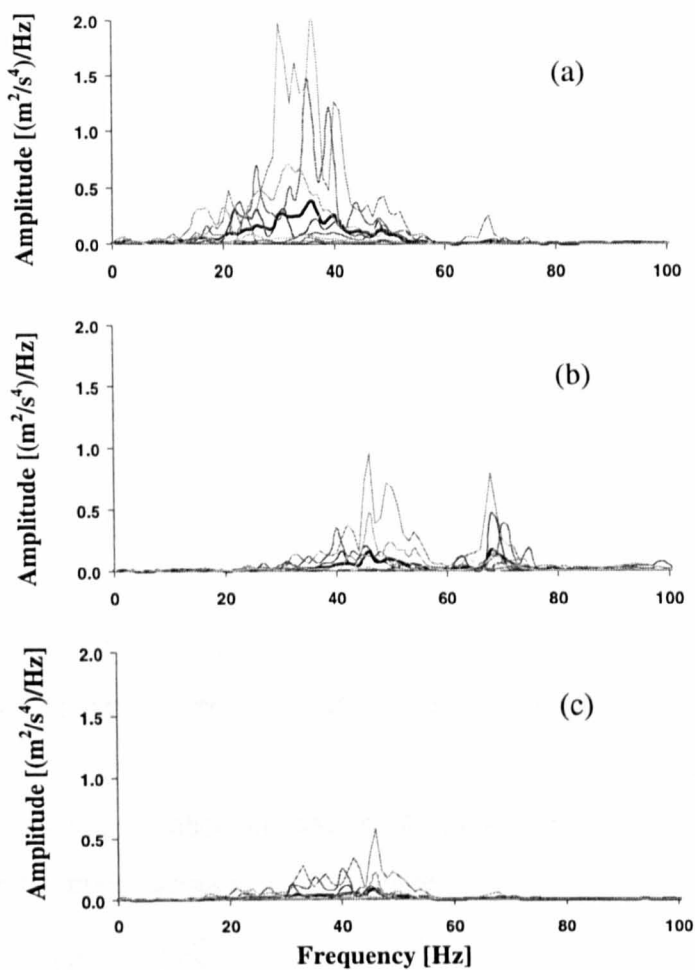
Figure 1.8   Acceleration power spectral densities at the steering wheel measured for a mid-sized European automobile while driving at 40 km/h over seven different road surfaces. The thick solid line indicates the average power spectral density of the data sets (adapted from Giacomin *et al.* 2004).

a) vertical direction; b) fore-and-aft direction; c) lateral direction.

1.4 Research Objectives

For diesel engine idle, most existing literature treats the effect of motor controller design on engine idle stability (Shim *et al.*, 1996; Bidan *et al.*, 1998; Hinze and Cheng, 1998; De Nicalao *et al.*, 1999) or it treats the subjective annoyance produced by diesel engine idle sound (Lowet *et al.*, 1998; Shafiquzzaman *et al.*, 2000; Gonzalez *et al.*, 2003). To date, no scientific research has evaluated the effect of fuel content on the human subjective response to engine idle vibration. In addition, no research has previously been performed to produce a model describing the human subjective response to diesel idle vibration perceived through the automotive steering wheel.

The research described in this thesis is focused on the digital signal processing analysis of diesel idle vibration in automobiles, and on the human subjective response to steering wheel idle vibration. The main objectives were to measure the engine and steering wheel idle vibration signature of diesel-engined automobiles which had different engine technologies and which operated under different fuel conditions, to determine the optimal wavelet-based signal processing method with which analyse the data, and to develop a model of human hand-arm perception of the resulting time-varying vibrotactile stimuli. The research activity therefore consisted of the following tasks:

- to carry out a literature survey of diesel engine idle vibration, of steering wheel vibration and of the existing methods for evaluating the human perception of hand-arm vibration;

- to measure the vibration emissions of several representative 4-cylinder diesel-engined automobiles under several fuel conditions;

- to identify the salient statistical characteristics of steering wheel idle vibration by means of time-varying signal analysis (wavelet analysis);

- to determine the growth function which best describes the human subjective response to the idle vibration stimuli occurring at the steering wheel.

The main questions which the research set out to answer were the following:

- What vibrational signatures occur at the steering wheel of diesel-engined automobiles when at idle? And how much are these related to the vibration signature measured at the engine?

- How do the vibration signatures change when changing from one fuel to another ? And how much can the signatures vary from one engine to another ?

- What is the most appropriate wavelet-based signal processing method to use for quantifying the statistical variation of diesel idle vibration signals ?

- What is the most appropriate psychophysical method to use for quantifying the human subjective response to the diesel engine idle vibration which arrives at the driver through the steering wheel ?

- How can the human subjective response to idle vibration stimuli, which are perceived through the steering wheel, be modelled ? And how might this be used in practice by the producers of fuels, engines and of complete automobiles ?

Chapter 2

A review of the Human Response to Hand-Arm Vibration

2.1 Introduction

When a vibrating device is held in the hands, the effect of interest is local to that source of vibration. In such cases the terms 'local vibration', 'hand-arm vibration' and hand-transmitted vibration are often used (Griffin, 1990). The last term is frequently used to refer to vibration occurring at the hand which is transmitted into the body. 'Whole-body vibration', in contrast, refers to macroscopic body movements of the type which arise when a person is standing on a vibrating surface, when lying supine on a vibrating surface or when sitting on a vibrating surface. This is the case of sitting on a car seat which vibrates, or standing on the vibrating floor of a train. In this thesis, human response to hand-arm vibration has been investigated.

Humans are normally exposed to vibration from daily activities on a regular basis. Studies have shown that high levels of vibration exposure to the hand and fingers can result in symptoms of

physiological disorder, such as peripheral vascular (Taylor *et al.*, 1975), neurological or muscular responses (Griffin, 1982; Pelmear *et al.*, 1992), and bone and joint disorders (Iwata, 1968). In addition, somatosensory perception and tactile function may be temporarily decreased (Nishiyama and Watanabe, 1981). Changes in tactile function have been linked to changes in the sensitivity of specific types of mechanoreceptive nerve endings (Brammer and Verrillo, 1988). Previous research on hand-arm vibration has mainly involved the occupational diseases and hazards associated with the working tools (e.g. chain saw, drills, etc.) used by industrial workers (Miura *et al.*, 1957; Griffin, 1981). Conversely, many vibration exposures of the hand occur at low magnitudes, or for short durations, and are more associated with discomfort or annoyance than injury or disease. This is the case of automobile steering wheel vibration (Mansfield and Marshall, 2001; Giacomin *et al.*, 2004).

Understanding the way in which vibration is transmitted to, and through, the hand-arm system (Stelling and Dupuis, 1996; Sörensson and Burström, 1997) is a necessary step towards the definition of the effects of vibration on human comfort, performance and health. Nevertheless, in many applications, knowledge of how much vibration occurs at various locations is of little value without knowledge of the relation between the vibration and its subjective judgement (Stevens, 1986; Gescheider, 1997). Therefore, the methods used to study hand-arm vibration operate at different levels whose objectives can be categorised as the following:

Mechanical response: an important approach to the problem of assessing human vibration has been to experimentally investigate the mechanical response of subjects to given stimuli. The results of such studies are often expressed in terms of mechanical impedance or transmissibility, and the values of the resonance frequencies.

Health effects and activity interference: since 1907 (HMSO, 1907) numerous investigations have treated the symptoms and methods of diagnosis of physiological, neurological, muscular, bone

and joint disorders due to hand vibration exposure. The interference produced by hand-arm vibration on work and other every-day activities has also been the subject of many studies.

Subjective response: experiments have been performed to quantify the subjective response to vibration in terms of equivalent comfort curves, vibrotactile thresholds, and frequency weightings. Also, knowledge of the relationship between the physical stimuli and the subjective responses has been used to define response scales which have a known relationship to discomfort.

The purpose of this chapter is to provide an introduction to the human mechanical and subjective response to hand-arm vibration, with emphasis on studies performed relative to steering wheel stimuli. The most popular psychophysical methods used to establish the relationship between the physical characteristics of the vibration stimuli and the associated subjective response judgement will be presented in Chapter 3.

2.2 Biodynamic Response of the Hand-Arm System

Measures of the vibration transmitted to the hand (via mechanical impedance) and through the hand and arm (via transmissibility measurements) provide invaluable insights into the relative importance of different vibration frequencies (Stelling and Dupuis, 1996; Sörensson and Burström, 1997). Biodynamic measurements are convenient tools for investigating the influence of variables such as hand-arm posture, body size, grip force and grip contact area on the likely effect of vibration at the hand (Reynolds and Soedel, 1972; Pyykkö *et al.*, 1976; Lundström and Burström, 1989). The dynamic response of the hand-arm system is typically quantified by means of transfer functions: d*riving-point mechanical impedance* in which the driving force acting on the system and resulting velocity of the system are measured at the same point and in the same direction, and *transmissibility* in which two measures of the same quantity are obtained at two different locations along the hand-arm system, such as the acceleration at the hand and the acceleration at the shoulder.

2.2.1 Driving Point Mechanical Impedance of the Hand-Arm System

The most frequently used method of reporting human mechanical response to hand-arm vibration is the driving point impedance measurement. It is defined as:

$$Z(f) = \frac{F(f)}{v(f)}$$

(2.1)

where F is the input force measured at the driving point, v is the response velocity measured at the driving point, and f is the frequency of oscillation. The mechanical impedance Z can be described as a mechanical structure's resistance to an applied vibration (Pyykkö et al., 1976; Lundström and Burström, 1989). For the hand-arm system, the driving-point mechanical impedance is usually measured using a T-bar handle that is rigid over the frequency range from 10 to 1000 Hz (ISO5349-1, 2001). The handle is attached to a vibration exciter (e.g. an electrodynamic shaker) to produce the input stimulus into the hand. The handle is also equipped with strain gauges for measurements of both the grip and the feed forces applied by the subject to the handle.

The mechanical impedance characteristics of the hand-arm system have been investigated by several researchers (Reynolds and Soedel, 1972; Mishoe and Suggs, 1977; Lundström and Burström, 1989; Gurram et al., 1995b). Considerable differences are known to exist among the impedance measurements reported by the different investigators. These differences may be due to variations in the experimental techniques used, the hand-arm postures used and the grip forces adopted.

Reynolds and Soedel (1972) studied the mechanical response of the hand-arm system to translational sinusoidal vibration in the frequency range from 20 to 500 Hz when gripping a handle. They concluded that arm position had only a minor effect on the impedance of the hand across the frequency range tested, but that grip tightness and hand pressure influenced the vibration response at frequencies greater than 60 Hz. They also suggested that once a method of grip had been established, the hand-arm system could be treated as a linear system.

Lundström and Burström (1989) investigated the mechanical impedance of the hand-arm system in the frequency range from 20 to 1500 Hz. Firmer grips as well as higher vibration levels resulted in higher impedance magnitudes for frequencies above 100 Hz. Below 100 Hz, increasing the vibration input lowered somewhat the hand-arm impedance, while the grip force had little or no influence. All impedance curves had a pronounced minimum in the frequency range from 50 to 150 Hz, while the overall tendency outside that frequency range was of increasing impedance with increasing frequency, indicating that remote elements of the arm become less active as the frequency rises, eventually reaching a situation where only the fingers vibrate with the handle.

Typical values of impedance have been defined by summarising the values reported in the literature for similar measurement conditions. The mechanical impedance of the hand-arm system under conditions representative of power-tool operation is shown in Figure 2.1 (Gurram et al., 1995b) for vibration along the directions X_h, Y_h and Z_h of the standardized coordinate system for the hand (refer to Figure 2.11 for a definition of the coordinate system). The dotted line shows the mean value of the data, while the dark solid lines indicate the maximum and minimum values found in the data. Also shown is a dashed line which represents the impedance values of a 4-degree-of-freedom biodynamic model.

From Figure 2.1 it can be seen that the mechanical impedance of the hand-arm system in the X_h direction increases in magnitude with frequency, with a maximum from 20 to 70 Hz. The variation in the mean impedance magnitude in the Y_h and Z_h directions is less pronounced, and more difficult to describe. The standard error in impedance magnitude approached 30-37 percent at 1000 Hz. From the analysis of their data, Gurram *et al.* have suggested that changes in the grip force caused variations in the mechanical impedance magnitude and phase estimates of less than 10 percent at all frequencies below 100 Hz.
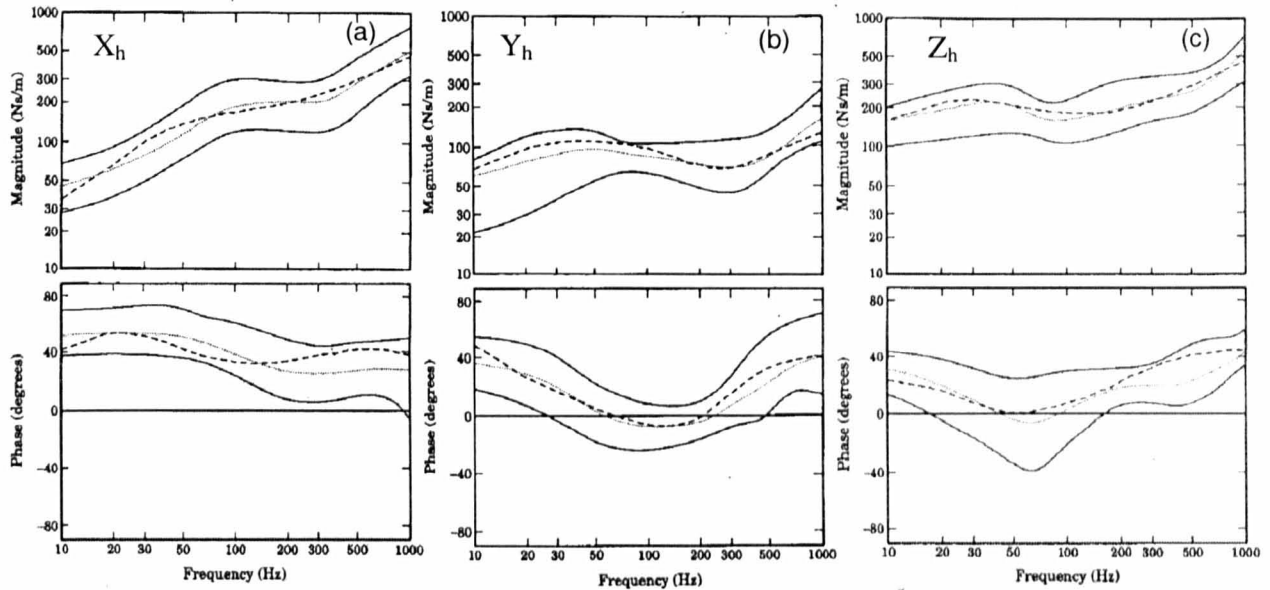
Figure 2.1 Mechanical impedance of the hand-arm system in the three orthogonal directions as defined in ISO 5349: (a) X_h direction (b) Y_h direction (c) Z_h direction. (reproduced from Gurram, 1995b).

2.2.2 Vibration Transmissibility through the Hand-Arm System

Transmissibility is normally expressed in terms of the measured acceleration since accelerometers are the mostly commonly used motion sensors (BS6842, 1987; ISO5349-1, 2001). When expressed in terms of acceleration, transmissibility is defined as:

$$H(f) = \frac{a_{out}(f)}{a_{in}(f)}$$

(2.2)

where the acceleration a is measured at reference points which represent the points of input and output to the system, and f is the frequency of the vibration. The acceleration at the input is usually measured by an accelerometer attached to the hand where the vibration enters, while the acceleration at the output is measured by one attached to a specific location of the body, such as the head , wrist, elbow, shoulder, neck, teeth, etc. (Pyykkö et al., 1976; Reynolds and Angevine, 1977; Sakakibara et al., 1986) by means of an appropriate device.

Common to the transmissibility results found in the literature is a considerable attenuation of vibration at frequencies above 100 Hz (Pyykkö et al., 1976), whereas vibration at frequencies below 40 Hz was generally found to be transmitted to the hand with little attenuation (Sörensson and Lundström, 1992). This suggests that the hand-arm system operates as a low-pass filter. Iwata et al. (1972) studied the properties of the hand-arm system by using varying psychophysical compression forces and an input acceleration level of 2 g in the frequency range from 6.3 to 100 Hz. They reported that at very low frequencies (from 6.3 to 20 Hz) the hand-arm system operates like an amplifier due to the presence of resonances.

Sörensson and Burström (1997) investigated the transmission of vibrational energy to three selected points along the hand and arm (i.e. knuckle, wrist and elbow). They estimated the transmissibility for two different kinds of vibration exposure: random vibration within the frequency range 20 to 5000 Hz, and sinusoidal vibration at eight different vibration frequencies from 20 to 1600 Hz. They found that the energy transmission to different parts of the hand and arm decreased with the distance from the vibration source. Moreover, a comparison with the random exposure showed that sinusoidal excitation lead to higher transmission of vibrational energy.

2.3 Subjective Response to Hand-Arm Vibration

With respect to human subjective response, Reynolds et al. (1977) have stated that the human subjective response to hand-arm vibration is composed of four main parameters: *quality, intensity, locus and affect. Quality* is the subjective difference that allows a name to be associated with a sensation, i.e. heat or cold, taste, smell, etc. *Intensity* represents the strength or amplitude of perception. *Locus* indicates the position from which the sensation originates. *Affect* is the characteristic of the sensation that allows a subject to classify the sensation as pleasant or unpleasant.

The subjective response to hand-arm vibration has been found to depend on many vibration variables (Griffin, 1990). In particular, research (Griffin, 1990; Giacomin and Onesti, 1999;

Haasnoot and Mansfield, 2003) has shown that the subjective response to mechanical vibration is highly dependent on the frequency of the vibration. This section therefore provides an overview of the main independent variables which affect the subjective response to hand-arm vibration.

2.3.1 The Cutaneous Mechanoreceptors

The human skin acts as a sensor to various forms of external energy such as mechanical, thermal, chemical or electrical stimuli. The sensory effect of stimulation of the skin is termed cutaneous sensitivity (Martin and Jessell, 1999). Research has demonstrated that the glabrous (non-hairy) skin of the hand contains different types of mechanoreceptors, the cutaneous end organs responsible for transducing mechanical energy into neural signals. Bolanowski and Gescheider (1988), in a series of experiments involving selective masking of the various tactile receptors, provided evidence for the existence of four main afferent fibre types in glabrous skin. These receptors are the Merkel's disks, Ruffini cylinders, Meissner's corpuscles and Pacinian corpuscles (see Figure 2.2). The four receptors form the so-called four-channel model of mechanoreception which is currently accepted by most psychophysical researchers (Bolanowski Jr and Gescheider, 1988; Hollins and Roy, 1996; Gescheider et al., 2001; Morioka, 2001).
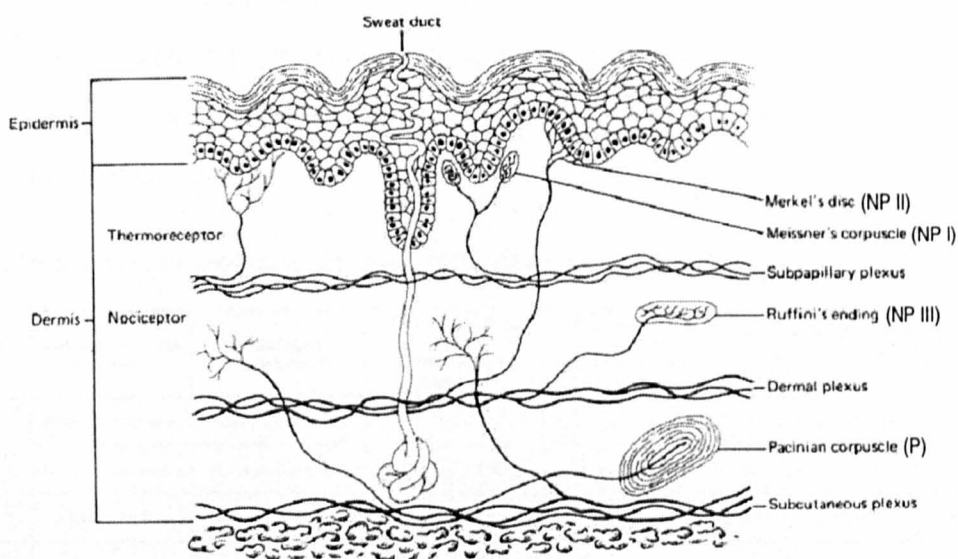
Figure 2.2 Cross-section of glabrous skin showing the different mechanoreceptors involved in vibrotactile perception (reproduced by Griffin, 1990).

Studies involving electrophysiological recording (Talbot et al., 1968; Mountcastle et al., 1972), direct recordings from human nerves (Knibestol and Vallbo, 1970; Johansson et al., 1982; Phillips et al., 1992) and psychophysics (Békésy, 1940; Verrillo, 1966b; Gescheider, 1976; Verrillo, 1985; Bolanowski Jr and Gescheider, 1988; Lamoré and Keemink, 1988; Hollins and Roy, 1996; Gescheider et al., 2001) have shown these mechanoreceptive fibres to possess distinct capacities to respond to specific frequency ranges of vibratory stimuli. The mechanoreceptive fibres are thus classified depending on how quickly they adapt to a steady stimulus, being defined as either fast acting (FA) or slow acting (SA). Slowly acting units continue to respond throughout the duration of the stimulus, whereas the response dies out quickly in the case of the fast acting units (Johansson *et al.*, 1982).

The four-channel model consists of the high frequency Pacinian (P) channel and the high frequency non-Pacinian NP II channel, along with the two low frequency channels non-Pacinian NP I and non-Pacinian NP III. Research has suggested that stimuli detection may be performed within the individual channel that is most sensitive to the signal in question (Bolanowski Jr and Gescheider, 1988; Hollins and Roy, 1996; Gescheider et al., 2001). Evidence to support the independence of the different sensory channels is found in studies of adaptation (Verrillo and Gescheider, 1977), of enhancement (Gescheider *et al.*, 1977) and of masking (Labs et al., 1978; Hamer et al., 1983). Table 2.1 summarises the salient characteristics of the four channel model of mechanoreception, while Figure 2.3 illustrates the differences in area and frequency selectivity between the four tactile channels.

Table 2.1 Properties of the four-channel model of mechanoreception.

Type of tactile channel	Associated neural receptors	Physiological characteristics	Frequency range response small contactor (0.008 cm²)	Frequency range response large contactor (2.9 cm²)	Frequencies of max sensitivity	Shape of threshold function	Spatial summation	Temporal summation
Pacinian (P) [*]	Pacinian corpuscles	fast adapting (FA 2)	none	high freq. (40 ÷ 700 Hz)	250 ÷ 300 Hz	U-shape	YES	YES
Non-pacinian (NP I) [**]	Meissner corpuscles	fast adapting (FA 1)	low freq. (3 ÷ 100 Hz)	low freq. (3 ÷ 35 Hz)	30 ÷ 50 Hz	flat	NO	NO
Non-pacinian (NP II) [***]	Merkel disks	slow adapting (SA 1)	high freq. (15 ÷ 400 Hz)	none	250 ÷ 300 Hz	U-shape	YES	YES
Non-pacinian (NP III) [****]	Ruffini cylinders	slow adapting (SA 2)	low freq. (0.4 ÷ 3 Hz)	low freq. (0.4 ÷ 3 Hz)	0.4 ÷ 2 Hz	flat	NO	NO

* Verrillo (1985). ** (Talbot *et al.*, 1968; Mountcastle *et al.*, 1972). *** (Labs *et al.*, 1978; Gescheider *et al.*, 1985). **** (Bolanowski and Gescheider,1988).
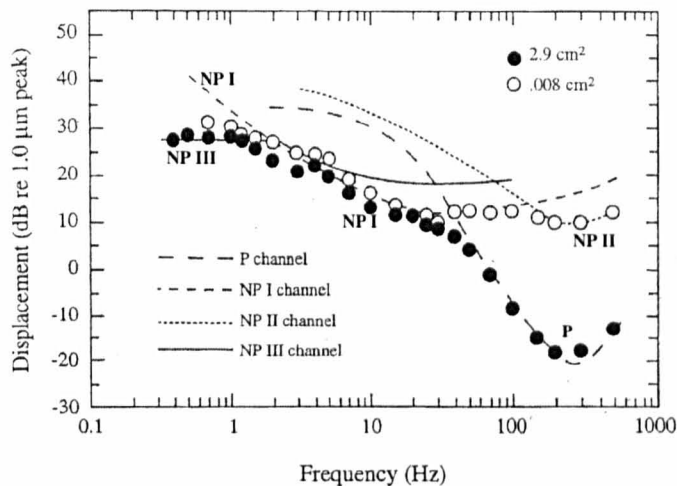
Figure 2.3   Detection threshold as a function of frequency and of contactor area for the four individual tactile channels (reproduced from Gescheider 2001).

2.3.2   Effect of Vibration Frequency on Subjective Response

The effect of frequency on human perceived discomfort has led several researchers to measure perception thresholds and annoyance thresholds. Research has shown that a constant vibration magnitude does not produce the same discomfort at all frequencies (Stevens, 1986; Griffin, 1990). Figure 2.4 presents a set of contours of equal sensation magnitude obtained by Verrillo *et. al.* (1969) using sinusoidal vibration stimuli applied to the skin of the index finger by means of a vibrating needle. Each curve describes the combinations of frequency and amplitude that result in judgments of equal subjective intensity. At threshold, the curve is U-shaped, resembling the vibrotactile perception threshold of the hand (Verrillo, 1985), and has a flattened portion in the frequency range below 40 Hz. As the vibration intensity increases the contours assume a smoother shape over the high frequency range from 100 to 1000 Hz. The flattering of the equal sensation curves as the vibration intensity increases is analogous to the behaviour of the well-known equal loudness contours for hearing (Moore, 2003), indicating that high-intensity sounds appear equally loud regardless of the frequency.
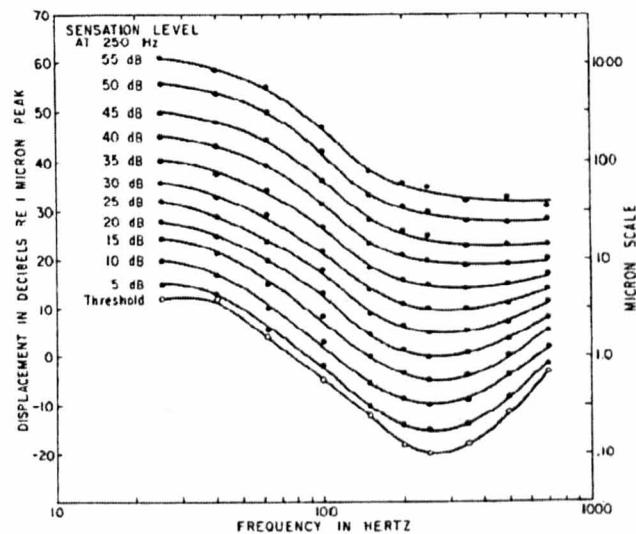
Figure 2.4   Equal sensation magnitude contours. Each curve describes the combinations of frequency and intensity that give rise to equal sensation magnitudes (reproduced from Verrillo et al 1969).

Research has suggested that, when plotted in terms of acceleration amplitude, human subjective response to hand-arm vibration decreases almost monotonically as a function of frequency. (Miura et al., 1959; Miwa, 1967; Reynolds et al., 1977; Verrillo, 1985; Griffin, 1990; Giacomin et al., 2001). Miwa (1967) for instance performed equal sensation and annoyance threshold tests for 10 subjects holding their palm flat against a vibrating plate, for vertical and horizontal vibration. Acceleration threshold was found to reach a maximum sensitivity at 100 Hz. Reynolds *et al.* (1977) studied the subjective response to vertical and axial direction translational handle vibration by measuring perception and annoyance threshold curves for eight test subjects. For a fixed acceleration amplitude, their results showed a general trend of reduced sensitivity with increasing frequency.

Most previous research on the subjective response to hand-arm vibration has investigated the change in perception threshold, or the change in the perceived intensity, at the finger and hand in the horizontal and vertical directions for translating handles or plates. The literature relative to rotational movement of handles, which is directly applicable to the vehicular steering wheel, is,

however, limited. Giacomin and Onesti (1999) produced equal sensation curves for the frequency range from 8 Hz to 125 Hz using sinusoidal excitation at reference amplitudes of 1.86 and 5.58 m/s^2. They concluded that a linear iso-comfort weighting might be acceptable at 5-10% accuracy for evaluating typical steering wheel vibration signals over the frequency range considered, and that grip tightness would not greatly effect the evaluation. Giacomin *et al.* (2004) have investigated the hand-arm perception of rotational steering wheel vibration by means of four equal sensation and one annoyance threshold tests. All equal sensation curves showed a decrease in human sensitivity to hand-arm vibration with increasing frequency. Giacomin *et. al.* suggested that two characteristic transition points existed in the curves of equal subjective response (see Figure 2.5) at frequencies of 6.3 Hz and in the interval of 50 to 80 Hz. The first was stated to be due to mechanical decoupling of the hand-arm system, while the second was claimed be due to the onset of Pacinian receptor output.
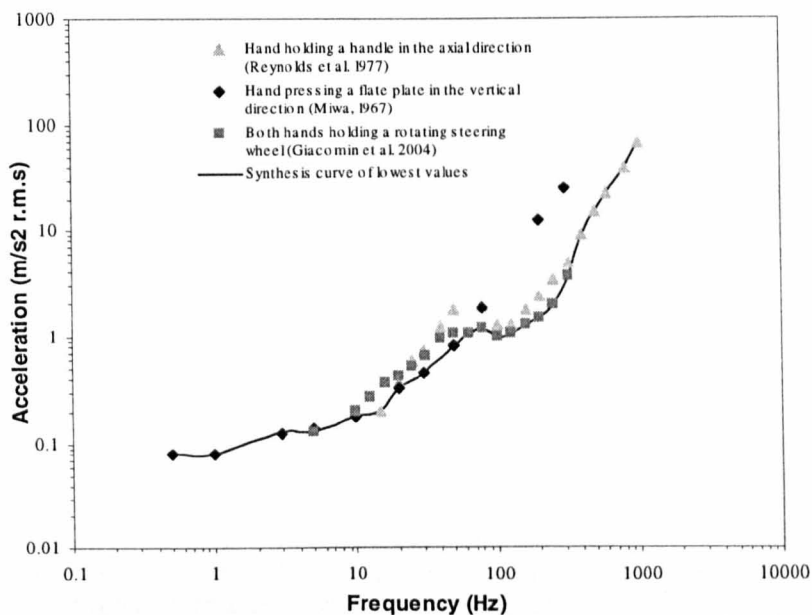
Figure 2.5   Synthesis curve of hand-arm system vibration perception: Equal sensation data from studies of translational and rotational vibration (reproduced from Giacomin et al. 2004).

International Organization for Standardization 5349-1 (2001) and British Standards Institution 6842 (1987) define a frequency weighting, called W_h, to assess the severity of hand-transmitted vibration over the frequency range 8-1000 Hz (refer to Figure 2.6). The same frequency weighting

W_h is used for each of the three axes of vibration at the point of entry of vibration to the hand. The frequency weighting W_h was primarily defined for use in reporting hand-arm exposures for the purpose of quantifying health effects. As the only internationally standardised frequency weighting, W_h has often been used in the automotive industry for evaluating steering wheel vibrational discomfort by means of measurements performed in both the translational and rotational directions of the wheel (Peruzzetto, 1988; Pak et al., 1991; Isomura et al., 1995). Giacomin et al. (2004) have proposed a frequency weighting, W_s (refer to Figure 2.6), for the purpose of evaluating the human subjective discomfort response to rotational vibrations of the type encountered in vehicles, over the frequency range from 3 to 315 Hz. Comparison of W_s to the W_h suggests important differences at low (3 to 6.3 Hz), intermediate (6.3 to 50 Hz) and high (greater than 50 Hz) frequencies. A particular point of note is the lower human sensitivity to vibration indicated by W_h at frequencies lower than 6.3 Hz.
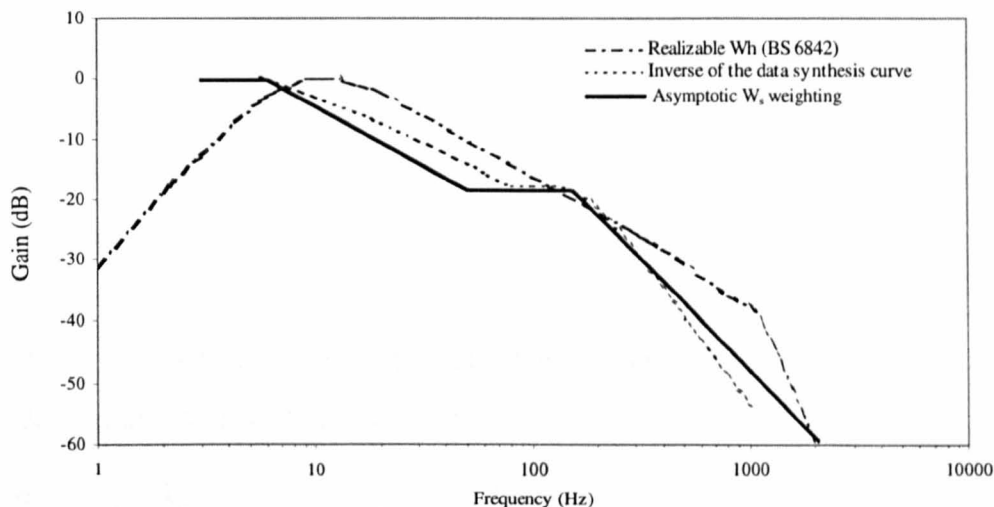
Figure 2.6 Comparison between the proposed frequency weighting W_s for rotational steering wheel vibration and the international standard frequency weighting W_h (reproduced from Giacomin et al., 2004).

2.3.3 Effect of Vibration Magnitude on Subjective Response

The magnitude of a mechanical vibration refers to the extent of its oscillatory motion. It can be measured in terms of either displacement, velocity, or acceleration. For practical convenience, the

magnitude of vibration is usually expressed in terms of the acceleration, whose units are m/s^2, and is usually measured by means of accelerometers (ISO 5349-1, 2001). Magnitude of hand-transmitted vibration is usually expressed as an average power of the acceleration, namely the root-mean-square value (m/s^2 r.m.s.) defined by:

$$r.m.s. = \left[\frac{1}{T} \int_0^T a^2(t)\,dt \right]^{\frac{1}{2}}$$
(2.3)

where T is the duration over which the r.m.s. value is determined, $a(t)$ is the instantaneous acceleration value and t is a time increment. The r.m.s. value has generally been adopted as the preferred method for quantifying the severity of human vibration exposures (ISO5349-1, 2001). The acceleration magnitude can also be expressed as acceleration level (in decibels, dB) by using a logarithmic scale. It is defined as:

$$L_a = 20 log_{10} \left(\frac{a_{r.m.s.}}{a_0} \right)$$
(2.4)

where $a_{r.m.s.}$ is the root mean square acceleration being measured, and a_0 is the reference level of 10^{-6} m/s^2 defined for acceleration (ISO1683, 1983). With the reference level of 10^{-6} m/s^2, an acceleration of 1 m/s^2 corresponds to 120 dB, while an acceleration of 10 m/s^2 corresponds to 140 dB.

Another measure used in the evaluation of vibration severity is the vibration-dose-value (VDV) which is defined as (BS-EN-ISO8041, 2005):

$$VDV = \left[\int_0^T a^4(t)\,dt \right]^{\frac{1}{4}}$$
(2.5)

where T is the duration over which the VDV value is determined and $a(t)$ is the instantaneous acceleration. The VDV value provides a cumulative measure of the vibration exposure, and being a fourth power method, has been shown in studies of whole-body vibration (Howarth and Griffin, 1991) to account for the greater effect on human subjective response of the high amplitude peaks which occur in the time history. While not having been formalised in any current international

standard, VDV values have been used (Giacomin and Fustes, 2005) for quantifying the human subjective response to hand-arm vibration since VDV is more sensitive to large amplitude accelerations than are r.m.s. values.

Several studies have attempted to answer the question how the human subjective response to hand-arm vibration changes as a function of the magnitude of the vibration. Verrillo *et al.* (1969) for example determined the rate at which the subjective intensity of the vibration grows as a function of the amplitude using sinusoidal vibration stimuli applied to the skin of the index finger by means of a vibrating needle. The resulting curves, shown in Figure 2.7, suggest that the subjective magnitude of the stimulation increases as the physical intensity of the vibration is increased. At low intensities, the subjective response was found to grow approximately linearly with respect to the intensity of the vibration stimulus at frequencies from 25 to 250 Hz. This result is in agreement with Zwislocki's theory of vibration sensitivity (Zwislocki, 1960) which states that sensory magnitude is approximately proportional to the stimulus intensity near threshold. The subjective response curves of Figure 2.7 are parallel at the upper intensities except for the 500 Hz stimuli which is steeper. This result was thought to be a reflection of the flattening of the equal sensation curves of Figure 2.4 as the vibration intensity increases.
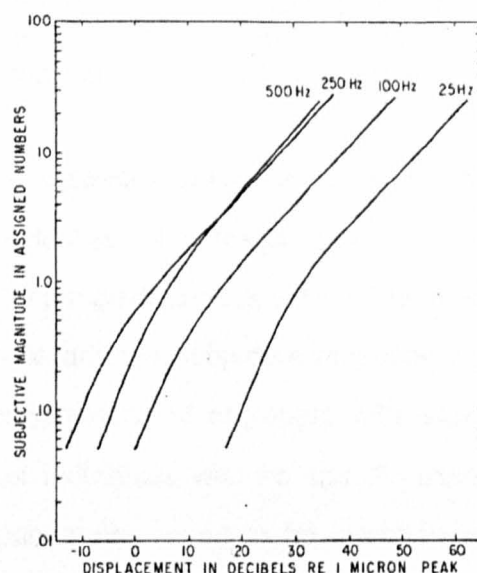
Figure 2.7 Subjective magnitude of suprathreshold vibration presented at the fingertip at frequencies of 25, 100, 250 and 500 Hz (reproduced from Verrillo *et al.* 1969).

Hollins and Roy (1996) investigated the perceived intensity of vibrotactile stimuli presented to the left index fingerpad of the hand at sinusoidal frequencies ranging from 10 to 200 Hz. They found that perceived intensity at a given frequency increased as a function of the physical amplitude in all the subjects, as shown Figure 2.8. They also found that frequencies between 25 and 75 Hz produced the most intense sensations.

Amplitude (dB re: 1 μm peak)
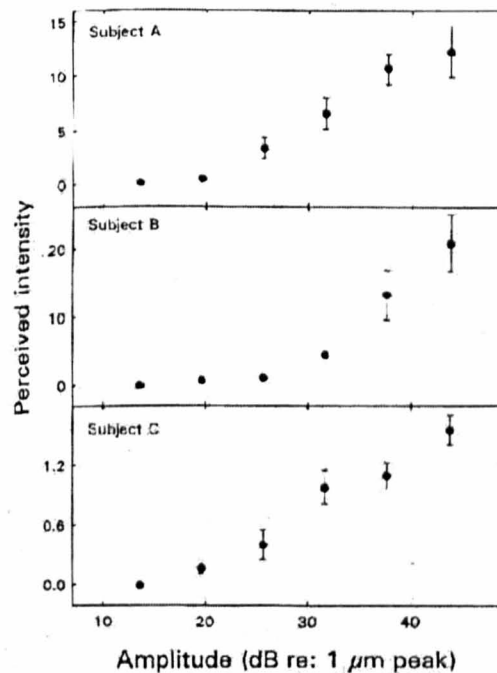
Figure 2.8   Perceived intensity of 10 Hz vibrotactile sinusoidal stimuli delivered to the index fingerpad as a function of amplitude. Data are shown as mean plus or minus one standard deviation (reproduced from Hollind and Roy, 1996).

Wos *et al.* (1988) studied the subjective response to hand-arm vibration as a function of the vibration intensity, using sinusoidal stimuli of frequencies of 30, 75 and 187 Hz at five amplitude values ranging from 26 to 5130 μm peak-to-peak values. The function describing the relationship between the stimulus amplitude and the subjective response was determined for two different groups of test subjects: one consisting of engineers with experience in analysing vibrational phenomena, and the other of individuals with no specific experience in analysing vibrational phenomena. Subjective response was found to be a negatively acceleration function of the vibration intensity. As shown in Figure 2.9, the experienced engineers were found to provide

higher intensity ratings at the test frequencies of 30 and 75 Hz. Figure 2.9 also presents the line of best fit through the mean subjective response values, which was a power function with exponent ranging from 0.72 to 1.10 (refer to section 3.3 for a definition of a power law).
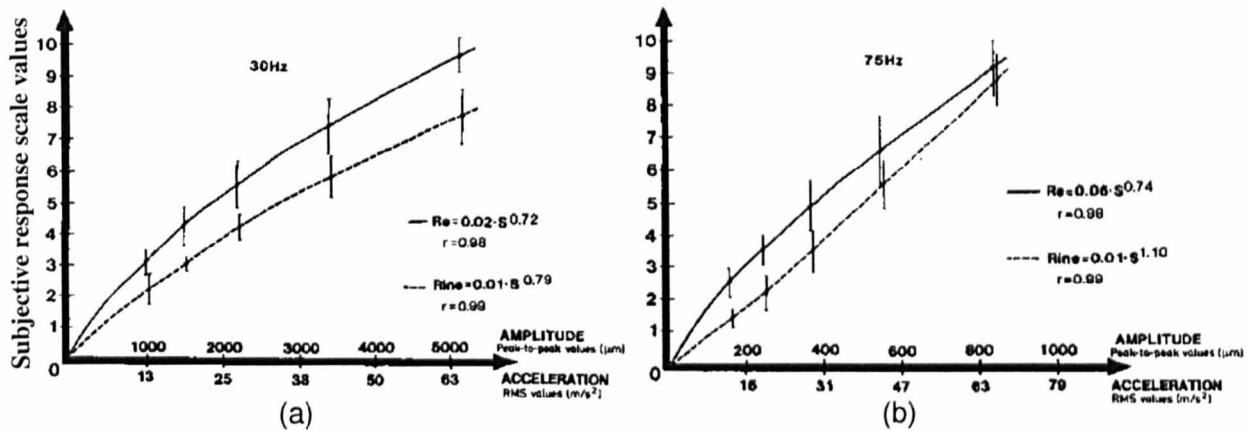
Figure 2.9   Subjective response to hand-arm vibration as a function of vibration intensity for sinusoidal stimuli delivered to the hand. Data are determined for both engineers with experience in analysing vibrational phenomena (indicated as Re),and individuals with no specific experience in analysing vibrational phenomena (indicated as Rine). Data are presented as mean value plus or minus one standard deviation.

(a) perceived vibration intensity obtained with sinusoidal vibration of 30 Hz.
(b) perceived vibration intensity obtained with sinusoidal vibration of 75 Hz.

An important case of the effect of amplitude is that of amplitude-modulated (AM) vibration. This stimulus type has been little investigated since the majority of the psychophysical studies have used sinusoidal or random stimuli for vibrotactile intensity perception (for a review see Verrillo and Gescheider, 1992). Evidence that the tactile system may have temporal processing abilities in detection of amplitude modulated stimuli can be found in earlier experiments of flicker perception on the skin by Békésy (1957). A work by Gescheider (1967) reported that two pulses stimuli separated by more than 10 ms were perceived as different stimuli. In terms of sensitivity to amplitude modulation, this implies that modulation frequencies up to 100 Hz (i.e.1/10ms) can be perceived.

One study, however, was that of Lamoré et al. (1986) who found that high-frequency (1000-2000 Hz) sinusoidal vibrations of the skin, which are normally imperceptible, induced maximum sensitivity when amplitude modulation was applied at modulation frequencies between 100 and 300 Hz. However, the use of high-frequency stimuli makes this an atypical study being outside the range of vibration frequency, up to about 350Hz (Verrillo, 1985), to which the tactile system is normally responsive. Research by Weisenberger (1986) on temporal sensitivity in the tactile system used modulated sinusoidal carrier frequencies within the range of human vibrotactile sensitivity as well as wide band and narrow band noise carriers. The results showed that the perception of amplitude modulation using sinusoids is superior to that with wide or narrow band noise. Weisenberger determined the threshold value of the depth of the modulation, which is the depth of the modulation necessary to just allow discrimination between a modulated and an unmodulated waveform. The results, shown in Figure 2.10, indicated that the modulation depth at threshold determined for an unmodulated sinusoidal carrier waveform of 25 Hz is about 0.2 for modulation frequency ranging from 5 to 10 Hz. As the carrier frequency increases up to 250 Hz the data showed large differences in modulation sensitivity reflecting the separate mechanoreceptive response systems at low (0.4-100 Hz) and high (40-700 Hz) frequencies. Weisenberg concluded that although not as sensitive to amplitude modulation as the auditory system, the vibrotactile system can reasonably be expected to resolve temporally varying waveforms.
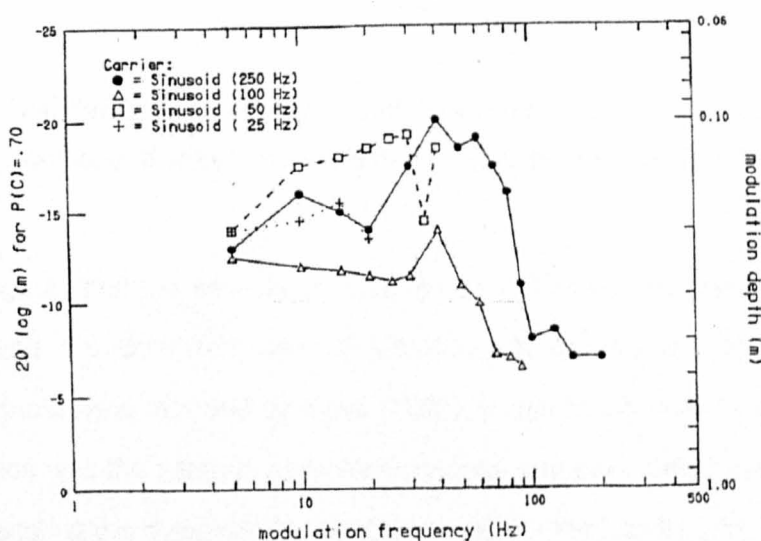
Figure 2.10 Modulation depth thresholds for detection of sinusoidal amplitude modulated stimuli with carrier frequency at 25, 50, 100 and 250 Hz (reproduced from Weisenberg, 1986).

2.3.4 Effect of Vibration Direction on Subjective Response

The vibration along one axis of a handle may differ greatly from that along other axis. International Organization for Standardization 5349-1 (2001) and British Standards Institution 6842 (1987) define the directions along which the vibration is transmitted to the hand, referring to the anatomical and basicentric co-ordinate system, as presented in Figure 2.11. The anatomical co-ordinate system is defined in both standards as centred on the hand in the head of the third metacarpal bone. The basicentric co-ordinate system, instead, is defined as centred on (or adjacent to) the vibrating surface. In practice, vibration measurements are usually made with respect to a basicentric co-ordinate system (ISO 5349-1, 2001).
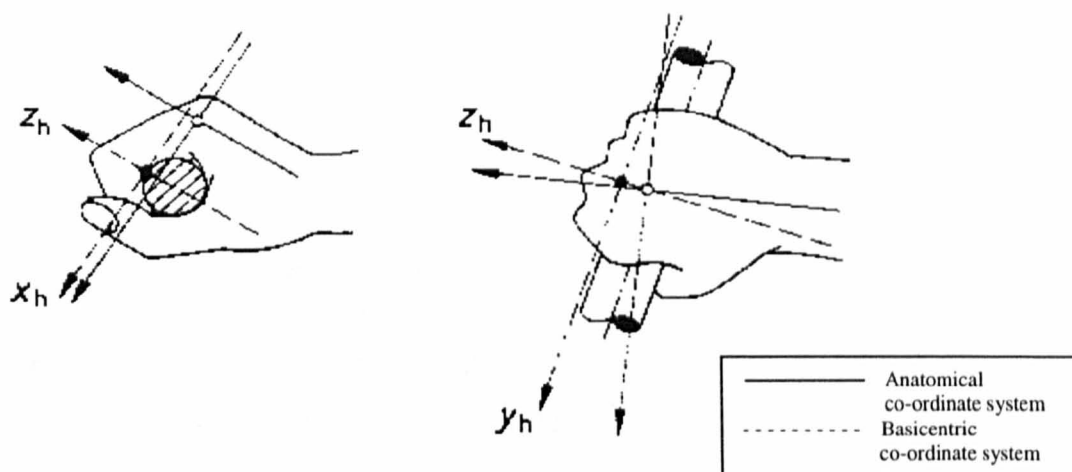
Figure 2.11 Standardized anatomical and basicentric co-ordinate system for the directions of vibration for the hand (reproduced from ISO 5349-1, 2001).

ISO 5349-1 suggests that the severity of vibration can often be sufficiently characterised by the acceleration along the dominant axis of vibration. In the studies of equal sensation and annoyance threshold tests reported by Miwa (1967), it was found that the subjective response to hand-arm vibration was the same in both the horizontal and the vertical directions, for one or two hands pushing against the plate, and for various shapes of the handle grip. Reynolds *et al.* (1977)

studied the subjective response to vertical and axial direction, translational, handle vibration for eight test subjects. For a fixed acceleration amplitude, they observed that vibration along the vertical direction caused the greatest discomfort, while vibration along the tubular handle caused the least discomfort.

For what regards perceived discomfort relative to an automotive steering wheel, Schröder and Zhang (1997) have investigated the subjective response to steering wheel acceleration stimuli measured along the three orthogonal axes on a mid-sized European passenger car for different driving speeds ranging from 30 to 70 Km/h over three different road surfaces. Correlation analysis between the subjective ratings and the measured steering wheel acceleration suggested that the vibration level along the vertical direction of the steering wheel correlated best with the subjective ratings of the drivers in the frequency range from 30 to 90 Hz, which is the frequency range where most of the vibration energy is present at the steering wheel (Peruzzetto, 1988; Amman *et al.*, 2001; Giacomin *et al.*, 2004).

2.3.5 Effect of Vibration Duration on Subjective Response

Extensive research has shown that the stimulus duration affects both the vibrotactile sensitivity at threshold (Verrillo, 1965; Gescheider, 1976; Verrillo, 1985; Gescheider *et al.*, 1990; Checkosky and Bolanowski Jr, 1992; Gescheider *et al.*, 1994b; Gescheider *et al.*, 1996; Gescheider *et al.*, 1999; Gescheider *et al.*, 2001) and at suprathreshold levels of stimulation (Verrillo *et al.*, 1969; Gescheider and Joelson, 1983). For stimuli frequencies greater than 40 Hz and stimuli durations shorter than approximately 0.5 seconds, the threshold amplitude for detection has been found to decrease monotonically with stimulus duration. The phenomenon is usually referred to as temporal summation or temporal integration. For stimuli frequencies greater than 40 Hz, the perception threshold does not change with increases in stimulus duration beyond 1.0 second. For vibration frequencies less than 40 Hz, no temporal summation has been observed.

Figure 2.12 illustrates the nature of the temporal summation effect in terms of perception thresholds for vibratory stimulation at 30 Hz and 200 Hz delivered to the hand. It can be seen that the non-Pacinian channels NP I and NP III have an approximately constant sensitivity at low frequencies below 40 Hz and thus do not present temporal integration properties (Verrillo, 1965; Gescheider, 1976; Bolanowski Jr and Gescheider, 1988; Gescheider *et al.*, 1994). Since increases in stimulus duration produce decreases in the thresholds of the Pacinian receptors (at 200 Hz) and the non-Pacinian NP II receptors (at 30 Hz), these two sensory systems are believed to be capable of temporal integration (Verrillo, 1965, 1966a; Gescheider, 1976; Gescheider *et al.*, 1985; Bolanowski Jr and Gescheider, 1988).
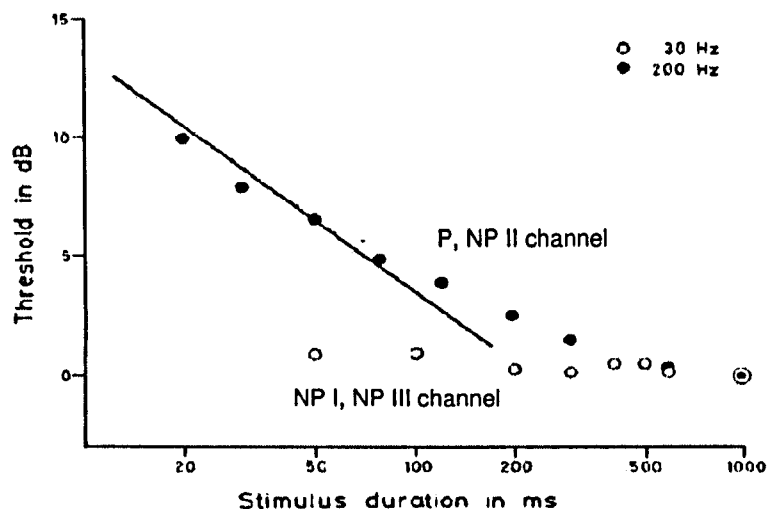
Figure 2.12 Temporal summation effects on vibrotactile perception threshold (reproduced from Gescheider, 1976):

Most laboratory studies in which subjects have been asked to judge the discomfort of vibration have been conducted with rather brief vibration exposures. For example Miwa (Miwa, 1968) has asked subjects to judge the relative discomfort produced by short periods of sinusoidal vibration, and pulsed sinusoidal vibration, for signal durations up to 6 seconds. He suggested that for vibration in the range 2-60 Hz there is no further increase in discomfort sensation for stimuli durations greater than approximately 2.0 seconds, whereas for vibration in the range from 60 to 200 Hz the same limit is approximately 0.8 seconds.

Chapter 3

Concepts from the Field of Psychophysics

3.1   Introduction

Psychophysics is the study of the relationship between the properties of physical stimuli and the psychological reactions to those properties (Coren and Ward, 1989). Sensation refers to the process of detecting and encoding the physical stimulus by means of the sensory system, which sends the information to the brain, while perception refers to the results of the mental processing of the brain, which involves relationships, context, past experience and memory. Figure 3.1 summaries the psychophysical process through which the sensory information passes from the physical stimulus to its perception, and subsequent subjective response. The first stage of the psychological process is the physical dimension. The stimulus can be represented as a single point along a certain dimension (e.g. the intensity of the vibration) and can be measured by instruments (such as accelerometers) that assign a value along a physical (objective) scale. The second stage is represented by the internal subjective experience. At this stage, the sensory

systems undergo a stimulus coming from the environment, and the perceptual experience creates an inner dimension of the stimulus. The last stage is represented by the subjective response. At this stage the human subject can report his or her subjective judgment of the stimulus based on his or her internal subjective experience.
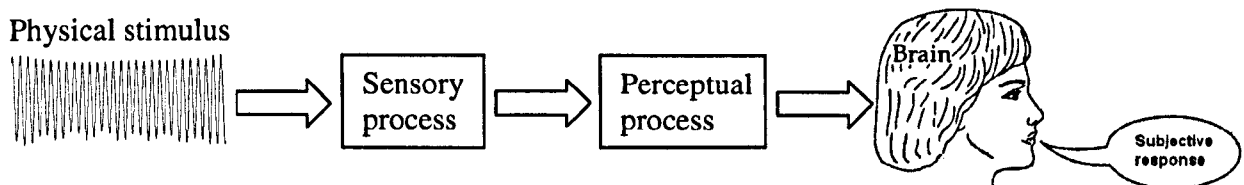
Figure 3.1 Psychophysical process.

Classical psychophysical methods, as proposed by E. H. Weber and Gustav Fechner (Guilford, 1954) as early as 1860, are concerned with the measurement of the sensory limits of the human sense organs. The *stimulus threshold* (also called *absolute threshold*) is defined as the smallest amount of stimulus energy necessary to produce a sensation. The *difference threshold* (DL) is defined as the amount of change in a stimulus required to produce a *just noticeable difference* (JND) in the sensation. For what regards tactile sensitivity, classical psychophysical methods have been used to determine vibration perception thresholds (Verrillo, 1985; Morioka, 1999) and to determine the difference threshold for the detection of changes in vibration amplitude for the hand-arm system (Knudson, 1928; Craig, 1972; Gescheider *et al.*, 1990).

Although the investigation of sensory thresholds provides valuable information about the senses, it does not in itself provide a complete picture of a sensory system, since absolute and difference thresholds are not stated in sensation units but rather in units of stimulus energy (Gescheide, 1997). It is assumed that many factors make a human subject respond differently on different occasions to identical levels of sensory experience (Marks and Stevens, 1965; Algom and Marks, 1984; Zwislocki, 1991). The exact relationship between physical quantities and the sensations they produce must therefore be determined experimentally. Psychophysical scaling methods are used in order to establish metric scales which describe the human subjective response.

Different psychophysical methods developed for the scaling of sensory attributes can measure the human subjective response to many forms of nonmetric (i.e. stimuli that can be arranged only on a nominal scale) (Stevens and Harris, 1962; Stevens, 1966) and metric stimuli (Verrillo, 1985; Gescheider *et al.*, 1990). Psychophysical scaling methods can be described as belonging to one of two major classes. One class involves indirect rating of the stimuli, where the psychophysical scale is constructed by means of statistical assumptions, which are imposed on the experimental data. In this case, the measure of sensory magnitude comes from the discrimination of differences between physical stimuli. On the other hand, the direct methods are based on scaling procedures which assume that human subjects are capable of making direct and meaningful evaluations of the magnitude of their sensory experiences. In psychophysical experiments involving the direct methods, the test subjects provide an estimate of their subjective response to the stimuli.

In the research presented in this thesis, psychophysical experiments were performed in order to investigate the human subjective response to hand-arm vibration. This chapter therefore presents an overview of the most commonly used scaling methods, and a review of the studies involving the modelling of the human subjective response to vibration.

3.2   Weber's Law and Fechner's Law

Psychophysical theory (Coren and Ward, 1989) has shown that to discriminate two stimuli as different it is necessary that they present a specific difference, ΔI, in the magnitude of the physical stimuli. The value of ΔI represents the smallest increment of a stimulus that can be detected. The proportion by which a stimulus intensity I must be changed in order to produce a just noticeable difference (JND) in sensation is referred to as the Weber fraction (WF):

$$\frac{\Delta I}{I} = c \tag{3.1}$$

where ΔI is the difference threshold in the physical stimulus of intensity I, and c is the Weber fraction. The difference threshold ΔI increases with increases in the magnitude of the vibration stimulus I, whereas c is a constant which depends on the type of stimulus. The Weber fraction indicates the amount by which a stimulus must differ from another stimulus so as to be detected. The smaller the Weber value, the greater the sensitivity to stimulus differences along a sensory dimension. The Weber fraction for hand-transmitted vibration has been found to vary from a minimum of 0.05 as found by Knudson (1928) in a study for the detection of changes in vibration amplitude using needles indenting the skin of the fingertips, to a maximum of 0.15 to 0.18 as found by Morioka (1999) in a study using sinusoidal vibration at frequencies from 8 to 500 Hz applied to a wooden handle. Common to all the studies is that the WF was found to be independent of stimulus frequency.

Classical psychophysical methods are based on the assumption that sensations are not directly measurable. Fechner, by assuming the validity of Weber's law of Eq. (3.1), derived indirect measures of sensory magnitude from the physical measurements of the difference thresholds in the stimulus magnitude. The general assumption made by Fechner and co-workers (Fullerton and Cattel, 1892; Thorndike, 1910) was that all the JND's were equal psychological increments in sensation magnitude, regardless of the size of difference threshold ΔI, since the JND, which represents the smallest detectable increment in a sensation, is always the same size psychologically. Thus, Fechner developed a scale of sensation magnitude by counting the number of JND's above absolute threshold for specific values of the stimulus intensity. Fechner proposed that the sensation magnitude increased with the logarithm of the stimulus intensity, deriving a general formula from the Weber's law, which is known as Fechner's law:

$$\Psi = c \, log \, I \qquad\qquad (3.2)$$

where Ψ is the sensation magnitude, I is the intensity of the stimulus in units above the absolute threshold, and c is the Weber fraction. Fechner's law is presented in Figure 3.2 where it can be seen that equal increments in sensation correspond to increasingly larger values of stimulus intensity as the stimulus intensity increases.
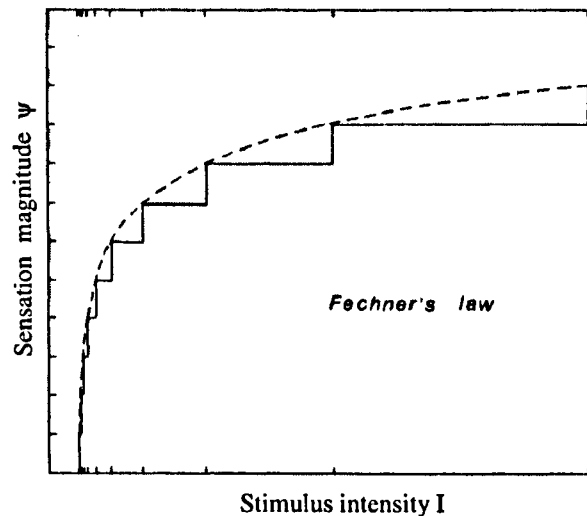
Figure 3.2   Relationship between stimulus intensity and perceived sensation
according to Fechner's law (reproduced from Stevens, 1986).

3.3   Stevens' Power Law

Stevens (1986) proposed that the psychophysical or perceived intensity of a stimulus was best related to the physical intensity by a power law relationship, which in its most general form is expressed as:

$$\Psi = \Psi_o + k(X - X_{th})^\beta$$ (3.3)

where Ψ is the subjective perceived magnitude, X is the stimulus magnitude, k is a constant determined from the measurement units, the two constants Ψ_o and X_{th} are the subjective and stimulus magnitudes at threshold, which indicate the starting point of the growth function on the response axis (y-axis) and on the stimulus axis (x-axis) respectively, and β is the power exponent defining the growth of the human response. The calculation of the Stevens's power exponent β is useful since it provides a metric which translates the measurable physical objective quantities into perceived subjective quantities. The form of the psychophysical function is influenced by the size of the exponent. An exponent of 1.0 corresponds to a linear function. An exponent of less than 1.0 corresponds to a concave downward function indicating a negatively accelerating relationship between perceived intensity and physical stimulus amplitude, while an exponent greater than 1.0 corresponds to a concave upward function indicating a positively accelerating relationship. Support that judgments of sensation intensity grow as power functions of stimulus intensity has

been provided by experiments on a large number of perceptual continua. Power function

exponents have been found to be as small as 0.33 for brightness (Stevens and Stevens, 1963)

and loudness (Stevens, 1955), and as large as 3.5 for electric shock on the fingertip (Stevens *et*

al., 1958). An example of the Stevens' power law obtained for three different modalities is

presented in Figure 3.3.
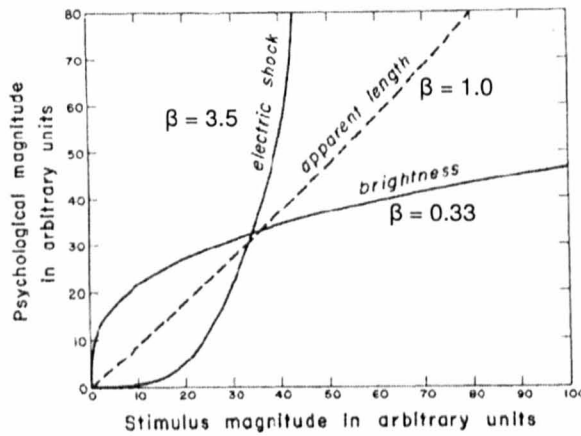
Figure 3.3   Relationship between stimulus intensity and perceived sensation according to
Stevens' power law (reproduced from Stevens, 1986).

In the case of vibrotactile perception, Stevens (Stevens, 1959) reported that the subjective

intensity of a 60 Hz vibration applied to the fingertip followed a power function with an exponent of

0.95, whereas for a 120 Hz vibration the exponent was 0.83 (Stevens, 1968). Similarly, Franzén

(Franzén, 1969) reported Stevens' power exponents of 0.95 for 50 Hz, 0.81 for 100 Hz, 0.70 for

150 Hz and 0.58 for 250 Hz (see Figure 3.4).
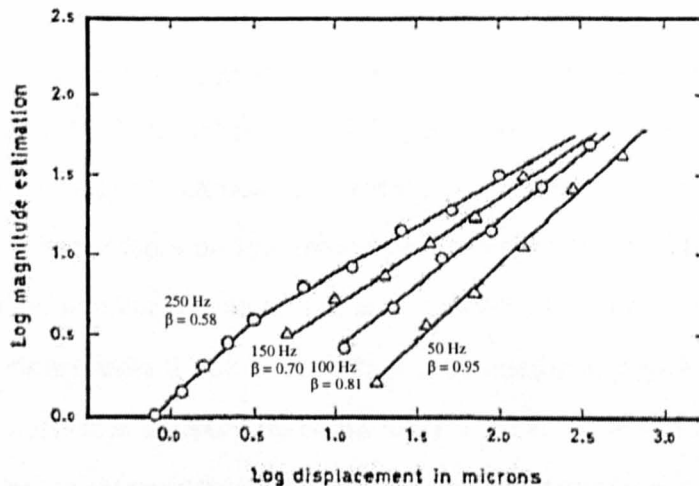
Figure 3.4   Subjective magnitude function of vibration stimuli presented at fingertip at
frequencies of 50 Hz, 100 Hz, 150 Hz and 250 Hz (reproduced from Franzen, 1969).

Although a considerable amount of evidence (Stevens, 1986; Baird, 1997; Gescheider, 1997) indicates that subjects obey the Stevens' power law (Eq. 3.3), the exponent values vary considerably across individuals within the same experiment (Marks and Stevens, 1965; Wanschura and Dawson, 1974; Logue, 1976; Hellman, 1981; Algom and Marks, 1984) and across time within individuals (Logue, 1976; Teghtsoonian and Teghtsoonian, 1983; Marks, 1991). The fact that this occurs, despite averaging across multiple responses for each stimulus, indicates that test subjects do not generally produce unique responses to the same stimuli (Poulton, 1989). This suggests that the power exponent might be influenced by the psychophysical scaling procedure used.

3.4   Psychophysical Scale Types

The type of scale achieved depends upon the character of the basic empirical operations performed during the psychophysical test and on the nature of the sensory attribute being scaled (Stevens, 1946; Marks, 1974a). Stevens (1986) distinguished two kinds of sensory continua according to whether the corresponding stimulus dimension is based on quantity (*"prothetic"*) or quality (*"metathetic"*). Vibratory amplitude and vibratory frequency are two separate stimulus dimensions, and the sensation evoked by each can be ordered by human subjects along the prothetic scale of changing intensity or the metathetic scale of changing quality, respectively.

Different scaling methods can be applied to a given set of data, leading to different conclusions (Marks, 1974a; Stevens, 1986; Gescheider, 1997). Four basic types of measurement scales have been defined: *nominal*, *ordinal*, *interval*, and *ratio* scale (Gescheider, 1997). A *nominal* scale categorises objects. The numbers on the nominal scale reflect only that the objects are different from one another. Such nominal scales do not use numbers quantitatively and, therefore, cannot provide a means of measurement. An *ordinal* scale uses numbers to rank objects with respect to some characteristic such that different numbers have a greater-than-less-than relation between them. The rank number represents the scale value for each measurement. However, in an ordinal

scale, it is not possible to determine the distance between the objects with respect to the characteristic being measured. In an *interval* scale, instead, the intervals between the scale values represent meaningful distances between amounts of the property measured. In this way, the difference between two scale values can be compared with the difference between two other scale values. In an interval scale, the size of the differences between numbers, as well as their ordinal relation, has meaning. However, the zero point of the scale can be set arbitrarily at the scale value of one stimulus, and does not represent the zero amount of the property measured. A *ratio* scale, on the other hand, as well as having the properties of order and distance, has a natural origin where the ratios of the scale values have meaning.

According to Stevens (1960), the methods for constructing psychological scales can be classified into three types: *confusion scaling, partition scaling and ratio scaling*. Each is designed to generate a numerical scale of sensory magnitude, although each requires a different kind of perceptual response from the test subject. *Confusion scaling* (also called discrimination scaling) requires a test subject to make discriminative responses between stimuli that differ by a certain number of JND's. It relies on the ability of the test subject to make comparative differences and to report whether the sensation produced by one stimulus is greater than or less than the sensation produced by another stimulus. Confusion scales of sensation are based on indirect scaling procedures, and are interval scales. *Partition or category scales* are obtained by direct scaling procedures in which the test subjects have to make direct judgments of the psychological differences among stimuli, and partition them into a limited number of categories. Partition scales are therefore interval scales since the intervals between the scale values represent differences between amounts of the property measured. *Ratio scaling* of sensation relies on the ability of the test subject to make direct judgments of the ratio relationships between the magnitudes of sensations. Table 3.1 summarizes the different type of psychological scales in terms of their properties.

Table 3.1 Main types of psychological scales.

Psychological process	Psychophysical scaling method	Scale type obtained	Empirical operations	Property of distance	Natural origin
Ranking scaling	Direct	Ordinal scale	Determination of greater or less	NO	NO
Confusion scaling	Indirect	Interval scale	Determination of equality of intervals or differences	YES	NO
Partition (category) scaling	Indirect				
Ratio scaling	Direct	Ratio scale	Determination of equality of ratios	YES	YES

3.5   Psychophysical Scaling Methods

3.5.1 Indirect Scaling Methods

In the case of indirect scaling procedures, the sensory magnitudes of the stimuli are inferred from measures of stimulus discriminability based upon comparative judgments. Thurstone's law of comparative judgement (Thurstone. 1959) is the indirect scaling method which is most frequently used to construct a psychophysical scale, due to its generality and reliability. Classical Fechnerian indirect methods based on JND counting are not considered suitable for constructing scales since they depend on only the distance between the stimuli on the psychological continuum, thus they do not take into account the statistical variability in the subjective estimates. In this section, Thurstone's law of comparative judgement is therefore presented since it is the best representative of the indirect scaling methods.

3.5.1.1 The Paired-Comparisons Method Using Thurstone's Model

In the method of paired-comparisons (Thurstone, 1959; David, 1988), all stimuli are presented to the test subjects in all possible pairs. The subjects are then required to make comparative judgments for all the pairs, and to state which of the two stimuli greater than the other with respect of the chosen semantic attribute (e.g. unpleasantness, intensity, etc.). The test subject is not required to judge the magnitude of the stimulus presented. The method of paired-

comparisons is not suitable when large numbers of stimuli are to be compared since the number of comparisons required by the method is equal to the number of possible combinations, which for a number n_s of stimuli is given by:

$$n_s(n_s - 1) = n_s^2 - n_s \qquad\qquad (3.4)$$

Thus, the number of comparative judgments increases with the square of the number of the stimuli considered.

Thurstone (1959) developed a mathematical model for deriving subjective scale values from comparative judgment proportions. Thurstone's model has been widely used in several scientific disciplines (Stevens and Harris, 1962; Ekman and Kûnnapas, 1963; Stevens, 1966; Franzén, 1969; Gescheider, 1997) because of its generality and ability to quantify numerous psychological qualities for which there are no obvious physical stimulus properties (Guilford, 1954). Thurstone's model assumes that a stimulus is capable of producing a range of momentary estimates of the position of the stimulus along the human internal psychological continuum (S_i values in Figure 3.5).
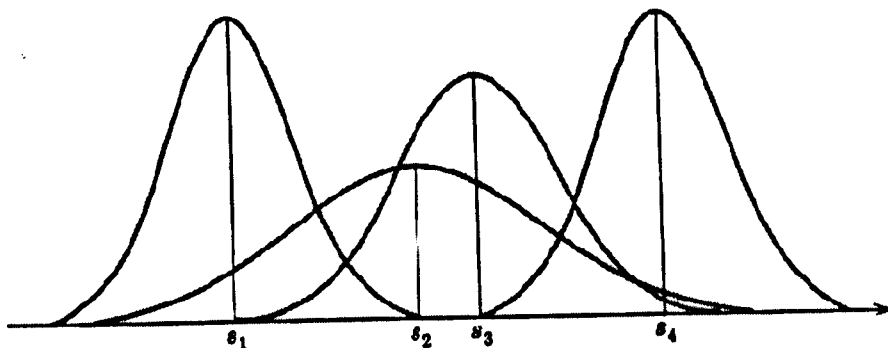
Figure 3.5   Distributions on the psychological continuum of discriminal processes associated with four different stimuli. S_i are the mean values of each discriminal distribution (reproduce from Torgerson, 1958).

The variations in the estimates are assumed to be normally distributed along the psychological continuum, and the standard deviation of each distribution is usually referred to as the discriminal dispersion. The difference between the means of two distributions specifies the difference on the psychological continuum between the sensations for two stimuli. Thurstone's law of comparative judgments is:

$$S_j - S_k = z_{jk}\sqrt{\sigma_j^2 + \sigma_k^2 - 2r_{jk}\sigma_j\sigma_k}$$ (3.5)

where S_j and S_k are the subjective scale values of stimuli j and k respectively, z_{jk} is the normal deviate corresponding to the proportion of times the stimulus j is preferred over the stimulus k when they are compared, σ_j and σ_k are the standard deviations of the distribution of momentary estimates and r_{jk} is the coefficient of correlation between the pairs of discriminal processes.

In order to determine the difference between two scale values, $S_j - S_k$, all the terms on the right-hand side of Eq. 3.5 must be known. From the results of all possible paired-comparisons, the observed frequencies expressing the number of times each stimulus was judged greater than each other stimulus are calculated, and next converted into the proportion of times each stimulus is judged greater than every other stimulus. This provides a proportion matrix P [ns x ns] (presented as Table 3.2) where the generic element $p_{j>k}$ is calculated as:

$$p_{j>k} = \frac{f_{j>k}}{n_{judgements}}$$ (3.6)

where $f_{j>k}$ is the number of times each stimulus j (in the jth column) was judged greater than stimulus k (in the kth row), and $n_{judgements}$ is the total number of judgements per stimulus pair. Since each stimulus is assumed to be judged greater than itself half of the time (Torgerson, 1958) values of 0.5 are placed on the diagonal positions.

Table 3.2 Matrix P of the proportion of times stimulus j is judged greater than stimulus k.

		stimulus j			
Matrix P	**A**	**B**	**C**	**D**	**E**
A	0.5	$p_{B>A}$	$p_{C>A}$	$p_{D>A}$	$p_{E>A}$
B	$p_{A>B}$	0.5	$p_{C>B}$	$p_{D>B}$	$p_{E>B}$
C	$p_{A>C}$	$p_{B>C}$	0.5	$p_{D>C}$	$p_{E>C}$
D	$p_{A>D}$	$p_{B>D}$	$p_{C>D}$	0.5	$p_{E>D}$
E	$p_{A>E}$	$p_{B>E}$	$p_{C>E}$	$p_{D>E}$	0.5

stimulus k

The value of the normal deviate z_{kj} in Eq. (3.5) corresponding to the element $p_{j>k}$ is obtained from statistical tables of the normal distribution (Hinton, 1999). However, the remaining parameters in Eq. (3.5) are still unknown. Thurstone (1959) presented five different cases of the law of comparative judgment in order to solve Eq. (3.5), by making assumptions that simplify the equation. They are:

Case I: the law is applied in its complete form as stated in Eq. (3.5), and the unknown terms must be estimated from the data. In Case I, repeated judgments are made by a single test subject.

Case II: as in Case I, the law is applied in its complete form, but many test subjects make a single judgment for each pair of stimuli.

Case III: an assumption is made that there is no correlation between the responses to any pair of stimuli, meaning that the responses for any two stimuli are independent. This assumption is based on the homogeneity of stimuli, meaning that the stimulus series has no distracting attributes and varies clearly in only one aspect. The term r_{jk} is therefore assigned a value of zero. The discriminal dispersions are assumed to be unequal, and need to be estimated from the experimental data.

Case IV: the discriminal dispersions are assumed to be approximately equal, but their values still must be estimated.

CaseV: the simplest solution of all is provided by making the additional assumption that the discriminal dispersions are equal.

The particular solution of the law used in deriving the scale values is dependent upon the circumstances of each particular scaling problem. Analytical procedures have been devised to give good estimates of the unknown terms when using one of Thurstone's five cases (Burros, 1951; Burros and Gibson, 1954; Guilford, 1954; Torgerson, 1958).

3.5.2 Direct Scaling Methods

Common to all the direct scaling methods is the assumption that the test subject is capable of estimating quantitative relations between subjective experiences and that he or she can assign numbers to stimuli to represent sensation magnitude (Stevens, 1986; Baird, 1997; Gescheider, 1997). Therefore no assumptions are imposed on the experimental data other than the constraints implied in the instructions given to the test subject.

3.5.2.1 The Method of Magnitude Estimation

This method requires subjects to directly judge some attribute of the stimulus by assigning numbers which should be chosen in proportion to the perceived sensation. The stimuli are randomly presented and there is no limit to the range of numbers a subject may use. Magnitude estimation thus offers the advantage of reducing the end effects that can be encountered by using fixed scale techniques such as semantic scales or numbered scales. However, a major disadvantage is that different subjects may give wildly different magnitude estimates (Teghtsoonian and Teghtsoonian, 1983; Algom and Marks, 1984; Zwislocki, 1991), and tend to avoid extreme judgmental ratios (Stevens and Greenbaum, 1966; Griffin and Whitham, 1976; Teghtsoonian and Teghtsoonian, 1978) which is referred to as the regression effect. Therefore subject training is required before the actual data is gathered. Inter-subject variability can be addressed in a number of ways. One is to present a reference stimulus and to tell the test subject that the sensation it produces has a specified magnitude, such as 10 or 100. On subsequent trials, other stimuli are presented, and the test subject is instructed to make his or her judgments reflect how many times greater one sensation is than another. Thus, the test subject is required to perform ratio estimations between the two sensations. In either variation of the method, the average of the numbers assigned to each stimulus is usually taken as its psychological scale value.

One important characteristic of direct scaling methods such as magnitude estimation is that they can be affected by large artefacts (Teghtsoonian, 1971; Poulton, 1989) which are directly dependent on the stimulus range used in the study. Also the preceding test signal (Cross, 1973; Ward, 1973; Allan, 1975) effects the test subject's response since it provides a contextual constraint on the subject's judgments. Therefore the Stevens' power law exponent obtained by means of magnitude estimation must be used with care. In particular, it should not be applied to stimuli having vastly different statistical properties and it should not be used to estimate human subjective response to stimuli which are outside the original test range.

3.5.2.2 The Method of Magnitude Production

The method of magnitude production is the inverse of the method of magnitude estimation. In this direct scaling method, the experimenter tells the test subject the numerical value of a reference stimulus. Next the test subject is required to adjust the magnitude of a comparison stimulus, such that the subjective sensation that it produces bears a required ratio to the sensation produced by the reference stimulus. The psychological function is derived by plotting the prescribed subjective magnitude values against the average setting of the stimulus obtained from the test. However, this method can result in a bias towards low settings, since subjects do not like exposing themselves to uncomfortable stimuli (Stevens and Greenbaum, 1966; Griffin and Whitham, 1976; Teghtsoonian and Teghtsoonian, 1978).

3.5.2.3 Category Scaling

Category scaling is a direct method to quantify subject opinion about a certain attribute of the stimulus presented (Stevens, 1986; Gescheider, 1997). It is an absolute method since the subject doesn't have to judge a succession of pairs of stimuli, but each stimulus separately. In this method the subject is required to assign each stimulus to a category such as comfortable, very uncomfortable or extremely uncomfortable. The categories may be defined by numbers, the numbers 1 to 7 being commonly used (Stevens and Galanter, 1957). The results obtained using

semantic scales depend on the question phrasing and on the number of words used on the scales. It is important that the choice of the attribute to describe the sensation be appropriate to the application. The number of useful semantic labels has been found to be limited by the human ability to resolve differences between stimuli and situations. Research (Pollack, 1952; Miller, 1956) suggests that the optimum is from 5 to 9 levels. A typical scale based on five levels is presented in Figure 3.6.

very uncomfortable	uncomfortable	average	comfortable	very comfortable

Figure 3.6 Example of a five level semantic category rating scale.

In vibration testing applications different studies have employed different phrases to describe the vibration, and widely differing results have been obtained (Hanes, 1970). The use of semantic scales normally involves large inter-subject differences due to the fact that each subject attaches a slightly different meaning to the descriptive label. It is a consequence of the fact that specific words activate specific cognitive categories. Subjects may use the same meaning throughout an experiment and thus produce a potentially useful set of data, yet not representing any absolute statistical significance.

3.5.2.4 Borg Category-Ratio Scale Method

Based on the observation that ratio scaling methods were unable to make inter-individual comparisons, Borg (1998) developed a category-ratio scale, referred to as the Borg category-ratio CR-10 scale, to be used in clinical studies for evaluating the human subjective responses to perceived intensity after physical exercise. Borg assumed that ratio scaling procedure, such as magnitude estimation, could not be used in clinical settings since the difference between two subjective responses were not due perceptual intensity evaluated, but were instead due to the difference in the use of numbers. The Borg category-ratio CR-10 scale combines the advantage of using categories of descriptive adjectives, with the advantage of obtaining a ratio scale for the

determination of the numerical subjective response values. The use of descriptive adjectives provides an "anchor" for the numbers which helps the test subject to make reliable judgments. The method assumes that the perceived sensations described by the same adjective will be experienced as the same by different test subjects, thus reducing the problem of response bias (Borg and Borg, 1992). An assumption of the Borg CR10 scale is that the range of perceptual intensities is approximately equal for different human subjects, in spite of the fact that the physical stimulus intensities may differ for different stimulus modalities. Thus the range from zero to the maximal perceived intensity is used as a frame of personal reference for the test subject. The Borg CR10 scale, shown in Figure 3.7, consists of a numerical scale from 0 (nothing at all) to 10 (extremely strong) with nine verbal anchors placed along the number scale in an approximately logarithmic fashion. The "extremely strong" 10 rating value is used to represent the strongest perception of the current attribute that has ever been experienced by the test subject. The rating "absolute maximum", which is located below the value 10 and is indicated by a dot "•", provides an opportunity for estimating the value of any test stimuli which dramatically exceed the subject's past experience.

0	Nothing at all	"No P"
0.3		
0.5	Extremely weak	Just noticeable
1	Very weak	
1.5		
2	Weak	Light
2.5		
3	Moderate	
4		
5	Strong	Heavy
6		
7	Very strong	
8		
9		
10	**Extremely strong "Max P"**	
11		
✦		
●	Absolute maximum	Highest possible

Figure 3.7   The Borg category-ratio CR-10 scale (reproduced from Borg, 1998).

Test subjects are instructed to use the scale by first finding the verbal anchor which best fits the perceived sensation, and by then choosing an appropriate numerical value from those associated with the verbal anchor. Subjects are allowed to use any number on the scale, fractions or decimals. If subjects experience the perceived intensity to be stronger than their own personal experience, they are allowed to choose a number greater than 10 in order to avoid ceiling effects (Gescheider, 1997).

Evidence of the reliability of the Borg CR 10 scale can be found in the study of the human subjective response to hand-arm vibration performed by Wos *et al.* (1988), who claimed that the Borg CR 10 scale is highly reliable, with reliability coefficients ranging from 0.841 to 0.986. Neely *et al.* (1992) have reported coefficients of determination (r^2) of 0.79 between Borg CR 10 results and subjective data obtained by means of a visual analogue scale, and also reported typical retest coefficients of determination of 0.98.

3.6   Relation Between Different Psychophysical Scales

Since the different psychophysical scaling methods generate different scales (see Table 3.1), various studies have been conducted to establish the relationships between them. For both kind of continua, those based on metric stimuli and those based on non-metric stimuli, Stevens (1966) has demonstrated that when the scales resulting from ratio scaling (direct judgement) are compared with the scales resulting from the use of an interval scale (category scaling or an indirect Fechner or Thurstone procedure) the relation is found to be approximately logarithmic. Figure 3.8 presents a comparison of a Fechnerian-based JND scale, a category scale and a magnitude estimation scale used to quantify the subjectively perceived duration of a noise stimulus. From Figure 3.8 it can be seen that the form of the psychophysical laws are different. Magnitude estimation produced a power function, the JND method of Fechner approximates a logarithmic function, and the category scale produced an intermediate result between the other two.
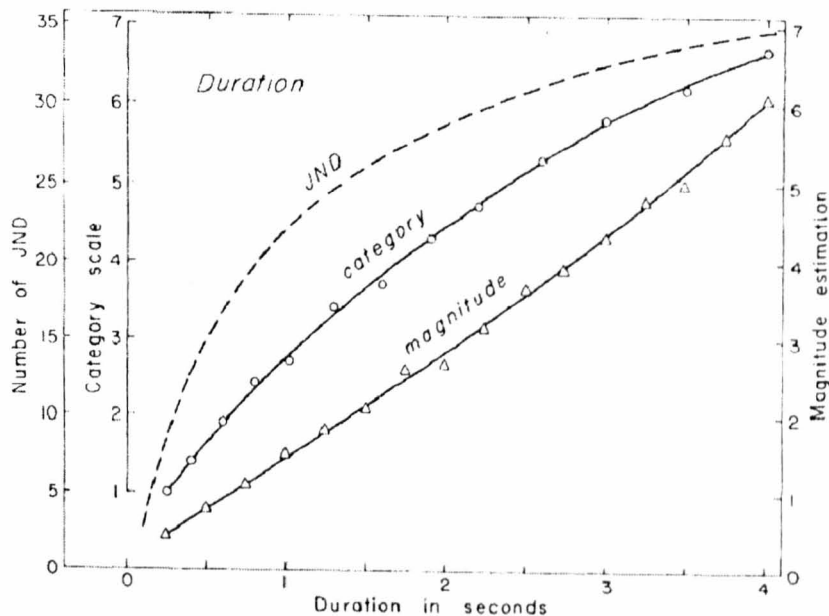
Figure 3.8   Subjective response functions obtained using JND counting, category scaling and magnitude estimation test protocols when measuring apparent duration of sound stimuli (reproduced from Stevens, 1966).

The difference between the results obtained using interval scales (JND, Thurstone and category scale) and those obtained using ratio scales (magnitude estimation, magnitude production) has been explained by Marks (1974b) in terms of "fundamentally different psychophysical processes that are involved in the two type of scales to describe a sensory/perceptual system". Marks further suggested that ratio scaling methods yield valid measures of sensory magnitudes, while scales produced by means of interval scales yield valid measures of sensory discriminability. Therefore the discriminability of two sensations was claimed to not correspond to the difference in magnitude between the two sensations. Marks defined discriminability as "the capacity of a sensory/perceptual system to respond differentially to a pair of stimuli". This capacity is measured in particular paradigms (e.g. paired comparison tasks) under conditions that minimize the influence of central mechanisms such as memory or decision making. However, both discriminability and subjective magnitude are considered to be equally meaningful dimensions of perceptual experience, each being measured most effectively by means of a different scaling procedure (Ward *et al.*, 1996; Gescheider, 1997).

Chapter 4

Concepts from the Field of Digital Signal Processing

4.1 Introduction

The main objective of signal processing analysis is to determine the statistical properties of a signal which can be used to identify and describe the nature of the signal being analysed (Bendat and Piersol, 1986; Piersol, 1992). The identified signal statistics provide objective metrics that can be used to quantify the overall effect of an individual signal condition, and to compare the signal properties of different sets of data. The effectiveness of a signal processing technique depends mainly on the type of signal being analyzed, and on the type of signal information that is to be determined from the measured signal (Bendat and Piersol, 1986; Piersol, 1992). As stated in the introductory Chapter 1, automotive engine idle vibration can be considered to be a mixture of harmonic components and non-stationary random components due to the reciprocating combustion event repeating every engine cycle (Dixon *et al.*, 1994; Rahnejat, 1998) and due to the random fluctuations in the crankshaft angular velocity that occur due to the stochastic nature

of the combustion process (Priede, 1992; Ozdor et al., 1994; Hinze and Cheng, 1998). These random phenomena cause the engine vibration signature to vary considerably with time (Shim et al., 1996; Stankovic and Bohme, 1998; Gaberson, 2001). This chapter provides an overview of a set of signal processing techniques which can be used to analyse temporally varying signals of the type produced by an automotive engine which is at idle.

4.2 Signal Types

A mechanical vibratory system can be described using a schematic representation as shown in Figure 4.1. The input time series x(t) represents the vibration source that excites the mechanical system S, producing a vibration time series response y(t).

Vibration   ────────▶ | **Mechanical System** | ────────▶ Vibration
source   x(t) | **(S)** | y(t)   response
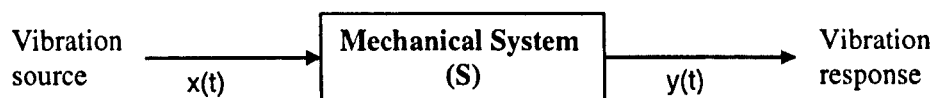
Figure 4.1   Schematic representation of a mechanical vibratory system.

Two broad classifications of signal are generally accepted by the scientific community (Bendat and Piersol, 1986): deterministic and nondeterministic. If the excitation acting on the vibratory system can be described by a mathematical function at any given time, the motion is said to be predictable or deterministic. A deterministic signal can further be characterized as being periodic or nonperiodic. A signal is periodic if it repeats with a characteristic period for all time. A signal is nonperiodic, instead, if it only exists for a finite time range (transient signal) or when one or more of the signal statistical parameters change with time (aperiodic). Periodic signals can further be characterized by having one single frequency (sinusoidal signal) or being a superposition of two or more harmonic waves (complex periodic). A generally accepted system of signal classification is presented in Figure 4.2.
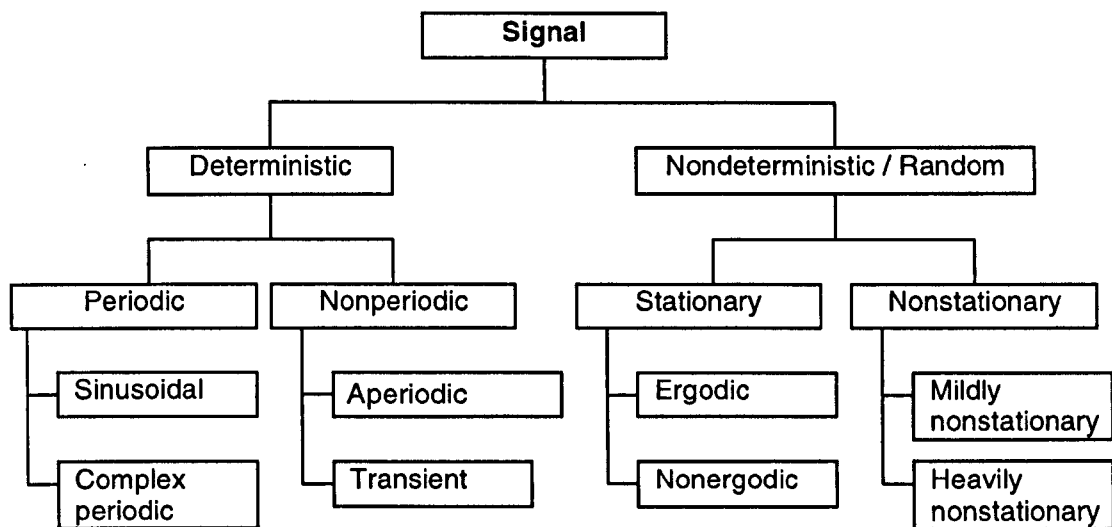
Figure 4.2 Classification of signals (adapted from Bendat and Piersol, 1996).

When the value of the excitation at a given time cannot be predicted, the excitation is instead said to be nondeterministic or random. In this case, the signal can be described only in terms of probability distributions and statistical averages computed over the ensemble of the sample records representing the random process. The probability distribution P(x) for a random process is defined as (Bendat and Piersol, 1986):

$$P(x) = \int_{-\infty}^{x} p(x)\,dx \qquad (4.1)$$

where p(x) is the probability density function (PDF) expressing the probability that the random variable takes a value between x and x+dx. A random process x(t) is said to be stationary if for any time t_1, t_2, ..., t_n, its probability distribution does not depend on time, i.e.

$$P\{x(t_1), x(t_2), ..., x(t_n)\} = P\{x(t_1+\tau), x(t_2+\tau), ..., x(t_n+\tau)\} \qquad (4.2)$$

where τ is an arbitrary time displacement. In practice, low order statistics are employed to describe random process, leading to the definition of the term "weak stationarity" to describe stationarity up to order 2. Under this condition, a stationary random process can be described by

the statistical averages up to the second order, computed over the ensemble of N_s sample records, i.e.

- the mean value $\mu_x = \dfrac{1}{N_s} \displaystyle\sum_{k=1}^{N_s} x_k(t)$;   (4.3)

- the mean square value: $\mu_x^2 = \dfrac{1}{N_s} \displaystyle\sum_{k=1}^{N_s} x_k^2(t)$;   (4.4)

- the variance $\sigma_x^2 = \dfrac{1}{N_s} \displaystyle\sum_{k=1}^{N_s} \left[x_k(t) - \mu_x \right]^2$;   (4.5)

- the auto-correlation function $R_{xx}(\tau) = \dfrac{1}{N_s} \displaystyle\sum_{k=1}^{N_s} x_k(t)\, x_k(t+\tau)$ (4.6)

By definition, the weakly stationary condition implies that the mean value, the mean square value and the variance are constant and independent of time, and that the auto-correlation function is dependent only on the time displacement τ. If the random process is stationary and the statistical properties as defined in Eq. (4.3) to (4.6) do not differ when computed over different sample records k, the random process is said to be ergodic.

An important characteristic of a stationary random process is that its instantaneous values at any time t have a probability density function given by:

$$p(x) = \frac{1}{\sigma_x \sqrt{2\pi}}\, e^{-(x-\mu_x)^2 / 2\sigma_x^2} \qquad\qquad -\infty < x < +\infty \qquad\qquad (4.7)$$

This probability density function, known as the Gaussian distribution, is commonly observed in nature, and is thus an important model used in the analysis of a random process. Its statistical characteristics can be completely specified using two parameters (refer to Eq. 4.7). This is not true for other random processes, whose behaviour cannot be adequately described without the use of several further metrics which define the departure from a Gaussian process.

A random process x(t) is said to be non-stationary if for any time t_1, t_2, ..., t_n, its probability distribution depends on time. Non-stationary signals can further be subdivided into two categories: mildy non-stationary and heavily non-stationary (Giacomin *et al.*, 1999). A mildy non-stationary signal is defined as a random process with a stable mean, mean square value and variance for most of the record, but with short periods of changed signal statistics due to the presence of transient behavior. A heavily non-stationary signal is defined as being similar to a mildly non-stationary signal, but with the presence of transient events over large intervals of the time history.

4.3 Time Domain Analysis

4.3.1 Global Signal Statistics

Global signal statistics (Bendat and Piersol, 1986; Erdreich, 1986) calculated from the time series are commonly used in order to describe data sets and to quantify the extent of any departures from stationary-Gaussian behaviour.

4.3.1.1 Root Mean Square Value

The root-mean-square (r.m.s.) value, which is a 2nd statistical moment, gives a measure of the overall energy of a signal. For a time series, the r.m.s. is defined as:

$$r.m.s. = \left\{ \frac{1}{N} \sum_{j=1}^{N} x_j^2 \right\}^{1/2}$$

(4.8)

where x_j is the instantaneous value of the sampled process $x(t)$ at time $t = j \Delta t$ and N is the number of the sampled values. The sampling interval Δt is equal to $1/f_s$ where f_s is the sampling frequency of the signal.

4.3.1.2 Skewness

The skewness, which is a 3rd statistical moment, characterizes the degree of asymmetry of a distribution around its mean value. It is dimensionless and it is expressed as:

$$S_{kew} = \frac{1}{N} \sum_{j=1}^{N} \left(\frac{x_j - \mu_x}{\sigma_x} \right)^3 \qquad (4.9)$$

For a symmetrical distribution, such as a harmonic waveform or for a stationary Gaussian process, the value of skewness is zero. Positive skewness indicates a distribution with an asymmetric tail extending toward more positive values. Negative skewness indicates a distribution with an asymmetric tail extending toward more negative values.

4.3.1.3 Kurtosis

The kurtosis, which is a 4th statistical moment, is highly sensitive to outlying data among the instantaneous values and therefore characterizes the relative peakedness or flatness of a distribution compared to the normal distribution. It is dimensionless and it can be expressed as:

$$K_t = \frac{1}{N} \sum_{j=1}^{N} \left(\frac{x_j - \mu_x}{\sigma_x} \right)^4 \qquad (4.10)$$

The kurtosis is an important metric since it helps quantify the extent of departure from stationary Gaussian distribution, for which the kurtosis value should be close to 3. Any positive deviation from this value indicates a relatively peaked distribution, whilst a kurtosis less than 3 indicates a relatively flat distribution. For a sinusoidal signal the kurtosis value is, instead, 1.5. For the purpose of hand-transmitted vibration evaluation, an estimate in terms of kurtosis is useful due to the close correspondence between this metric and the 4th power methods, where the 4th power reflects an increased human sensitivity to high amplitude events (Howarth and Griffin, 1991).

4.3.2 Running Statistical Measures

When the data of interest have average properties that are time varying, running time averages are often used to describe the data (Piersol, 1992). For each of the signal statistics described in section 4.3.1, the running time averages can be accomplished by executing Eq. (4.8) to Eq. (4.10) repeatedly over short, contiguous time intervals of duration $T_w \ll T$, where T is the length of the

original signal. A running statistical measure can therefore provide a useful tool for tracking the variation in the signal statistics over time. The basic requirement in the computation of a running average is to select an averaging time window T_w that is short enough not to smooth out the time variations present in the signal, but long enough to suppress statistical sampling errors in the average value estimate at any time. Procedures (Erdreich, 1986) for selecting the optimum time window T_w usually depend on the nature of the analysed signal, as in the case of a rotating machine presenting a periodicity feature of a dynamic event over time.

Another signal parameter that is occasionally calculated as a running statistic is the crest factor (CF). The crest factor is defined as the ratio between the maximum instantaneous value, $\left| x_{j\text{max}} \right|$, present in the sampled process time history and the calculated r.m.s. value, i.e.

$$CF = \frac{\left| x_{j\,max} \right|}{r.m.s.} \tag{4.11}$$

For a sinusoidal signal the crest factor is 1.41. For a stationary Gaussian random process crest factor values should usually lie in the range between 3.5 and 4.5 (Giacomin *et al.*, 2000). By its definition, the crest factor is rarely used as a global statistic since it is determined by the amplitude of the single largest peak present in the signal. Thus a global crest factor value cannot be representative of a multiple peak, non-stationary waveform (Erdreich, 1986).

4.3.3 Time-varying Auto-Covariance method

Another sliding window method which has proven useful in several fields (Li et al., 2000; Li and Jung, 2002; Wang and Jung, 2002) is the time-varying auto-covariance (TVA) method. The advantage of using a TVA method is that it allows not only tracking of the signal energy variation over time as in the case of the running r.m.s. estimate, but also directly reveals the periodicity of the variation. The TVA method requires the decomposing of the original time history into a series of short segments of length T_w which are assumed to be stationary, whereby the classical auto-covariance function can be determined.

The classical auto-covariance function is a tool for detecting deterministic periodic data which might be masked in a random background (Bendat and Piersol, 1986). This technique is thus particularly useful for describing the harmonic periodic motion which occurs in engine idle vibration due to the cyclic operation of the engine (Dixon *et al.*, 1994; Rahnejat, 1998). For a signal $x(t)$, the auto-covariance function describes the self-similarity of the values of the data at one time with the values at another time. It is expressed as (Bendat and Piersol, 1986):

$$C_{xx}(\tau) = E\{[x(t)-\mu_x]\cdot[x^*(t+\tau)-\mu_x]\} \tag{4.12}$$

where E is the expected value operator. * denotes the complex conjugate, μ_x is the mean value of $x(t)$, and τ is the time displacement (also called tau lag) by which the signal is shifted to assess self-similarity. For the particular case of a process which has a mean value of zero, the auto-covariance function becomes the auto-correlation function expressed by Eq. (4.6). For a zero-mean process, the detection of the signal periodicity is based on the properties of the auto-correlation function, namely:

(a)   for a deterministic, periodic signal of infinite length (Figure 4.3a), the $R_{xx}(\tau)$ persists periodically with the same cycle period (CP) as the underlying signal x(t), does not show peak decay, and all side lobes have the same height as the central lobe at zero lag (see Figure 4.3b). The cycle period is given by the time lag τ of the first-right peak neighboring the zero lag ($\tau = 0$);

(b) $R_{xx}(\tau)$ has its maximum at zero time lag ($\tau = 0$) and it is equal the mean square value of x(t).

Thus, $\dfrac{1}{N}\displaystyle\sum_{k=1}^{N} x_k^2(t) = R_{xx}(0)$;

(c)   for a narrow-band random signal (shown in Figure 4.4c) which is characterized by a distribution of frequency content only in a narrow band of frequencies, the $R_{xx}(\tau)$ diminishes to zero for large time displacements (see Figure 4.4d). While for a broad-band random signal, which is characterized by a distribution of frequency content in a wider band of frequencies, the $R_{xx}(\tau)$ diminishes more rapidly to zero
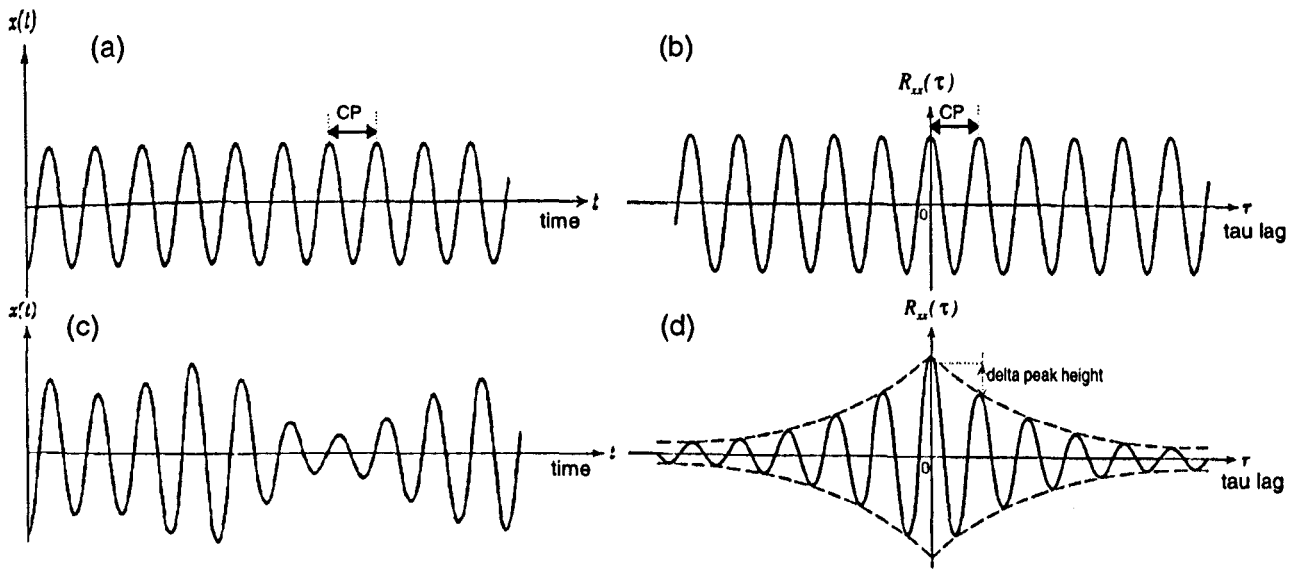
Figure 4.3. Time domain representation of a signal and of its associated auto-correlation function (reproduced from Bendat and Piersol, 1986).

(a)   time history of a sinusoidal waveform of frequency 1/CP.

(b)   auto-covariance function of a sinusoidal waveform of frequency 1/CP.

(c)   time history of a narrow-band random signal.

(d)   auto-covariance function of a stationary random signal.

By calculating Eq. (4.12) in the time window T$_w$, it is possible to extract for each segment the cycle period CP. The estimated CP for each window is then converted to frequency f using the relationship $f = \dfrac{1}{CP}$ in order to track the changes in the frequency over time. A quantitative measure of the variability of the amplitude of the signal can also be obtained from the autocorrelation function by calculating the height of the first dominant right side lobe peak. For a

finite length signal with changing amplitude the height of the auto-correlation central lobe provides, as shown for the property (b), the mean square value, a measure of the energy content of the signal within the time window, whereas the side lobe peaks decay such that with higher amplitude variability there is larger peak decay. Hence, from the array of each of the auto-correlation function, the difference between the height of the central lobe and that of the first right side lobe (indicated in Figure 4.3d as delta peak height) provides a measure of the variability of the signal energy over time.

Figure 4.4 presents a typical result (Li and Jung, 2002) obtained for a signal whose frequency decreases from a initial frequency of 1.0 Hz to final frequency of 0.1 Hz (a chirp signal) shown in Figure 4.4(a), and for a sinusoidal signal of constant amplitude and same frequency of 1.0 Hz, shown in Figure 4.4(a'). The windowed auto-covariance sequences for the two signals, which are zero-mean processes, are presented in Figures 4.4b and b' in the time-lag plane as a two-dimensional intensity plot, with amplitude coded by a gray scale. As indicated by the intensity plot of Figure 4.4(b), the magnitude of the TVA for the chirp signal shows a gradual "fanning" of the peaks indicating a monotonic decrease of the frequency, while the amplitude of the side lobes slightly decay in time on either side of the central lobe, as shown by the changes of the intensity from white to black. The resultant increase in the cycle period CP (in seconds) is illustrated in Figure 4.4(c). In contrast to the fanning nature of TVA sequences of the chirp signal, the TVA sequence of the sinusoidal signal of Figure 4.4(a') is characterized by having the time lag τ of the first side lobe constant as a function of time t, see Figure 4.4(b'), indicating a constant value of the frequency of the sinusoidal signal . The peak amplitude of the side lobs remains also constant being the amplitude of the sinusoidal signal constant. The resultant cycle period CP, indicating the constant period of the sinusoidal signal, is illustrated in Figure 4.4(c').
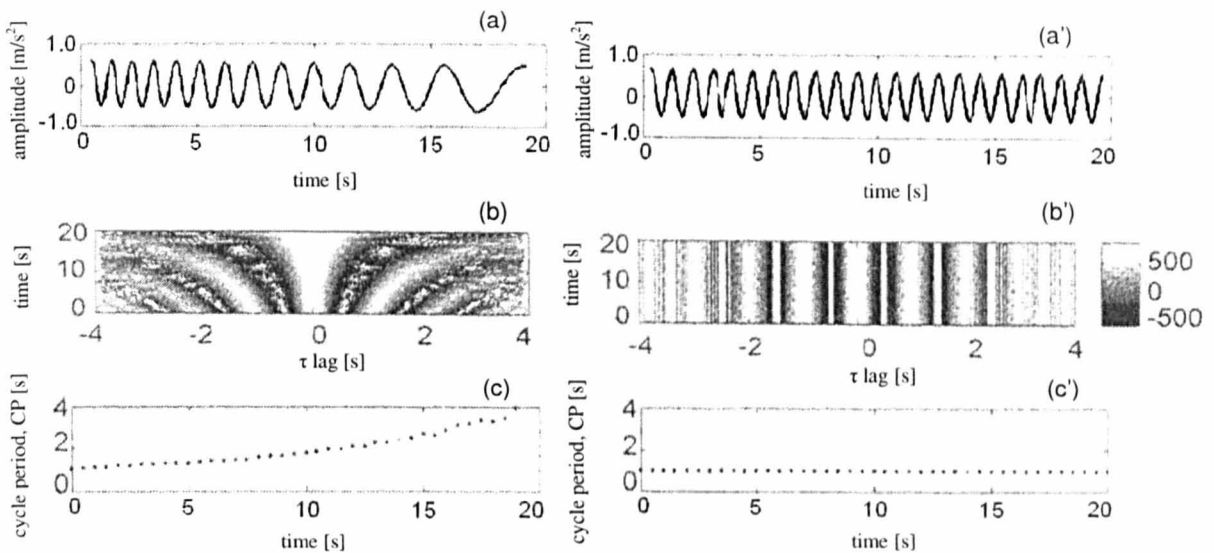
Figure 4.4   Time-varying auto-covariance method (reproduced from Li and Jung, 2002).

(a)   time history of a chirp signal consisting of a initial frequency of 1.0 Hz and final frequency of 0.1 Hz.

(a')   time history of a sinusoidal signal consisting of a frequency of 1.0Hz.

(b)   time-varying auto-covariance sequences obtained for the chirp signal, presented as an intensity plot in the time-lag plane.

(b')   time-varying auto-covariance sequences obtained for the sinusoidal signal, presented as an intensity plot in the time-lag plane.

(c)   cycle period of the chirp signal as a function of time.

(c')   cycle period of the sinusoidal signal as a function of time.

4.4 Frequency Domain Analysis

4.4.1 Fourier Transform

Spectral analysis is widely used to analyse vibration signals (Piersol, 1992; Rahnejat, 1998). The mathematical function used to transform a time data series x(t) into the frequency domain is called the Fourier transform (Oppenheim and Schafer, 1975; Newland, 1994). The Fourier transform decomposes any periodic signal into a summation of its harmonic components. For a time data series x(t) measured over the time interval [0, T], sampled at N equally spaced points at distance Δt_s apart, the discrete Fourier transform (DFT) is defined as:

$$X_k(f_k) = \frac{1}{N} \sum_{n=0}^{N-1} x_n e^{-i(2\pi k n/N)} \qquad \text{n,k = 0, 1, 2, ..., (N-1)} \qquad (4.13)$$

computed at the discrete frequency values:

$$f_k = \frac{k}{T} = \frac{k}{N\Delta t_s} = \frac{k f_s}{N} \qquad \text{k = 0, 1, 2, ..., (N-1)} \qquad (4.14)$$

where $f_s = \frac{1}{\Delta t_s}$ is the sampling frequency. The Fourier components X_k are unique only out to k =

N/2, that is out to the frequency $f_k = 1/(2\Delta t_s) = f_s/2$ which is called the Nyquist frequency f_N.

The Nyquist frequency f_N represents the maximum usable frequency available in a signal taken

at a given sampling frequency f_s. The most widely used algorithm for computing the Fourier

components expressed in Eq (4.13) is the fast Fourier transform (FFT) (Bendat and Piersol,

1986). The calculation of the Fourier transform defined in Eq. (4.13) is based on the fundamental

assumption that the time series is periodic over the period $T = N\Delta t_s$ being analyzed.

Once a Fourier transform is used to convert data from the time domain to the frequency domain,

a useful representation which is commonly used in the case of random vibration signals is the

autospectral density function, also called the power spectral density (PSD) (Bendat and Piersol,

1986; Newland, 1994). The PSD being a power density function represents the rate of change of

the mean square value with frequency. In this way, it avoids the problem that random signals,

producing a continuous frequency spectra, have the signal energy measured within a certain

frequency band which depends on the width of that band (Bendat and Piersol, 1986). In addition,

because the Fourier transform in Eq. (4.13) is computed only on one time interval, the spectrum

will not be typical of the complete time history. Thus, averaging of the spectra from different

intervals of the signal is performed in order to obtain a more accurate representation. The PSD of

a time series is therefore defined as:

$$G_{xx}(f) = \frac{2}{n_d T} \sum_{i=1}^{n_d} |X_i(f,T)|^2 \qquad f > 0 \qquad (4.15)$$

where $X_i(f,T)$ is the FFT of the signal computed over the ith data interval of duration T as defined in Eq. (4.13), and n_d is the number of averages used in the calculation. The segment duration T determines the frequency resolution $\Delta f = 1/T = f_s/N$ for the FFT computation, and is normally chosen based on the characteristics of the type of data being analysed. Figure 4.5 shows the effect of frequency resolution on the calculation of the PSD of a vibration signal recorded in a helicopter.
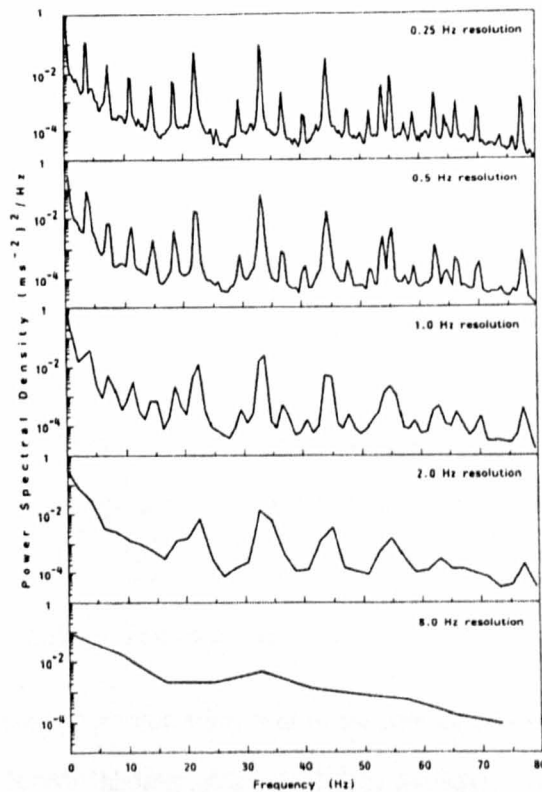
Figure 4.5   Effect of frequency resolution on the power spectral density of a vibration signal (reproduced from Griffin, 1990).

4.5 Time-Frequency Domain Analysis

The averaging process associated with the methods described in the previous sections can lead to a loss of information regarding the transient events present in the signal, and can lead to the smoothing and averaging of time variant characteristics in the signal statistics. An extension of

the classical analysis, which is based on the assumption of the stationarity of the signal, to the analysis of a signal whose characteristics change in time, leads to the definition of time-frequency analysis (Piersol, 1992; Newland, 1994; Mallat, 1998). Time-frequency analysis has proven useful in obtaining information about the signal properties as a function of time (Staszewski, 1998a). The most commonly used forms of time-frequency analysis are the short time Fourier transform (STFT) (Hodges *et al.*, 1985; Gade and Gram-Hansen, 1996; Lim and Witer, 2000), the Wigner-Ville distribution (WVD) (Chiollaz and Favre, 1993; Staszewski et al., 1997; Ren *et al.*, 1999) and the wavelet transform (Li *et al.*, 1999; Lee and White, 2000; Gaberson, 2001). The advantages and drawbacks of these methods are discussed in details in by Gade and Gram-Hansen (1996). In particular, the wavelet transform has the advantage of a linear representation and as such does not suffer from interference terms as in the case of Wigner-Ville distribution, especially for the analysis of multicomponent signals (Feldman, 1995). Also, wavelet based analysis offers the advantage of a multiresolution analysis over the time-frequency plane compared to the STFT and the WVD where the time-frequency resolution remains uniform (Mallat, 1998). Of the various time-frequency analysis methods, this section presents the signal processing techniques which are most suitable for extracting quantitative measures of signal variability.

4.5.1 Short Time Fourier Transform

The most logical first step in considering a time-frequency representation of a signal is to evaluate the FFT over a finite length sliding window and to evaluate how the frequency content of these segments change over time. This is called the short time Fourier transform (STFT), and it is defined as (Newland, 1994):

$$STFT = X(\tau_w, f) = \int_{-\infty}^{+\infty} x(t) w(t - \tau_w) e^{-i2\pi f t} dt \qquad (4.16)$$

where w(t) is a function that divides the signal into segments, called the window function, f is the frequency and τ_w is the position of the window in time. By computing the FFT of the data points within each segment, it is possible to produce a number of localised spectra, each corresponding

to a windowed segment. In engineering applications, it is useful to refer to the energy content of the signal (Lim and Witer, 2000). This is represented by the square of the modulus of the STFT, called the spectrogram (Newland, 1994).

In contrast to the classical Fourier transform which adopts infinite time support sines and cosines as its basis analyzing functions, the STFT adopts a window function that is typically non zero only in the analysed segment and is set to zero outside. The main drawback of the STFT calculation consists in the localization property given by the size of the time-frequency window. The size of the window in the time domain is defined by its duration Δt and in the frequency domain by its bandwidth Δf. The time-frequency resolution is bounded according to the Heisenberg uncertainty principle (Messiah, 1961; Chui, 1992):

$$\Delta t \Delta f \geq \frac{1}{4\pi} \tag{4.17}$$

Therefore, the STFT does not allow a high degree of resolution in both the time and the frequency domains simultaneously. A good frequency resolution (Δf small) can be achieved if a large time window is used. This however produces poor time resolution (Δt large). Conversely, a good time resolution (Δt small) can be achieved if a small time window is used. This however produces a poor frequency resolution (Δf large). Another limitation of the STFT is that all spectral estimates have the same constant bandwidth. Thus, once the size of the analysing window is fixed to suit either the frequency or the time resolution, it remains fixed over the entire time-frequency plane. Figure 4.6 shows an example of problem of time-frequency resolution which occurs with a STFT spectrogram of a synthesized signal consisting of the sum of two sinusoids and an impulse signal. The sum of the two sinusoids consisted of two harmonics of 10 Hz and 50 Hz (Figure 4.6a) defined as the following:

$$y(t) = sin(2\pi 10t) + 5 \, sin(2\pi 50t) \tag{4.18}$$

The power spectral density of the combination of the sum of the two sinusoids and an impulse is shown in Figure 4.6b, while the STFT spectrogram is presented in Figure 4.6c. It is possible to observe from the PSD that the combined signal presents in the frequency domain two main components which have different frequency bandwidth. However, the STFT spectrogram is unable to distinguish the different frequency bandwidth of the two components due to the constant frequency resolution Δf which cannot be made simultaneously appropriate for both the frequency components. In addition, for a fixed frequency resolution in the frequency domain, the time resolution is poor in the time domain being the STFT unable to detect simultaneously the change of the amplitude which is created by the impulse event at about 0.5 s.
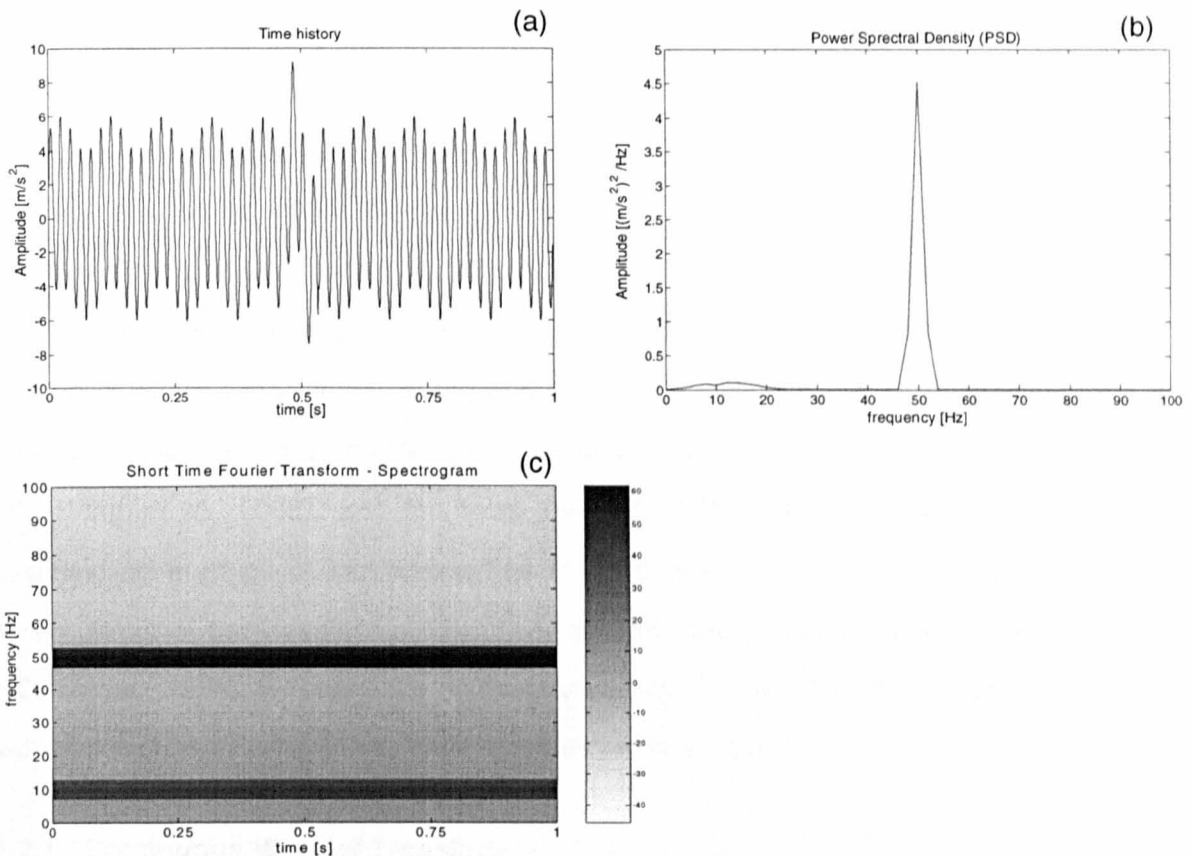
Figure 4.6   STFT calculation for the combination of the sum of two sinusoids consisting of 10 Hz and 50 Hz harmonic components and an impulse signal.

     (a)   acceleration time history.
     (b)   power spectral density.
     (c)   STFT spectrogram.

In order to overcome to the problem of the constant bandwidth analysis of the STFT, an alternative approach is to use a relative frequency resolution (also called a constant-Q analysis) (Chui, 1992) whereby the bandwidth Δf changes with the change of frequency f. In this case what remains constant is the ratio:

$$\frac{\Delta f}{f} = \text{constant}$$
(4.19)

Such analysis leads to the development of the wavelet transform which is the subject of the next section.

4.5.2 Wavelet Transform

The wavelet transform is a useful mathematical tool for the analysis of non-stationary signals, since it performs multi-resolution analysis in both the time and frequency domains (Chui, 1992; Newland, 1994; Mallat, 1998). The wavelet transform has a wide variety of applications such as signal processing, image processing, data compression and pattern recognition (Mallat, 1998). In the field of mechanical signal processing, wavelet analysis has proven useful for performing fault detection of rotating machinery (Wang and McFadden, 1996; Wang *et al.*, 2001; Zheng *et al.*, 2002), for signal feature extraction (Hong *et al.*, 1996; Staszewski, 1998b; Gutter and Kantz, 2001; Peng *et al.*, 2002), and for noise reduction (Pasti *et al.*, 1999; Lin and Qu, 2000). Depending on the type of information that is to be determined from the analysed signal, two different forms of the wavelet transform are defined. The continuous wavelet transform (Chui, 1992; Mallat, 1998) is presented in section 4.5.2.1, while the discrete wavelet transform (Daubechies, 1992; Burrus *et al.*, 1998) is presented in section 4.5.2.3.

4.5.2.1 Continuous Wavelet Transform

The continuous wavelet transform (CWT) is founded on a linear transformation that decomposes an arbitrary signal $x(t)$ of one variable into a superposition of elementary functions of two variables a and b:

$$\psi_{a,b}(t) = \psi^* \left(\frac{t-b}{a} \right)$$ (4.20)

obtained by a process of translating and scaling a basic function $\psi(t)$, called the mother wavelet,

where b is a translation parameter indicating the time locality, and a ($a>0$) is a scale or dilation

parameter indicating the level of resolution of the wavelet. The CWT is defined as (Chui, 1992):

$$W_\psi(a,b) = \frac{1}{\sqrt{a}} \int_{-\infty}^{\infty} x(t) \psi^* \left(\frac{t-b}{a} \right) dt$$ (4.21)

where $W_\psi(a,b)$ are the scaled wavelet coefficients, the factor $1/\sqrt{a}$ is a normalization term to

keep constant the total energy of the scaled wavelets at different scales, and * denotes complex

conjugation. In order to obtain a time-frequency localization the wavelet function $\psi(t)$ needs to be

a function that decays sufficiently fast. A function $\psi(t)$ to be used as the analysing wavelet must

satisfy the admissibility condition (Chui, 1992):

$$C_\psi = \int_{-\infty}^{+\infty} \frac{|F(\omega)^2|}{|\omega|} d\omega < \infty$$ (4.22)

where $F(\omega)$ is the Fourier transform of $\psi(t)$. Eq. (4.22) requires the analysing function $\psi(t)$ to

have finite energy, and guarantees that the signal $x(t)$ can be recovered from its wavelet

transform decomposition.

With reference to the family of the scaled wavelets $\psi\left(\frac{t-b}{a} \right)$, the wavelet transform can be

interpreted as a decomposition of the signal into a set of localized window filters centred on the

frequency f_x of the signal. The local resolution of the wavelet transform in time and frequency

domain depends on the scale factor a, since it controls the width of the wavelet. The multi-

resolution property is determined by the duration and bandwidth of the analyzing functions, given

by:

$$\Delta t = a\,\Delta t_\psi\,, \qquad\qquad \Delta f = \frac{\Delta f_\psi}{a} \qquad\qquad (4.23)$$

where Δt_ψ and Δf_ψ are the duration and bandwidth of the basic wavelet function, respectively. By using all of the scales, the full frequency range of interest can be covered. In particular, from Eq. (4.23) it can be seen that using a large scale value a, which corresponds to a dilated version of the base wavelet, permits a fine frequency domain resolution (Δf smaller), especially at low frequencies where a wide time window (Δt larger) is needed to capture the complete signal information. Use of a small scale value a, which corresponds to a compressed version of the base wavelet, permits a fine time domain resolution (Δt smaller) at high frequencies where a narrow time window is needed to permit the high frequency components to be revealed. These situations are illustrated in Figure 4.7b.
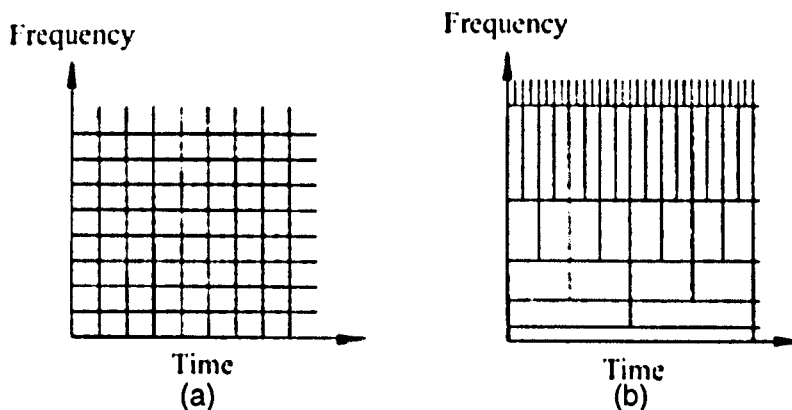
Figure 4.7   Time-frequency resolution grid.

(a) short time Fourier transform: a square box indicates constant resolution.
(b) wavelet transform: a rectangular box indicates multiresolution.

In contrast to the STFT, where the time-frequency resolution is uniform (see Figure 4.7a), the length of the analyzing wavelet changes both in time and in frequency. In contrast to Fourier analysis which has an infinite domain of definition, the wavelet basis functions have finite domains allowing a better identification of non-stationary characteristics (Chui, 1992; Newland, 1994).

A number of different real or complex-valued wavelet functions can be used to compute the wavelet transform (Chui, 1992). In order to measure the time evolution of the frequency content of a signal, a complex-valued wavelet function which can separate the amplitude and phase information is required. In engineering applications, a so called progressive wavelet function is often used (Delprat *et al.*, 1992; Staszewski and Tomlinson, 1994). It is defined as a function that is complex-valued, satisfies the admissibility condition (Eq. 4.22), and does not have any negative frequencies, as in practice only positive frequency components are meaningful. One of the analyzing wavelet functions that is most frequently used for signal feature extraction is the Morlet wavelet (Staszewski and Tomlinson, 1994; Li *et al.*, 1999; Lee and White, 2000; Lin and Qu, 2000; Rubini and Meneghetti, 2001; Wang *et al.*, 2001; Zheng *et al.*, 2002) which is defined as the product of a complex exponential wave and a Gaussian envelope (Chui, 1992):

$$\psi(t) = e^{i2\pi f_0 t} \cdot e^{-t^2/2} \qquad\qquad (4.24)$$

where f_0 is the frequency of oscillation inside the modulated envelope, and t is the time. The frequency f_0 is also called the center frequency of the base wavelet function. Figure 4.8 presents an example of the Morlet wavelet function in both the time and frequency domains for different values of the scale factor a and for $\omega_0 = 2\pi f_0 = 15\,\text{rad/s}$, which correspond to fifteen oscillations inside the Gaussian envelope. In Figure 4.8 is represented only the real part of the complex-valued Morlet function for simplicity. It can be seen that the base Morlet function ($a = 1.0$) is scaled in time and amplitude so as to have a fixed number of oscillations inside the envelope. It can also been seen that the value of the scale factor a balances the time-frequency resolution of the wavelet function: as the scale value increases the wavelet is wider in time, and both the center frequency f_c and the frequency bandwidth of the scaled wavelet decrease, leading to a better frequency resolution at low frequencies.

CWT results are often presented graphically in the time-scale plane (Chui, 1992; Mallat, 1998; Staszewski, 1998a). In order to compare wavelet data with power spectra or with the results of

time-frequency analysis, a conversion from scale to frequency can be performed using the relationship (Abry, 1997):

$$a = \frac{f_s \cdot f_0}{f_x} \tag{4.25}$$

where f_x is the frequency of the signal at which the scaled wavelet is focused, and f_s is the sampling frequency of the signal.
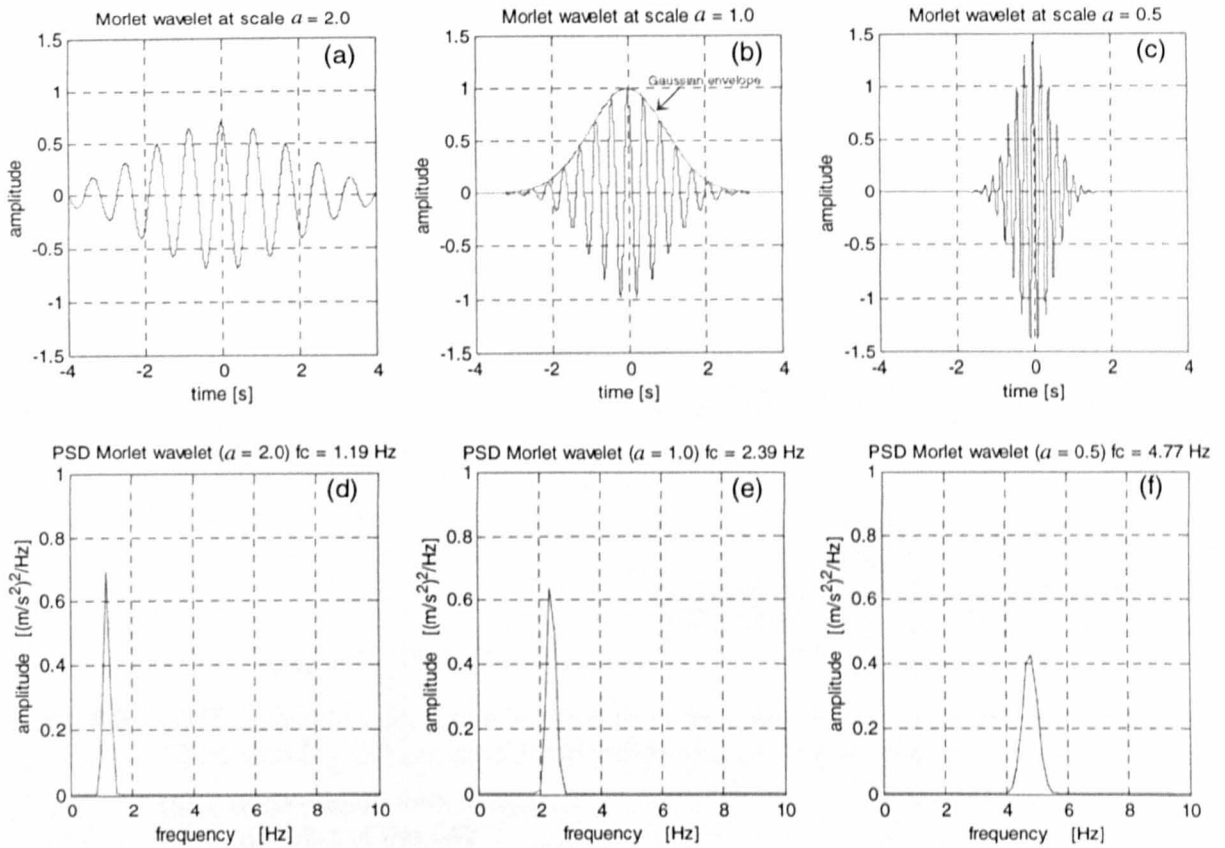
Figure 4.8   Example of scaled Morlet wavelets ($\omega_0 = 15$ rad/s) in the time and the frequency domain for different scale values a.

(a), (b), (c) time domain representation for scale values a =2.0, a =1.0, a =0.5, respectively.
(d), (e), (f) frequency domain representation for scale values a =2.0, a =1.0, a =0.5, respectively.

Figure 4.9 presents an example of a CWT computed using the Morlet function as the analyzing wavelet with a value of center frequency ω_0 =15 rad/s. Figure 4.9b presents the modulus of the CWT of the signal consisting of the sum of two sinusoids of 10 Hz and 50 Hz and an impulse

(shown in Figure 4.9a) used for the computation of the spectrogram of the STFT. In contrast to the STFT where the frequency resolution remains constant for all the frequency components present in the signal (see Figure 4.6c), the CWT allows the energy of the signal to be distributed at different resolutions along the frequency axis providing a better frequency resolution at the low frequencies. This is shown in Figure 4.9b where the strong 50 Hz carrier frequency produces a darker band along the time axis, whereas the low frequency of 10 Hz sine component is separated by the component at about 15 Hz, which is due to the presence of the impulse. In addition, the CWT provides simultaneous local information of the signal temporal variation. Thus, the CWT avoids the limitation of the STFT which provides, instead, poor time resolution when a good frequency resolution is produced. The presence of the impulse is indicated in the CWT map by the increase of the modulus around the point where the impulse exists, at about 0.5 s.
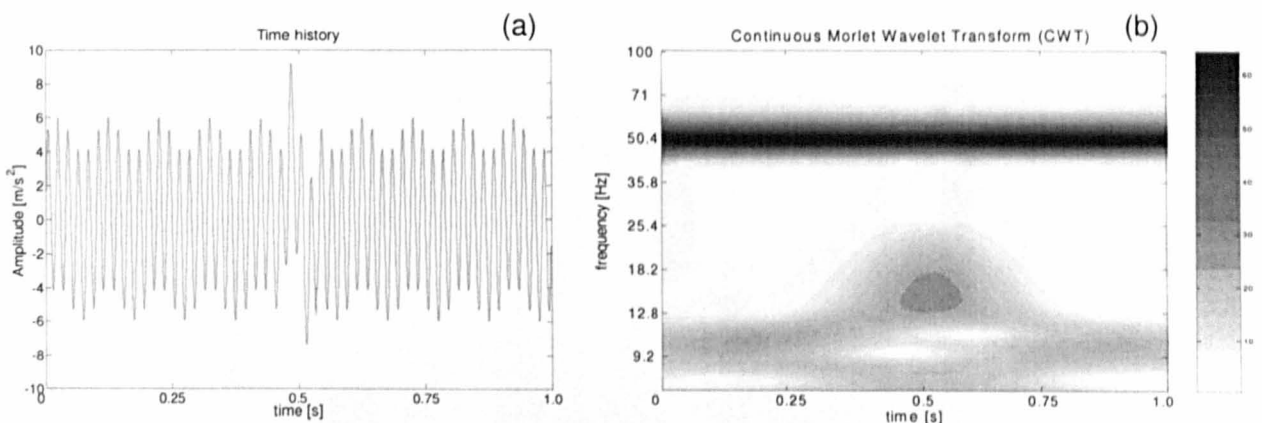
Figure 4.9 CWT calculation for the combination of the sum of two sinusoids consisting of 10 Hz and 50 Hz harmonic components and an impulse signal.

(a)   acceleration time history.
(b)   modulus of the CWT.

The CWT has proven useful for performing feature extraction (Dalpiaz and Rivola, 1997; Staszewski, 1998a; Lin and Qu, 2000; Gutter and Kantz, 2001; Peng et al., 2002). Figure 4.10 presents an example of the CWT of the acceleration vibration signal measured for a casing which embodies a cam mechanism for reciprocal translation motion (Dalpiaz and Rivola, 1997). The two transient events occurring in the acceleration time history (Figure 4.10a) are clearly localized in time in the CWT map (Figure 4.10b). Here a variation in the amplitude appears as an alternating

intensity from white to black areas in the CWT map. In order to detect the changes in the amplitude of the casing vibration, a cross-section of the CWT was extracted relative to the frequency of interest of 690 Hz. This frequency is presented as a dashed line in Figure 4.10b. The amplitude variations obtained from the cross section are shown in Figure 4.10c. The extraction of the cross-section clearly highlights the transient phenomena occurring at specific times. However, the use of the extraction of the cross section at a particular frequency does not allow tracking of the instantaneous frequency variation of the frequency of interest. In this case, the so-called ridge and skeleton of the CWT are used as explained in the next section.
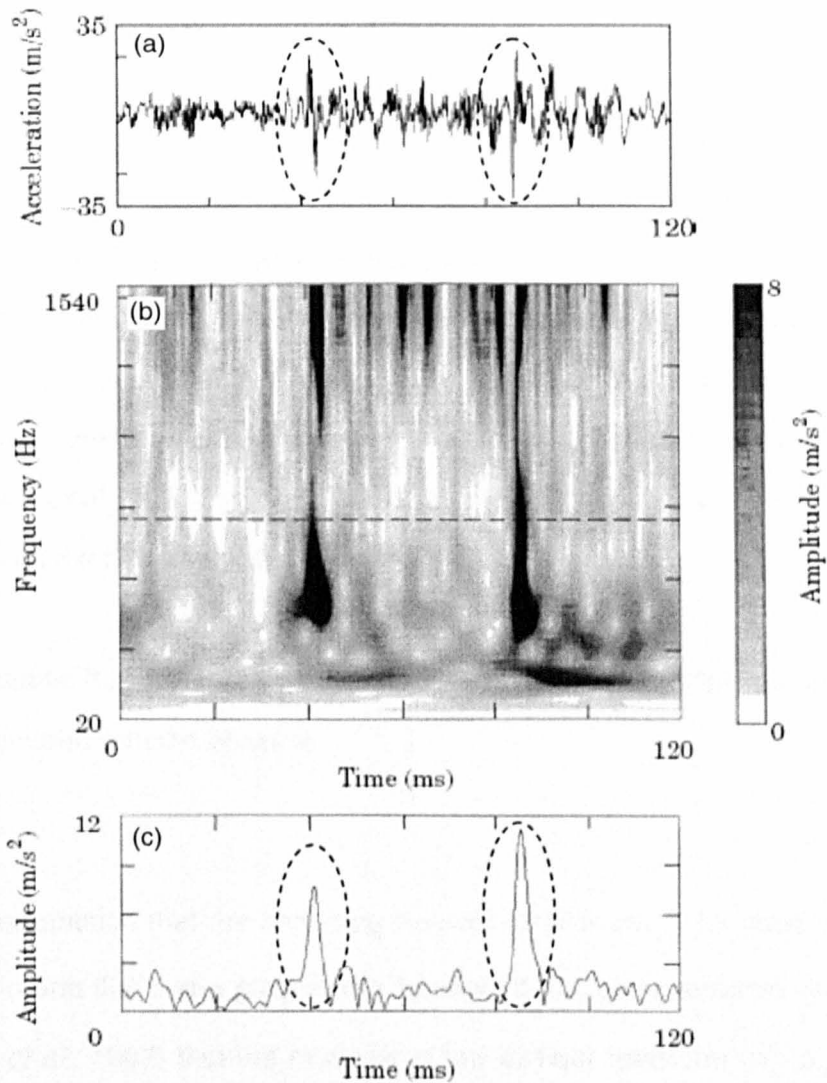
Figure 4.10 Application of the CWT of the acceleration vibration signal measured for a casing embodying a cam mechanism for reciprocal translation motion (reproduced from Dalpiaz and Rivola, 1997).

(a)   original vibration time history.
(b)   modulus of the CWT.
(c)   Cross-section of the CWT extracted at the frequency of 690 Hz.

4.5.2.2 Extraction of the CWT ridge and the skeleton

The extraction and quantification of the instantaneous signal features has proven useful in many engineering applications such as in system identification procedures (Carmona *et al.*, 1997; Staszewski, 1998a; Bellizzi *et al.*, 2001) sonar detection (Bertrand and Bertrand, 1985) and speech processing (McAulay and Quatieri, 1986). Many algorithms have been proposed which allow the extraction of the instantaneous characteristics of the signal such as the Hilbert transform based envelopes and instantaneous frequencies (Feldman, 1994a, b, 1995) and the extraction of the ridge of the CWT (Delprat *et al.*, 1992; Carmona *et al.*, 1997). However, the Hilbert transform based procedures do not provide effective results for multicomponent signals, and bandpass filtering pre-processing are also required (Feldman, 1995). This can produce difficulty in the interpretation of the results and even failure if the system vibration modes are close in frequency. On the other hand, the wavelet-based algorithms altogether are based on the calculation of the modulus or phase of the CWT. The most common and simple approach uses the localization properties of the modulus of the CWT (Carmona et al., 1997). The methods based on the phase of the CWT, instead, are often difficult to interpret, especially in the presence of noise (Delprat *et al.*, 1992; Carmona *et al.*, 1997). In this section, the algorithm based on the modulus of the CWT is therefore presented for its simplicity of application.

Under the assumption that the analysed signal x(t) is asymptotic, i.e. that the signal amplitude, A, varies slowly compared with the phase ϕ:

$$\left|\frac{d\phi}{dt}\right| >> \left|\frac{1}{A}\frac{dA}{dt}\right| \tag{4.26}$$

and under the assumption that the analysing wavelet function $\psi(t)$ has good localization in the frequency domain and that it is a progressive function, it has been demonstrated (Delprat *et al.*, 1992; Carmona *et al.*, 1997) that the modulus of the wavelet transform $\left|W_\psi(a_0,b)\right|$ on the time-frequency plane is mainly concentrated around the so-called "ridge" of the wavelet transform. By definition (Delprat *et al.*, 1992; Carmona *et al.*, 1997), the ridge of the CWT provides the

frequency values along which the modulus of the wavelet coefficients reach their maximum. Mathematically, the term local maxima is used to describe any point (a_0, b_0) in the time-scale plane such that the modulus of the wavelet coefficient $|W_\psi(a_0, b)|$ is locally maximum at the point $b = b_0$ (Mallat, 1998):

$$max|W_\psi(a,b)|\Big|_{b=b_0} = max|W_\psi(a,b_0)| = |W_\psi(a_0,b_0)| \qquad (4.27)$$

The curve $a = r(b)$ in the time-scale plane (a,b) along which all points (a_0, b_0) are modulus maxima is called ridge of the wavelet transform. Assuming a progressive complex-valued analyzing wavelet function, and assuming that its Fourier transform is maximum at its center wavelet frequency ω_0, It has been demonstrated (Delprat et al., 1992; Carmona et al., 1997) that the curve $a = r(b)$ is related to the instantaneous frequency of the signal by the formula:

$$r(b) = \frac{\omega_0}{\phi'(b)} \qquad (4.28)$$

where $\phi'(b)$ is the rate of change of the phase $\phi(t)$ of a signal which has the instantaneous frequency:

$$v_j = \frac{1}{2\pi}\frac{d\phi(t)}{dt} = \frac{1}{2\pi}\phi'(t) \qquad (4.29)$$

The ridge therefore provides a powerful method to visualize the instantaneous frequency variation of a signal. The values of the coefficients restricted to the ridge form the "skeleton" of the wavelet transform, which gives the distribution along the time-axis of the magnitude of the wavelet coefficients (Carmona et al., 1997; Staszewski, 1998a; Bellizzi et al., 2001). The instantaneous envelope representing the local maxima amplitude variation is provided by the modulus of the skeleton. In this way, it is possible to obtain the instantaneous amplitude variation of the signal.

Figure 4.11 presents an example of the extraction of the ridge and skeleton from the CWT of a simulated impulse response from a single degree-of-freedom (SDOF) system with cubic stiffness non-linearities (Staszewski, 1998a). In this study the extraction of the envelope was used to estimate the damping present in the system. The impulse response of the system is illustrated in Figure 4.11a. The CWT was calculated using a Morlet wavelet function. The CWT of the transient response is illustrated in Figure 4.11b in the form of a modulus contour plot. The decaying nature of the impulse response can be seen in the amplitude of the envelope characteristic with the highest peak at about 10 s as shown in Figure 4.11c. Figure 4.11d presents, instead, the ridge of the CWT representing the instantaneous frequency of the system. Figure 4.11d also shows that the results are effected by small disturbances which are obtained only at both ends of the instantaneous frequency.
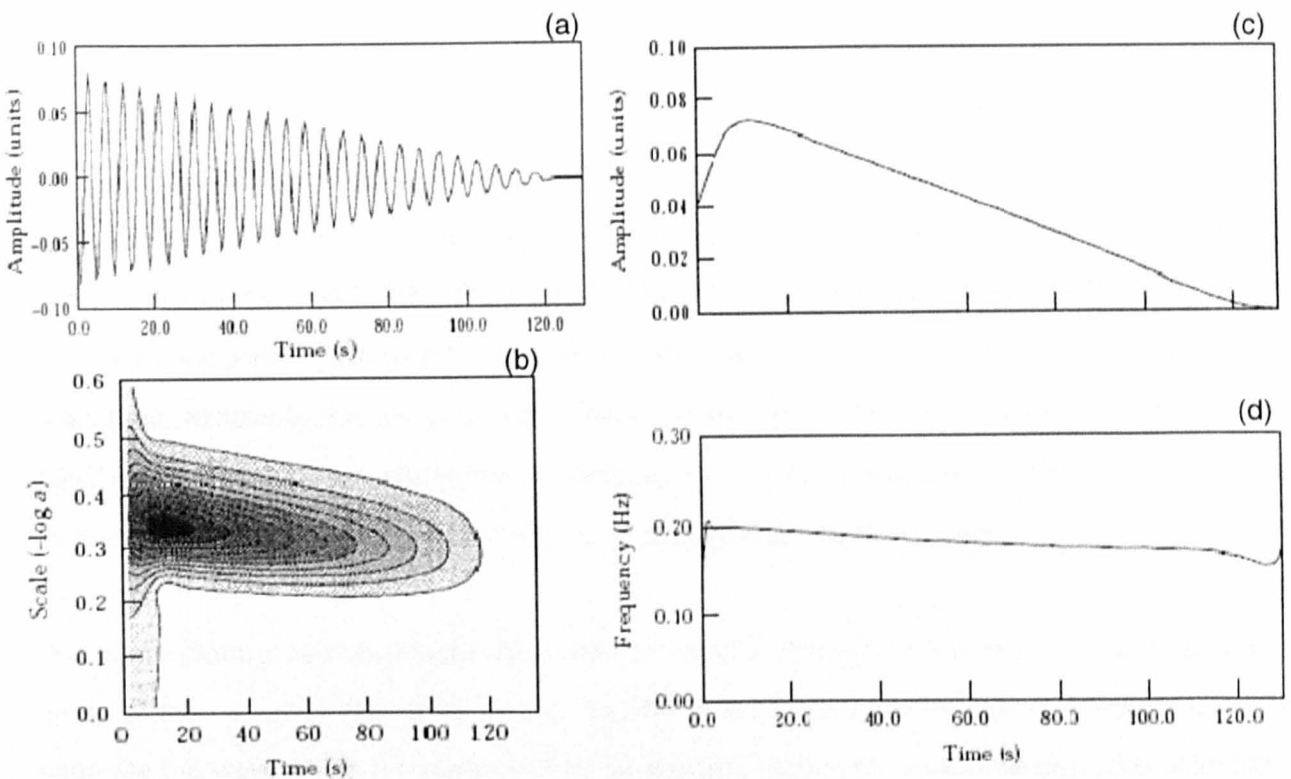
Figure 4.11   Ridge and skeleton of the CWT obtained for a simulated impulse response from a single degree-of-freedom (SDOF) non-linear system (reproduced from Staszewski, 1998).

    (a)   Impulse response function from the SDOF non-linear system.
    (b)   Amplitude of the continuous wavelet transform of the impulse response function.
    (c)   Instantaneous envelope.
    (d)   Instantaneous frequency.

4.5.2.3 Discrete Wavelet Transform

Time-frequency CWT analysis can be confined to a discrete set of translation and scale parameters such as the dyadic framework $a_j = 2^j$ and $b_{j,k} = k/2^j$. A function $\psi(t)$ is called an orthogonal wavelet if the function

$$\psi_{j,k}(t) = 2^{j/2}\psi(2^j t - k), \qquad \text{with } j = 1,2,...J \qquad (j,k \in Z) \qquad (4.30)$$

forms an orthonormal basis (Daubechies, 1992), where J denotes the number of levels j of the wavelet decomposition and k represent the number of wavelet coefficients. The orthogonal wavelet transform (OWT) then becomes:

$$x_k^j = \int_{-\infty}^{\infty} x(t)\psi_{j,k}(t)dt \qquad (4.31)$$

In contrast to the CWT (Mallat, 1998), the orthogonality of the OWT avoids redundancies in the analysis (Daubechies, 1992). Orthogonality ensures mutual independence between the wavelet coefficients. A number of wavelet functions satisfy the admissibility conditions for orthogonal analysis (Newland, 1994). The Daubechies wavelet functions (Daubechies, 1992), also called compactly-supported orthonormal wavelets, have been shown to provide good analyzing properties, especially for the purpose of data compression and feature selection (Staszewski, 1998b), statistical patter recognition (Hong et al., 1996), irregularity detection (Wang and McFadden, 1995; Smallwood, 1998) and noise reduction (Pasti et al., 1999).

The nomenclature used for Daubechies wavelets is DN, where N is a scalar value indicating the order of the wavelet. The order of the wavelet indicates the number of coefficients used to generate the wavelet. As the number of its coefficients increases, a wavelet becomes smoother, meaning more differentiable (Newland, 1994). Generally, different wavelet families make different trade-offs between how compactly the basis functions are localized in space and how smooth they are (Newland, 1994; Staszewski, 1998b). More compactly supported, and less smooth, wavelets are normally adopted for the analysis of non-stationary data with discontinuities and

transient events (Staszewski, 1998b). This is the case of the lower order Daubechies D4 wavelet. Less compactly supported and smoother wavelets are better for the analysis of stationary and periodic data presenting a more regular pattern. This is the case of the higher order Daubechies D20 wavelet.

The advantage of using an OWT consists of decomposing the analysed signal into different frequency bands. Each level j of the decomposition is obtained by convolving the signal with low-pass and high-pass filters, and down-sampling based on powers of two. The Mallat algorithm (Mallat, 1998) implements this decomposition scheme using filters. The outputs of the high-pass filter are called the "detail coefficients" $cD_{j,k}$, while the outputs of the low-pass filter are called the "approximation coefficients" $cA_{j,k}$. Given the sampling frequency f_s at each level j, the detail and approximation coefficients lie within a frequency band given by:

$$cD_{j,k} \qquad \left[2^{-(j+1)} f_s, 2^{-j} f_s \right] \qquad\qquad (4.32)$$

$$cA_{j,k} \qquad \left[0, 2^{-(j+1)} f_s \right] \qquad\qquad (4.33)$$

The decomposition process is iterated with successive approximation components being decomposed in turn, while the details are saved each time. The detail coefficients represent the high-frequency components that contain the finest information of the signal at the first-levels of the decomposition iteration. The approximation coefficients, on the other hand, represent the low-frequency components that contain the coarsest information of the signal at the last level of the decomposition. The decomposition process is iterated until the individual approximation components consist of a single sample. The number of decomposition levels is bounded by the length of the analysed signal (Newland, 1994). When the number of data points in the analysed signal is $N=2^J$, the algorithm allows a maximum of J+1 levels of decomposition. An example of a 3-order level wavelet decomposition consisting of J+1 = 4 wavelet levels is presented in Figure 4.12.
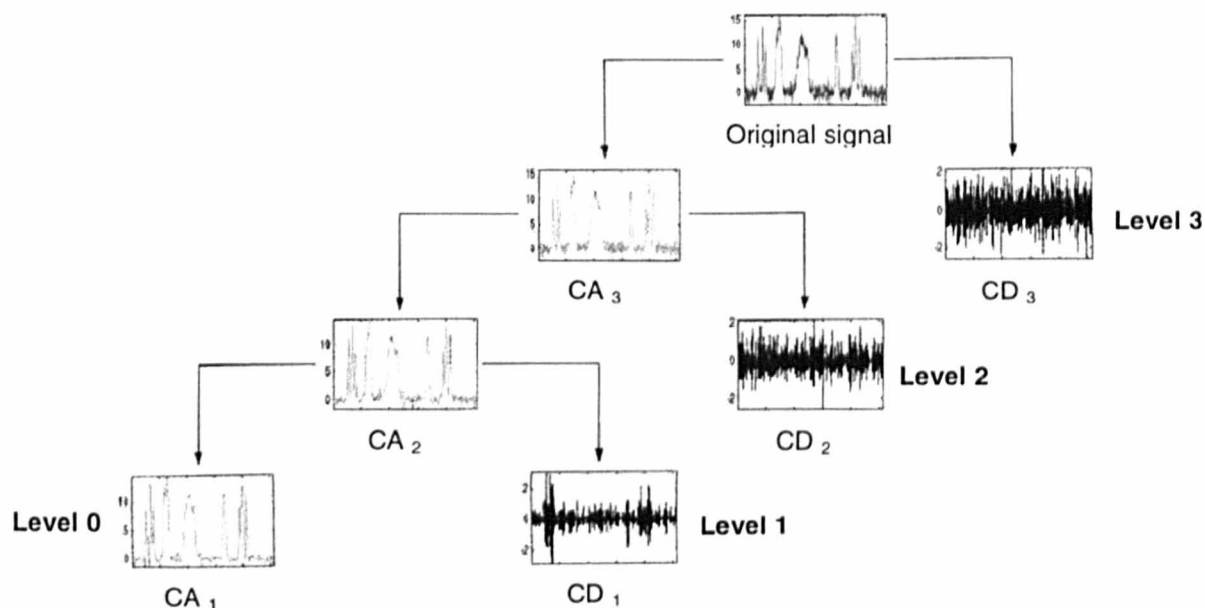
Figure 4.12 Example of a 3-order level discrete wavelet decomposition tree consisting of 4 wavelet levels (adapted from Mathworks Inc, Version 6, September, 2000).

The details coefficients obtained for a level j can be recombined to reconstruct the time domain signal belonging to the specific frequency band (Newland, 1994; Mallat, 1998). The objective of such a process is to identify a frequency band, or level j, where the salient characteristics of the analysed signal appear more evident and clear than in the original time history. The orthogonal property of the OWT ensures that any detail signals can be analysed independently by means of an appropriate choice of wavelet level. Once the detail signal levels of interest are identified, it is possible to perform a local analysis on each to extract the signal features of interest.

In the case of the discrete orthogonal transform, the results normally consist of a set of signal features which are extracted from each frequency band of the signal rather than a map of the magnitude or phase of the wavelet coefficients as used with the CWT (Mallat, 1998). This is because the discrete number of scales (or levels j) used in the computation of the OWT are limited by the value of the sampling rate of the signal ($J=\log_2 N$). Frequency resolution is therefore insufficient for fine analysis.

Figure 4.13 presents an example of the OWT decomposition of the vibration signal measured for an automotive gearbox with a wheel rotational frequency of 37.5 Hz, and a meshing vibration frequency of 600 Hz (Staszewski, 1998b). The OWT analysis was applied to $N=2^8=256$ samples, producing thus $J = 8$ levels. Figure 4.13a presents the reconstruction in the time domain of the detail components for each level j, whereas Figure 4.13b presents the wavelet details in the frequency domain. The upper window of Figures 4.13a and 4.13b shows the original data used for the decomposition. In particular, the meshing frequency H_1 (600 Hz) and its harmonics H_2 (1200 Hz), H_3 (1800 Hz), H_4 (2400 Hz), and H_5 (3000 Hz) are seen dominate the original PSD (Figure 4.12b). By using an eight level wavelet decomposition, it was possible to observe that the harmonic H_2 was dominant on level 7, while the meshing frequency H_1 was dominant on level 6.
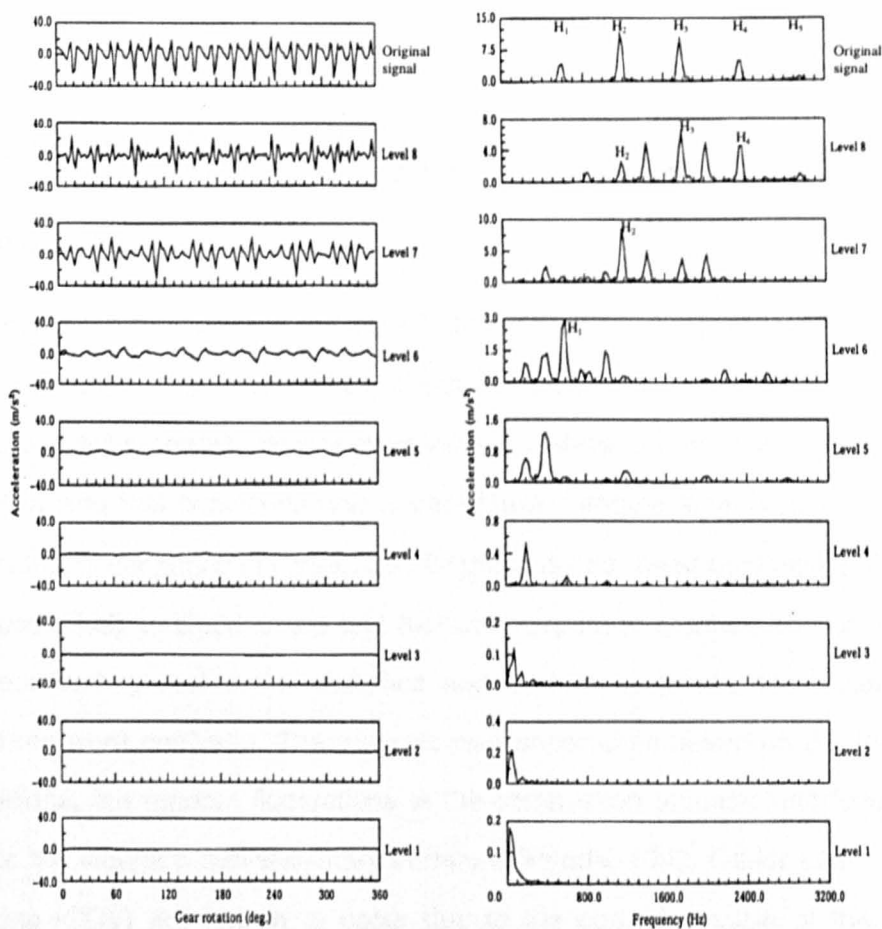
Figure 4.13   Orthogonal wavelet decomposition of the vibration signal measured for an automotive gearbox (reproduced from Staszewski, 1998b).

(a)   reconstruction of the wavelet detail components in time domain.
(b)   power spectra densities of the wavelet detail components.

Chapter 5

An Examination of Diesel Idle Vibration

5.1 Introduction

This chapter investigates the nature of the idle vibration emission of representative diesel-engined automobiles. In particular, the experimental measurements and the signal analysis described here were used to quantify the typical statistical variation which occurs in the diesel idle vibration signature under varying fuel conditions and under different engine technologies. The reason for analysing the statistical variations in diesel idle vibration was the need to identify salient statistical properties that could help to discriminate one fuel with respect to another, and between different types of engines. Both global signal statistics and cycle-to-cycle statistical variations in the vibration signatures were analysed. The analysis was undertaken based on the knowledge that under idle conditions, the random fluctuations of the combustion process introduce time-varying forces that make the vibration non-stationary in nature (Priede, 1992; Ozdor *et al.*, 1994). Cycle-to-cycle variations (CCV) are known to occur due to the operating cycle of the engine when combustion takes place (Ball *et al.*, 1998; Randall, 2001; Liu *et al.*, 2002). Different fuel content, or a different engine technology, can affect this variability (Ando and Motomochi, 1987;

Kouremenos *et al.*, 1996; Satgé de Caro *et al.*, 2001; Lee *et al.*, 2004). One of the resultant effects of the random variation in the combustion process is the cycle-to-cycle variation (CCV) in the cylinder pressure rate (Pischinger et al., 1979; Ozdor *et al.*, 1994). The effect of combustion process CCV on engine power output, fuel consumption and pollution has traditionally been quantified by measuring the cyclic variability of the pressure data. One such measure which is frequently reported in the literature is the coefficient of variation in the indicated mean effective pressure (IMEP) (Matekunas, 1983; Heywood, 1988). The IMEP is defined as:

$$COV_{IMEP} = \left(\frac{\sigma_{IMEP}}{\mu_{IMEP}} \right) \cdot 100 \, [\%] \qquad\qquad (5.1)$$

where the IMEP is defined as the theoretical constant pressure which must be exerted to produce the same total power during the power stroke of the engine, σ_{IMEP} is the standard deviation in IMEP pressure and μ_{IMEP} is the mean IMEP. When the coefficient of variation COV_{IMEP} exceeds 10 percent (Heywood, 1988), engine performance is normally degraded, and tends to generate complaints of a "rough" idle vibration from drivers (Hoard and Rehagen, 1997).

Similar to the pressure-based metrics of the cyclic variability, the work presented in this chapter aimed to define a set of coefficients of variation which quantify the change in the vibration statistics that is caused by the changes of fuel type and engine technology. The objective of the analysis presented in this chapter was to describe the statistical variation of the vibration signals, so as to identify objective signal parameters which could be used as vibration stimuli descriptors for quantifying the human subjective response to the steering wheel idle vibration. The main objectives of the analysis were:

- to measure the engine idle vibration signature of diesel-engined automobiles under various fuel conditions;
- to measure the steering wheel idle vibration signature of diesel-engined automobiles under various fuel conditions;
- to identify how much the steering wheel vibration signature was related to the engine idle vibration signature;

- to quantify the percentage variation of the global and cycle-to-cycle signal statistics of the engine and the steering wheel vibration when changing from one fuel to another.

In order to achieve these objectives, the analysis of the diesel idle vibration was conducted as described in the flowchart of Figure 5.1.
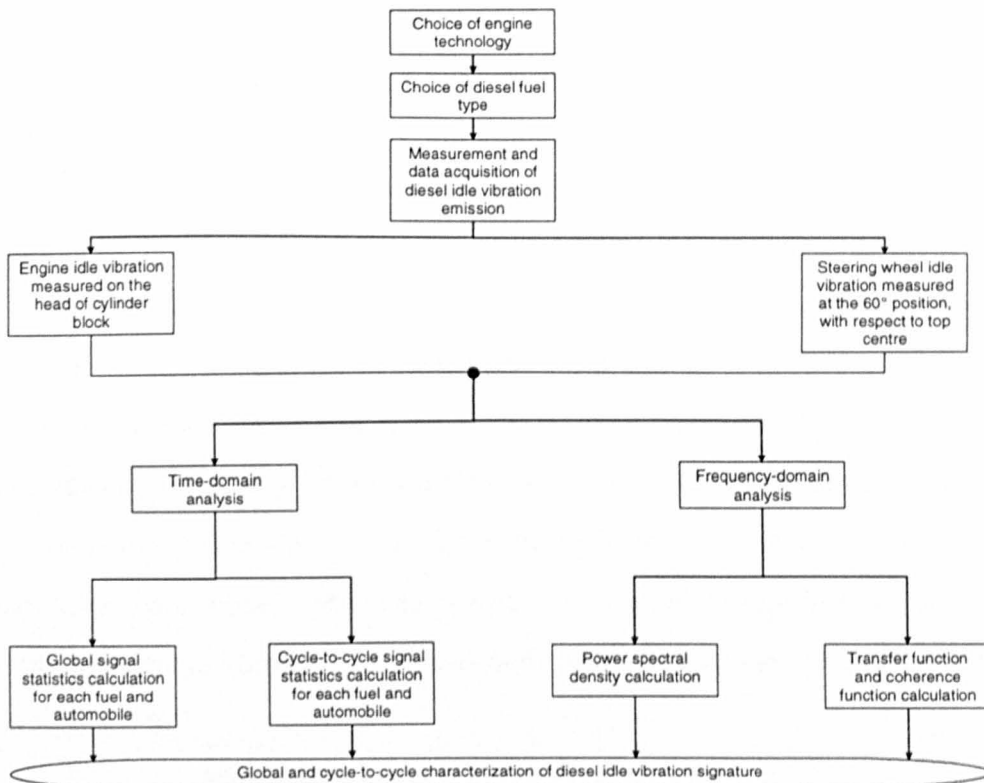
Figure 5.1   Flowchart describing the analysis of diesel idle vibration conducted in Chapter 5.

5.2   Experimental Idle Vibration Tests

5.2.1 Choice of Diesel Fuel Properties

The most important fuel properties influencing the combustion process are the fuel ignition quality, volatility, viscosity and density (Owen and Coley, 1995). The effect of fuel properties on engine performance will be discussed in the following sections.

5.2.1.1 Fuel Cetane Number

Among the chemical properties of a diesel fuel that can affect engine performance, the cetane number (C.N.) value is generally recognized as the most important predictor of combustion quality (Owen and Coley, 1995). The cetane number represents a measure of the tendency of the fuel to ignite spontaneously in the combustion chamber. A fuel with a high cetane number (C.N. > 50) presents higher ignition quality due to a shorter ignition delay period, which is the time between the beginning of ignition and the appearance of the pressure rise inside the cylinder (Heywood, 1988). On the other hand, a low cetane number fuel presents a long ignition delay which leads to an accumulation of fuel prior to ignition, causing a rapid pressure rise and very high peak pressures once combustion takes place. Thus, for a lower cetane number, the combustion process is characterised by higher heat release and faster pressure rise times, producing rougher engine operation. Typical C.N. values required by national standards and by fuel quality guide specifications (Owen and Coley, 1995) are from 40 to 59. A typical cetane number value for a commercial diesel fuel is reported to be 49. In the research presented in this thesis, a set of twelve diesel fuels were tested under idle conditions. In order to represent diesel fuels having different combustion characteristics, the cetane number of the test fuels ranged from 27.1 to 77.0 as shown in Figure 5.2.
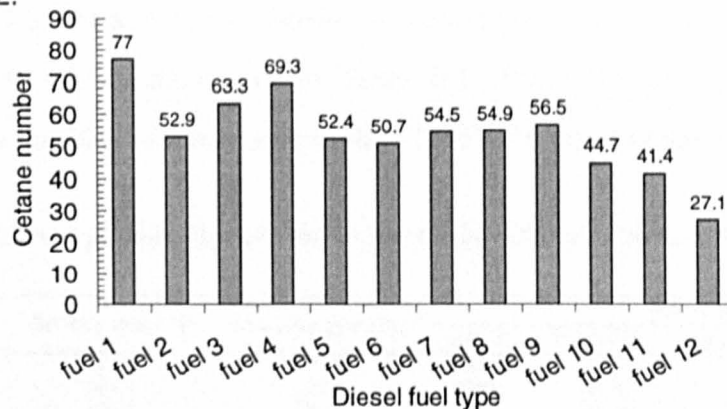
Figure 5.2   Cetane numbers of the test fuels.

5.2.1.2 Fuel Volatility

The physical property of diesel fuel volatility (Owen and Coley, 1995) refers to its evaporation characteristics, expressed in terms of the temperature at which successive portions are distilled

from a sample of fuel under controlled heating in a standardized apparatus. The distillation curve for a particular fuel is defined by the temperatures at which various amounts of fuel are distilled. Standard measures (ASTM-D-86-96, 1996) of volatility recorded during the distillation process are the initial boiling point (IBP), the final boiling point (FBP) and the percent of condensate recovered. A low temperature at IBP reflects the ease with which the fuel will start to vaporize, while the FBP gives an indication of the extent to which complete vaporization of the fuel may be expected in the combustion chamber. Diesel fuel specifications within the European Union (BS EN 590, 1997) require that diesel fuels must have at least 85% recovery at 350 °C, and a maximum of 65% recovery at 250 °C, with a minimum IBP temperature of 180 °C.

In terms of engine performance, lowering the temperature at the IBP, and thus increasing the volatility, often raises the vapor pressure, which can lead to vapor lock in the fuel injection system (Hills and Schleyerbach, 1977). On the other hand, a fuel with a high boiling point tends not to burn completely, which results in an increase of carbonaceous fuel deposits on injector tips. For cold weather starts and smooth cold weather idle, a low boiling point temperature (T50%) of 245 °C is usually recommended (Owen and Coley, 1995).

For the fuels used in the research of this thesis, the percent of condensate recovered at 250 °C ranged from 20.5% to 73.5% as shown in Table 5.1. Table 5.1 also presents the initial temperature (IBP) and the 50% recovery temperature (T50%) for each of the test fuels.

Table 5.1 Chemical and physical properties of the twelve Diesel fuels tested in the research.

Fuel	Cetane Number	Density (kg/m3)*	Viscosity (mm2/s)**	Volatility		
				IBP °C	T50% [°C]	Recovery at 250 °C [Vol %]
1	77.0	773.1	——	188.0	273.5	35.5
2	52.9	824.1	2.27	176.0	250.0	50.0
3	63.3	826.9	3.19	188.0	286.4	22.5
4	69.3	811.4	2.94	183.5	280.2	29.0
5	52.4	837.3	2.93	178.0	268.5	39.0
6	50.7	837.3	3.40	188.5	285.0	25.5
7	54.5	830.1	2.72	169.5	274.5	33.5
8	54.9	817.7	1.95	179.0	229.4	73.5
9	56.5	837.6	3.33	194.0	284.6	26.5
10	44.7	847.4	2.22	154.5	238.5	57.5
11	41.4	836.1	1.93	153.0	235.0	61.0
12	27.1	915.3	——	193.0	289.0	20.5

* Density at 15 °C   IBP = initial boiling point
** Kinematic viscosity at 40 °C   T50% = 50% recovery temperature
** —— data not available

From Table 5.1, it can be seen that fuel 8 was characterized by the lowest boiling point temperature T50% value, which indicated the lowest distillation curve, and was thus the fuel with the highest volatility. Fuel 12, on the other hand, was characterized by the highest boiling point temperature T50% value, which indicated the highest distillation curve, and thus represented the fuel with the lowest volatility.

5.2.1.3 Fuel Viscosity

Fuel viscosity is defined as the resistance of the fuel to flow (Owen and Coley, 1995). It is usually expressed in terms of kinematic viscosity, measured in centistokes (cSt) mm^2/s. Viscosity is related to the performance of the fuel injection equipment, particularly at low temperatures where an increase in viscosity leads to a smaller quantity of injected fuel. On the other hand, a low viscosity fuel can produce leakage from the pumping elements, reducing the volume of fuel delivered, particularly at low speeds (Grigg *et al.*, 1986). National specifications for automotive diesel fuel (BS EN 590, 1997) impose an upper limit on viscosity to ensure that the fuel will flow readily during cold starting, and a minimum limit to avoid the possibility of power loss at high temperatures. Typical viscosity values required by the BS EN 590 standard are a maximum level of $5.0 \ mm^2/s$ at 40 °C for the cold start region, and a lower limit of $2.5 \ mm^2/s$ at 40 °C to minimize the risk of hot restart problems. The viscosity level of the twelve test fuels used during the course of the research described in this thesis ranged from 1.93 to $3.40 \ mm^2/s$ at 40 °C in order to represent typical fuel conditions (see Table 5.1).

5.2.1.4 Fuel Density

Fuel density is defined as the mass per unit volume, and it is expressed in kilograms per cubic meter (kg/m^3). The importance of fuel density is primarily related to the heating value of the fuel, and thus to the energy available to generate power. Fuel density properties do not feature in all technical specifications (Owen and Coley, 1995), however since fuel injection equipment operates on a volume metering system, a change in density will influence engine output due to the different

mass of fuel injected. A higher density fuel tends to produce more engine power and less fuel consumption (Heinze, 1986). Typical density limits for the European market (BS EN 590, 1997) are between a minimum of 820 and a maximum of 860 kg/m³. The fuel density values of the twelve test fuels used in this research ranged from 773.1 to 915.3 kg/m³ in order to represent typical fuel conditions (see Table 5.1).

5.2.1.5 Relation between Chemical and Physical Fuel Properties

For partially or fully warmed-up engines, research has shown that the physical characteristics of diesel fuel do not significantly affect the ignition delay (Wong and Steere, 1982). For cetane numbers, ranging from 38 to 53, tests running fuels of different IBP volatility have shown no discernible differences in the ignition delay period. Therefore, in a warmed-up engine, variations in fuel atomization, spray penetration and vaporization rate are small over a wide range of cetane number values. In the case of cold starting performance, research (Cole et al., 1986) has shown that increasing the cetane number by means of additives provides benefits in terms of the amount of time required to achieve a stable idle condition. Figure 5.3 presents the effect of diesel fuel additives on the time to reach stable idle for fuels with different initial cetane number and different viscosity and volatility properties. As shown in Figure 5.3, the time to stable idle decreases more quickly with the cetane number than with changes in the other physical properties of the fuel.
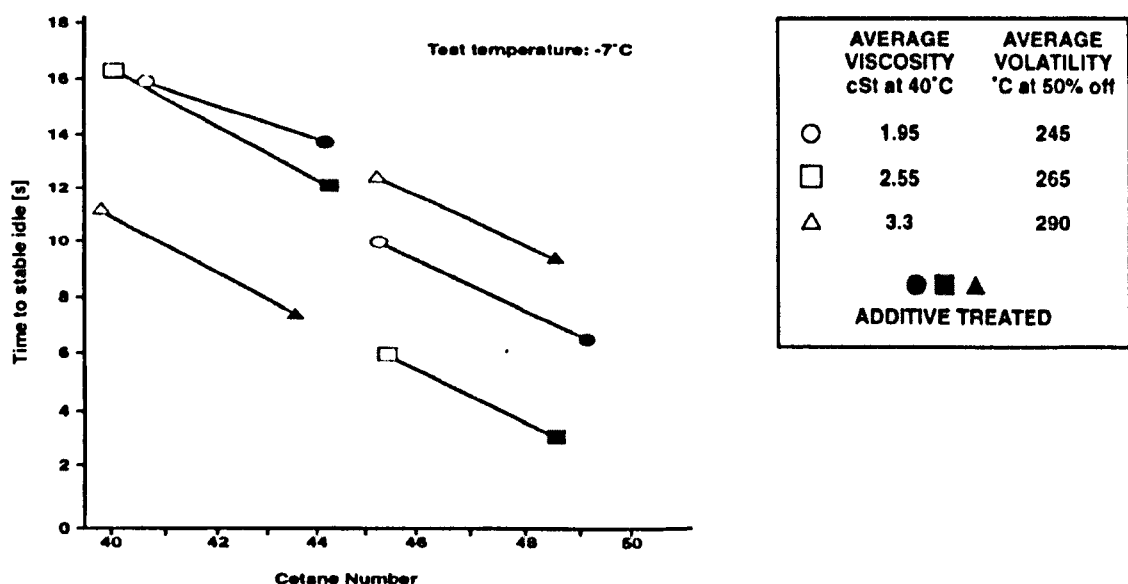
Figura 5.3 Influence of cetane number on the time to reach stable idle when cold starting a direct-injection Diesel engine (reproduced from Cole et al., 1986).

Owing to the influence of the cetane number on cold starting time, and owing to the fact that the other physical characteristics of diesel fuel do not significantly affect the ignition delay, the effect of fuel type on the idle vibration signature presented in this thesis has been analysed primarily in terms of cetane number.

5.2.2 Choice of Engine Technology

Diesel engines can be divided into two basic categories according to their combustion chamber design (Heywood, 1988): direct-injection (DI) engines (Figure 5.4a) and indirect-injection (IDI) engines (Figure 5.4b). In the case of DI engines, the fuel is injected directly into a single combustion chamber formed by the confined space between the cylinder head and the crown of the piston as it reaches its highest position. IDI engines, on the other hand, have a combustion chamber which is divided into two regions, and the fuel is injected and burned first in the prechamber, which is connected to the main chamber via a nozzle or orifice.

(a)   (b)
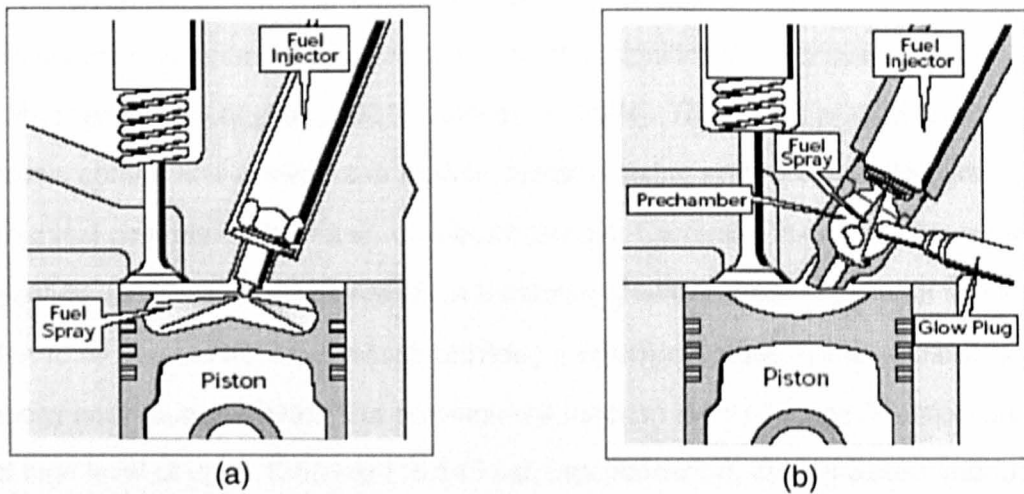
Figure 5.4   Combustion chamber configurations (reproduced from Riesenberg and Faupel, 1999).

        (a)   Direct-injection (DI).
        (b)   Indirect-injection (IDI).

In direct injection engines, the mixing of fuel and air depends mostly on the spray characteristics and on air motion (Heywood, 1988). Thus, high-speed DI engines generally require fuels of high

ignition quality, with short delay characteristics, which in turn require a high cetane number value. IDI engines, in contrast, provide higher fuel vaporization and mixture formation in the main combustion chamber through the use of the narrow connecting passage of the prechamber. Good mixing of fuel and air is achieved by means of the high turbulence, which is created by the rapid transfer of air from the cylinder into the prechamber during compression. The resulting pressure drop between the prechamber and the main chamber produces a gas flow which enhances the mixing and combustion of the fuel and air. The higher turbulence achieved in the IDI engines make this type of engine capable of using fuels of poorer ignition quality, and thus fuels with lower cetane number (Heywood, 1988; Owen and Coley, 1995). However, the increased volume, combustion chamber surface area and turbulence of IDI engines put them at a disadvantage in terms of thermodynamic efficiency and, ultimately, fuel economy.

The IDI engine was developed primarily to overcome the reduced mixing of fuel and air which characterises DI engines, limiting them to the use of fuels of high quality for the passenger car market. Recently, however, the availability of high pressure fuel-injection systems and of electronic engine management systems has permitted significant advances in direct injection (DI) engine performance (Monaghan, 1981; Ivaldi *et al.*, 2004). The use of piezoelectric injectors and an electronic control unit allows more flexible injection timing and fuel metering compared to the old mechanical controls of the rotary distributor pumps. Currently, the most widely used form of direct-injection is the common-rail system, a terminology which refers to a single fuel injection line connected to all the fuel injectors, which provides a common pressure accumulator called a "rail" (Riesenberg and Faupel, 1999). The common-rail function is to maintain injection pressure at a constant high level of up to 1350 bar (19,845 psi) independent of engine speed and fuel quantity. This is achieved by means of an electronic engine management system which continually adjusts the fuel feed pressure according to the engine speed and the throttle position. Sensor data from the camshaft and the crankshaft is used by the electronic control unit to adjust the fuel injection so as to adapt it to actual demand, consequently improving fuel efficiency and emissions. (Riesenberg and Faupel, 1999).

In order to introduce statistical variation into the data, two different diesel automobiles, which had substantially different engine characteristics, were used in the research described in this thesis. The vehicles were:

- Renault 19 1.9 L – turbocharged engine with mechanical indirect injection (IDI) and prechamber system;

- Ford Focus 1.8 L – turbocharged engine with common-rail direct injection (DI) system.

Table 5.2 lists the basic engine specifications for the two automobiles.

Table 5.2   Engine specifications of the two test automobiles.

	Automobile model	
	Renault 19 1.9L	**Ford Focus 1.8L**
Specification	1.9 litre Turbocharged diesel, indirect injection (IDI), precombustion chamber system	1.8 litre Turbocharged diesel, direct injection (DI), common rail fuel-injection system
Engine Type	Four-cylinder, dual overhead cam	Four-cylinder, dual overhead cam
Bore	80 mm	82.50 mm
Stroke	93 mm	82 mm
Displacement	1870 cm^3	1753 cm^3
Compression Ratio	21.5/1	19.40/1

The two test automobiles were chosen based on the knowledge that the effect of diesel fuel on engine performance depends on engine design, engine size and on the engine operating conditions (Heywood, 1988). In particular, an older engine having a prechamber-based indirect combustion system and mechanical distributor pump (Renault 19) was chosen along with an automobile having a modern direct injection common-rail system (Ford Focus 1.8). The new automobile, characterized by common-rail technology, was expected to provide better combustion stability than the older vehicle equipped with a mechanical injection pump (Renault 19). Both automobiles were equipped with 4-cylinder engines. The decision to focus the research on 4-cylinder engines was taken due to the popularity of this configuration, and due to time constraints which did not allow for the testing of more than a single engine layout.

5.2.3 Vibration Measurements

Vibration measurements were made at the engine block and at the steering wheel on each

automobile in order to determine the properties of the vibration signals occurring at the two subsystems, and to evaluate how much the steering wheel vibration signature was related to the engine idle vibration signature. Measurement positions at the engine block structure are typically taken at the head gasket level (Priede *et al.*, 1969) In the research described in this thesis, the measurement point chosen to record the engine vibration was on the upper part of the cylinder block near the engine transfer hook (see Figure 5.5a). A metal plate exists at this point which is convenient for mounting the accelerometer at the required gasket level. The measurement point chosen to record the steering wheel vibration was taken on the surface of the steering wheel at the 60° position with respect to top centre (see Figure 5.5b). This location coincides with a typical grip position of the driver's hand when holding an automotive steering wheel (Giacomin and Gnanasekaran, 2005).

(a)   (b)
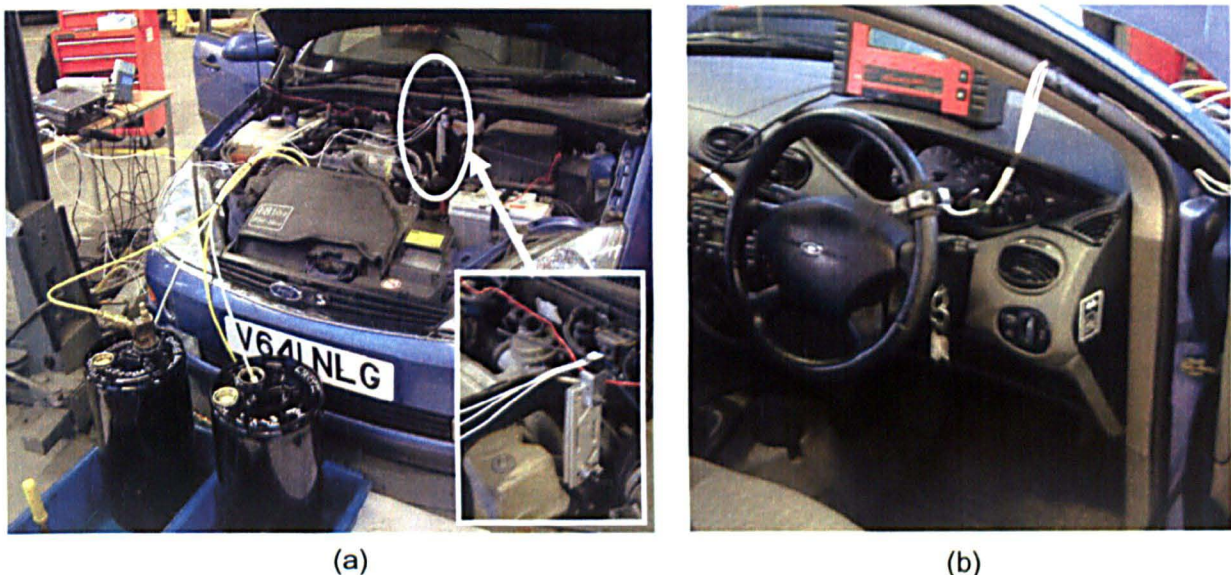
Figure 5.5   Test measurement points. Photos are relative to the Ford Focus 1.8 L.
        (a)   accelerometer position at the engine block.
        (b)   accelerometer position at the steering wheel.

The directions of measurement for the engine block and for the steering wheel were taken along the three principal axes (see Figure 5.6) of the automobile as defined by SAE standard SAE J 670e (1974). The X-axis was towards the front of the car, the Y-axis was to the left and the Z-axis was upwards. In this thesis, the X-axis at the engine block will be referred as to the engine

transverse direction (X) since it was in the horizontal plane normal to the crankshaft axis of both automobiles. The Y-axis will be referred as to the axial direction since it was along the crankshaft axis and the Z-axis will be referred as the vertical direction. The directions of measurement at the steering wheel were taken as described in section 1.3.
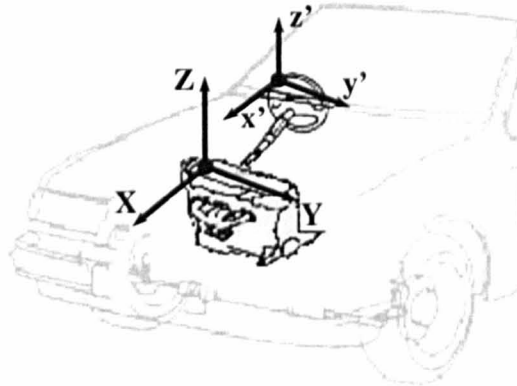
Figure 5.6   Measurement axis of the vibration recordings performed at the engine block and at the steering wheel.

The engine block and steering wheel vibrations were measured by means of two tri-axial piezoresistive accelerometers (*Entran EGAS3-CM-25*). The accelerometer at the engine block measurement position was fixed by means of an aluminium block, mounting plates and screws. The accelerometer at the steering wheel measurement position was fixed by means of an aluminium clamp and mounting screws. The geometrical dimensions of the engine block mounting plates and of the steering wheel clamp are provided in Appendix A. The acceleration signals were amplified by means of an *Entran MSC6* signal-conditioning unit (Entran, 1991), and stored using 6 channels of a Sony PC 216A Digital Audio Tape (DAT) recorder (Sony, 1994) and monitored by a *Tektronix TDS 210* digital oscilloscope (Tektronix, 1999). The specifications of the accelerometers, and of the test equipment are provided in Appendix A. The amplifier and the DAT recorder were run using a battery so as to eliminate electronic noise from vehicle systems. The DAT sampling rate chosen for the vibration measurements was 5 kHz. The rate of 5 kHz was sufficient to ensure that the vibration signals were recorded with adequate definition at the maximum frequency of interest of 1000 Hz. The maximum analysis frequency of 1000 Hz was

chosen based on the guidance provided by the International Organization for Standardization 5349-1 (2001), which defines the frequency range most associated with the effects of hand-arm vibration as that from 8 to 1000 Hz.

The vibration measurements were performed at the Road Test Laboratory at Shell Cheshire Innovation Park in Thornton, England, where engineers specialised in engine and vehicle testing performed the change of fuel for each recording session. In particular, for each fuel, two tanks where used (see Figure 5.5a) to feed in the fuel and to remove it at the end of each recording session. Precision manometer gauges were used to monitor the loading of the fuel. After each change of fuel, each engine was left to idle for approximately 10 minutes so as to purge the fuel feed system, and so as to stabilize temperature and injection conditions. After the 10 minute warm-up, the engine and steering wheel signals were sampled for two minutes in order to obtain acceptable confidence in estimating the statistics of the time histories (Brunt and Emtage, 1997; Ball *et al.*, 1998). The test conditions for both test automobiles are summarised as the following:

- vehicle parked with engine at idle;
- transmission in neutral and handbrake actuated;
- no human subject sitting in the car during the test or holding the steering wheel;
- twelve diesel fuels having different cetane numbers;
- data recorded over 2 minutes for each fuel;
- 20 °C environmental temperature and 40% humidity.

The recorded signals were reacquired and analysed at the University of Sheffield Perception Enhancement Systems Laboratory by means of a *Hewlett Packard 9000 C110 Unix workstation* running the *Fourier Monitor* module of the *LMS CADA-X 3.5B* software (LMS International, 1996), using a 12-*channel Difa Systems Scadas front-end unit*. The signals were resampled at 2048 Hz, a rate which was adequate for the purpose of evaluating hand-arm vibration in the range from 8 to 1000 Hz.

5.3   Signal Processing and Statistical Analysis

5.3.1 Time and Frequency Parameters for a 4-Cylinder Engine

In order to analyse the engine idle vibration, some basic time and frequency parameters (Priede, 1992) for a four-cylinder, four-stroke engine had to be determined, as shown in Table 5.3. The time parameters for one working cycle of a four-cylinder engine are illustrated in Figure 5.7.

Table 5.3 Time and frequency parameters for a four-cylinder, four-stroke engine.

Time constant	Formula	Unit	Eq.
nominal idle speed of the crankshaft	n	[r/min]	(5.2)
period of one revolution of the crankshaft	$T_{REV} = \dfrac{(60\,sec/min)}{(n)}$	[s]	(5.3)
period of one working cycle of the engine	$T_C = 2T_{REV}$	[s]	(5.4)
rotational frequency of the crankshaft	$F_{REV} = \dfrac{1}{T_{REV}}$	[Hz]	(5.5)
engine working cycle repetition frequency	$F_C = 1/T_C$,	[Hz]	(5.6)
engine firing frequency	$F_F = \dfrac{(cylinders) \cdot (n)}{(2\,rev/cycle) \cdot (60\,sec/min)}$	[Hz]	(5.7)
period between consecutive cylinder firings	$T_F = \dfrac{1}{F_F}$	[s]	(5.8)
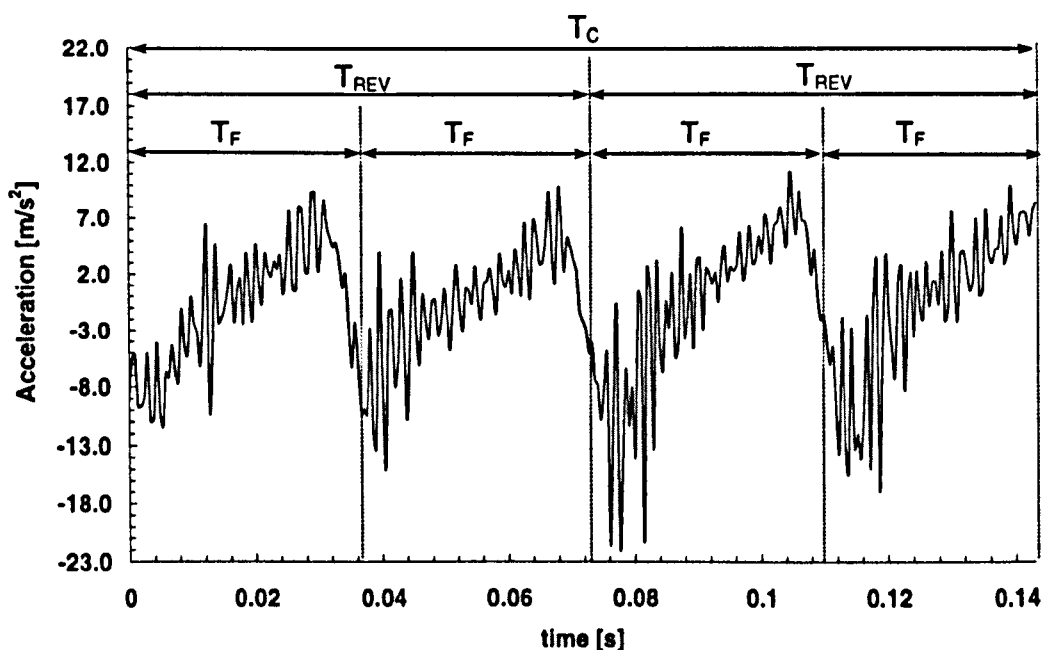
Figure 5.7   Time parameters for one working cycle of a four-cylinder engine.

5.3.2   Global Signal Statistics and Cycle-to-Cycle Variation Analysis

As mentioned in the introductory Chapter 1, in a reciprocating internal combustion engine the combustion forces can be considered as having a periodic engine cycle component, and a random component which is caused by the fluctuations of the combustion process. In the case of a four-cylinder, four-stroke engine, there is only one firing stoke per cylinder every second crankshaft revolution, which is the period of one engine working cycle (T_c). However, the combustion cycle does not repeat exactly every engine cycle due to the random fluctuations of the combustion process from cycle-to-cycle (Ozdor *et al.*, 1994; Hinze and Cheng, 1998) and due to an unequal distribution of fuel from cylinder-to-cylinder (Ando and Motomochi, 1987; Stout *et al.*, 2003). Due to the random variations in the combustion process, it was decided that the statistical variations in the vibration signature should be analysed in terms of both global signal statistics and cycle-to-cycle statistics. The root-mean-square value, kurtosis value and crest factor were calculated in order to:

- quantify the variations in the global signal statistics when changing from one fuel to another;
- quantify the variation in the cycle-to-cycle statistics when changing from one fuel to another;
- compare the behaviour of the two test automobiles under the various fuel conditions.

The root-mean-square and kurtosis values were calculated over the complete two-minute signal as global statistics. In order to reflect the cyclic engine variability, running statistical measures of root-mean-square, kurtosis and crest factor were also calculated on a cycle-to-cycle basis. The statistical values were computed for the acceleration time series of both the measurement points.

5.3.2.1 Selection of a Single Engine Cycle

In order to determine the statistical variations on a cycle-to-cycle basis, it was necessary to define the length of the time window over which to compute each signal statistic. For the calculations presented in this research, the time window was chosen equal to the period of one engine working cycle T_C (Eq. 5.4) since the combustion forces, which represent the main source of vibration for a internal combustion engine at idle, act periodically one every second crankshaft revolution, which is the period of one engine working cycle (T_C).

A general procedure would require the acquisition of the engine instantaneous angular velocity signals in order to be able to identify the starting point of each thermodynamic cycle involving the firing of all four engine cylinders (Liu *et al.*, 2002). The measurement of a tachometer signal via a shaft encoder can provide this information. Unfortunately, at the moment of the experimental measurements, it was not possible to install a shaft encoder since this would have damaged the physical structures of the automobiles that were tested. Therefore the identification of the period of one working cycle, within the full length of the sampled vibration, was made by means of an analytical routine programmed using the MATLAB software (Mathworks Inc, Version 6, September 2000). The starting point of each engine cycle was taken to be the point where the energy level was minimum after four complete combustion events of duration T_F. Four complete combustion events were chosen since, for a 4-cylinder engine, there are four power strokes within the period of one engine working cycle. Subsequently, by selecting a time window equal to the average period of a working engine cycle T_C, it was possible to extract each single engine cycle from the measured vibration time series.

5.3.2.2 Number of Engine Cycles for Statistical Stability

When statistical data are computed for engine data, a common problem (Brunt and Emtage, 1997) is to know how many engine cycles should be processed in order to ensure a high statistical confidence in the results. The maximum number of cycles acquired at the time of the

experimental test is usually determined by the amount of data that can be stored, and by the maximum acceptable data processing time. The optimal number of cycles, over which to compute the cycle-to-cycle signal statistics, is normally chosen to be the minimum number of cycles required to produce stable statistics. Process stability here refers to a process that is not changing its characteristics of mean and variance, when all the variations have been shown to arise from random causes (Oakland, 1996). Further, stability is here determined with respect to the statistical values which are found when calculated using the whole length of the time history.

In order to evaluate the effect of the number of cycles on the stability of the signal statistics, various time intervals of the signal, which included a variable number of cycles n_c, were randomly selected and grouped into a number K of samples. For a given sample which contained a fixed number n_c of cycles, a total of N_s observations were collected in order to compute the mean and the variance of that sample. The number of observations N_s used to compute the sample estimate represented the sample size. The parameter used to evaluate the stability of the process was the r.m.s. value. The r.m.s. value was chosen since it provided, for each sample K, the average energy value relative to the time interval which included a number n_c of cycles. For each sample K consisting of N_s observations, the mean was calculated as:

$$\overline{X}_K = \frac{1}{N_s} \sum_{i=1}^{N_s} x_i \tag{5.9}$$

where the variable x_i is the r.m.s. value calculated for each observation N_s in each sample K. The stability of the signal was assessed by calculating how closely the r.m.s. values for each sample estimated the global r.m.s. of the complete time history. Closeness was quantified by means of the normalized mean square error (MSE) of the sample mean (Bendat and Piersol, 1986) of each sample K:

$$MSE_K = \frac{1}{N_s \cdot \overline{\overline{X}}} \sum_{i=1}^{N_s} \left(x_i - \overline{\overline{X}}\right)^2 \cdot 100 \ [\%] \tag{5.10}$$

where $\overline{\overline{X}}$ is the global r.m.s. of the whole time history, and N_s is the number of observations for

each sample. The mean square error was normalized with respect to the global r.m.s. value for convenience of comparison between the various types of fuel and the different engine technologies. The value of 100 in Eq. (5.10) was used to express the MSE in percent. The mean square error provided a measure of the variability of the sampling distribution of the sample means $\overline{X_k}$ around the target value, i.e. the global r.m.s. of the whole signal. In order to provide an additional indication of how closely the sample values estimated the global r.m.s., confidence intervals were calculated at the confidence value of 99.7 % as defined by Oakland (1996):

$$\overline{\overline{X}}_K \pm 3\sigma_K \tag{5.11}$$

where $\overline{\overline{X}}_K$ is the overall average of the sample means and σ_K is the standard deviation across the number of samples K.

5.3.3 Indices of Variability

In order to quantify the changes in the vibrational signal statistics which were caused by the fuel type and by the engine technology, a coefficient of variation (CV) was determined for each signal statistic. In analogy to the coefficient of variation (Eq. 5.1) based on pressure-related parameters, which is used as a measure of combustion stability, a coefficient of variation was calculated based on the statistical parameters of the vibration signals:

$$CV = \left(\frac{\sigma}{\mu}\right) \cdot 100\% \tag{5.12}$$

where σ and μ are the standard deviation and the mean values of the distribution of the underlying statistic being calculated for each fuel condition for each automobile tested. The coefficient of variation was chosen because it is a normalised index, being obtained by dividing the variability (σ) around the mean value by the mean value itself (μ). For the case of the cycle-to-cycle variation analysis, the coefficient of variation of Eq. (5.12) calculated for each fuel m constituted a coefficient of *intra-fuel* variability (CV_m), which represented the percentage variation of the signal statistics occurring in the vibration signature from cycle-to-cycle for each fuel type. In

order to compare the cycle-to-cycle signal statistical variations calculated for each fuel type, and to compare the behaviour of the two test automobiles, two overall measures of variation were determined across all test fuels. The coefficients of variation CV_m obtained for each fuel m were averaged to determine an overall index of *intra-fuel variability* S_1, defined as:

$$S_1\% = \text{average index of variation across all fuels} = <CV_m>$$ (5.13)

where the symbol $<>$ represents the average taken across all fuels. The overall index of *intra-fuel* variability $S_1\%$ permitted a comparison of the variability in the acceleration signals between the two automobiles. Further, the standard deviation σ_{CVm} of the distribution of the CV_m obtained for each fuel m was divided by the index $S_1\%$ to determine an overall index of *inter-fuel variability* $S_2\%$. The overall index of *inter-fuel variability* $S_2\%$ which provided a measure of the percentage variation of the signal statistics between different fuel conditions, which was defined as:

$$S_2\% = \left(\frac{\sigma_{CVm}}{<CV_m>}\right)\cdot 100\%$$ (5.14)

Similarly, an overall index of the *inter-fuel* variability $S_2\%$ was calculated for the global signal statistical analysis as in Eq. (5.12) where μ and σ were the mean and standard deviation of the global statistics determined across all fuel conditions.

In order to facilitate the data analysis, a baseline difference value of 13% was established, and all signal statistics which produced a coefficient of variation greater than 13% were analysed. The 13% figure was chosen based on the knowledge that the just-noticeable-difference value (see section 3.2) for human perception of hand-transmitted vibration varies from a minimum of approximately 5% for the detection of changes in vibration magnitude using needles indenting the skin of the fingertips (Knudson, 1928), to a maximum of 15 to18% for the perception of hand-arm vibration using a wooden handle (Morioka, 1999). The just-noticeable-difference, which indicates the intensity by which a stimulus must differ from another stimulus so as to be detected (Coren and Ward, 1989), provides a useful threshold value which must be exceeded if humans are to detect differences in vibration.

5.3.4 Frequency Domain Analysis

For the analysis presented in this thesis, acceleration power spectral density calculations were performed rather than power spectra due to the desire to accurately quantify the spectral amplitudes of the many random components of the engine vibration signatures. In this and successive chapters, acceleration power spectral densities are presented in order to quantify the frequency distribution of the vibrational energy in the various vibration signatures. In this chapter, examples are also presented of the acceleration transmissibility function $H(f)$ defined as:

$$H(f) = \frac{G_{xy}(f)}{G_{xx}(f)}$$

(5.15)

where $G_{xx}(f)$ is taken in the context of this thesis to be the PSD of the engine block acceleration (input reference), and $G_{xy}(f)$ is the cross-spectral density of the engine block and the steering wheel acceleration (output response) (Bendat and Piersol, 1986). Confidence statements about the accuracy and the reliability of the transmissibility function are often required in order to assist the interpretation of the results. This can be achieved by estimating the presence of measurement noise in the output signal, and by calculating how much the measured output signal is linearly related to the input signal at each frequency by means of the coherence function:

$$\gamma^2(f) = \frac{|G_{xy}(f)|^2}{G_{xx}(f)G_{yy}(f)}$$

(5.16)

where $0 \leq \gamma^2(f) \leq 1$, and $G_{yy}(f)$ is the PSD of the output y(t). A value of zero means that none of the power in the output signal is linearly related to that in the input signal, and that it is not due to the input signal but to the measurement noise. A value of one, on the contrary, means that all the power is linearly related and that no measurement noise is present in the output signal. All the spectral calculations presented in this thesis were performed using the following parameters:

- original data length of 2 minutes;
- sampling frequency of 2048 Hz;
- FFT block size of 2048 samples;

- frequency resolution of 1.0 Hz;
- Hanning window;
- window function overlap of 90%.

5.4   Experimental Results

The 2 minutes of acceleration data from each experimental test meant that a total of 800 engine cycles were acquired for the engine and steering. In light of the studies on statistical analysis performed by Brunt and Emtage (1997) and by Ball *et al.*, (1998), 800 engine cycles were considered acceptable for estimating the overall statistical properties for the expected range of data variability. The time constants for the four-cylinder, four-stroke, engines are listed in Table 5.4.

Table 5.4 Time constants for the test engines when at idle.

Automobile model	Engine type	Number of cylinders	n r/min	T_C (s)	T_{REV} (s)	T_F (s)	F_C (Hz)	F_{REV} (Hz)	F_F (Hz)
Renault 19	IDI engine	4	840	0.143	0.071	0.036	7	14	28
Ford Focus 1.8	DI engine	4	780	0.154	0.077	0.038	6.5	13	26

5.4.1 Global Signal Statistical Variation among Fuels

Figures 5.8 and 5.9 present an example of typical idle acceleration time histories from the Renault 19 and the Ford Focus 1.8, relative to the condition of fuel 8 (C.N. 54.9). Parts (a) (b) and (c) of Figure 5.8 present the engine block acceleration time histories as measured for the Renault 19 along the X, Y, Z directions, while parts (d) (e) and (f) present the steering wheel acceleration time histories along the x', y', z' axes respectively. Figure 5.9 presents the same information for the Ford Focus 1.8. One second of time history is presented, which corresponds to approximately 7 complete engine cycles, involving 28 individual cylinder combustions. The time histories suggest changes in combustion duration T_F (time between consecutive cylinder firings), amplitude modulation of the combustion activity from cycle-to-cycle, and an unequal distribution of combustion peaks. In addition, the time histories suggest that the transmission of the vibrational energy from the engine to the steering wheel differed for the two automobiles, resulting more attenuated for the Ford Focus 1.8 than for the Renault 19.
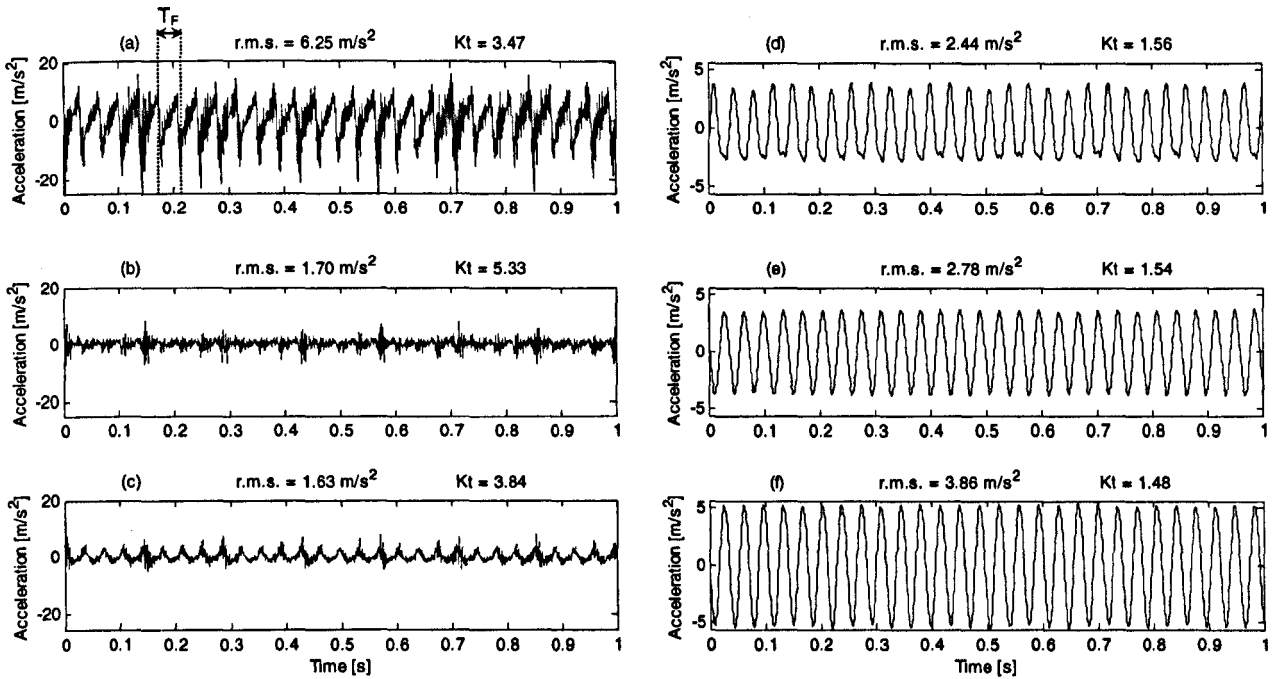
Figure 5.8   Idle acceleration time histories measured for the Renault 19 (IDI) for fuel 8 (CN = 54.9).

Engine block vibration along (a) transverse, (b) axial, (c) vertical directions.

Steering wheel vibration along (d) fore-and-aft, (e) lateral, (f) vertical directions.
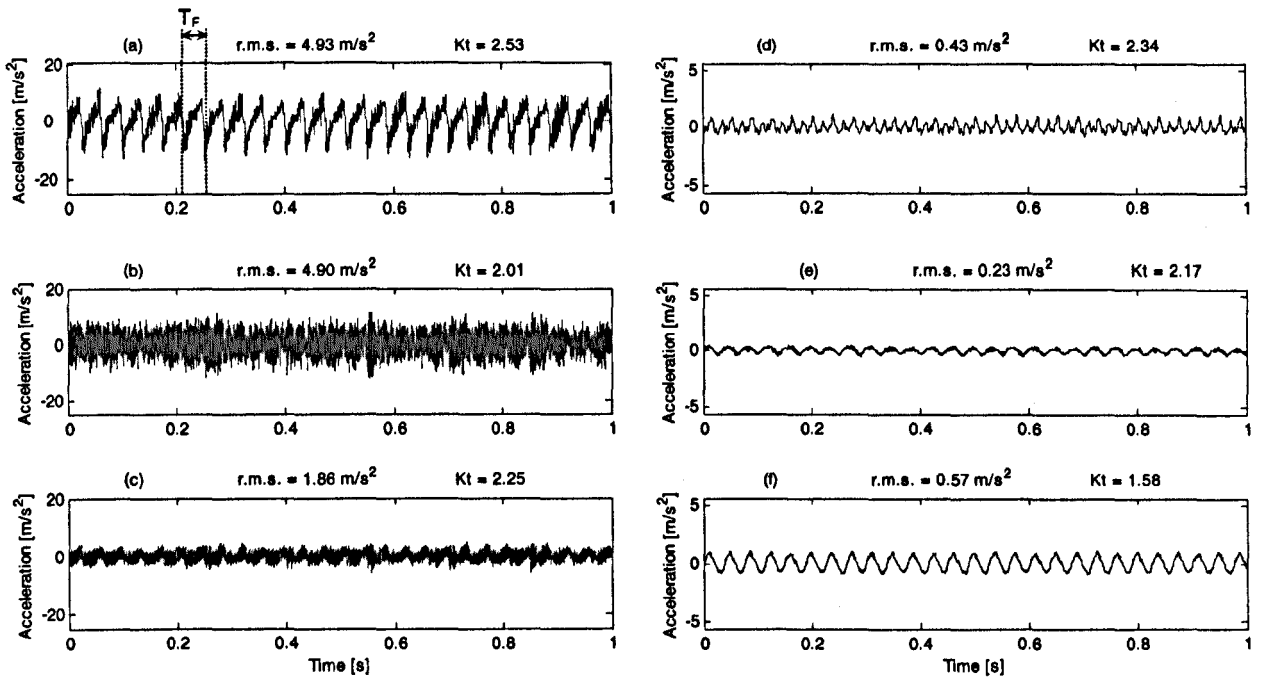
Figure 5.9   Idle acceleration time histories measured for the Ford Focus 1.8 (DI) for fuel 8 (CN = 54.9).

Engine block vibration along (a) transverse, (b) axial, (c) vertical directions.

Steering wheel vibration along (d) fore-and-aft, (e) lateral, (f) vertical directions.

Figure 5.10 presents histograms containing the engine block and steering wheel r.m.s. vibration levels for each fuel along the three directions measured for each automobile. All statistics were computed over the full 800 consecutive engine cycles acquired. The histograms are arranged in order of fuel cetane number, from the highest to the lowest. Figure 5.10a shows that the transverse direction (X-axis) measured at the engine block for the Renault 19 was the direction with the highest vibration level. This was not always true, however, for the engine block acceleration signals measured for the Ford Focus 1.8 (Figure 5.10c), where the r.m.s. levels along the X and Y axis were generally similar. As far as the steering wheel vibration levels are concerned, the vertical direction (z'-axis), along the tangent of the steering wheel, was the direction with the highest energy for both automobiles (Figures 5.10b and d). Further, the vibration measured at the steering wheel was more attenuated for the Ford Focus than for the Renault 19. The acceleration level at the wheel for the Ford Focus was only approximately 1/10th of the levels at the engine block.
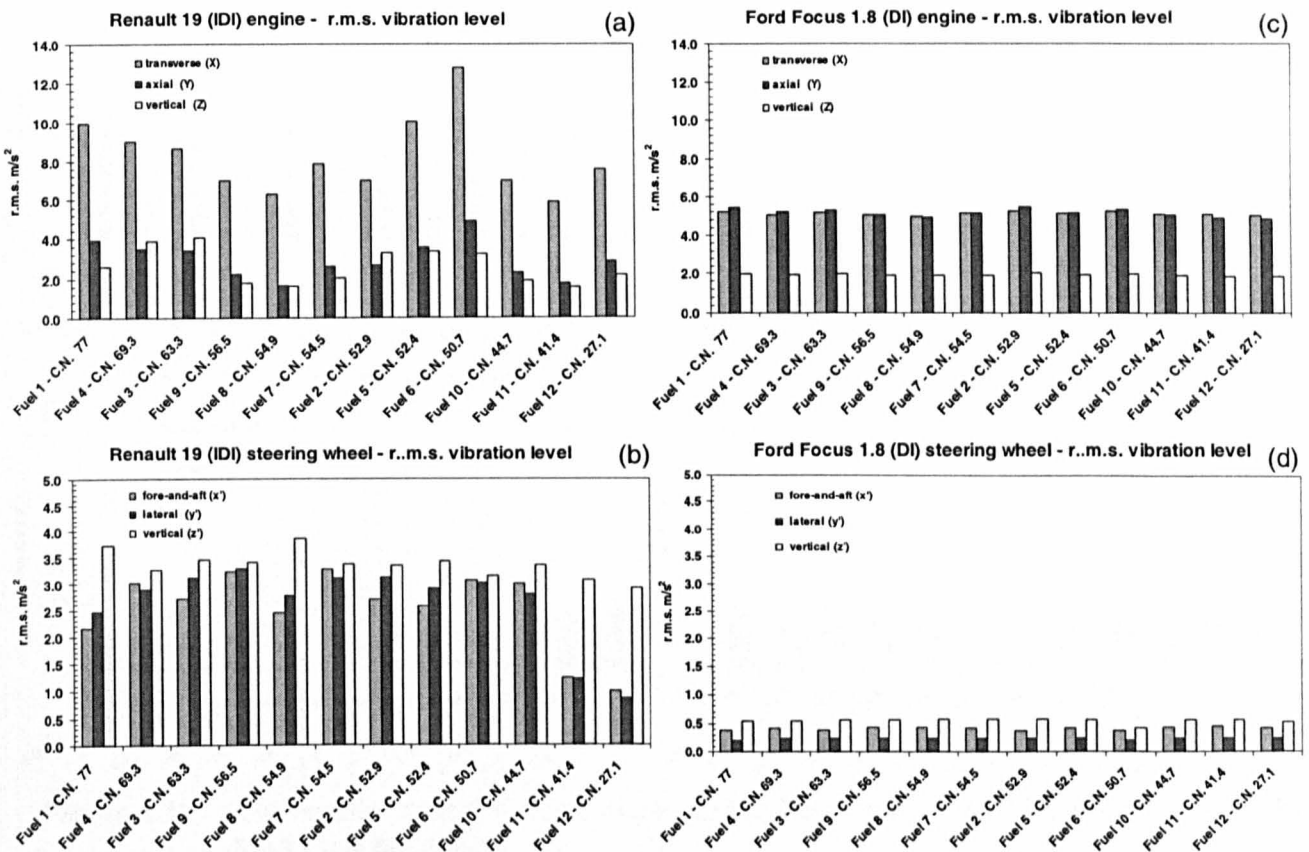
Figure 5.10 Idle vibration global r.m.s. levels for the Renault 19 and for the Ford Focus 1.8 for the 12 fuel conditions.

    (a) engine block acceleration r.m.s. levels measured for the Renault 19 (IDI).
    (b) steering wheel acceleration r.m.s. levels measured for the Renault 19 (IDI).
    (c) engine block acceleration r.m.s. levels measured for the Ford Focus 1.8 (DI).
    (d) steering wheel acceleration r.m.s. levels measured for the Ford Focus 1.8 (DI).

The mean r.m.s. values and the coefficients of variation (CV) among fuels calculated as in Eq. (5.12) are reported in Table 5.5 for both the engine block and the steering wheel along the three directions. The statistics presented in Table 5.5 were calculated excluding the results for fuels 11 and 12, since their properties resulted to be not representative of any legally certifiable fuel (BS EN 590, 1997). Comparison of Figures 5.10a,c and 5.10b,d, suggested that the IDI-engined Renault 19 was more affected by fuel quality than the DI-engined Ford Focus 1.8, having higher coefficients of variation for both measurement points (refer to Table 5.5). The fact that the changes for the Ford Focus were less marked than for the Renault 19 may be attributable to the presence of the common rail fuel injection system.

Figure 5.11 presents histograms of the global kurtosis values for the engine block and for the steering wheel for each fuel along the three directions measured for each automobile.
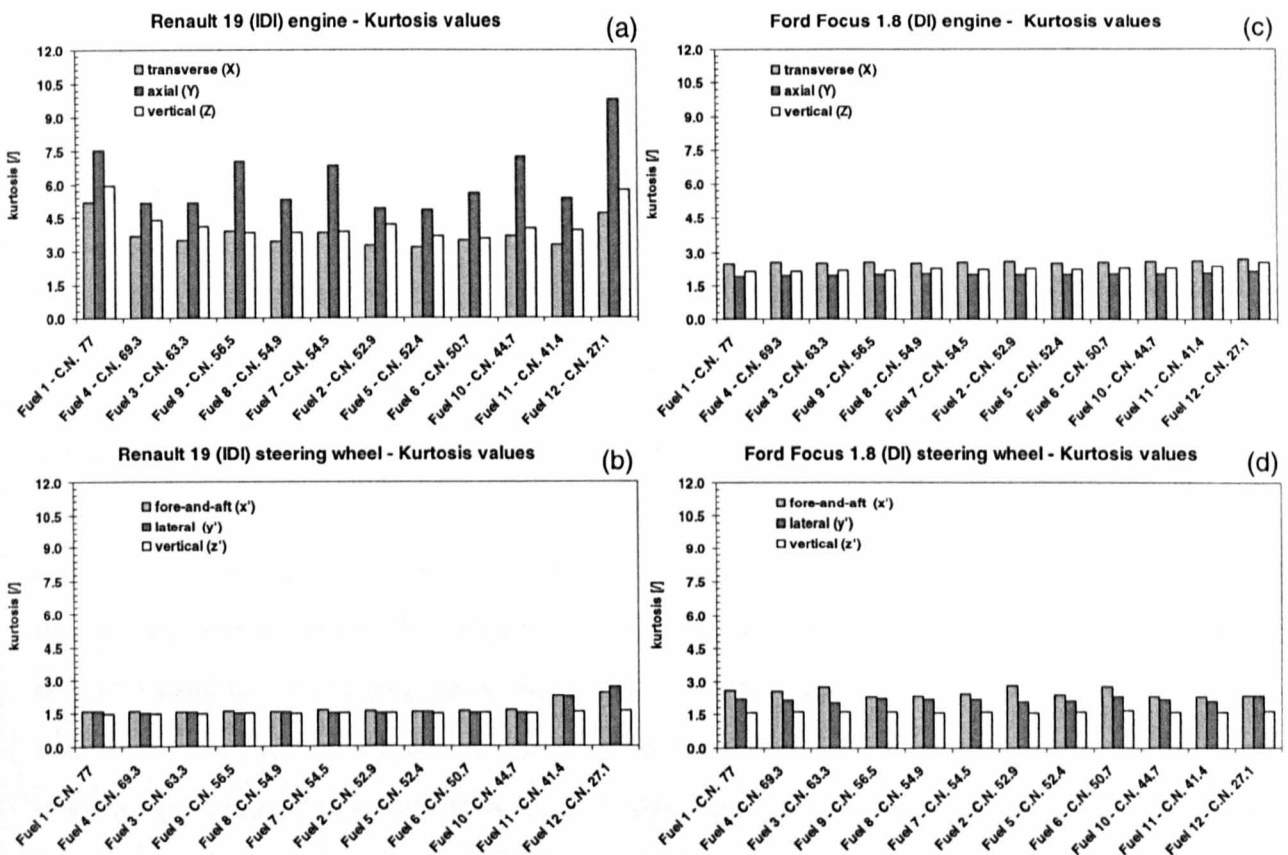
Figure 5.11   Idle vibration global kurtosis values for the Renault 19 and for the Ford Focus 1.8 for the 12 fuel conditions.

(a)   engine block global kurtosis values for the Renault 19 (IDI).
(b)   steering wheel global kurtosis values for the Renault 19 (IDI).
(c)   engine block global kurtosis values for the Ford Focus 1.8 (DI).
(d)   steering wheel global kurtosis values for the Ford Focus 1.8 (DI).

Figures 5.11a and 5.11c relative to the engine block show deviation from a kurtosis value of 3.0, reflecting the presence of transient events. From a comparison of the engine block data of Figures 5.11a and 5.11c, the influence of the fuel on the kurtosis statistics was found again to be more evident for IDI-engined Renault 19 than for the DI-engined Ford Focus 1.8 (refer to Table 5.5). As far as the steering wheel data is concerned (Figure 5.11b and 5.11d), the kurtosis values were approximately 1.5, which is the kurtosis value of a sinusoidal wave. The mean kurtosis values and the overall indices of inter-fuel variability $S_2\%$ calculated across all 10 fuels are reported in Table 5.5.

Table 5.5   Global signal statistics and indices of *inter-fuel* variability ($S_2\%$) determined across all 10 Diesel fuels for the Renault 19 (IDI) and for the Ford Focus 1.8 (DI).

	Automobile model							
	Renault 19 1.9L (IDI)				Ford Focus 1.8L (DI)			
Engine block global statistics	r.m.s.		kurtosis		r.m.s.		kurtosis	
	average across fuels	inter-fuel variability $S_2\%$	average across fuels	inter-fuel variability $S_2\%$	average across fuels	inter-fuel variability $S_2\%$	average across fuels	inter-fuel variability $S_2\%$
Transverse - X axis	8.55 m/s²	23.15%	3.74	15.31%	5.12 m/s²	2.09%	2.54	1.42%
Axial - Y axis	3.06 m/s²	31.40%	5.97	17.60%	5.19 m/s²	3.56%	1.98	1.95%
Vertical - Z axis	2.77 m/s²	32.75%	4.16	16.29%	1.93 m/s²	2.85%	2.21	2.35%
Steering wheel global statistics	r.m.s.		kurtosis		r.m.s.		kurtosis	
	average across fuels	inter-fuel variability $S_2\%$	average across fuels	inter-fuel variability $S_2\%$	average across fuels	inter-fuel variability $S_2\%$	average across fuels	inter-fuel variability $S_2\%$
Fore and aft - x' axis	2.82 m/s²	12.78%	1.58	1.44%	0.40 m/s²	6.31%	2.55	7.90%
Lateral - y' axis	2.95 m/s²	8.05%	1.51	1.56%	0.23 m/s²	6.88%	2.17	4.13%
Vertical - z' axis	3.43 m/s²	6.24%	1.48	0.66%	0.55 m/s²	3.15%	1.61	1.54%

In terms of the variation in the signal statistics across the various fuel conditions, the global steering wheel kurtosis value cannot be considered capable of discriminating one fuel with respect to another since it presented variation not greater than 8% when changing from one fuel to another. With respect to the research objective of identifying physical signal parameters which could be used for quantifying the human subjective response to steering wheel idle vibration, the information provided by the global signal statistics did not clearly suggest an objective metric to discriminate different fuel conditions for both test automobiles. The coefficients of variation were found to be less than 13% for the steering wheel data across all the test fuels and across the two test automobiles. Being characterised by variations that were less than the human just-

noticeable-difference for vibration level discrimination, the diesel idle global statistics did not appear to be strong candidates for measures of human response. Further, each of the global statistics provided only a single number for the idle vibration signature. In the case of vibration signals characterized by non-stationary events, there is concern among engine vibration researchers regarding the current practice of using single numbers to quantify the effect of the complete vibration signature (Brunt and Emtage, 1997; Ball *et al.*, 1998). The difficulty is that global statistics provide an averaged value of the whole signal, with the loss of all inter-cycle statistical information.

5.4.2 Cycle-to-Cycle Signal Statistical Variation

The first step in the cycle-to-cycle statistical analysis was to determine the minimum number of engine cycles (each consisting of four combustions in the case of 4-cylinder engines), which should be used for calculating the statistical values. It was decided to investigate the engine data along the transverse (X-axis) direction, since this direction has been considered the most informative in studies involving the vibration monitoring of reciprocating engines (DeBotton *et al.*, 2000). For each fuel, a series of time intervals, which included a number n_c of engine cycles, was randomly selected from the original time history and grouped into a number K of samples. Each sample contained a number N_s of randomly selected observations of the same time duration, which included a fixed number n_c of engine cycles. In order to calculate the statistical estimates over a large number of observations, it was decided to select K=20 samples, containing N=10 members, to give a total of 200 individual estimates of the r.m.s. value. The choice of the 10 members for each sample K was based on the total of 800 engine cycles of data available, which provided a maximum of 80 engines cycles for the statistical calculations. Each sample included a number n_c of engine cycles from 1 to 80, as shown in Table 5.6.

Table 5.6   Twenty samples defined for the purpose of determining the minimum number of engine cycles required for the cycle-to-cycle statistical analysis. Each sample contained 10 randomly selected members, and had a time duration which included a number n_c of engine cycles.

Sample number	K=1	K=2	K=3	K=4	K=5	K=6	K=7	K=8	K=9	K=10	K=11	K=12	K=13	K=14	K=15	K=16	K=17	K=18	K=19	K=20
Number of cycles included (n_c)	1	2	3	4	5	10	15	20	25	30	35	40	45	50	55	60	65	70	75	80

The sample means $\overline{X}_K$ (Eq. 5.9) were calculated and plotted against the correspondent number of cycles n_c. Figures 5.12a and 5.12b present the sample means calculated for the engine acceleration time history for fuel 8 for both the Renault 19 and the Ford Focus 1.8. The global r.m.s. of the complete time history is represented by the horizontal line. Two further horizontal lines define the 99.7% confidence limits for the estimate of the mean of the complete time history. Figures 5.13a and 5.13b present the normalized mean square error MSE_K (Eq. 5.10) of each sample for the Renault 19 and for the Ford Focus 1.8, respectively.

The stabilization analysis showed that the r.m.s. value computed over more then 45 cycles presented a mean square error less than 0.01% for both automobiles (see Figure 5.13). The stabilization analysis was conducted for all the 10 legally certifiable diesel fuels, and similar results to those shown of Figure 5.13 were found in all cases. It was therefore decided to perform the cycle-to-cycle analysis using a number of cycles greater than 45. A total of 55 cycles was chosen as the optimal number of cycles for determining the cycle-to-cycle signal statistics.
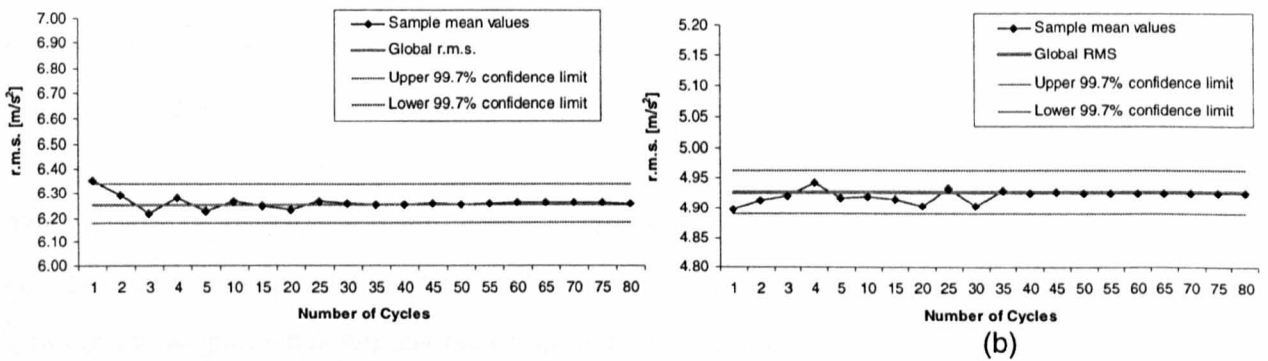
Figura 5.12 Stabilization of the sample mean as a function of the number n_c of engine cycles for fuel 8 (CN 54.9).

    (a) engine block, transverse direction, Renault 19.
    (b) engine block, transverse direction, Ford Focus 1.8.
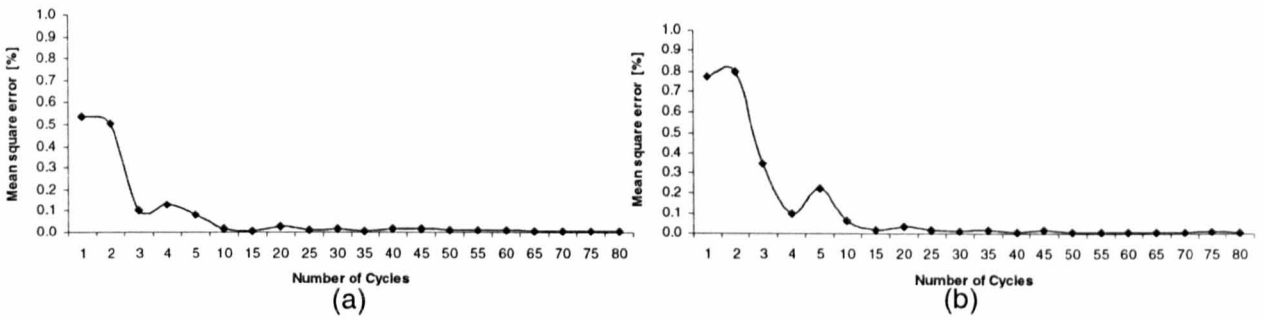
Figure 5.13   Normalised mean square error between the sample mean and the mean of the complete 800 cycles time history as a function of the number n_c of engine cycles.

(a) engine block, transverse direction, Renault 19.
(b) engine block, transverse direction, Ford Focus 1.8.

The running r.m.s., kurtosis and crest factor statistics were determined for each engine cycle of the engine block and steering wheel vibration signals. Figure 5.14 presents the cycle-to-cycle variations computed over 55 consecutive cycles of the engine block acceleration time histories for each fuel and each automobile tested. Figure 5.15 presents, instead, the cycle-to-cycle variations computed over 55 consecutive cycles of the steering wheel time histories for each fuel and each automobile tested. The overall indices of *intra-fuel* variability $S_1\%$ and *inter-fuel* variability $S_2\%$ which were determined across all 10 fuels are presented in Table 5.7 and Table 5.8 for both automobiles and both measurement points.

The coefficients of cycle-to-cycle *intra-fuel* variation, CV_m, calculated for each fuel, permitted a comparison of the variability in the acceleration time history between the two automobiles. In the case of the engine block signals (see Figure 5.14), when the coefficients of cycle-to-cycle *intra-fuel* variation, CV_m were averaged across all ten fuels, the overall indices of *intra-fuel* variability $S_1\%$ were found similar for the Renault 19 and the Ford Focus 1.8. However, the overall indices of *inter-fuel* variability $S_2\%$ determined across all 10 fuels, which provided a measure of the variation in the vibration signatures between different fuel conditions, suggested that the indirect-injection (IDI) engine of the Renault 19 was the most affected by fuel quality. The more irregular

response to fuel quality of the IDI-engined Renault 19 may be attributed to the presence of the mechanical injection system for this type of engine, compared to the DI-engined Ford Focus equipped with the common rail system. Despite the fact that the Renault 19 was an IDI-engined automobile, and thus was potentially capable of using fuels of poorer ignition quality due to the higher turbulence and higher mixing of fuel and air achieved in the combustion prechamber, the engine block analysis suggested that the action of the electronic controller of the common rail system of the Ford Focus was better able to compensate fuel differences.

As far as the steering wheel vibration is concerned (see Figure 5.15), the overall index of the cycle-to-cycle *intra-fuel* variability (S_1%) of the steering wheel vibration signature of the Renault 19 was found to be lower than that of the Ford Focus 1.8. Although the engine vibration levels and the variation in the engine vibration statistics were similar for the Renault 19 and the Ford Focus, differences in the mechanical properties of the steering system lead to greatly different vibrational behaviour at the steering wheel. Compared to the global *inter-fuel* statistical variation values S_2% calculated for the steering wheel which were all found to be less than 13 percent across all ten fuels for both automobiles (refer to Table 5.5), the cycle-to-cycle *inter-fuel* statistical variation values provided, instead, S_2% variability greater than 13 percent (refer to Table 5.8). Being characterised by values greater than the human just-noticeable-difference value for hand-arm vibration, the index of *inter-fuel* variability S_2%, which represented the percentage variation between different fuel conditions, suggested that the differences between fuels were likely to be perceived by the driver when holding a steering wheel at idle.
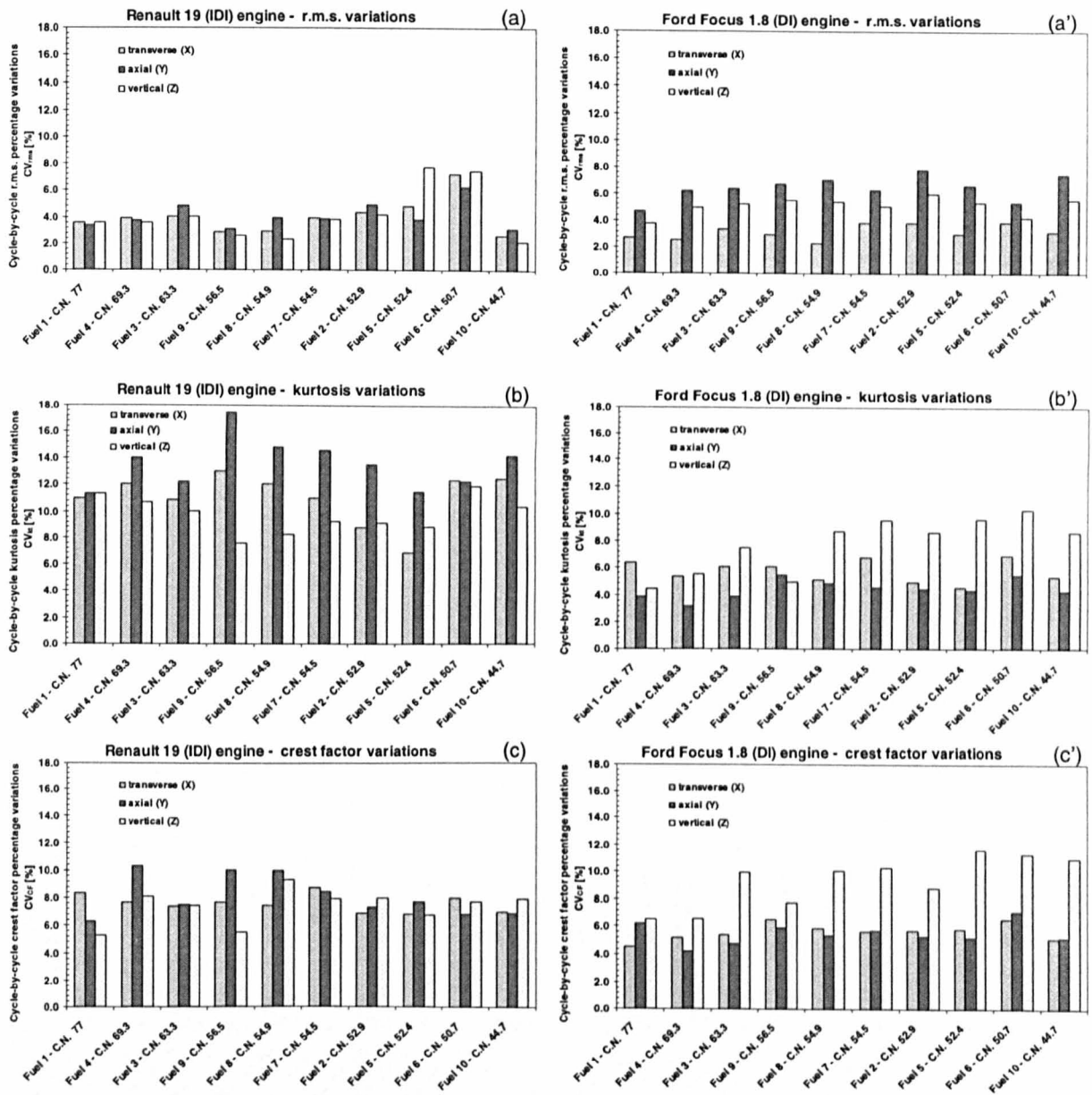
Figura 5.14 Cycle-to-cycle coefficients of *intra-fuel* variation for the engine block idle vibration signature for fuels 1 to 10 for the Renault 19 and for the Ford Focus 1.8.

(a), (a')   Coefficient of r.m.s. cyclic variation, CV_{rms}.
(b), (b')   Coefficient of kurtosis cyclic variation, CV_{Kt}.
(c), (c')   Coefficient of crest factor cyclic variation, CV_{CF}.
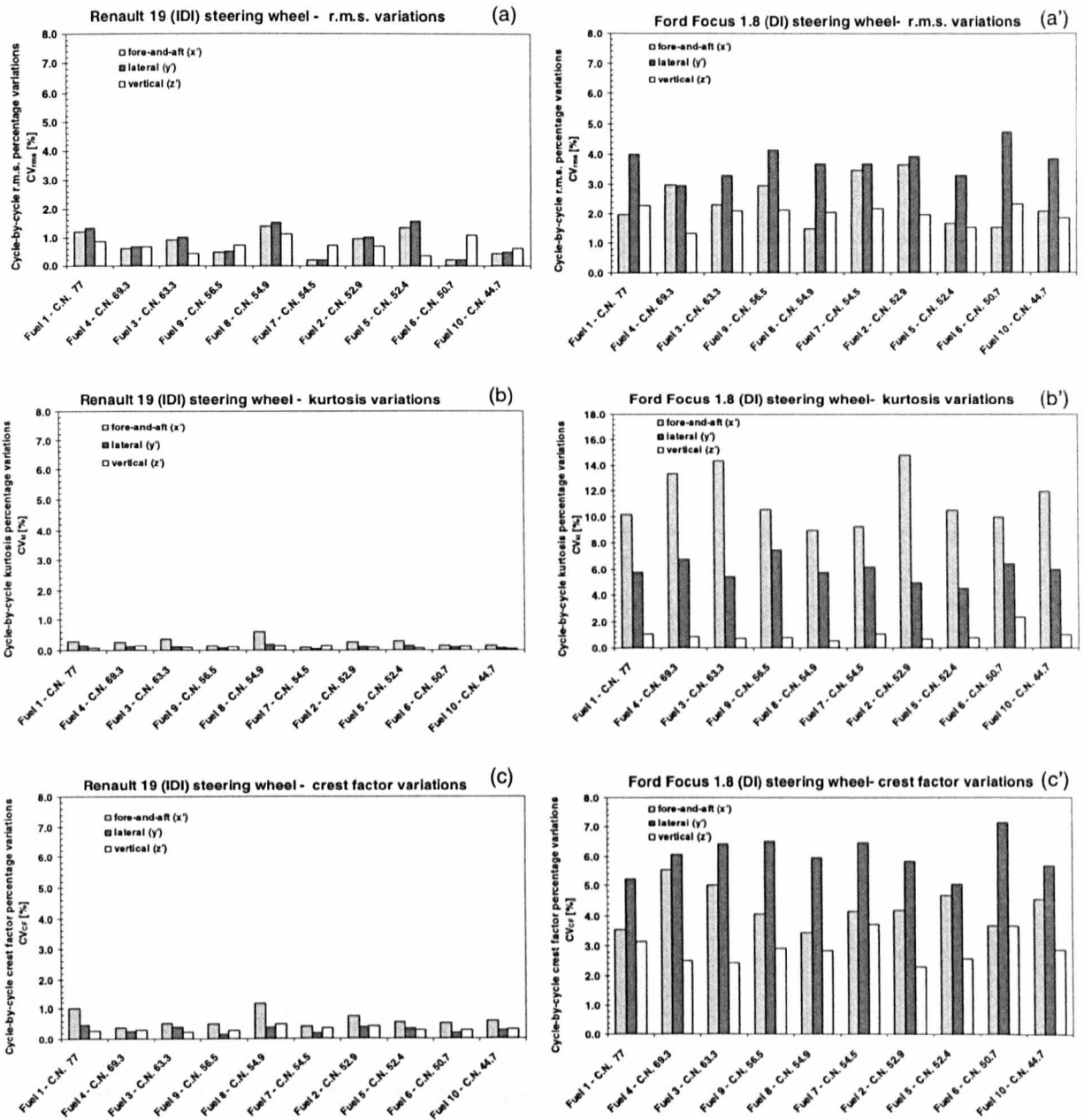
Figura 5.15   Cycle-to-cycle coefficients of *intra-fuel* variation for the steering wheel idle vibration signature for fuels 1 to 10 for the Renault 19 and for the Ford Focus 1.8.

(a), (a')   Coefficient of r.m.s. cyclic variation, CV_{rms}.
(b), (b')   Coefficient of kurtosis cyclic variation, CV_{Kt}.
(c), (c')   Coefficient of crest factor cyclic variation, CV_{CF}.

Table 5.7 Cycle-to-cycle indices of *intra-fuel* variability ($S_1\%$) determined across all 10 Diesel fuels for the Renault 19 (IDI) and for the Ford Focus 1.8 (DI).

	Automobile model					
	Renault 19 1.9L (IDI)			Ford Focus 1.8L (DI)		
Engine block CCV statistics	r.m.s	kurtosis	crest factor	r.m.s	kurtosis	crest factor
Transverse - X axis	4.05%	11.02%	7.59%	3.14%	5.75%	5.63%
Axial - Y axis	4.13%	13.55%	8.12%	6.47%	4.42%	5.48%
Vertical - Z axis	4.18%	9.72%	7.41%	5.10%	7.77%	9.38%
Steering wheel CCV statistics	r.m.s	kurtosis	crest factor	r.m.s	kurtosis	crest factor
Fore and aft - x' axis	1.17%	0.27%	0.63%	2.40%	11.35%	4.26%
Lateral - y' axis	1.30%	0.12%	0.30%	3.74%	5.90%	6.08%
Vertical - z' axis	0.74%	0.11%	0.32%	1.97%	0.96%	2.88%

Table 5.8 Cycle-to-cycle indices of *inter-fuel* variability ($S_2\%$) determined across all 10 Diesel fuels for the Renault 19 (IDI) and for the Ford Focus 1.8 (DI).

	Automobile model					
	Renault 19 1.9L (IDI)			Ford Focus 1.8L (DI)		
Engine block CCV statistics	r.m.s	kurtosis	crest factor	r.m.s	kurtosis	crest factor
Transverse - X axis	32.65%	17.15%	8.39%	17.17%	14.13%	11.19%
Axial - Y axis	23.86%	13.68%	18.05%	14.47%	16.12%	14.55%
Vertical - Z axis	47.22%	14.02%	16.67%	12.99%	26.84%	20.05%
Steering wheel CCV statistics	r.m.s	kurtosis	crest factor	r.m.s	kurtosis	crest factor
Fore and aft - x' axis	33.51%	18.72%	15.65%	68.41%	57.04%	40.55%
Lateral - y' axis	13.34%	14.41%	10.58%	69.10%	38.83%	35.14%
Vertical - z' axis	16.66%	25.65%	17.16%	33.98%	33.03%	22.93%

5.4.3 Frequency Analysis Results

Fourier analysis was performed for the engine block and steering wheel time histories. As an example, Figures 5.16 and 5.17 present the power spectral densities of the time histories presented in Figures 5.8 and 5.9. The discussion is, however, applicable to the data sets of both automobiles and all 10 test fuels since the energy distribution in the frequency domain of the diesel idle vibration showed similar features for all data sets. From Figures 5.16a and 5.17a it can be seen that the spectra of the engine block along the transverse (X-axis) direction are characterized by two regions of significant energy: a low frequency region (up to 200 Hz) with

harmonic components at the firing frequency and its multiples, and a high frequency region (200-800 Hz) characterized by broad peaks that are not related to engine speed, but are instead due mainly to bending vibrations of the engine structure (Priede *et al.*, 1969; Anderton *et al.*, 1970; Priede, 1992). The low frequency region (0-200 Hz) can be interpreted in terms of engine harmonic orders: for a four-cylinder four-stroke diesel engine the rotational frequency of the crankshaft F_{REV} (Eq. 5.5) represents the fundamental engine order harmonic H_1 (Dixon *et al.*, 1994; Rahnejat, 1998). For the IDI-engined Renault 19 idling at 840 rpm, the fundamental frequency H_1 was at 14 Hz, whereas for the DI-engined Ford Focus 1.8 idling at 780 rpm the fundamental frequency H_1 was at 13 Hz (see Table 5.4).
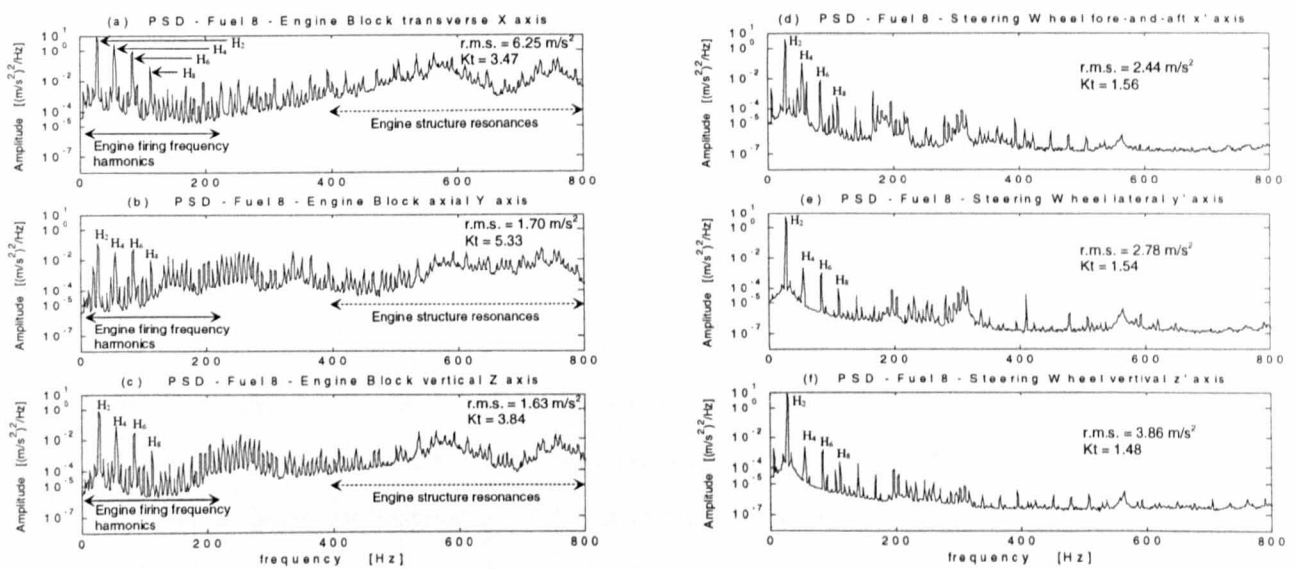
Figure 5.16   Acceleration power spectral densities of the Diesel idle vibration measured for the Renault 19 (IDI) and fuel 8 (CN = 54.9).

Engine block PSD along (a) transverse, (b) axial, (c) vertical directions.

Steering wheel PSD along (d) fore-and-aft, (e) lateral, (f) vertical directions.
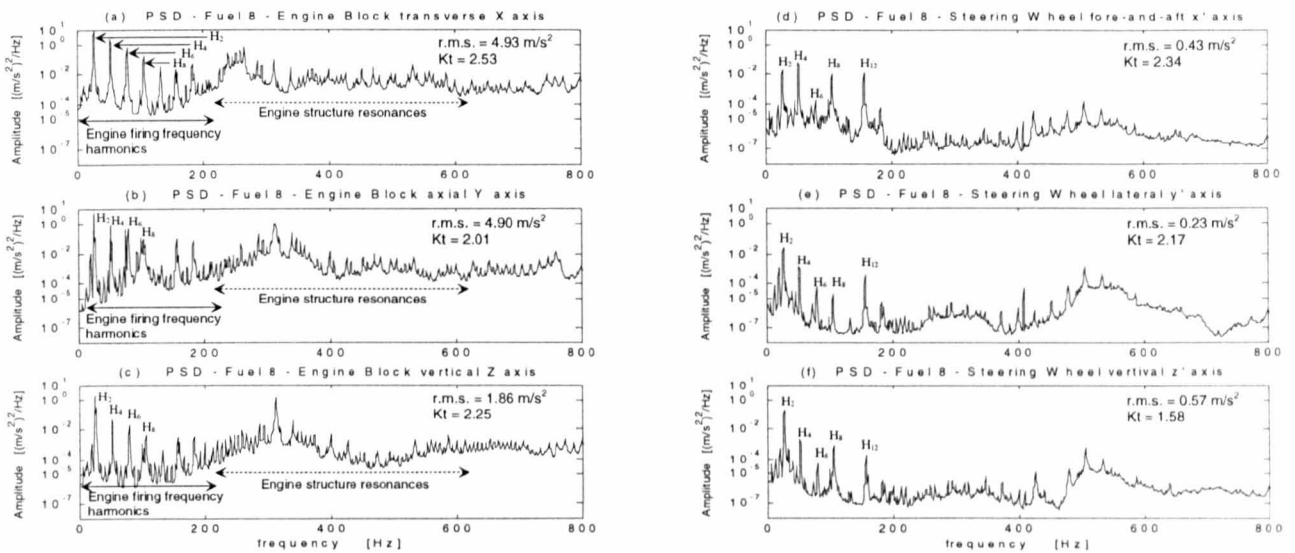
Figure 5.17   Acceleration power spectral densities of the Diesel idle vibration measured for the Ford Focus 1.8 (DI) and fuel 8 (CN = 54.9).

Engine block PSD along (a) transverse, (b) axial, (c) vertical directions.

Steering wheel PSD along (d) fore-and-aft, (e) lateral, (f) vertical directions.

As can be see from Figures 5.16 and 5.17:

- for both diesel engines the major peak occurred at twice the rotational frequency of the crankshaft. For a four-cylinder engine the amplitude of this second-order engine harmonic H_2 is caused by both the effect of second-order mechanical unbalance and the action of the combustion process, which occur at the firing frequency F_F (see Eq. 5.7);

- a second and third noticeable peak exist, called H_4 and H_6 respectively, at four and six times the rotational frequency. These peaks are also caused by the combustion process;

- the amplitudes of the harmonics are characterized by a monotonic decay law.

Regarding the vibrational behaviour of the engine in the axial (Y-axis) and vertical (Z-axis) directions, the vibration energy along these directions presented in the low frequency range similar features to the transverse (X-axis) direction in terms of engine order harmonics, but with lower intensity (see Figures 5.16 and 5.17). In the high frequency range from 200 to 800 Hz the spectrum of the IDI engine differed from the DI engine due to an increased bandwidth of the vibrational energy associated with the bending frequencies of the engine structure, and with the cylinder combustion processes. The DI engine had vibrational energy mostly at frequencies in the

range from 200 to 400 Hz, while for the IDI engine the range was mostly from 200 to 800 Hz. The increased frequency bandwidth of the vibration for the IDI engine might be attributable to the cavity resonances of the combustion chamber associated with the different combustion chamber geometry of the two engines. The cavity resonances in the combustion chamber of a IDI diesel engine are typically found to be in the range from 750 Hz to 3000 Hz (Scott, 1973; Ren *et al.*, 1999) and from 4000 Hz to 5000 Hz for a DI engine (Brammer and Muster, 1975; Hickling *et al.*, 1979). For a IDI engine, the presence of the prechamber, communicating by a small passage with the main chamber, acts as a coupled resonator system of the Helmholtz type (Priede, 1992) which determines lower cavity resonances than those for a DI engine of the same bore size. This leads to lower combustion resonance frequencies which could be excited more easily by the cylinder pressure pulsations of the combustion process.

The power spectral densities of the steering wheel acceleration signals presented in part (d), (e) and (f) of Figures 5.16 and 5.17 are typical of the frequency domain results for all the test data, showing that for all three directions and for both cars the energy conveyed to the steering wheel covered only the low frequency range up to 200 Hz. In addition, the vertical z' direction was found to be the direction where the vibration level was the highest.

Figure 5.18 presents the acceleration power spectral densities, transmissibility functions, and coherence functions calculated for both cars between the engine block (along the transverse X-axis direction) and the steering wheel (along the vertical z'-axis direction). The transverse X direction was chosen for the engine block data since this direction was the most informative in terms of engine harmonics. The vertical z' direction for the steering wheel data was chosen since along this direction the energy level was the highest. The transfer functions suggest that:

- the energy conveyed to the steering wheel was mostly due to the even-order engine harmonics, from H_2, H_4 ,H_6 to H_{12}, which originate from the moving parts of the engine;

- most of the vibration originating from the combustion process was attenuated along the transmission path to the steering system.
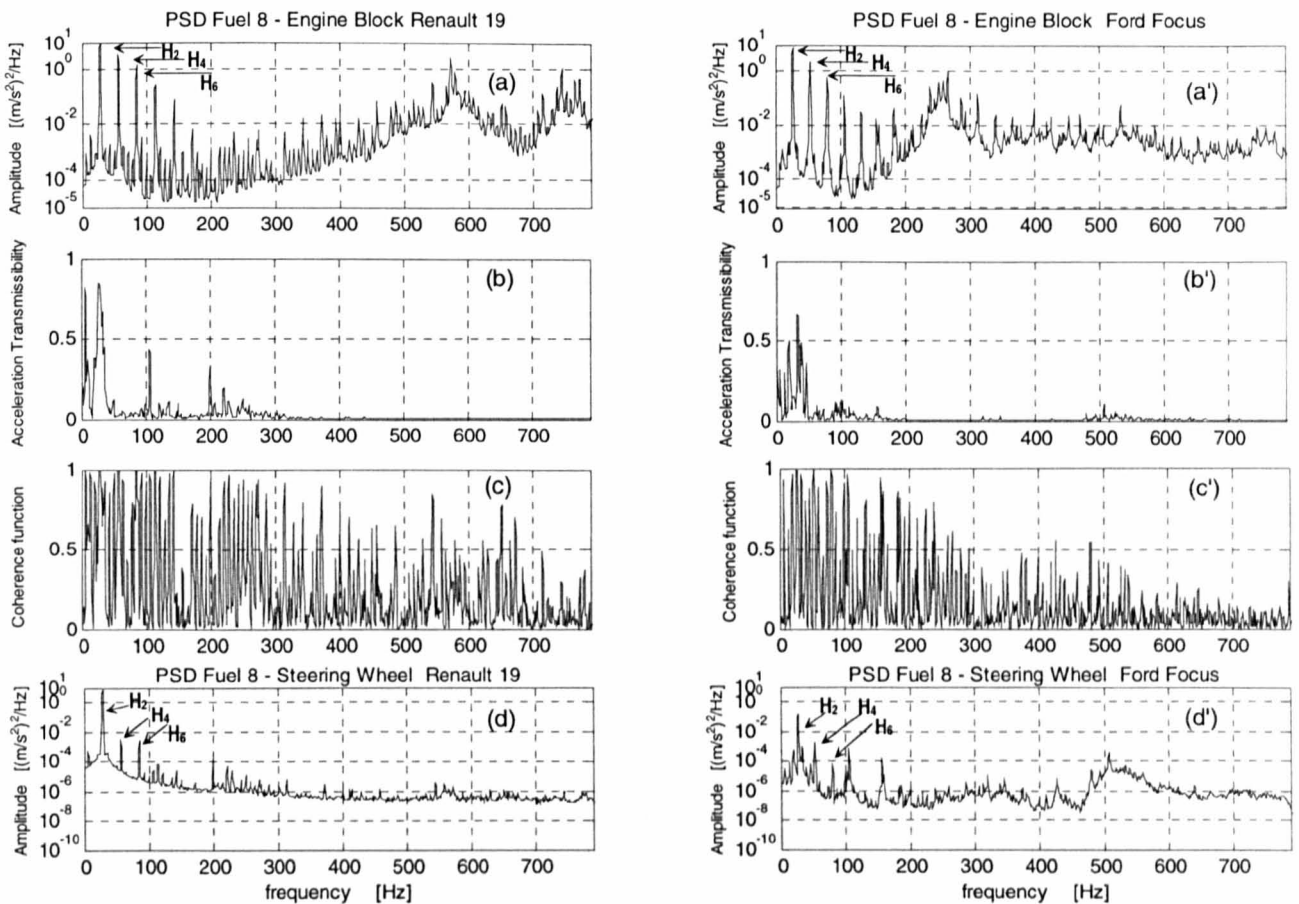
Figure 5.18   Frequency-domain characterisation of the Diesel idle vibration measured for fuel 8 for the Renault 19 and for the Ford Focus 1.8.

(a), (a') acceleration power spectral density of the engine block (X-axis).

(b), (b') transmissibility function from engine block to steering wheel.

(c), (c') coherence function from engine block to steering wheel.

(d), (d') acceleration power spectral density of the steering wheel (z'-axis).

5.4.3.1 Comparisons between Fuels and Automobiles

Comparisons of the power spectral densities are presented here for the transverse X direction of the engine block, since this direction was the most informative in terms of engine harmonics. For the steering wheel, the vertical z' direction has been chosen since the energy level was higher in this direction. Figure 5.19 presents a comparison of the power spectral densities calculated for the engine block signals measured for both test automobiles for two different fuels. Test results

from a fuel having a higher cetane number of 56.5 (fuel 9) are presented in Figures 5.19a and 5.19c, while results for a fuel having a lower cetane number of 44.7 (fuel 10) are presented in 5.19b and 5.19d. Comparison of the power spectral densities relative to the two fuel conditions and the two automobiles suggests that amplitude differences caused by the fuel properties only occurred in the higher frequency range from 200 to 800 Hz, which coincides with the frequency range where the response of the engine structure is greatest (Priede *et al.*, 1969; Anderton *et al.*, 1970; Priede, 1992). In the lower frequency range, up to 200 Hz, no evident differences were found in terms of the amplitudes of the engine harmonics.
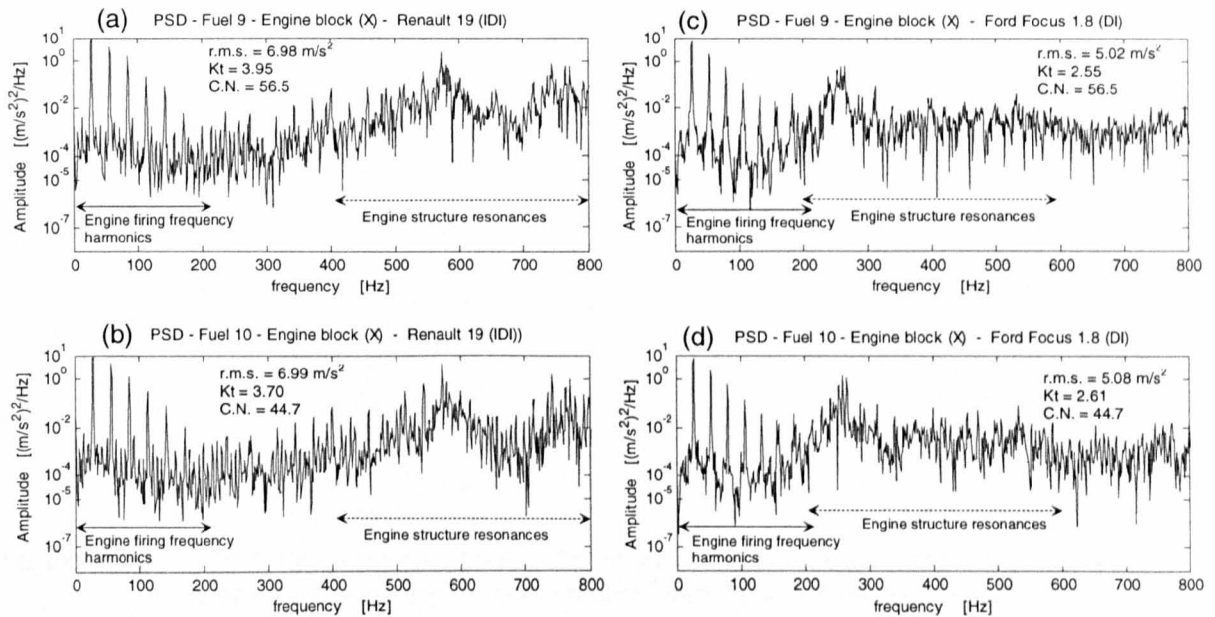
Figure 5.19   Acceleration power spectral densities of the Diesel engine idle vibration measured along the transverse (X-axis) direction for both test automobiles.

engine block PSD measured for the Renault 19 (IDI) (a) fuel 9, (b) fuel 10.

engine block PSD measured for the Ford Focus 1.8 (DI) (c) fuel 9, (d) fuel 10.

Figure 5.20 presents the acceleration power spectral densities calculated for the steering wheel signals measured for both test automobiles using the same two fuels. Comparison of the power spectral densities suggests that use of fuels of different quality did not lead to evident differences in either the frequency values or the amplitude values of the engine harmonics from $H_{1/2}$ to H_{12}. On the other hand, comparison of the results for the two different automobiles suggests important

differences. Large sidebands occurring at frequencies above and below the second-order engine harmonic H_2, and separated from the harmonic H_2 by the half-order engine rotational frequency $H_{1/2}$, are seen more prominent for the DI-engined Ford Focus 1.8 than for the IDI-engined Renault 19. The presence of the sidebands around the second order engine harmonic H_2 suggests that the steering wheel idle vibration is characterized by amplitude modulation.
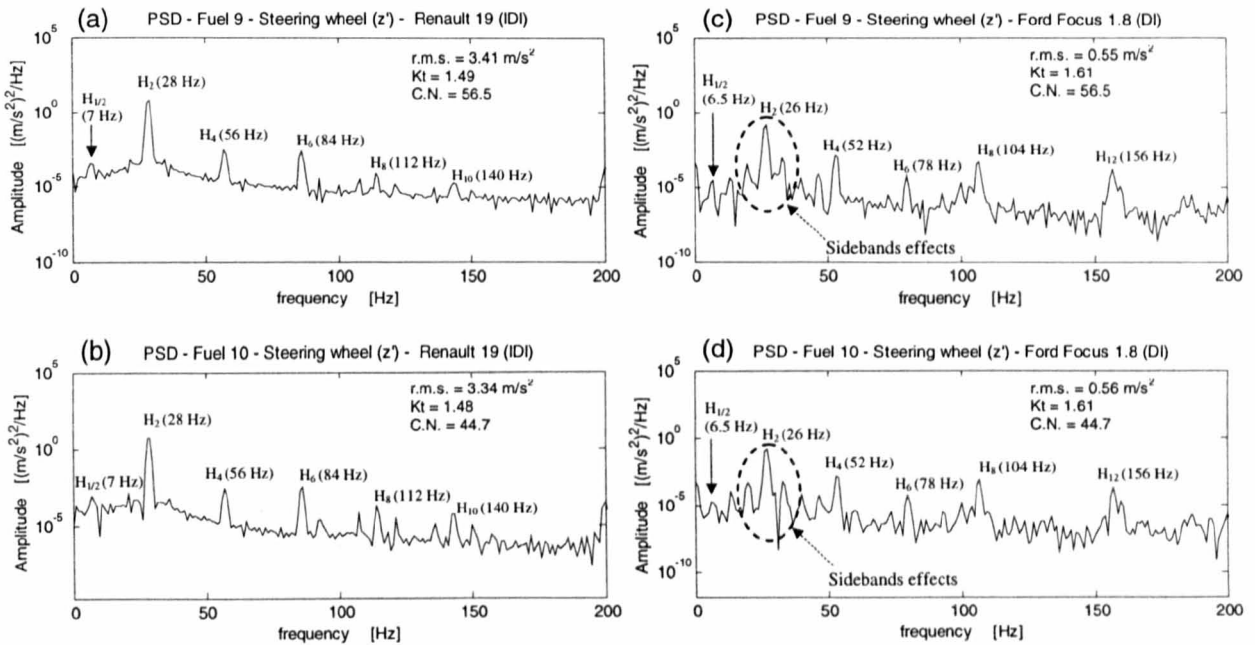
Figure 5.20 Acceleration power spectral densities of the Diesel steering wheel idle vibration measured along the vertical (z'-axis) direction for both test automobiles.

steering wheel PSD measured for Renault 19 (IDI) (a) fuel 9, (b) fuel 10.

steering wheel PSD measured for the Ford Focus 1.8 (DI) (c) fuel 9, (d) fuel 10.

Amplitude modulation is in fact a commonly observed characteristic of the measured vibro-acoustic signatures of rotating machinery, indicating in general a deterioration or irregularity in machine operation (McFadden, 1986; Staszewski *et al.*, 1997; Dalpiaz *et al.*, 2000). The modulation components are known as "sidebands" (Hartmann, 2000). Comparison of the steering wheel power spectral densities suggests that the use of fuels of different quality might lead to different levels of amplitude modulation of the second-order engine harmonic H_2.

5.5   Summary

A set of vibration recordings were performed on the engine block and on the steering wheel using two automobiles which had different injection systems, under different diesel fuel conditions. The first automobile was a Renault 19 1.9 L with mechanical indirect injection and a prechamber system. The second was a Ford Focus 1.8 L which had a common-rail direct injection system. Both cars were equipped with a four-cylinder, 4 stroke engine. The acceleration time histories measured at the engine block and at the steering wheel were analysed using a combination of time domain and frequency domain analysis in order to identify the typical characteristics of diesel idle vibration, and to quantify the statistical variations which occur in the vibration signature due to the change of fuel type and engine technology. Both global signal statistics and cycle-to-cycle statistical variations in the vibration signatures were analysed for all ten reference fuels. A set of coefficients of variation were defined to quantify the change in the vibration statistics. The objective of the analysis of the statistical variations was to identify physical signal parameters which could be used as vibration stimuli descriptors for quantifying the human subjective response to the steering wheel idle vibration.

Global signal statistics were determined using the complete 2 minute vibration signal acquired, which was equivalent to 800 consecutive engine thermodynamic cycles, whereas the cycle-to-cycle statistical variations were determined over a time interval of 8 seconds which was equivalent to 55 complete engine thermodynamic cycles. A total of 55 cycles was identified as the optimal number of engine cycles for ensuring a high statistical confidence and stability of the results when determining the cycle-to-cycle signal statistics.

The fuel-related changes in the vibration signatures at the engine block were quantified by means of the index of *inter-fuel* variability $S_2\%$ which provided a measure of the variation in the vibration signature between different fuel conditions. The results suggested that the indirect-injection (IDI) engine of the Renault 19 was more affected by fuel quality than the DI-engined Ford Focus,

having higher coefficients of variation for both the global *inter-fuel* statistical variability S_2% (refer to Table 5.5) and the cycle-to-cycle *inter-fuel* statistical variability S_2% (refer to Table 5.8). Despite the fact that the Renault 19 was an IDI-engined automobile, and thus was potentially capable of using fuels of poorer ignition quality, the engine block analysis suggested that the action of the electronic controller of the common rail system of the Ford Focus was better able to compensate fuel differences.

As far as the steering wheel vibration is concerned, the *inter-fuel* variabilities S_2% calculated in terms of the global statistics (refer to Table 5.5) were found to be less marked for the Ford Focus than for the Renault 19. However, the global *inter-fuel* statistical variation values S_2% were all found to be less than 13 percent across all ten fuels for both automobiles. Being characterised by variations that were less than the human just-noticeable-difference for vibration level discrimination, the global statistics did not appear to be strong candidates for measures of human subjective response to steering wheel idle vibration. On the other hand, the cycle-to-*cycle inter-fuel* variation values S_2% of the steering wheel vibration signature of the Ford Focus were found to be higher than that of the Renault 19, and were all found to be greater than 13 percent across all ten fuels for both automobiles. This result suggested that the steering wheel idle vibration can be best described on a cycle-to-cycle basis in relation to defining objective signal parameters which can be used to quantify the human subjective discrimination of different fuel conditions.

The frequency analysis performed for the engine block and for the steering wheel signals has shown that the transmission of the diesel idle vibration from the engine to the wheel reduced the frequency bandwidth of the vibration to only the low-order harmonics of the engine rotational frequency. The second-order engine harmonic H_2 was found to account for most of the energy of the steering wheel idle vibration. For a 4-cylinder, 4-stroke engine, harmonic H_2 is caused by both second-order unbalance of the mechanical components and by irregularities of the combustion process in the individual cylinders, which occur at the engine firing frequency. The dominant role of harmonic H_2 in the case of a 4-cylinder engine corroborates the analytical results of Rahnejat

(1998) and the experimental measurements performed by Dixon *et. al.* (1994).

Comparison of the engine block power spectral densities suggested that the vibrations measured for the two engines differed in terms of amplitude only in the frequency range from 200 to 800 Hz, which coincides with the frequency range where the response of the engine structure is greatest. The DI engine of the Ford Focus had vibrational energy mostly at frequencies in the range from 200 to 400 Hz, whereas for the IDI engine of the Renault 19 the range was mostly from 200 to 800 Hz. The increased vibration bandwidth of the IDI engine is thought to be due to the different cavity resonance characteristics, which are associated with the different combustion chamber geometries adopted by the two engines. In the lower frequency range, up to 200 Hz, no evident differences were found in terms of the amplitudes of the engine harmonics.

The presence of sideband components in the power spectral densities of the steering wheel vibration at frequencies above and below the second-order engine harmonic H_2 suggested that the steering wheel idle vibration can be considered as amplitude-modulated stimuli whose amplitude changes over time due to the combustion event repeating every engine working cycle at the half-order engine rotational frequency $H_{1/2}$. Comparison of the steering wheel power spectral densities relative to fuels of different cetane number suggested that the use of fuels of different quality can lead to different levels of amplitude modulation of the second-order engine harmonic H_2.

Chapter 6

Time-Frequency Analysis of Diesel Idle Vibration

6.1   Objectives of the Time-Frequency Analysis

In the previous chapter it was noted that the appearance of amplitude modulation sidebands around the second-order engine harmonic in the steering wheel power spectral densities suggested that the frequency and amplitude of the signal might change over time. In addition, cycle-to-cycle variations were observed to occur in the steering wheel acceleration time histories due to combustion variations during the engine operating cycle.

This chapter describes a wavelet time-frequency analysis that was performed in order to establish whether the variation in the diesel idle vibration could be best characterized as being due to changes in the instantaneous signal character, or due instead to more slowly developing differences which occur across complete thermodynamic engine cycles. The wavelet transform was used since it provides a simultaneous time-frequency analysis, giving local information

pertaining to the temporal variations in the spectral content of the signal (Chui, 1992; Newland, 1994; Mallat, 1998). Thus, the wavelet transform avoids the well-known limitations of classical Fourier-based methods when applied to signals whose characteristics change over time. Both the continuous wavelet transform and the discrete orthogonal transform were applied to the steering wheel acceleration time histories of both automobiles for all 10 fuels. The wavelet analysis was performed with the aim of identifying which of the two wavelet-based methods provided the more sensitive tool for analysing steering wheel idle vibration, and in order to define signal parameters which could be used as vibration stimuli descriptors for quantifying the human subjective response to the steering wheel idle vibration.

The continuous wavelet transform was considered suitable for the extraction of instantaneous signal features from the steering wheel signatures. In particular, the ridge and skeleton of the CWT (Delprat *et al.*, 1992; Carmona *et al.*, 1997; Staszewski, 1998a) were thought to provide effective tools for visualizing and quantifying the instantaneous frequency and amplitude variation of the engine-order harmonics as a function of time. On the other hand, the orthogonal wavelet transform was considered suitable for separating the harmonic components of the steering wheel idle vibration signature into independent frequency bands, facilitating the extraction of signal features for each frequency band of interest. The advantage of using an orthogonal wavelet analysis consisted of decomposing the analysed signal into different wavelet levels, which each had the potential of revealing salient signal features (Smallwood, 1998; Staszewski, 1998b; Gaberson, 2001). Once decomposed into wavelet levels, the variation of the harmonic contents of the signal from cycle-to-cycle could be quantified by means of time-varying auto-covariance analysis (Li *et al.*, 2000; Li and Jung, 2002; Wang and Jung, 2002) performed on the wavelet level containing the harmonic of interest. Thus, quantitative assessments of the variation in the steering wheel vibration were made by means of:

(a)   extraction of the instantaneous frequency and envelope characteristics by means of the ridge and skeleton of the continuous wavelet transform (CWT);

(b)   extraction of the cyclic variation from the discrete orthogonal wavelet transform (OWT) using time-varying auto-covariance (TVA) analysis.

From the array of the instantaneous and cycle-to-cycle characteristics extracted from all the steering wheel idle vibration signals, coefficients of variation (CV=SD/mean) were calculated and compared in order to:

- determine whether the changes were due more to differences in instantaneous value or to differences from cycle-to-cycle;

- verify which properties changed from one fuel, or vehicle, to another.

Figure 6.1 summarizes the computations and comparisons performed. All signal processing algorithms employed were coded in the MATLAB software environment (Mathworks Inc, Version 6, September 2000a, b).
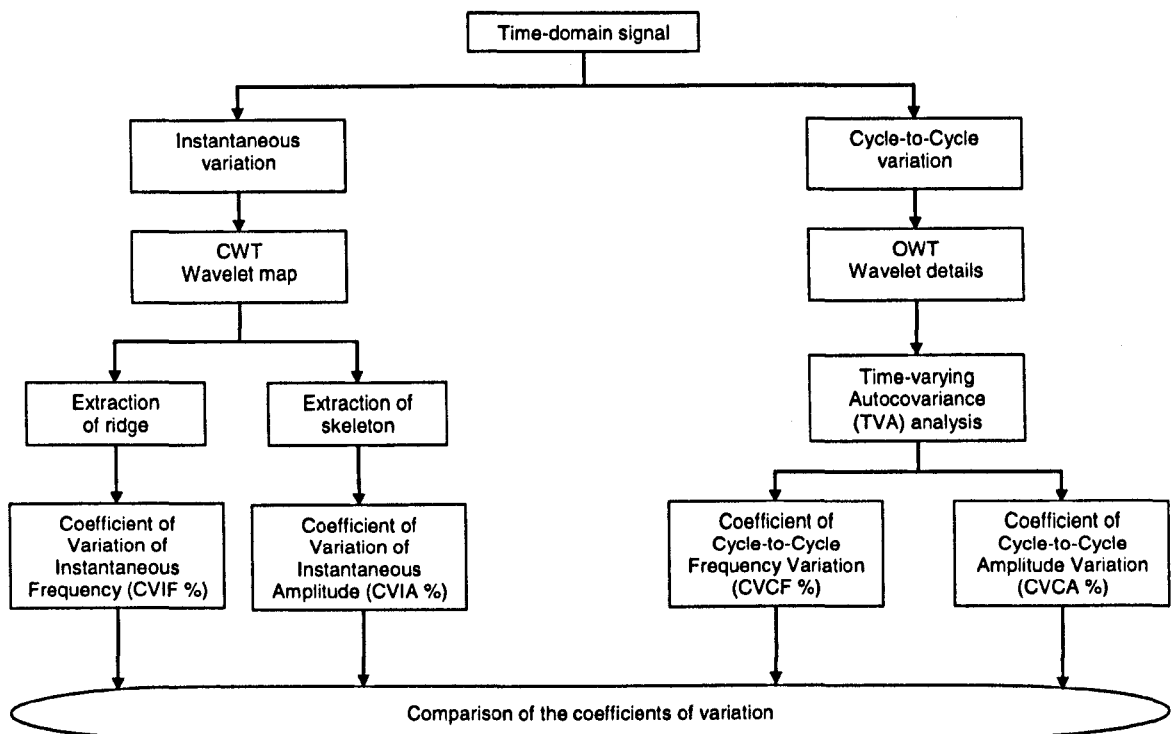
Figure 6.1   Flowchart illustrating the time-frequency analysis performed for the steering wheel idle acceleration signals.

6.2   Continuous Wavelet Analysis

As observed in the previous chapter, the steering wheel idle vibration acceleration spectra were mainly characterised by the second-order engine harmonic H_2 and by the even-order harmonics up to H_{12}. Due to the fact that the extraction of the ridge from the modulus of the CWT gives exact values only when the signal frequency components are localized far away from each other along the frequency axis (Delprat et al., 1992), the choice of the wavelet analysis parameters was made so as to separate the different engine order harmonics, avoiding frequency interactions on the time-frequency plane of the CWT map. This can be understood by recalling that the wavelet transform can be interpreted as a filtered version of the decomposed signal (refer to section 4.5.2.1), with the filter characteristics chosen so as to provide good time-frequency localization (Farge et al., 1994; Mallat, 1998). Therefore, the wavelet filter parameters were chosen in order to focus the analysis around one dominant engine order harmonic at a time.

6.2.1   Choice of the Analysing Wavelet Function

A number of different wavelet functions that satisfy the admissibility condition (Eq. 4.22) can be used as the analyzing wavelet for the calculation of the CWT. The Morlet wavelet function was used for the analysis in this research. It has been demonstrated (Delprat et al., 1992) that the Morlet wavelet function is the best candidate for use when extracting a ridge or skeleton of the CWT due to its property of having a Gaussian envelope (refer to Eq. 4.24) and due to its satisfying the admissibility condition (Eq. 4.22) for values of the wavelet center frequency $\omega_0 \geq 5$ (Kronland-Martinet and Morlet, 1987; Delprat et al., 1992). Being a wavelet function characterized by identical exponential decay each side of centre, it has good localization properties in the frequency domain (Delprat et al., 1992; Mallat, 1998). The Morlet wavelet is therefore considered well suited to the analysis of the ridge of multi-component signals, particularly when the signal components do not interact in the time-frequency plane. The continuous wavelet transform involving the Morlet wavelet function has been widely used for the detection of changes in signal

properties and for signal feature extraction. Examples include fault detection in ball bearings (Rubini and Meneghetti, 2001), gear fault detection (Wang et al., 2001; Zheng et al., 2002) signal feature extraction (Staszewski and Tomlinson, 1994; Lin and Qu, 2000), detection of abnormal engine combustion resonances (Li et al., 1999), and the analysis of impact harshness of road automobiles (Lee and White, 2000).

6.2.2 Choice of the Morlet Wavelet Parameters

An algorithm was implemented in the MATLAB software (Mathworks Inc, Version 6, September 2000b) in order to perform the continuous wavelet analysis. The selection of the parameters needed as inputs for the algorithm were based on both the analyzing wavelet function and the analysed signal. In particular, the wavelet parameters were: the center frequency of the wavelet ω_0, the sampling frequency f_w of the wavelet function, and the total number of scales a, which defined the position of the wavelet filter in the frequency domain. The signal parameters were instead: the sampling frequency f_s of the analysed signal which determines its time resolution, and the frequency band where to focus the wavelet analysis, as specified by the minimum (f_{min}) and maximum (f_{max}) frequency values of interest.

Typically, the Morlet wavelet function as defined in Eq. (4.24) is used with a center frequency of approximately $\omega_0 = 5$ rad/s, which is well suited for the analysis of localized abrupt changes in a signal (Staszewski and Tomlinson, 1994) and for impulsive events (Li et al., 1999). For the analysis of the instantaneous signal characteristics presented in this research, a value of $\omega_0 = 15$ rad/s was chosen, since it provided good frequency selectivity. The center frequency of the Morlet wavelet was chosen large enough to avoid interference between the different harmonic components, guaranteeing their separation in the time-frequency plane.

Figure 6.2 presents an example of the effect of the center frequency ω_0 on the time-frequency resolution obtained when computing a CWT of a steering wheel acceleration signal. Figure 6.2a presents the steering wheel time-history as measured on the Ford Focus relative to fuel 8, while Figures 6.2b, 6.2c and 6.2d present the CWT modulus obtained for three different values of wavelet center frequency, namely $\omega_0 = 5$ rad/s, $\omega_0 = 10$ rad/s and $\omega_0 = 15$ rad/s. Four harmonics can be observed in the CWT modulus: $H_{1/2}$ (6.5 Hz), H_2 (26 Hz), H_4 (52 Hz) and H_8 (104 Hz). By comparing the three wavelet maps, it can be seen that the value of $\omega_0 = 15$ rad/s, shown in Figure 6.2d, provides a better localization and separation of the harmonics in the time-frequency plane. Lower values of the center frequency produce, instead, a "smearing" effect causing interferences between the different harmonics. The choice of center frequency $\omega_0 = 15$ rad/s was considered to provide good frequency selectivity since it provided a frequency bandwidth (Eq. 4.23) of the base wavelet function as small as $\Delta f_\psi = 0.23$ Hz, determined as the half-power bandwidths in the frequency domain (Bendat and Piersol, 1986).

As illustrated in Figure 4.8 (refer to section 4.5.2.1), the narrower the scaled version of a wavelet is in the time domain, the wider it is in the frequency domain. This increases the frequency overlap between adjacent wavelets, which brings about redundancy at higher frequencies (Farge *et al.*, 1994; Mallat, 1998). Care must therefore be taken when choosing the number of scales to use in a time-frequency wavelet analysis. The optimum number of scales ns was chosen to be 300 since this value provided a frequency resolution Δf of 0.05 Hz, a value that was considered reasonable for estimating instantaneous frequency or amplitude variations greater than the just-noticeable-difference value of 0.13 for hand-arm vibration.
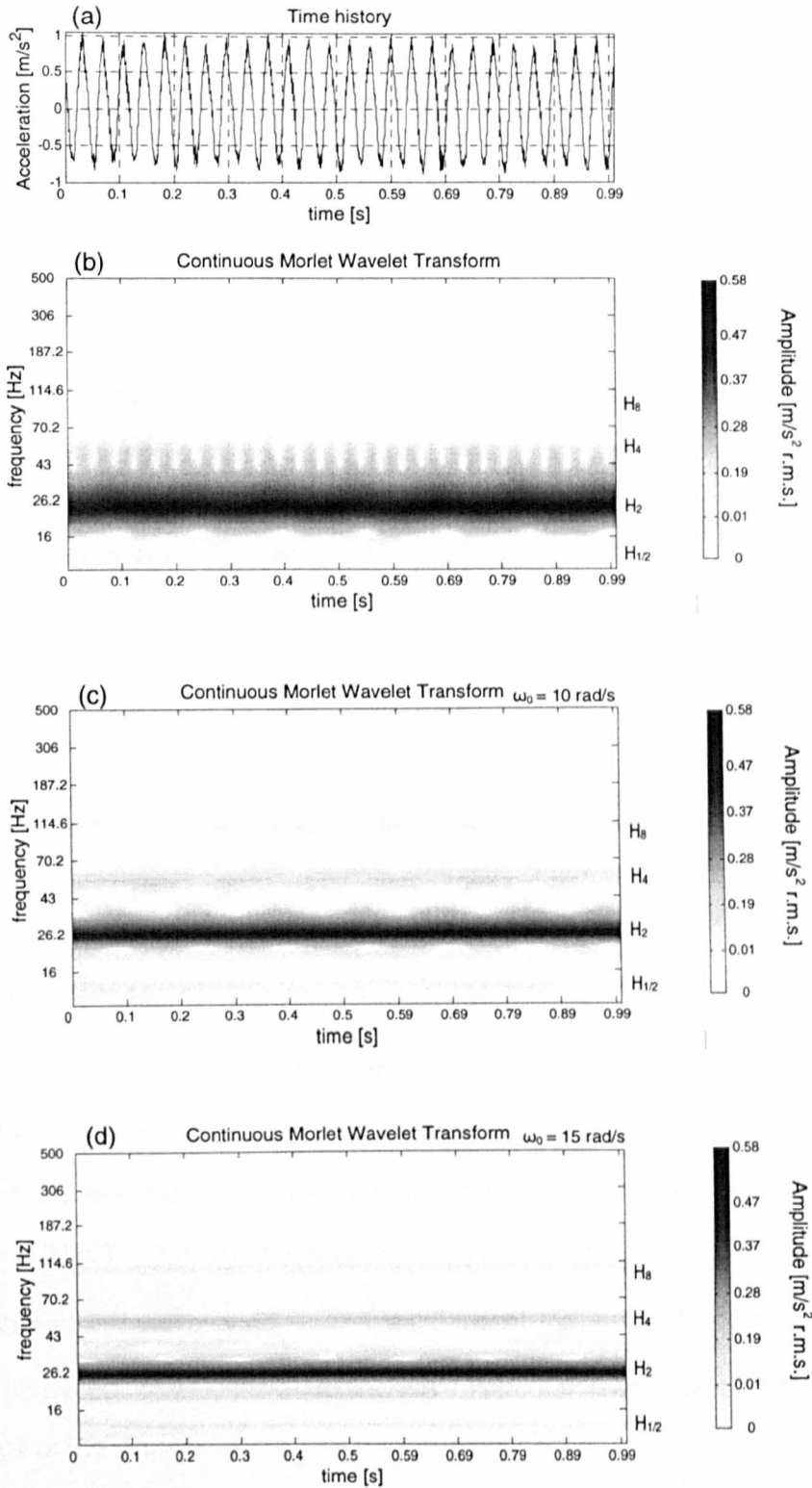
Figure 6.2 Effect of the Morlet wavelet center frequency value on the time-frequency resolution of the continuous wavelet transform.

(a)   original steering wheel idle acceleration time history.

(b), (c), (d)   modulus of the CWT in the time-frequency plane for three different values of the center frequency ω_0.

The sampling frequency f_w of the wavelet function is defined as the number of data points used to digitally implement the wavelet (Mathworks Inc, Version 6, September 2000b). The value of the wavelet sampling frequency f_w was chosen as high as the sampling frequency of the signal, $f_s =$ 2048 Hz, in order to minimise numerical error, and to focus the analysis on the low frequency components (large scale values).

All of the CWT wavelet maps presented in this thesis have been calculated using equation 4.25. The modulus of the CWT was normalized to the root-mean-square value of the signal in order to facilitate the comparison of the various wavelet maps.

6.2.3 Extraction of the Ridge and Envelope

Calculation of the ridge of the CWT provided direct information on the instantaneous frequency changes of the acceleration signals measured at the steering wheel. Ridge extraction was implemented in the MATLAB software (Mathworks Inc, Version 6, September 2000b). The software program identified all the points (a_0, b_0) in the time-scale plane where the modulus of the wavelet coefficient $|W_\psi(a_0, b)|$ was maximum at the point $b = b_0$ along the time axis. The computed modulus of the wavelet coefficients was obtained by means of the MATLAB algorithm as an output matrix of size [ns X N], where ns is the total number of the scale values a used in the computation of the wavelet transform, and N is the number of the sampled points of the time history of duration T (N = T * f_s). The collection of all the frequency values obtained for each time position $b = b_0$ formed the wavelet ridge. The modulus of the wavelet coefficients forming the ridge, as described by Eq. (4.27), provided the instantaneous amplitude of the signal which is called the envelope of the signal.

Figure 6.3 presents the flowchart of the algorithm used for the computation of the ridge and the envelope from the coefficients of the continuous wavelet transform.
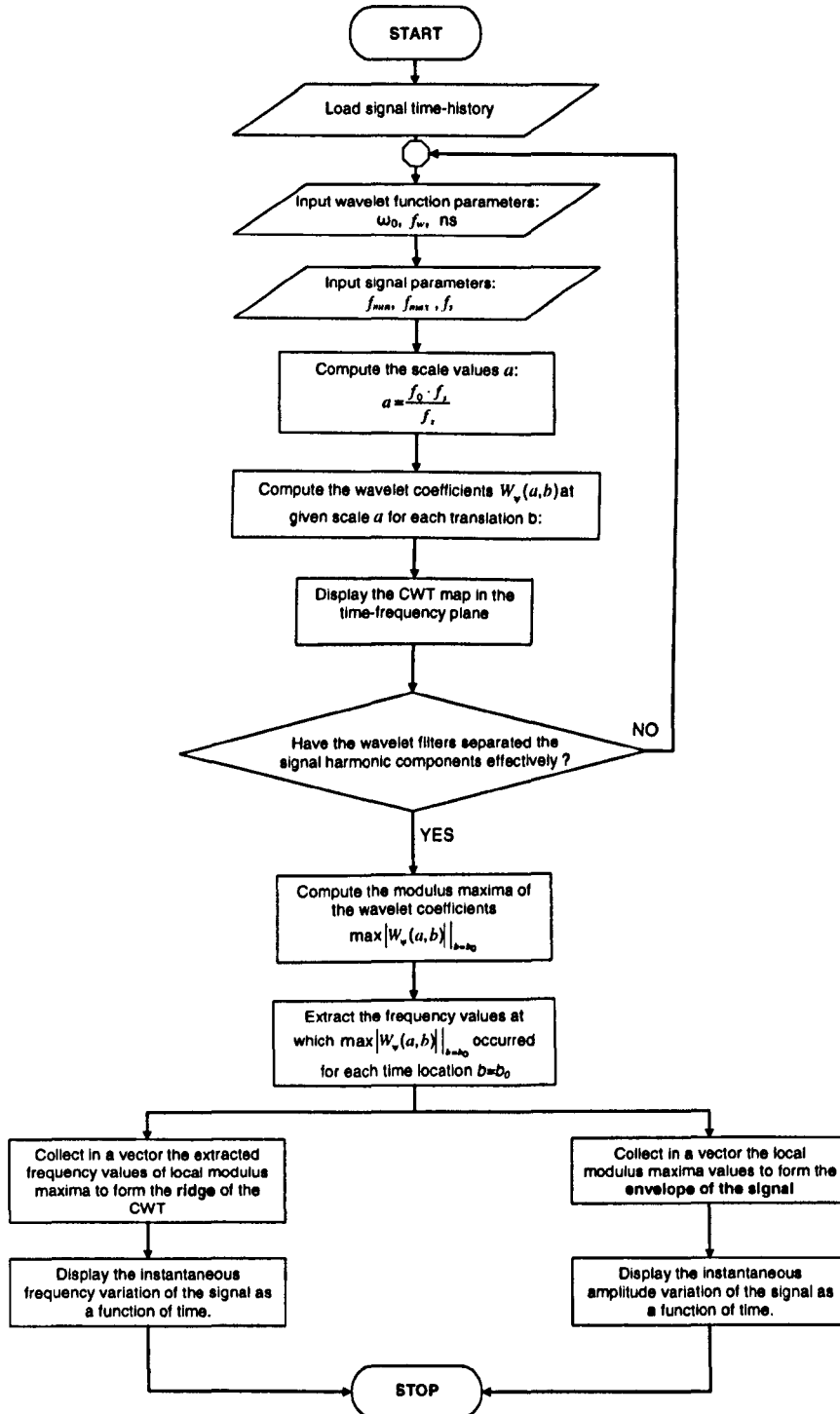
Figure 6.3 Flowchart of the algorithm used to extract the instantaneous signal variation values using the continuous wavelet transform.

6.2.4 Indices of Instantaneous Variability

In order to quantify the frequency and amplitude variation of the various harmonics present in the steering wheel idle vibration signal, a coefficient of instantaneous variation was defined for each harmonic for each fuel m:

$$CVI_m = \left(\frac{\sigma}{\mu}\right) \cdot 100\% \tag{6.1}$$

where σ and μ are the standard deviation and the mean values of the distribution of the underlying signal feature being calculated. Using the wavelet ridge, the percentage variation of the instantaneous frequency values, referred to as CVIF%, was calculated. Using the wavelet envelope, the percentage variation of the instantaneous amplitude values, referred to as CVIA%, was calculated (refer to Figure 6.1).

In order to compare the behaviours of the two test automobiles, and to compare the sensitivity of the two wavelet-based methods, an overall measure of variation was determined across all test fuels. The coefficients of variation obtained for each fuel m were averaged in order to determine an overall index of *intra-fuel* variability S_I defined as:

$$S_1\% = \text{average coefficient of variation across all fuels} = <CVI_m> \tag{6.2}$$

where the symbol < > represents the average taken across all fuels.

6.2.5 Application of the Continuous Wavelet Analysis to Steering Wheel Idle Vibration

Figure 6.4 presents a modulus intensity plot of the CWT of the engine block acceleration of the

Renault 19 relative to fuel 8. Figure 6.5(b) suggests that most of the energy in the vibration signal was centred at the firing frequency of 28 Hz, which is the second-order engine harmonic, and at the even order harmonics of the engine rotational frequency of 14 Hz. The high frequency range from 400 to 1024 Hz is characterized by the impulsive nature of combustion process, represented by a more discrete pattern, showing transitions from white (low energy) to black (high energy), indicating the periodicity of the firing process.
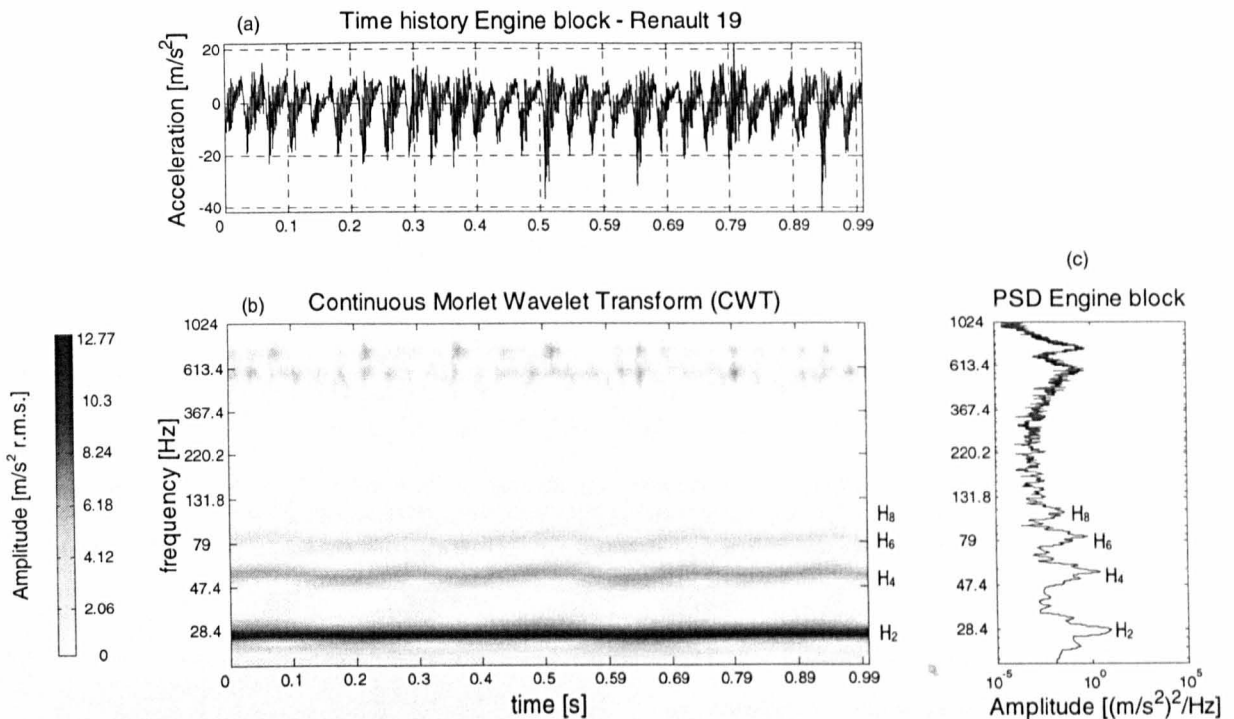
Figure 6.4   Example of continuous wavelet transform as applied to the engine block vibration measured for the Renault 19 and fuel 8.

(a) Time-history of the engine block vibration.

(b) Modulus of continuous wavelet transform obtained using the Morlet wavelet.

(c) Power spectral density of the engine block vibration.

In order to examine the sensitivity of the wavelet-based signal processing method to changes in the instantaneous characteristics of the steering wheel vibration, the ridge and skeleton of the CWT were extracted for the harmonics H_2 and H_4. It was decided to investigate these two harmonics since they were the most prominent. Table 6.1 presents the lower (f_{min}) and upper (f_{max}) frequency cutoff values used in the CWT analysis were of harmonics H_2 and H_4.

Table 6.1 Lower and upper frequency cutoff values of the bands used in the CWT analysis of the second and fourth-order engine harmonics.

Automobile model	Renault 19 1.9L		Ford Focus 1.8L	
Engine harmonic	second-order H_2 (28 Hz)	fourth-order H_4 (56 Hz)	second-order H_2 (26 Hz)	fourth-order H_4 (52 Hz)
lower frequency (f_{min})	20.5 Hz	48.5 hz	18.5	44.5 Hz
upper frequency (f_{max})	35.5 Hz	63.5 Hz	33.5	59.5 Hz

Referring to the analysis which focused on harmonic H_2, Figures 6.5(b) and 6.5(b') present the modulus of the CWT for 55 engine cycles (8 seconds of steering wheel time history) for fuel 8 for both the Renault 19 and the Ford Focus 1.8. Here, the variation of the firing frequency H_2 resulted in an almost horizontal band along the time axis, indicating low frequency variability, whereas the amplitude modulation took the form of an alternating intensity from white to black. The plots in Figure 6.5(c) and 6.5(c') show the instantaneous frequency characteristics extracted from the wavelet ridge, while Figures 6.5(d) and 6.5(d') show the envelope of the harmonic obtained from the wavelet skeleton. Figure 6.6 presents the same calculations for the continuous wavelet transform which focused on harmonic H_4, for both of the automobiles tested.
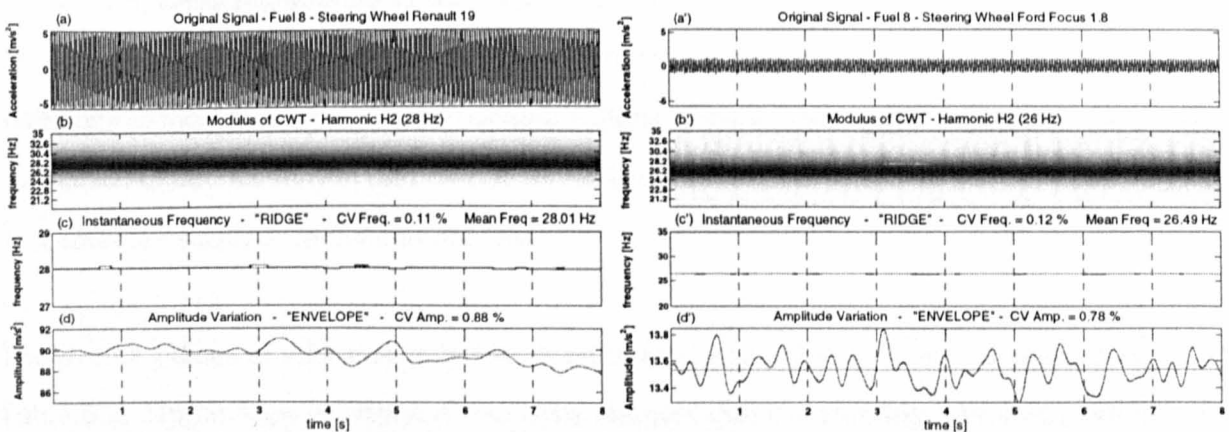
Figure 6.5 Ridge and envelope extracted from CWT analysis which focused on the harmonic H_2 of the steering wheel idle acceleration of the Renault 19 and the Ford Focus 1.8.

(a), (a') Original time history of the steering wheel signal.

(b), (b') Modulus of CWT.

(c), (c') Instantaneous frequency (wavelet ridge).

(d), (d') Instantaneous amplitude (signal envelope).
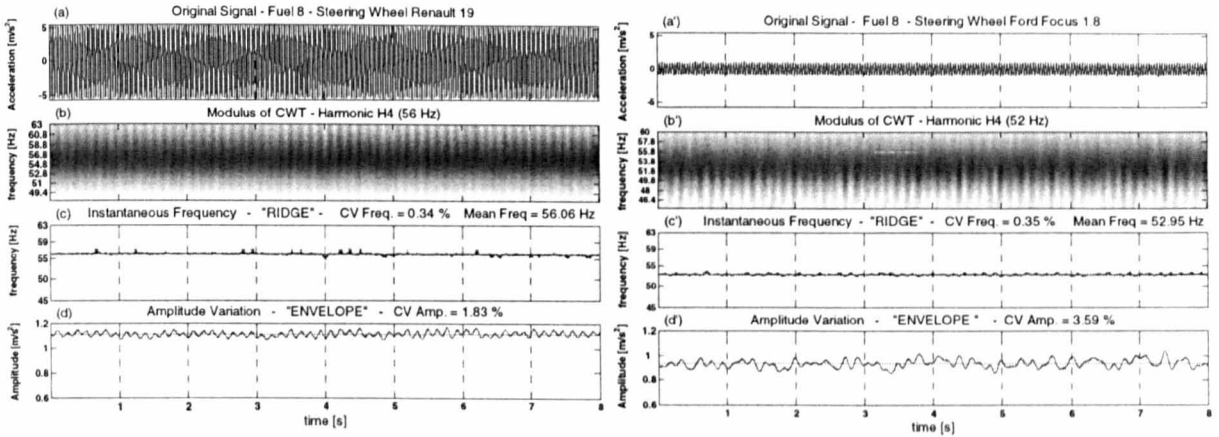
Figure 6.6   Ridge and envelope extracted from CWT analysis which focused on the harmonic H_4 of the steering wheel idle acceleration of the Renault 19 and the Ford Focus 1.8.

(a), (a') Original time history of the steering wheel signal.

(b), (b') Modulus of CWT.

(c), (c') Instantaneous frequency (wavelet ridge).

(d), (d') Instantaneous amplitude (signal envelope).

The coefficients of instantaneous variation describing the changes in ridge frequency and those describing the changes in envelope amplitude are presented in Figure 6.7 for the data set of 10 diesel fuels, arranged in order of decreasing cetane number. From Figure 6.7 it can be seen that the variations in the amplitude of the signal harmonics H_2 and H_4 were found to be higher than the variations in the frequency. The percentage variations were found larger in the case of the fourth harmonic H_4, but this may in part be due to the smaller modulus values of this harmonic, and thus to greater sensitivity to measurement noise.

The overall indices of *intra-fuel* variability S_1 calculated across the 10 diesel fuels are presented in Table 6.2. The indices of *intra-fuel* variability suggest that the steering wheel idle vibration was better described by amplitude modulation (a mean value of S_1 of 2.47 percent determined across both automobiles) than by frequency modulation (a mean value of S_1 of 0.28 percent determined across both automobiles).
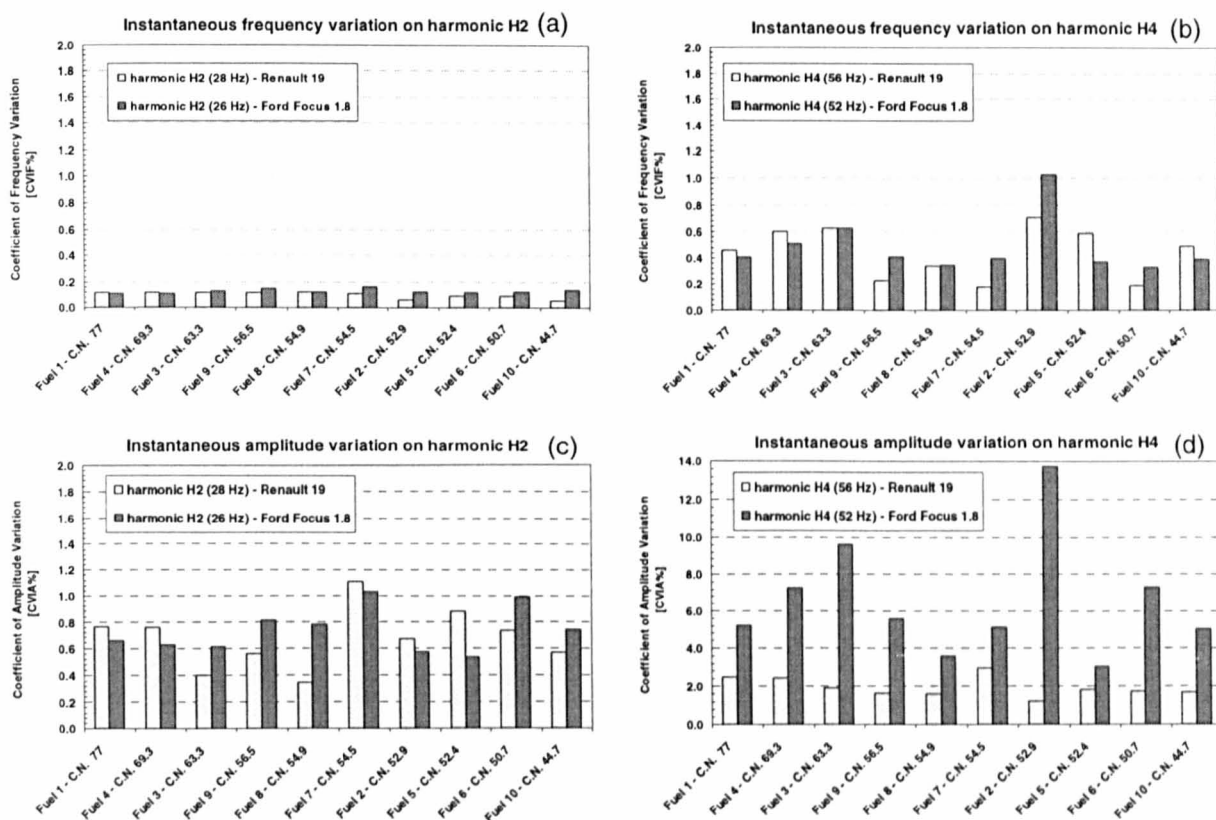
Figure 6.7 Coefficients of instantaneous variation of the steering wheel harmonics determined by means of the continuous wavelet transform for the Renault 19 and the Ford Focus 1.8 for 10 diesel fuels.

    (a)   instantaneous frequency variation (CVIF%) of the second-order engine harmonic H_2.

    (b)   instantaneous frequency variation (CVIF%) of the fourth-order engine harmonic H_4.

    (c)   instantaneous amplitude variation (CVIA%) of the second-order engine harmonic H_2.

    (d)   instantaneous amplitude variation (CVIA%) of the fourth-order engine harmonic H_4.

Table 6.2 Global index of *intra-fuel* variability S_1 (expressed as a percentage) determined by means of the continuous wavelet transform for 10 diesel fuels for steering wheel harmonics H_2 and H_4 for the Renault 19 and the Ford Focus 1.8.

Engine harmonic	second-order H_2		fourth-order H_4		Mean value of S_1 (percent)
Automobile model	Renault 19 1.9L	Ford Focus 1.8L	Renault 19 1.9L	Ford Focus 1.8L	
Instantaneous frequency variation	0.10	0.12	0.44	0.48	0.28
Instantaneous amplitude variation	0.68	0.73	1.95	6.55	2.47

In order to identify any statistically significant differences among the two automobiles, a one-factor ANOVA (Hinton, 1999) test was performed at a 95 percent confidence level using the coefficients of instantaneous variation of the steering wheel harmonics as the independent variable. Statistically significant differences between the two vehicles were found for the variation in the amplitude of both harmonics H_2 and H_4. Therefore, the extent of the variation in the amplitude of the steering wheel harmonics can be considered to be vehicle dependent. On the other hand, differences in the frequency variation between the two automobiles were found significant at a 95 percent confidence level for only the second-order harmonic H_2.

6.3 Orthogonal Wavelet Analysis

6.3.1 Choice of the Orthogonal Wavelet Decomposition Variables

For the orthogonal wavelet analysis of the steering wheel signals, the Daubechies wavelet of the 20th order (D20) was chosen as the analysing wavelet. Compared to a lower Daubechies order, the D20 wavelet is less compactly supported in time and is smoother, thus closer to a smooth harmonic function (Newland, 1994; Burrus *et al.*, 1998). This makes the D20 suitable for the analysis of deterministic signals that contain periodicity (Staszewski, 1998b). At the same time, the D20 wavelet provides acceptable frequency selectivity (Newland, 1994).

In order to adequately analyse the steering wheel vibration signals, an optimal number of wavelet levels had to be chosen so as to separate the even-order engine harmonics into different levels. Referring to the Mallat algorithm which was used for the wavelet decomposition (see section 4.5.2.3), the order of the decomposition is bounded by a maximum value that depends on the number N of the data samples in the analysed signals:

$$J_{max} = log_2(N) + 1 \tag{6.3}$$

and by a minimum value that depends on both the sampling frequency f_s of the analysed signal and the upper frequency limit of the frequency band of the wavelet detail in which the signal has

to be reconstructed. Thus, the minimum number of the orthogonal wavelet decomposition levels necessary to capture the frequency band of interest is given by:

$$J_{min} = log_2\left(\frac{f_s}{f_D}\right)$$ (6.4)

where f_D is the upper limit of the frequency band relative to the wavelet details where the reconstructed signal lies. For the current application, the steering wheel signatures of the two test automobiles contained a dominant second harmonic H_2, which had a mean frequency of 28 Hz for the Renault 19 and of 26 Hz for the Ford Focus. Thus the upper limit of the wavelet details was select to be f_D = 32 Hz, which provided the minimum level:

$$J_{min} = log_2\left(\frac{2048}{32}\right) = 6$$ (6.5)

The maximum level of the decomposition was chosen based on the knowledge that the higher the level of the decomposition, the larger the number of wavelet coefficients representing the signal finer details (Newland, 1994; Burrus *et al.*, 1998; Staszewski, 1998b). Based on the analysis presented in section 5.4.2, where 55 cycles was considered the optimal number of cycles to obtain confidence in estimating the cycle-to-cycle signal statistics, the orthogonal wavelet analysis was also applied to 55 engine cycles. Since the vibration signals were sampled at 2048 Hz, the total of 55 consecutive engine cycles was approximately equivalent to 8 seconds (2^{14} = 16384 samples) of steering wheel acceleration time history. The orthogonal wavelet transform was applied to each data set consisting of $N = 2^{14}$ = 16384 samples. Thus, a total number of J+1 = 15 levels was used. For the steering vibration data, 15 decomposition levels were sufficient to separate the engine harmonics into separate frequency bands. Table 6.3 presents the frequency bands of the 15 levels of wavelet decomposition used to analyse the steering wheel signals, which had been recorded using a sampling frequency f_s of 2048 Hz.

Table 6.3 Frequency bands of the orthogonal wavelet decomposition tree of 15 levels used to analyse the steering wheel vibration data which had been sampled at 2048 Hz.

Wavelet decomposition level	Frequency bands
Original signal	[0 - 1024 Hz]
Level 14	[512 - 1024 Hz]
Level 13	[256 - 512 Hz]
Level 12	[128 - 256 Hz]
Level 11	[64 - 128 Hz]
Level 10	[32 - 64 Hz]
Level 9	[16 - 32 Hz]
Level 8	[8 - 16 Hz]
Level 7	[4 - 8 Hz]
Level 6	[2 -4 Hz]
Level 5	[1 - 2 Hz]
Level 4	[0.5 - 1 Hz]
Level 3	[0.25 - 0.5 Hz]
Level 2	[0.125 - 0.25 Hz]
Level 1	[0.0625 - 0.125 Hz]
Level 0	[0 - 0.0625 Hz]

6.3.2 Time-Varying Auto-Covariance Analysis to Extract Cyclic Variation

From the orthogonal wavelet levels containing the harmonics of interest, the extraction of the cyclic information was achieved by means of time-varying auto-covariance analysis. In order to examine the changes in the frequency and amplitude of each harmonic on a cycle-by-cycle basis, a sliding window of finite length T equal to the average period of a working cycle Tc was employed on the selected wavelet level. For each window and for each wavelet level of interest, the time lag τ of the first-right peak neighboring the zero lag $(\tau = 0)$ provided the duration in seconds of the period of each harmonic. The estimated cycle period CP (see Figure 6.8) was then converted to frequency by means of the relation $f = \dfrac{1}{CP}$. The difference between the height of the central lobe and that of the first right side lobe (indicated in Figure 6.8 as Delta Peak Height) provided a measure of the energy of each harmonic, in units of m/s^2 r.m.s. By calculating, for each window, the cycle period CP and the delta peak height it was possible to track the changes of frequency and amplitude from cycle-to-cycle.
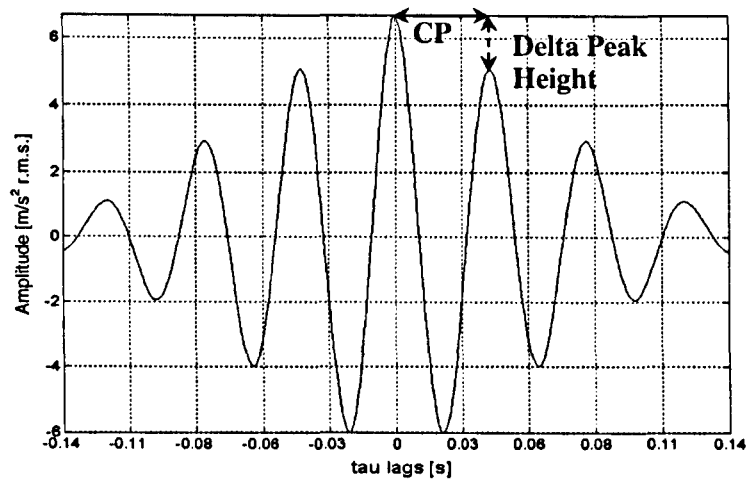
Figure 6.8 Example of auto-covariance sequence obtained over one time window Tc for the analysis of the steering wheel vibration of the Renault 19. CP indicates the cycle period.

6.3.3 Indices of Cycle-to-Cycle Variability

In order to quantify the cycle-to-cycle signal variation of the data obtained by means of the combined analysis consisting of the orthogonal wavelet transform and the TVA method, a coefficient of cycle-to-cycle variation was defined for each fuel m as:

$$CVC_m = \left(\frac{\sigma}{\mu}\right) \cdot 100\% \qquad (6.6)$$

where σ and μ are the standard deviation and the mean values of the distribution of the underlying signal feature being calculated. From the calculated cycle periods of each harmonic obtained by means of the windowed auto-covariance sequences, the percentage variation of the frequency from cycle-to-cycle, referred as CVCF%, was calculated. From the calculated peak heights of the windowed auto-covariance sequences, the percentage variation of the amplitude from cycle-to-cycle, referred as CVCA%, was calculated (refer to Figure 6.1).

As in the case of the CWT analysis, the coefficients of variation obtained for each fuel m were averaged in order to determine an overall index of *intra-fuel* variability S_1 defined as:

$S_1\%$ = average coefficient of variation across all fuels = $<CVC_m>$ (6.7)

where the symbol $<>$ represents the average taken across all fuels.

6.3.4 Application of the Orthogonal Wavelet Analysis to the Steering Wheel Idle Vibration

Figures 6.9 and 6.10 present the Daubechies 20 analysis results for each of the 15 levels of the orthogonal wavelet decomposition of the steering wheel acceleration measured along the vertical direction for the Renault 19 when using fuel 8. For the Renault 19 diesel engine at idle at 840 rpm, the fundamental frequency H_1 was 14 Hz, and the second-order engine harmonic H_2 was 28 Hz. Figure 6.9 presents the reconstruction in the time domain of the wavelet components for each level j, whereas Figure 6.10 presents the wavelet components in the frequency domain in the form of power spectral densities. The upper window of Figures 6.9 and 6.10 shows the original data used for the decomposition. From Figure 6.9 it can be seen that the orthogonal wavelet transform enhances the selection of the signal features in different frequency levels. In particular, the 15 wavelet levels revealed that most of the signal energy could be represented in the time-domain by the wavelet details components at the 10th level and at the 9th level, which correspond to the frequency bands from 32 to 64 Hz, and from 16 to 32 Hz. An examination of the power spectral densities (shown in Figure 6.10) of the wavelet detail reconstructions shows that the 9th level of the decomposition contains the second-order engine harmonic H_2, which had a mean frequency of 28 Hz.
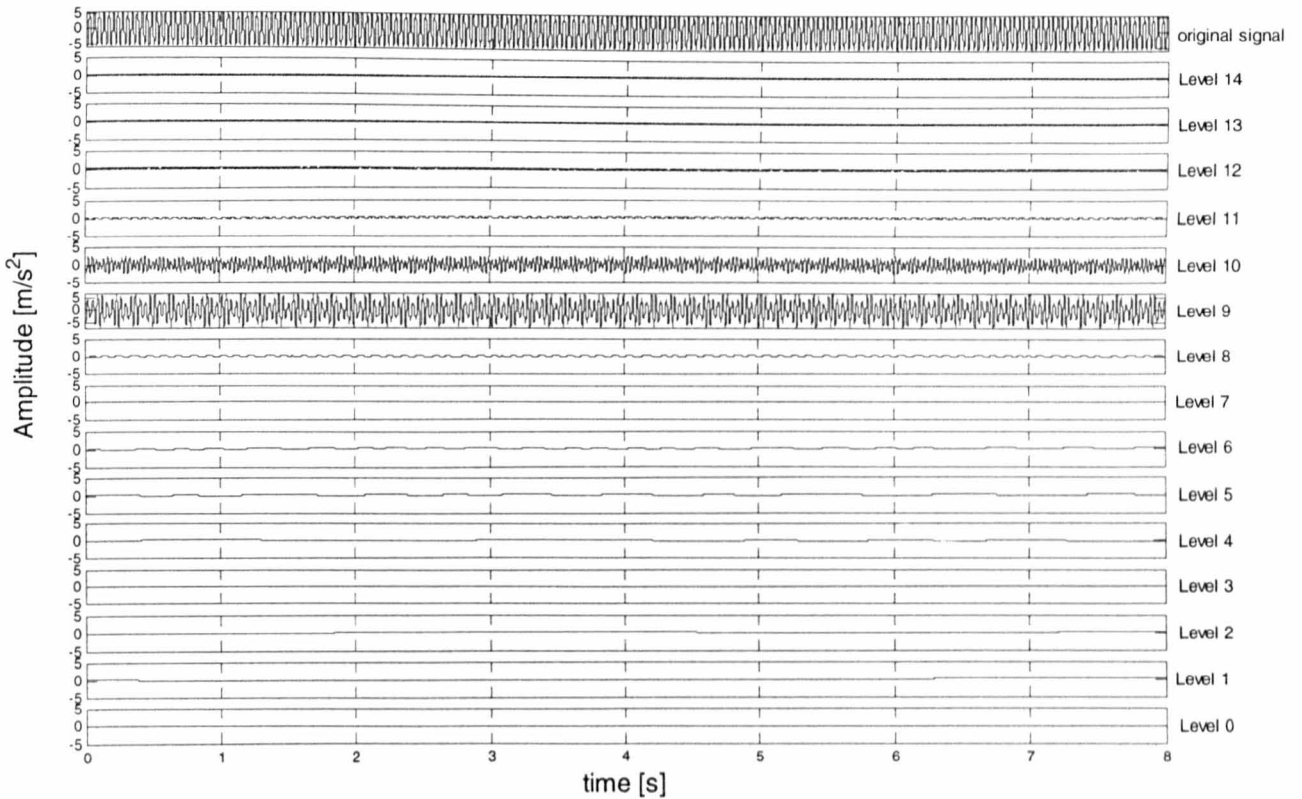
Figure 6.9   Daubechies 20 orthogonal wavelet decomposition based on 15 wavelet levels, for the steering wheel idle acceleration measured for the Renault 19 and fuel 8.
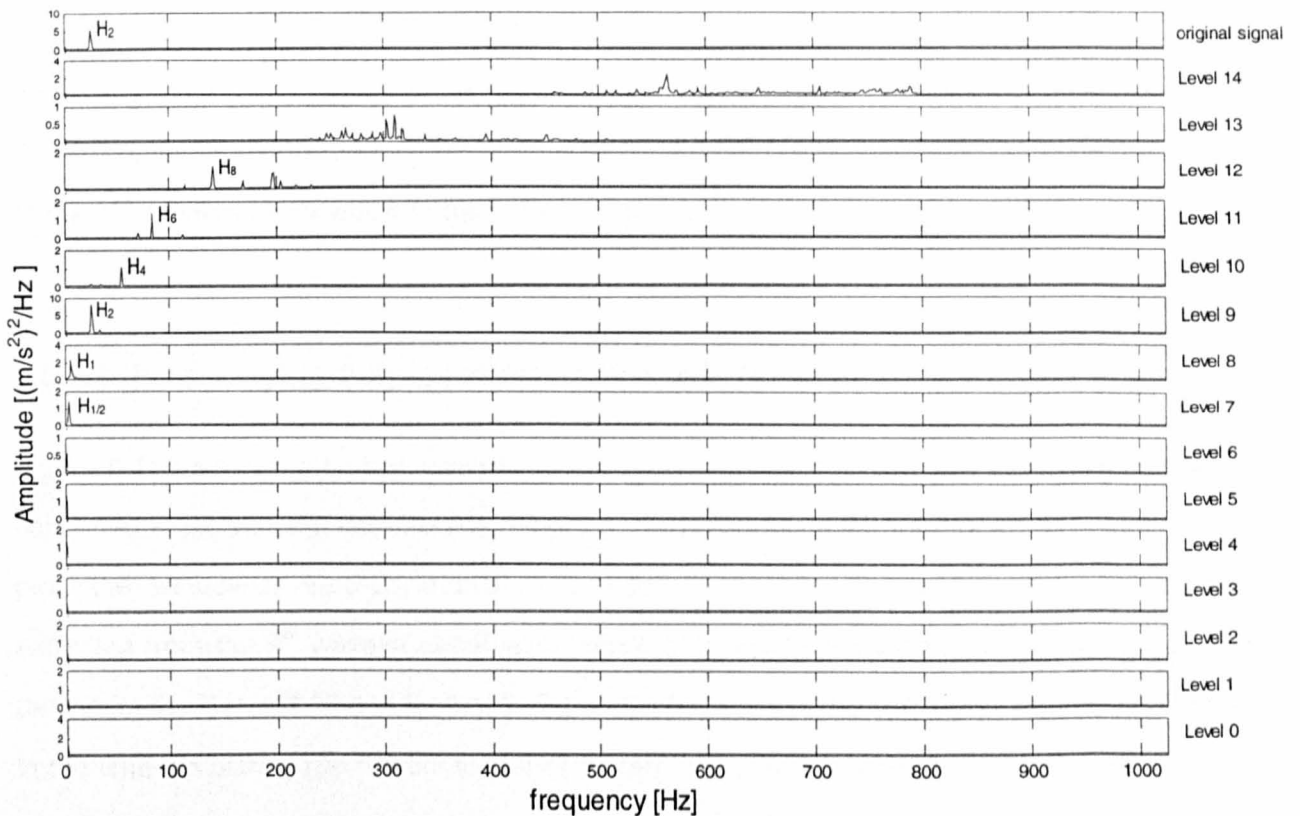
Figure 6.10   Power spectral densities of the Daubechies 20 orthogonal wavelet decomposition based on 15 wavelet levels for the steering wheel idle acceleration measured for the Renault 19 and fuel 8.

From Figure 6.10 it is possible to observe that 15 decomposition levels were sufficient to separate the steering wheel harmonics into different frequency bands. It can be seen that the fourth-order engine harmonic H_4 (56 Hz) was dominant in the 10th level of the decomposition, the sixth-order engine harmonic H_6 (84 Hz) was dominant in the 11th level, and the eighth-order engine harmonic H_8 (112 Hz) was dominant in the 12th level. Similar results were found for the orthogonal wavelet decomposition analysis of the steering wheel vibration signature of the Ford Focus 1.8. For the Ford Focus 1.8 engine at idle at 780 rpm, the fundamental frequency H_1 was 13 Hz, and the second-order engine harmonic H_2 was 26 Hz. The wavelet levels where the energy was mostly concentrated were the 9th and 10th levels of the decomposition. In particular, the second-order engine harmonic H_2 (26 Hz) was dominant in the 9th level of the decomposition, whereas the fourth-order engine harmonic H_4 (52 Hz) was dominant in the 10th level.

Based on the orthogonal wavelet decomposition of the signals from all 10 fuels and both automobiles, the 9th level and the 10th level of the wavelet detail components were selected for analysing the cyclic variation of the steering wheel signal using the time-varying auto-covariance method. The 9th level and the 10th level were chosen since they were the wavelet levels containing most of the energy of the signal. The analysis of the 9th level made it possible to track the frequency and amplitude variation of the second-order engine harmonic H_2, while the analysis of the 10th level made possible to track the variation of the fourth-order engine harmonic H_4.

6.3.4.1 Time-Varying Auto-Covariance Analysis Results

Figure 6.11 presents a typical example of the application of TVA analysis to the signal features contained in the wavelet detail levels. Figure 6.11a presents, in the form of a 3-D colour intensity plot, the windowed auto-covariance sequences in time-lag-covariance space which were extracted from the 9th wavelet detail level, which contained the second-order harmonic H_2. The data is for the Renault 19 and for fuel 8. Figure 6.11b presents the corresponding 2-D contour plot in the time-lag plane. The red contour lines at zero lag ($\tau = 0$) represents the central peaks of the

auto-covariance calculated for each window. The side lobe peaks on either side are yellow in colour, indicating lower values. From Figure 6.11a it can be seen that the amplitude of the central lobe (τ =0) changed with time, suggesting that the amplitude of the second harmonic H_2 is characterised by variation from cycle-to-cycle. Observation of Figure 6.11b suggests, instead, that there is little variation in the frequency of harmonic H_2 since the time lag of the first side lobe peaks were nearly constant as a function of time.
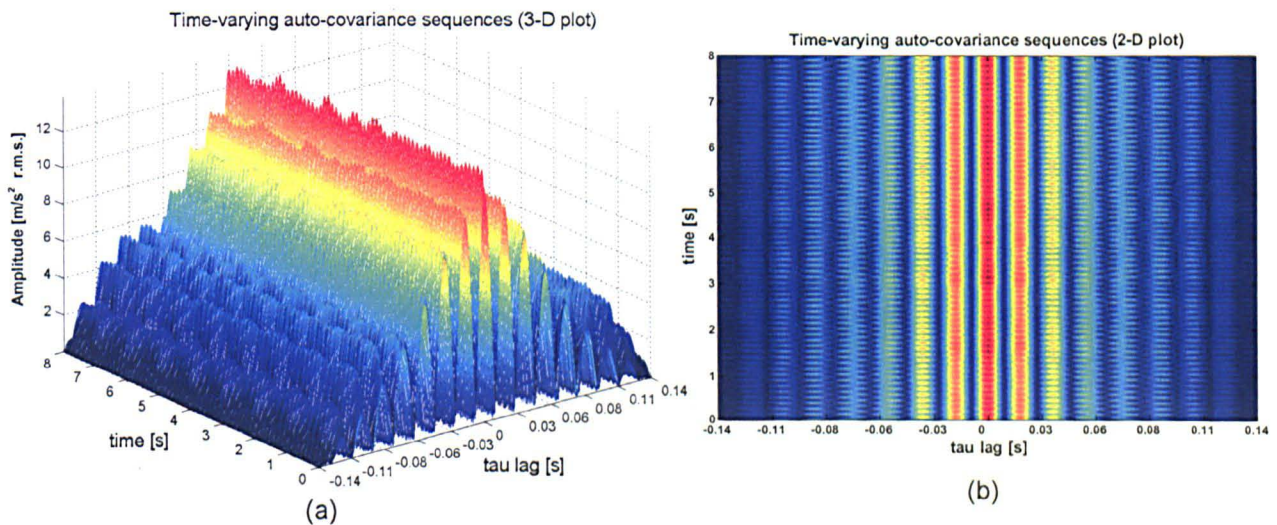
Figure 6.11   Example of the windowed time-varying auto-covariance analysis as applied to the 9th wavelet detail level of the steering wheel idle acceleration measured for the Renault 19 and for fuel 8.

(a)   three-dimensional plot in the time-lag-covariance space.
(b)   two-dimensional plot in the time-lag plane.

Figure 6.12 presents an example of the TVA analysis which was performed for each of the wavelet levels of interest. Figure 6.12a presents the steering wheel acceleration time history for the Renault 19 for fuel 8, while Figure 6.12b presents the 9th wavelet level which contained the second-order harmonic H_2. The changes in the mean firing frequency $\left(\dfrac{1}{CP}\right)$ over time are presented in Figure 6.12c, while Figure 6.12d presents the amplitude variations from cycle-to-cycle (Delta peak height). From Figure 6.12c, it can be noted that the frequency variation of harmonic H_2 was characterised by low variability (CV = 1.27 percent), being almost a constant value of 28 Hz. This is in-line with the results obtained from the CWT analysis of the same

automobile and fuel (refer to Figure 6.5). On the other hand, Figure 6.12d suggests that the periodicity of the amplitude variation is that of the half-order engine harmonic $H_{1/2}$ (7 Hz). This confirms the observation made in the frequency domain analysis of the steering wheel vibration signature (refer to section 5.4.3) where sideband components were located above and below the second harmonic H_2 of the engine rotational frequency, separated from H_2 by a modulation frequency equal to the half-order engine rotational frequency $H_{1/2}$. As in the case of the CWT analysis, the presence of amplitude modulation characterises the diesel idle vibration occurring at the steering wheel. Amplitude modulated waveforms were also found for the other fuel conditions, and for the Ford Focus automobile.
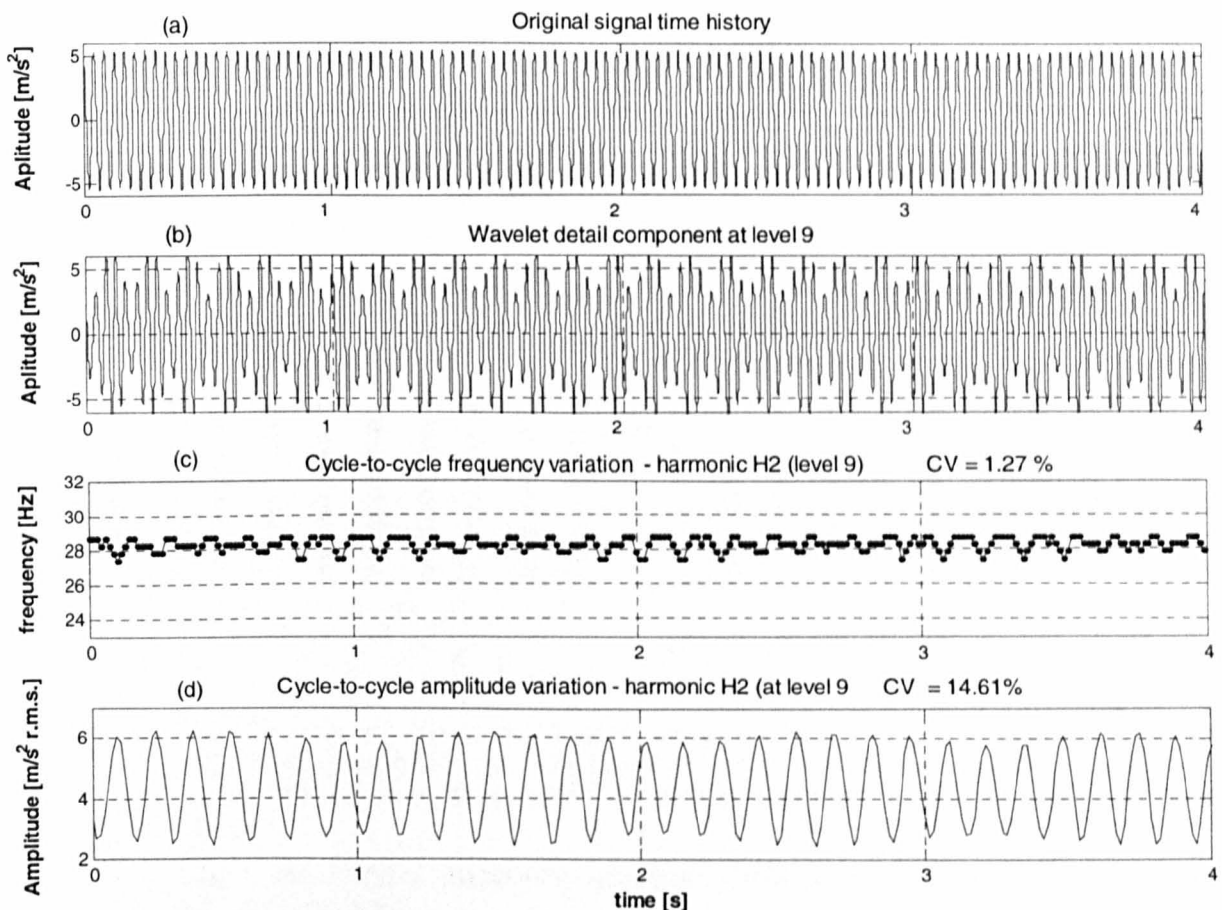
Figure 6.12 Analysis of the cycle-to-cycle statistical variation based on the 9th level of the wavelet decomposition which focused on the harmonic H_2 of the steering wheel idle acceleration of the Renault 19 for fuel 8.

(a)   original time history of the steering wheel idle acceleration.
(b)   wavelet detail component at the 9th level containing harmonic H_2.
(c)   cycle-to-cycle frequency variation.
(d)   cycle-to-cycle amplitude variation.

The coefficients of variation describing the changes in frequency, and those describing the changes in the amplitude from cycle-to-cycle, are presented in Figure 6.13 for the data set of 10 diesel fuels and for both test automobiles. The plots are relative to the analysis of the second-order engine harmonic H_2 and the fourth-order engine harmonic H_4. It can be seen that the amplitude variations from cycle-to-cycle (Figure 6.13c and d) were found to be higher than the variations associated with the changes in the frequency (Figure 6.13a and b).
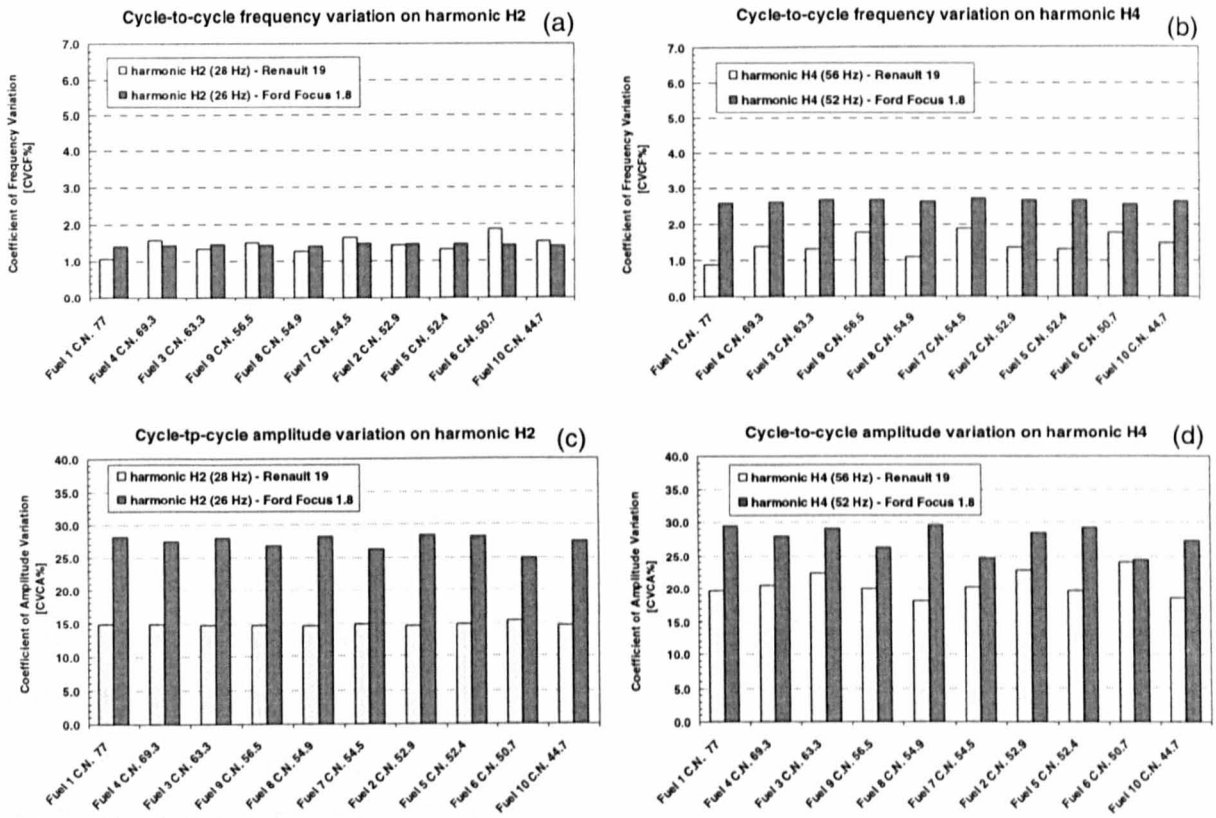
Figure 6.13   Coefficients of the cycle-to-cycle variation of the steering wheel harmonics determined by means of the orthogonal wavelet transform and the time-varying auto-covariance method for the Renault 19 and the Ford Focus 1.8 for 10 diesel fuels.

(a) Cycle-to-cycle frequency variation (CVCF%) of the second-order engine harmonic H_2.

(b) Cycle-to-cycle frequency variation (CVCF%) of the fourth-order engine harmonic H_4.

(c) Cycle-to-cycle amplitude variation (CVCA%) of the second-order engine harmonic H_2.

(d) Cycle-to-cycle amplitude variation (CVCA%) of the fourth-order engine harmonic H_4.

The overall indices of *intra-fuel* variability S_1 calculated across the 10 diesel fuels are presented in Table 6.4. As in the case of the CWT analysis, the time-varying auto-covariance analysis revealed that the steering wheel idle vibration was better described by amplitude variation (a mean value of S_1 of 22.61 percent determined across both automobiles) than by frequency variation (a mean value of S_1 of 1.73 percent determined across both automobiles).

Table 6.4 Global index of *intra-fuel* variability S_1 (expressed as a percentage) determined by means of the orthogonal wavelet transform and TVA analysis for 10 diesel fuels for steering wheel harmonics H_2 and H_4 for the Renault 19 and the Ford Focus 1.8.

Engine harmonic	second-order H_2		fourth-order H_4		Mean value of S_1
Automobile model	Renault 19 1.9L	Ford Focus 1.8L	Renault 19 1.9L	Ford Focus 1.8L	(percent)
Cycle-to-cycle frequency variation	1.45	1.43	1.42	2.63	1.73
Cycle-to-cycle amplitude variation	14.78	27.45	20.61	27.63	22.61

In order to identify any statistically significant differences among the two automobiles, a one-factor ANOVA (Hinton, 1999) test was performed at a 95 percent confidence level using the coefficients of cycle-to-cycle variation of the steering wheel harmonics as the independent variable. Statistically significant differences between the two vehicles were found for the variation in the amplitude of both harmonics H_2 and H_4. Therefore, the extent of the variation in the amplitude of the steering wheel harmonics can be considered to be vehicle dependent. On the other hand, differences in the frequency variation between the two automobiles were found significant for only the fourth-order harmonic H_4.

6.4   Comparison of Signal Processing Method Performance

A comparison of the sensitivity of the two wavelet-based signal processing methods used for quantifying the statistical variation in the steering wheel signals was made in terms of the overall and mean indices of *intra-fuel* variability S_1% calculated for the H_2 and H_4 harmonics for both automobiles. Table 6.5 presents the results obtained with the continuous wavelet transform

analysis and the combined analysis consisting of the orthogonal wavelet transform and of the time-varying auto-covariance method.

Table 6.5 Comparison of the indices of *intra-fuel* variability S_1 (expressed as a percentage) for the steering wheel harmonics H_2 and H_4 based on the results of the CWT and TVA analysis for 10 diesel fuels for the Renault 19 and Ford Focus 1.8.

Signal feature extracted	Engine harmonic	second-order H_2		fourth-order H_4		Mean value of S_1 (percent)
	Method of analysis	Renault 19 1.9L	Ford Focus 1.8L	Renault 19 1.9L	Ford Focus 1.8L	
Frequency variation	Continuous wavelet transform (CWT)	0.10	0.12	0.44	0.48	0.28
	Time-varying auto-covariance (TVA)	1.45	1.43	1.42	2.63	1.73
Amplitude variation	Continuous wavelet transform (CWT)	0.68	0.73	1.95	6.55	2.47
	Time-varying auto-covariance (TVA)	14.78	27.45	20.61	27.63	22.61

The wavelet-based TVA method produced larger values of *intra-fuel* variability, and thus appears to be the most sensitive measure of idle irregularity. The greater sensitivity may be attributable to the fact that the TVA method was computed as a running average on a cycle-to-cycle basis, offering an efficient representation of the changes in the total combustion energy from one engine cycle to another. Further, as an averaged value, the variation in the TVA would also be expected to be more robust against electrical and other forms of measurement noise by which the CWT analysis can be affected (Delprat *et al.*, 1992; Bellizzi *et al.*, 2001).

The analysis of the cycle-to-cycle amplitude variation, by means of the orthogonal wavelet transform and the TVA method, determined higher *intra-fuel* variation values. A mean value of *intra-fuel* variability S_1% of 22.61 percent, determined across both automobiles, suggested that the variation in the steering wheel idle vibration could be best characterized as due to more slowly developing differences which occurred across complete thermodynamic engine cycles rather than

by changes in the instantaneous signal character obtained by means of the CWT method (a mean value of $S_1\%$ of 2.47 percent determined across both vehicles). In addition, both methods provide an indication of the nature of diesel idle vibration by showing that the vibration data is more affected by amplitude variation (a mean value of $S_1\%$ of 12.54 percent between the two methods) than frequency variation (1.01 percent) for the 10 diesel fuels and the two automobiles tested.

6.5   Summary

The time-frequency wavelet-based analysis of Chapter 6 was performed in order to establish whether the variation in the diesel steering wheel idle vibration could be best characterized as due to changes in the instantaneous signal character caused by the rapid variation in the combustion peaks, or due instead to more slowly developing differences which occur across complete thermodynamic engine cycles. Both the continuous wavelet transform and the orthogonal wavelet transform were used to identify which of the two wavelet methods provided the most sensitive tool for analysing steering wheel idle vibration. The calculation of the ridge and skeleton of the continuous wavelet transform was used for quantifying the instantaneous frequency and amplitude variation of the engine-order harmonics as a function of time. On the other hand, the orthogonal wavelet transform combined with the time-varying auto-covariance analysis was used for separating the harmonic components of the steering wheel idle vibration signature into independent frequency bands, and for extracting the signal features for each frequency band of interest on a cycle-to-cycle basis.

The continuous wavelet transform used for all the calculations the Morlet wavelet function, with a center frequency $\omega_0 = 15$ rad/s which provided good time-frequency localization and separation of the different engine order harmonics on the time-frequency plane of the CWT map. For the orthogonal wavelet analysis of the steering wheel signals, the Daubechies wavelet of the 20th order (D20) was chosen as the analysing wavelet to provide acceptable frequency selectivity. For

the steering wheel idle vibration, 15 levels of the orthogonal wavelet decomposition were found to be sufficient to separate the different engine order harmonics into individual frequency bands.

Both the continuous wavelet transform and the orthogonal wavelet transform were applied to 8 seconds of steering wheel acceleration time history, which included 55 complete thermodynamic engine cycles. The analysis of the instantaneous and cyclic variation of the signal properties was focused on the second-order H_2 and fourth-order H_4 engine harmonic since these components were the most prominent. In order to quantify both the instantaneous signal variation and the cycle-to-cycle variation of the harmonic components present in the steering wheel signals, a set of coefficients of variation were defined and calculated for each fuel type. When averaged across all ten reference fuels, an overall index of intra-fuel variability $S_1\%$ was determined in order to compare the behaviours of the two test automobiles and to assess the sensitivity of the two wavelet-based methods.

The time-frequency wavelet-based analysis has confirmed that the diesel idle vibration occurring at the steering wheel is better described in terms of amplitude variation than in terms of frequency variation. The periodicity of the amplitude fluctuation was found to be that of the half-order engine harmonic $H_{1/2}$. The coefficients of variation describing the changes in the amplitude were found to be greater (a mean value of 12.54 percent between the two methods) than those describing the changes in the frequency (a mean value of 1.01 percent between the two methods) for all fuels and both automobiles tested. Statistically significant differences of the global index of *intra-fuel* variability $S_1\%$ calculated between the two vehicles were found for the variation in the amplitude of both harmonics H_2 and H_4. Therefore, the extent of the variation in the amplitude of the steering wheel harmonics was considered to be vehicle dependent.

The sensitivity of the time-frequency analysis based on the continuous wavelet transform was compared to that of the combined analysis consisting of the orthogonal wavelet transform and of the time-varying auto-covariance method. The wavelet-based TVA method produced larger

values of *intra-fuel* variability, and thus appears to be the more sensitive measure of idle irregularity. A mean value of *intra-fuel* variability $S_1\%$ of 22.61 percent, determined for the cycle-to-cycle amplitude variation, suggested that the variation in the steering wheel idle vibration can be best characterized as due to more slowly developing differences between complete thermodynamic engine cycles rather than by changes in the instantaneous signal character obtained by means of the CWT method (a mean value of $S_1\%$ of 2.47 percent, refer to Table 6.5).

Chapter 7

Human Subjective Response to Amplitude-Modulated Steering Wheel Vibration

7.1   Introduction

The digital signal processing analysis presented in the previous chapters identified amplitude modulation as the principal physical characteristic of the steering wheel vibration of automobiles when at idle. In the case of a four-cylinder four-stroke engine at idle, amplitude modulation occurs due to the action of the half-order engine harmonic on the second-order engine harmonic.

The experimental testing activities described in this chapter were performed in order to investigate the growth in the human subjective response to amplitude-modulated vibration stimuli of the type caused by a four-cylinder diesel engine idle in passenger cars. The objective of the analysis was to develop a model of the human hand-arm perception of the diesel idle vibration as perceived through the automotive steering wheel. Due to the lack of available data in the scientific

literature regarding the human response to amplitude-modulated vibration of the type caused by engine idle, it was decided to perform a systematic analysis by modelling the diesel idle vibration which occurs at the steering wheel using analytically defined amplitude-modulated stimuli. Analytical signals were used in the experiments which are described in this chapter because the analysis performed in the previous chapters established that the steering vibration signals were mostly characterised by amplitude modulation. By defining analytic test signals it was possible to reduce the number of statistical parameters which describe the test stimuli to only one, the modulation depth m as defined in section 7.2.

Due to the possible bias which is introduced by the choice of the psychophysical test protocol (Gescheider, 1997; Laming, 1997), two psychophysical studies, each consisting of two experiments, were performed. Four experimental conditions, determined by the combination of two semantic descriptors and two test methods, were used to examine the human subjective response to steering wheel idle vibration. In this research, the semantic descriptors of "unpleasantness" and "roughness" were chosen as metathetic (Stevens, 1986) descriptors for judging the quality of the stimulus. The semantic attribute of unpleasantness was chosen as descriptor since it has been found to be used by experienced drivers to describe vehicle idle quality (Hoard and Rehagen, 1997). The sensory attribute of roughness was chosen based on Wiesenberger's experiments where the amplitude-modulated stimuli were frequently reported as feeling "rougher" than the unmodulated stimuli (Weisenberger, 1986). Experiment I and II of study 1 used the method of Thurstone's Law of Comparative Judgment (Thurstone, 1959) which provided an indirect scaling method. Experiment III and IV of study 2 used the category-ratio Borg CR-10 scale (Borg, 1998) which provided a direct scaling method. The paired comparison procedure was chosen because it provides accurate sensory distances from one stimuli to the next on the psychophysical scale (Biermayer *et al.*, 2001; Pielemeier *et al.*, 2001). Performing only a comparative judgement the test subject performs one of the lowest possible forms of cognitive processing, reducing the influence of external subjective factors (Nunnally and Bernstein, 1994). In contrast, direct scaling procedures involve a conscious imposition of the subjective personal experience in a rating task (Zwislocki, 1991). The direct scaling method of the

category-ratio Borg CR-10 scale was chosen because it affords the opportunity to measure perceived sensations on a common scale by using semantic labels for anchoring numbers, thus avoiding the problem of the response bias which occurs with the competing direct methods such as magnitude estimation or ratio scaling (Borg and Borg, 1992).

In the research presented in this thesis, only one-axis of vibration has been considered when studying the human subjective response to steering wheel vibration. The vertical direction along the tangent to the steering wheel has been chosen since research (Pak *et al.*, 1991; Schröder and Zhang, 1997) has shown that the vertical vibrations of the steering wheel best correlate with the subjective ratings of the drivers, especially in the frequency range from 30 to 90 Hz. In addition, vibration measurements performed in automobiles under representative driving conditions (Peruzzetto, 1988; Schröder and Zhang, 1997; Amman *et al.*, 2001; Giacomin *et al.*, 2004) have shown that acceleration magnitudes at the steering wheel along the vertical direction are normally greater than those along either the fore-and-aft or the lateral direction. The signal processing analysis described in chapters 5 and 6 of this thesis confirm this finding for the case of diesel idle vibration.

7.2   Steering Wheel Reference Stimuli

The choice of the reference stimuli for the study of the human subjective response to steering wheel idle vibration was based on the nature of the diesel idle stimuli, as revealed by the digital signal processing analysis of the steering wheel accelerations measured for the IDI-engined Renault 19 and the DI-engined Ford Focus 1.8. Of the two test automobiles, the acceleration time histories recorded from the DI-engined Ford Focus 1.8 were chosen as the reference stimuli since this type of automobile was characterised by a modern engine technology compared to the IDI-engined Renault 19, and thus more representative of current automobiles at idle. With respect to the problem of the human response to vibration stimuli, the DI-engined Ford Focus 1.8 presented higher coefficients of *intra-fuel* variability ($S_1\%$) of the signal statistics (refer to Table 5.7 and Table 6.5), and higher modulation sideband frequencies in the steering wheel power spectral

densities (refer to Figure 5.20). Therefore, the DI-engined Ford Focus 1.8 stimuli were chosen

due to their greater statistical richness. The nature of the steering wheel idle vibration which

occurred with the DI-engine Ford Focus 1.8 is illustrated in Figure 7.1. Figure 7.1 presents both

the time histories and the frequency spectra obtained with a fuel which had a high cetane number

(fuel 9, C.N. 56.5) and with a fuel which had a low cetane number (fuel 10, C.N. 44.7). Amplitude

modulation is evident in the form of sidebands about the second-order engine harmonic H_2 at

approximately 26 Hz. Amplitude modulation of this form can be conveniently and compactly

represented by means of the modulation depth parameter m (Hartmann, 2000). The modulation

depth is defined as the amount of change in the amplitude of the waveform, expressed as the

proportion:

$$m = \frac{(A_{max} - A_{min})}{(A_{max} + A_{min})} \tag{7.1}$$

where A_{max} is the maximum amplitude of the signal and A_{min} is the minimum amplitude. Thus a

value of $m = 1.0$ describes an amplitude variation of the carrier sinusoid from zero to its maximum

value, whereas a value of $m = 0.0$ describes the unmodulated version of the carrier signal (i.e. a

sine wave).
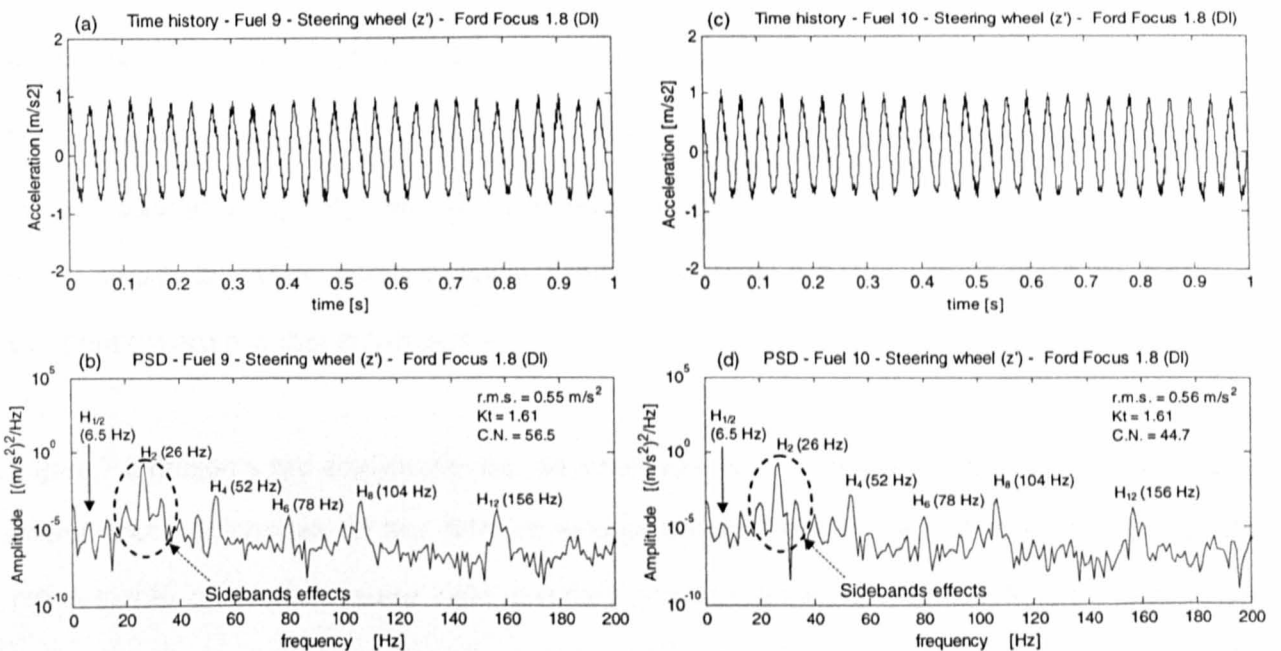
Figure 7.1 Steering wheel idle vibration along the vertical (z') direction for the Ford Focus 1.8 for
two different fuels.

(a), (b) time history and PSD obtained for fuel 9 (C.N. 56.5).
(c), (d) time history and PSD obtained for fuel 10 (C.N. 44.7).

At frequencies below 40 Hz, which is the frequency range where most of the steering wheel vibrational energy occurred, all the measured idle vibration signals can be best described as sinusoidal amplitude modulated waveforms of the form:

$$A(t) = A_0 \left[1 + m\ sin(2\pi f_m\ t + \varphi)\right] \cdot sin(2\pi f_c\ t + \theta) \tag{7.2}$$

where $A(t)$ is the instantaneous amplitude of the signal, A_0 is the amplitude of the carrier signal, m is the modulation depth, f_m is the modulation frequency, f_c is the carrier frequency, t is the time increment, and φ and θ are the phases of the modulating and carrier signals respectively. Using trigonometry (Hartmann, 2000), the function $A(t)$ can be rewritten as a sum of sines and cosines of the form:

$$A(t) = A_0\ sin(2\pi\ f_c\ t) + A_0\ \frac{m}{2}\left[cos\ 2\pi(f_c - f_m)\ t\right] - A_0\ \frac{m}{2}\left[cos\ 2\pi(f_c + f_m)\ t\right] \tag{7.3}$$

The resulting waveform of Eq. (7.3) has a frequency spectrum consisting of a main component at the carrier frequency f_c, and modulation sideband components that are above and below the carrier, displaced by the modulation frequency f_m. In an amplitude-modulated waveform the upper sideband at $(f_c + f_m)$ and the lower sideband at $(f_c - f_m)$ are characterised by having the same amplitude. When the modulation depth m is equal 1.0, the amplitude of the sideband components are half that of the carrier A_0.

Figure 7.2 presents two analytically defined amplitude-modulated waveforms and their associated power spectral densities for two different modulation depths $m = 0.2$ and $m = 1.0$, while all the other signal parameters were held constant (carrier amplitude $A_0 = 0.5$ m/s^2, modulation frequency $f_m = 7$ Hz, carrier frequency $f_c = 28$ Hz, phases φ and θ equal to zero). From the

r.m.s. values provided in Figure 7.2 it can be seen that the increase of the modulation depth produced an increase in the average energy of the signal. For amplitude-modulated signals, the increase in root mean square amplitude has been shown (Viemeister, 1979; Hartmann, 2000) to be equal to

$$\left(1+\frac{m^2}{2}\right)E_0 \tag{7.4}$$

where E_0 is the average energy of the unmodulated version of the carrier signal ($m = 0.0$), defined as the r.m.s. acceleration amplitude of a sinusoidal motion of peak amplitude A_0:

$$E_0 = a_{r.m.s.} = \frac{A_0}{\sqrt{2}} \tag{7.5}$$
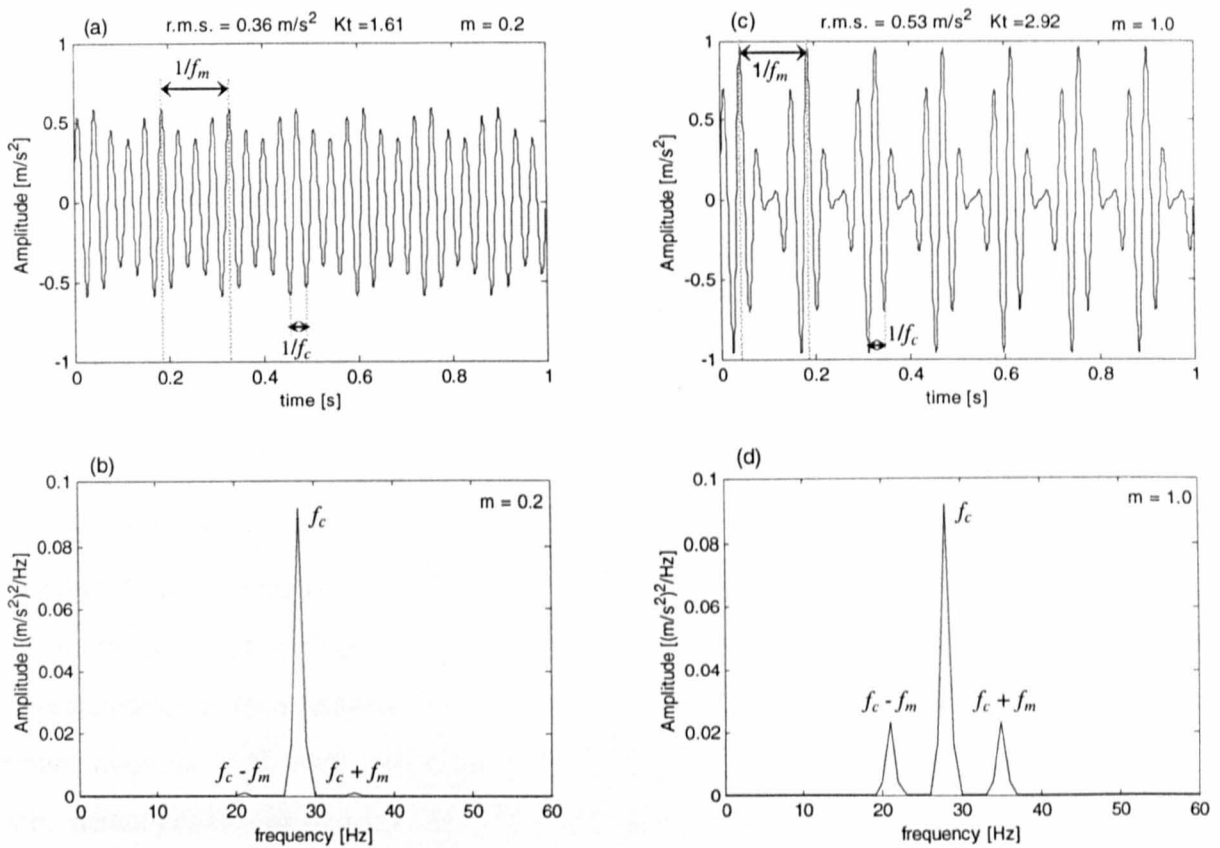
Figure 7.2 Analytically defined amplitude-modulated waveforms.

(a), (b)   time domain and frequency domain representation of a weakly modulated condition ($m = 0.2$).

(c), (d)   time domain and frequency domain representation of a strongly modulated condition ($m = 1.0$).

When investigating the growth in the human subjective response to amplitude-modulated stimuli, it is therefore necessary to compensate for the increased total energy. Failure to control the energy of the stimuli would lead to a situation where the human response was caused by both the overall signal energy and the actual shape of the waveform. In the research described here, signal energy was normalised so as to isolate the signal waveform as the single factor being investigated.

For the case of the Ford Focus 1.8, which is a four-cylinder diesel engine at idle at 780 rpm, the firing frequency harmonic (H₂) of 26 Hz was the carrier frequency f_c and the half-order engine harmonic (H₁/₂) of 6.5 Hz was the modulation frequency f_m. The r.m.s. acceleration chosen for the unmodulated version of the sinusoidal carrier signal was taken to be the r.m.s. value of the peak corresponding to the frequency harmonic H₂ of 26 Hz in the power spectral density of the steering wheel idle vibration. From the modulus value of the steering wheel PSD, the root mean square amplitude for the test stimuli was determined as:

$$a_{r.m.s.} = \sqrt{PSD(f) \cdot \Delta f}$$ (7.6)

where $PSD(f)$ is the amplitude of the underlying power spectral density of the harmonic in question and Δf is the frequency resolution of the spectrum. The r.m.s. acceleration value chosen for normalising the various test stimuli was taken to be the mean r.m.s. value obtained for the ten different fuel conditions. Across the ten different fuel conditions, the r.m.s. accelerations corresponding to the amplitude of the harmonic at 26 Hz ranged from 0.31 to 0.43 m/s², with an mean value of 0.41 m/s², as presented in Table 7.1. The value of the amplitude of the unmodulated carrier signal used for the test stimuli was thus taken to be

$$A_0 = \sqrt{2} \times a_{r.m.s.} = \sqrt{2} \times 0.41 = 0.58 \, m/s^2$$ (7.7)

Table 7.1   PSD amplitudes of the 26 Hz second harmonic H_2, equivalent H_2 r.m.s. amplitude and r.m.s. amplitude for the complete steering wheel vibration signal for the ten test fuels.

Fuel	PSD(f) amplitude at 26 Hz [(m/s^2)^2/Hz]	r.m.s. at 26 Hz [m/s^2]	Global r.m.s. [m/s^2]
Fuel 1 - C.N. 77	0.164	0.41	0.54
Fuel 4 - C.N. 69.3	0.158	0.40	0.53
Fuel 3 - C.N. 63.3	0.174	0.42	0.55
Fuel 9 - C.N. 56.5	0.169	0.41	0.55
Fuel 8 - C.N. 54.9	0.186	0.43	0.57
Fuel 7 - C.N. 54.5	0.184	0.43	0.57
Fuel 2 - C.N. 52.9	0.186	0.43	0.58
Fuel 5 - C.N. 52.4	0.175	0.42	0.56
Fuel 6 - C.N. 50.7	0.094	0.31	0.41
Fuel 10 - C.N. 44.7	0.176	0.42	0.56
Mean value	0.167	0.41	0.54

7.2.1 Choice of Acceleration Test Signals

Diesel engine idle vibration occurring at the steering wheel of automobiles was simulated by means of sinusoidal amplitude modulated acceleration time histories using the mathematical expression of Eq. (7.2). In the experiment the test stimuli were chosen so as to represent a four cylinder diesel engine at idle at 780 rpm. The carrier frequency was therefore taken to be the second-order engine harmonic H_2 of 26 Hz, and the modulation frequency was taken to be the half-order engine harmonic $H_{1/2}$ of 6.5 Hz. The test stimuli were thus characterised by amplitude modulation sidebands at 19.5 Hz and 32.5 Hz as defined by Eq. (7.3).

In order to study the growth in the human subjective response to amplitude-modulated vibration stimuli as a function of the modulation depth m, a set of seven acceleration time histories were

defined which had seven different values of modulation depth m equal to 0.0, 0.1, 0.2, 0.4, 0.6,

0.8, and 1.0. Since the average energy of a signal is increased when the carrier is modulated, all

the seven stimuli were scaled to have equal r.m.s. acceleration amplitude in order to eliminate

changes in overall perceived intensity due to changes in modulation depth. In this way, the

modulation depth parameter m represented the only test parameter. The reference r.m.s.

acceleration value chosen was 0.41 m/s², which was obtained by averaging all of the automobile

idle test data, as discussed in section 7.2.

The duration of each test stimuli was chosen to be 4 seconds based on the knowledge that the

tactile system of the human hand does not present temporal integration properties below

approximately 40 Hz (Gescheider et al., 1994) and based on the results of experiments reported

by Miwa (1968) who suggested that for vibration in the range 2 to 60 Hz there is no further

increase in discomfort sensation for stimuli durations greater than approximately 2 seconds. In all

the experiments, the phase of both the carrier and the modulating waves were chosen equal to

zero (φ =0, θ = 0) for simplicity. In addition to the r.m.s. acceleration, the vibration dose value

(VDV) was also calculated for all the seven signals by integrating the fourth power of the

acceleration $A(t)$ of Eq. (7.2) as defined in British Standard BS 6841 (1987):

$$VDV = \left[\int_0^T A^4(t)\, dt \right]^{1/4} \qquad\qquad (7.8)$$

where T is the duration over which the VDV value is measured and $A(t)$ is the instantaneous

acceleration amplitude of the signal. The VDV value provides a cumulative measure of the

vibration exposure, and being a fourth power method, it accounts more accurately for the greater

effect on human response to vibration of high amplitude peaks which occur in the time history

(Griffin, 1990). Figure 7.3 presents the seven time history test signals used in all psychophysical
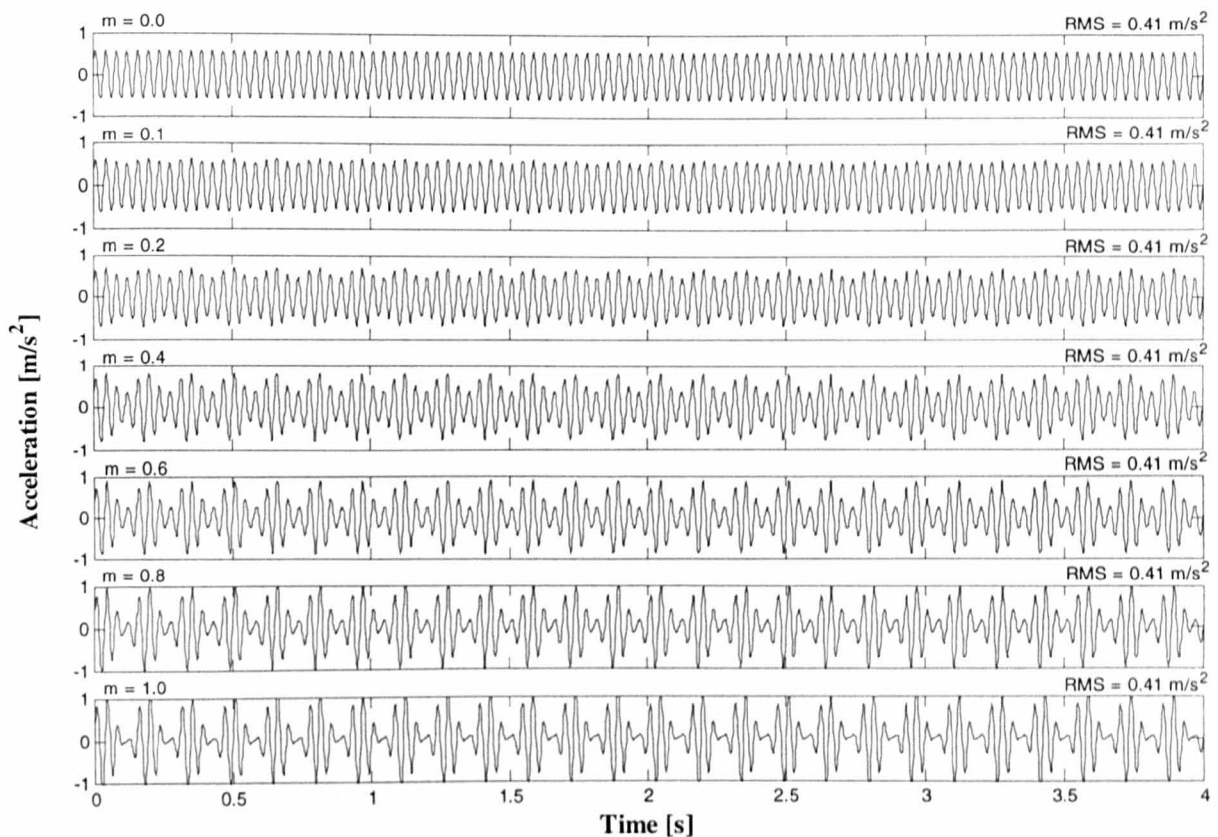
experiments.

Figure 7.3   Test signals used in all psychophysical experiments.

7.3   Experimental Apparatus

7.3.1   Test Facility Specification

The test facility adopted in this study for applying rotational vibration to a seated test subject used an existing steering wheel test rig, shown in Figure 7.4a, which was built in the Perception Enhancement Systems laboratory at the University of Sheffield. A schematic representation of the steering wheel test rig and of the associated signal conditioning and data acquisition systems is shown in Figure 7.4b. The test rig consisted of two steel plates (800 mm x 400 mm and 25 mm thickness) welded onto seven columns consisting of square section steel tube (10 mm x 10 mm and 5 mm wall thickness). The test rig design reproduced the sitting posture of a small European automobile.

(a)   (b)
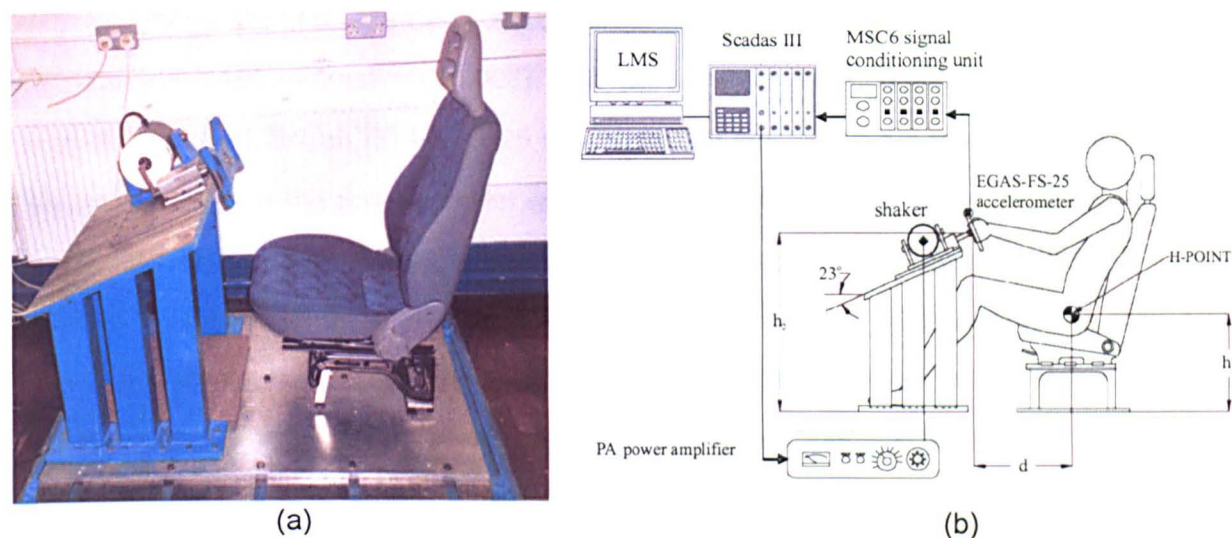
Figure 7.4   Steering wheel rotational vibration test rig.
                        (a) photograph of the steering wheel test rig
                        (b) schematic representation of the test rig and associated electronics.

The rotational steering system consisted of a rigid 325 mm diameter aluminium wheel connected to a steel shaft which was mounted onto two SKF precision bearings encased in a square steel casing and preloaded at 1.5 Nm torque. The steering wheel consisted of a 5 mm thick central plate with 3 mm thick cylinders welded at the extremities. The steering wheel was made of aluminium in order to obtain a first natural frequency greater than 300 Hz. The steering wheel had a mass of 1.22 Kg and a natural frequency of 410 Hz. The use of a rigid steering wheel guaranteed that no vibration attenuation occurred before reaching the hand-arm system. In contrast, the use of a real steering wheel would have compromised the analysis in the frequency range of the vibration test stimuli since vibration modes of the wheel itself are normally found in the frequency range from 20 to 60 Hz (Kim *et al.*, 1985; Pottinger and Marshall, 1986; Fujikawa, 1988; Demers, 2001), thus sometimes coinciding with the engine firing frequency when at idle (20-28 Hz).

Rotational vibration was applied by means of a G&W V20 electrodynamic shaker, which was connected to the shaft by means of a steel stinger rod, and which was driven by a PA100 amplifier (Gearing and Watson Electronics Ltd, 1995). Bench control and data acquisition were

performed by means of a LMS Cada-X 3.5 E software and a 12-channel Difa Systems Scadas III front-end unit (LMS International, 2002). The acceleration obtained at the steering wheel was measured using an Entran EGAS-FS-25 accelerometer located on the top left side of the wheel. The specifications of the accelerometer and of the vibration equipment are provided in Appendix A. The acceleration was measured in the tangential direction. The accelerometer signal was amplified by means of an Entran MSC6 signal-conditioning unit (Entran Devices Inc., 1991). Table 7.2 presents the main geometric dimensions of the test rig, which were based on average data taken from a small European automobile. The car seat was directly taken from a 1997 Fiat Punto and was fully adjustable in terms of horizontal position and back-rest inclination as in the original vehicle. Test rig usage conformed to the health and safety recommendations of British Standards Institution BS 7085 (1989).

Table 7.2 Geometric dimensions of the steering wheel rotational vibration test rig.

Geometric Parameter	Value
Seat H point height from floor, h_1	275 mm
Horizontal distance adjustable from H point to steering wheel hub centre, d	390-550 mm
Steering wheel hub centre height above floor, h_2	710 mm
Steering column angle with respect to floor	23 °
Steering wheel handle diameter	12.5 mm
Steering wheel diameter	325 mm

7.3.2 Accuracy of Test Facility Signal Reproduction

A set of calibration tests were performed so as to check the nominal vibration sensitivity of the bench. The tests were designed so as to assess the performance of the whole vibration instrument, in terms of the operating range over which the output stimulus that reaches the human-hand of the test subject can be considered a linear function of the input stimulus to the test rig system. Gaussian white noise voltage input signals were used to assess the performance of the test apparatus over the nominal frequency range of human hand-arm vibration up to 1000

Hz, as defined in British Standards Institution BS 6842 (1987). A white Gaussian random signal, which is characterised by a continuous and flat frequency spectrum, was chosen since it permits the testing of the device over the whole frequency spectrum using the same average intensity. When loaded by a human hand-arm system and tested at eight reference Gaussian white noise amplitudes ranging from 0.5 r.m.s. m/s^2 to a maximum of 4 r.m.s. m/s^2, the test bench transfer function was found to be linear between 40 and 250 Hz. The test rig was found capable of reproducing stimuli to frequencies in excess of 300 Hz, and presented a first resonance frequency at about 350 Hz.

According to the British Standards Institution BS 6840-2 (1993) for sound reproduction fidelity, signal distortion is defined as an error phenomenon that causes the appearance of extraneous signals at the output of a test equipment. These errors are directly based on the frequency content of the input signal. The parameter generally used to evaluate the fidelity of signal reproduction is termed the total harmonic distortion (THD), which is specified by the standard BS EN 60268-5 (1997). When loaded by a human hand-arm system and tested at frequencies of 4.0, 8.0, 16.0, 31.5, 63.0, 125 and 250 Hz at amplitudes of 0.2, 2.0 and 20.0 m/s^2 r.m.s., the test bench provided a maximum total harmonic distortion (THD) of 15% at 4 Hz and 20 m/s^2 (Giacomin *et al.*, 2004). With both increasing frequency and decreasing amplitude the THD dropped to a minimum of 0.002% at 250 Hz and 0.2 m/s^2. During the tests, which measured the bench tangential direction total harmonic distortion, a linear fore-and-aft direction acceleration measurement was also performed at the same point on the rigid wheel. Unwanted fore-and-aft acceleration was found to be no greater than −50 dB with respect to the tangential acceleration in all cases measured.

A specific evaluation was performed in order to determine the accuracy of the test facility when reproducing the target test stimuli. The test facility calibration procedure evaluated the ensemble of the LMS software, the front end electronics unit, the shaker, the accelerometer and the signal conditioning units. The accuracy of the signal reproduction was quantified by measuring the

maximum r.m.s. error between the actuated and the target signal. Amplitude-modulated vibratory stimuli were generated which had a sinusoidal carrier frequency of f_c = 26 Hz and a modulation frequency of f_m = 6.5 Hz. Seven levels of modulation depth parameter m were used, which provided seven amplitude-modulated stimuli which differed in the r.m.s. value as defined by Eq. (7.4). The r.m.s. values of the target calibration stimuli ranged from a minimum of 0.410 r.m.s. m/s^2 to maximum of 0.615 r.m.s. m/s^2 in order to cover the operational range of the steering wheel idle vibration (refer to Table 7.1). Pretesting involving the amplitude-modulated stimuli revealed that the test bench produced unequal harmonic sidebands, due to the frequency response of the shaker. Compensated drive voltage signals were therefore defined which included the effect of frequency response of the shaker. The compensated drive signals were created by scaling the FFT amplitudes of the carrier and of the sideband frequencies of the test signals, and by subsequently applying the inverse FFT to obtain the drive signal in the time-domain. The compensatory process was iterated so as to equalise the harmonic sidebands to the desired target values. As an example of the process, Figure 7.5 presents the power spectral density of the target test stimuli and of the bench response signal for modulation depth m = 1.0 for both the uncompensated (Figure 7.5a) and the compensated (Figure 7.5b) drive voltage signals. In this case, with frequency compensation, the modulated acceleration stimulus was reproduced at the human test subject with an r.m.s. error of less than 5%.
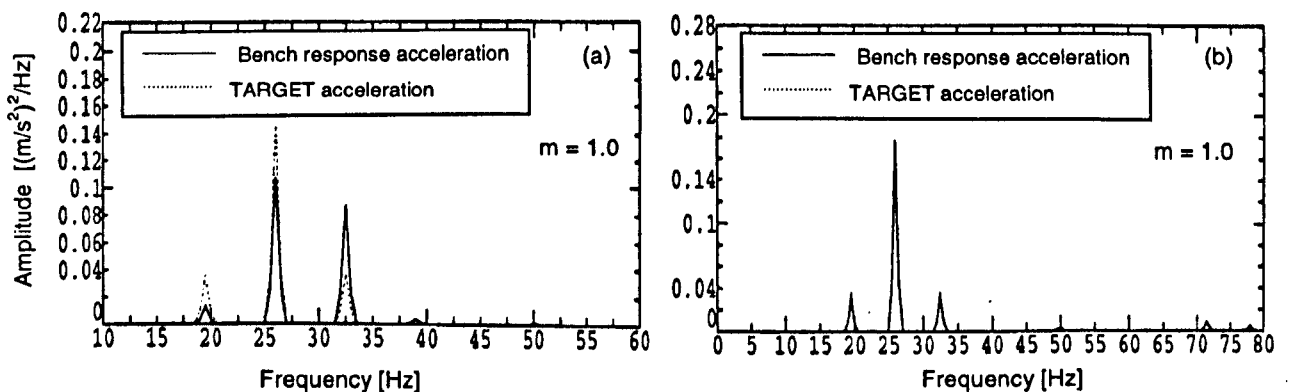
Figure 7.5   Accuracy of test facility steering wheel acceleration signal reproduction.
(a) comparison between target and bench response acceleration before compensation.
(b) comparison between target and bench response acceleration after compensation.

Each of the seven compensated amplitude-modulated drive voltage stimuli was tested. Each stimulus was used three times, during which the actuated acceleration response was recorded by means of the Entran EGAS-FS-25 accelerometer placed on the top left side of the steering wheel. Four test subjects were used in the process, and the maximum and minimum actuated r.m.s. acceleration values were determined. The actuated r.m.s. values were then expressed as a percentage of the target r.m.s value, as presented in Table 7.3.

Table 7.3 Steering wheel test bench stimulus reproduction accuracy for amplitude-modulated vibratory stimuli (three repetitions of each of the seven stimuli with f_c = 26 Hz, f_m = 6.5 Hz, and r.m.s. values from 0.410 to 0.615 m/s^2).

Modulated Signal	m = 0.0	m = 0.1	m = 0.2	m = 0.4	m = 0.6	m = 0.8	m = 1.0
Minimum actuated r.m.s. [m/s^2]	0.407	0.409	0.407	0.427	0.466	0.515	0.608
Target r.m.s. [m/s^2]	0.410	0.412	0.418	0.443	0.484	0.541	0.615
Maximum actuated r.m.s. [m/s^2]	0.418	0.416	0.425	0.451	0.518	0.576	0.676
Maximum error %	1.951	0.971	1.675	1.806	7.025	6.470	9.919

7.4 Study 1: Procedure of the Paired-Comparisons Method

7.4.1 Test Methodology for Experiment I and II

Experiments I and II of study 1 used a paired-comparison protocol of the type commonly used in the automotive industry for subjective evaluation of vehicle quality (Biermayer et al., 2001; Pielemeier et al., 2001). In its most common form, the method of paired-comparisons consists of presenting two stimuli of fixed duration, separated with a fixed gap between the two signals. The subjects are asked to state which of the two stimuli is thought to be greater than the other, with respect to a chosen semantic attribute. Torgerson (1958) identified four ways in which the order of presentation of the test stimuli can be optimised so as to avoid bias in the obtained results:

(a) Arranging pairs so that there is no detectable, systematic, pattern of "correct" responses.

(b) Arranging pairs so that there is no systematic variation in the difficulty of judgement.

(c) Keeping pairs which have one stimulus in common maximally separated in the order of presentation.

(d) Varying the order of presentation from trial to trial to eliminate learning and fatigue effects.

In order to avoid the biasing effects of the first (a) factor identified by Torgerson, the order of presentation of each stimulus pair was fully randomised. In order to avoid the bias introduced by factor (b), a counter-balancing procedure was used. The counter-balancing procedure consists of arranging the members of the pairs such that each stimulus appears first half of the times and appears second half of the time. In this way, it is possible to avoid that either the first or the second stimulus are always preferred. In order to accomplish (c), care was taken to maximise the distance between adjacent pairs which happened to have a stimulus in common. In order to reduce bias resulting from learning and fatigue effects as per factor (d), the order of presentation of the pairs was fully randomised for each test subjects. In addition, a "practice" set was added at the beginning of the test in order to familiarize the participant with the test method and with the nature of the signals being used. The subjective responses from this set were not recorded. The actual testing began from the subsequent set of trials.

After presenting each pair of stimuli, the test subject was asked to indicate which stimuli he or she considered to be "more unpleasant" in experiment I and to be "rougher" in experiment II. If the test subject identified the first signal as being more unpleasant (or rougher), the experimenter stored the number "1"on the answer table used to collect the subjective responses. Alternatively, the number "2" was entered if the test subject identified the second signal as being more unpleasant (or rougher).

All possible pairings of the seven test stimuli were used in order to fully counter-balance the test. The result was a total of 42 paired-comparisons given by $n_s \cdot (n_s - 1)$ where $n_s = 7$ is the number

of the test stimuli. In order to reduce testing time, no stimulus was presented with its duplicate as a pair (Torgerson, 1958). Each subjective evaluation consisted of a 4-second test signal followed by a 2-second gap followed by the other 4-second test signal. Each paired comparison therefore required 10 seconds, a duration which was chosen so as to keep the stimulus short enough to permit both signals to remain in human short-term memory (Gilson and Baddeley, 1969). Additionally, in order to reduce the annoyance caused by presenting a total of 42 pairs, each run of 42 pairs was divided into seven sets of six paired stimuli each. A break of 5 seconds after the presentation of each set was used to relax the hand from the grip of the steering wheel. The complete paired-comparisons test (all 42 pairs) lasted approximately 16 minutes for each test subject. An example of a complete test run of 42 pairs, and the associated answer table used to collect the subjective responses is presented in Appendix B.

7.4.2 Test Subjects for Experiment I and II

For each of the two test conditions of experiment I and II, an independent group of 25 individuals was tested. The two groups of 25 test subjects were independent in the sense that none of the persons who participated in experiment I, participated also in experiment II. The test groups consisted of Sheffield University staff and students whose age, height and weight characteristics are summarised in Table 7.4. On average, 92% of the subjects drove 2 to 10 hours per week, and all declared that they were in good physical and mental health.

Table 7.4 Physical characteristics of the two groups of test subjects used in the paired-comparison procedure of study 1.

		Age [years]	Height [cm]	Mass [kg]
Experiment I (n=25)				
Subjective	Mean (SD)	27.4 (7.93)	1.7 (0.08)	70.4 (14.10)
unpleasantness	Minimum	20.0	160.0	45.0
(Paired-comparison)	Maximum	56.0	190.0	100.0
Experiment II (n=25)				
Subjective	Mean (SD)	29.3 (5.12)	1.7 (0.09)	74.1 (16.39)
roughness	Minimum	22.0	160.0	48.0
(Paired-comparison)	Maximum	41.0	188.0	111.2

(SD) Standard deviation

7.4.3 Test Protocol for Experiments I and II

For each test subject, a strict test protocol was adhered to in which a predetermined sequence of events, each of fixed time duration, was performed. Upon arrival in the laboratory, each participant was given an information sheet and a consent form describing the purpose, procedure, risks and time commitment of their participation. After providing written consent, a short questionnaire regarding their physical characteristics, health, driving experience and history of previous vibration exposure was presented. The information describing the experiment was then presented to the test subject by the experimenter using a set of fixed verbal instructions. The test procedure adhered to the fixed phases and mean time durations outlined in Table 7.5. The information sheet, which contained the consent form, questionnaire and fixed verbal instructions used for the paired comparison procedure is presented in Appendix B.

Since grip type and grip strength (Reynolds and Keith, 1977) are known to affect the transmission of vibration to the hand-arm system, the subjects were asked to maintain a constant palm grip on the steering wheel using both hands. In addition, they were asked to maintain the grip strength which they felt they would use when driving on a winding country road. Room temperature was maintained in the range from 20 to 25 °C so as to avoid significant environmental effects on the skin sensitivity (ISO13091-1, 2001). The test facility and test protocol were reviewed and found to meet the University of Sheffield guidelines for good research practice.

Table 7.5 Steering wheel vibration testing protocol used for all subjects in the paired-comparison procedure of experiment I and II.

Phase	Tasks performed and information obtained
Questionnaire and Instruction Sheet (~2 minutes)	The subject was asked to read the intended purpose of the experiments and to sign a consent agreement form. Each subject provided personal details and completed a short questionnaire.
Adjustment of Driving Posture (~1 minute)	The subject was asked to remove heavy clothing, watches, or jewellers. They were then asked to adjust the seat position and backrest angle so as to simulate a driving task as realistically as possible.
Preparation for Test (~2 minutes)	The subject was required to maintain a constant palm grip on the steering wheel using both hands, as when driving on a winding country road. Subjects were also asked to wear ear protectors to avoid audio cues and to wear opaque glasses and to close their eyes to avoid any visual distractions.
Familiarization with test procedure (3 pairs x 10 seconds)	A familiarization period was used to acquaint the subject with the use of paired-comparisons procedure. Each subject was presented 3 stimuli pairs containing the highest modulation depth m, the lowest modulation depth, and a intermediate value.
Paired-comparison tests (42 pairs x 10 seconds)	Two 4-sec vibration signal stimulations separated by a temporal gap duration of 2 sec were used. Seven amplitude-modulated stimuli were chosen to construct all the 42 possible pairs. All the seven stimuli were scaled to the same reference energy of 0.41 r.m.s. m/s^2. Each run of 42 pairs was presented in seven sets of six paired stimuli. After presenting each signal subjects were asked to indicate which of the two stimuli they considered more unpleasant (for experiment I) or rougher (for experiment II).
Breaks (6 x 5 seconds)	A short break of 5 sec was made after finishing every set of six paired-comparisons to avoid annoyance effects.

7.4.4 Results Obtained from Experiments I and II

The construction of the psychophysical scale of the subjective response to the amplitude-modulated stimuli was determined according to the scaling method of Thurstone's Law of Comparative Judgement under the assumption of Case III (refer to section 3.5.1). Thurstone's Case III model was chosen since it assumes that there is no correlation between the responses to any pair of stimuli, and that the standard deviations of the discriminal distributions of the estimates for any two stimuli are unequal. Thurstone's Case III thus provides a general model for analysing the subjective responses values. Recalling that under the assumption of Case III, the scale separation $S_j - S_k$ between each pair of stimuli on the psychological continuum is given by

$$S_j - S_k = z_{jk} \sqrt{\sigma_j^2 + \sigma_k^2}$$ (7.9)

The scaling procedure requires the determination of the standard deviations σ_j and σ_k of the discriminal distributions of the stimuli j and k respectively, and the normal deviate z_{jk} corresponding to the proportion of times the stimulus j is preferred over the stimulus k when they are compared. For each of the 42 pairs of stimuli which were presented to each of the 25 test subjects, the observed frequencies expressing the number of times each stimulus was judged greater than each other stimulus were calculated, and arranged in a square matrix F [n_s x n_s] where n_s = 7 for the case of these experiments. The matrix F of observed frequencies was then converted into a matrix P which expressed the proportion of times each stimulus j (in the jth column) was preferred over the stimulus k (in the kth row). Having used a counter-balancing procedure, each stimulus pair was evaluated twice for the test group of 25 subjects, thus the total number of judgements per stimulus pair consisted of 50 observations.

The matrix P obtained from experiment I for the case of the unpleasantness dimension is presented as Table 7.6, while the matrix P obtained from experiment II for the case of the

roughness dimension is presented as Table 7.7. Values of 0.5 were placed on the diagonal position since each stimulus was assumed to be judged greater than itself half of the time (Torgerson, 1958). Each frequency percentage value of $p_{j>k}$ was next converted into the normal deviated z_{jk} which was obtained from a table of the normal distribution (Hinton, 1999). The matrices Z of normal deviates are presented as Tables 7.8 and 7.9 for experiments I and II respectively. The generic element z_{jk} is positive for all values of $p_{j>k}$ over 0.50, and negative for all values $p_{j>k}$ under 0.50. Thus a value of 0 is entered in the matrix Z in the diagonal position whereby $p_{j>k} = 0.5$. The matrices P and Z relative to experiment II presented extreme values for some stimuli pairs (as shown by the grey shaded areas in Tables 7.7 and 7.9), indicating an absolute preference for one stimulus over the other. In these cases, the separation interval between the stimuli cannot be accurately determined since the assumption that these stimuli overlap on the psychophysical continuum would not be tenable. (Torgerson, 1958; Nunnally and Bernstein, 1994). To obtain reliable data when the matrix Z presents extreme values Guilford (1954) suggests not using values more extreme than +2.0 < z_{jk} < -2.0, which arise from proportions of approximately 0.977 < $p_{j>k}$ < 0.023. Therefore these data were eliminated from the scaling procedure, and the corresponding cells in matrix Z were left vacant. Analytical and graphical procedures have been devised by Burros and Gibson (1954) for dealing with missing data in the matrix Z, as it is the case of experiment II (refer to Table 7.9). These procedures provide estimates of the standard deviations σ_j and σ_k of the discriminal distributions of the two stimuli j and k of Eq (7.9). On the other hand, similar analytical procedures to determine the same quantities are also given by Burros (1951) for use when the matrix Z is complete, as in the case of experiment I (refer to Table 7.8).

The procedures specified by Burros (1951) for the complete condition of the Matrix Z, and by Burros and Gibson (1954) for the incomplete condition, both provide formulas for estimation of the standard deviation for the dispersion of stimulus j, expressed in terms of the variance V_{z_j} of the

elements z_{jk} in each column of matrix **Z**. Therefore, for any two stimuli j and j+1, and thus for any two values of modulation depth, there will be as many estimates of the differences of Eq. (7.9) as there are filled pairs of cells in the j and j+1'th columns of matrix **Z**. The averages of these estimates over the number n_k of terms, which are summed for each column j, are taken as the estimates of the difference of the scale values. The scale values themselves for all stimuli are then obtained from the differences by arbitrarily allocating the zero point of the scale to the stimulus with the lowest scale value, and by adding the successive differences.

Table 7.6   Matrix **P** of the proportion of times stimulus j was judged "more unpleasant" than stimulus k in experiment I.

		stimulus j					
	mod_0.0	**mod_0.1**	**mod_0.2**	**mod_0.4**	**mod_0.6**	**mod_0.8**	**mod_1.0**
mod_0.0	0.50	0.38	0.50	0.70	0.86	0.90	0.94
mod_0.1	0.62	0.50	0.56	0.74	0.86	0.92	0.86
mod_0.2	0.50	0.44	0.50	0.74	0.88	0.94	0.90
stimulus k **mod_0.4**	0.30	0.26	0.26	0.50	0.78	0.86	0.96
mod_0.6	0.14	0.14	0.12	0.22	0.50	0.62	0.76
mod_0.8	0.10	0.08	0.06	0.14	0.38	0.50	0.72
mod_1.0	0.06	0.14	0.10	0.04	0.24	0.28	0.50

Table 7.7   Matrix **P** of the proportion of times stimulus j was judged "rougher" than stimulus k in experiment II.

		stimulus j					
	mod_0.0	**mod_0.1**	**mod_0.2**	**mod_0.4**	**mod_0.6**	**mod_0.8**	**mod_1.0**
mod_0.0	0.5	0.48	0.62	0.92	0.96	0.98	0.96
mod_0.1	0.52	0.5	0.62	0.86	0.96	0.98	0.96
mod_0.2	0.38	0.38	0.5	0.84	0.98	1	0.96
stimulus k **mod_0.4**	0.08	0.14	0.16	0.5	0.88	0.86	0.94
mod_0.6	0.04	0.04	0.02	0.12	0.5	0.64	0.82
mod_0.8	0.02	0.02	0	0.14	0.36	0.5	0.58
mod_1.0	0.04	0.04	0.04	0.06	0.18	0.42	0.5

Table 7.8   Matrix **Z** of normal deviates corresponding to the observed proportion element $p_{j>k}$ of matrix **P** in experiment I.

		stimulus j					
Matrix Z	mod_0.0	mod_0.1	mod_0.2	mod_0.4	mod_0.6	mod_0.8	mod_1.0
mod_0.0	0	-0.305	0.000	0.524	1.080	1.282	1.555
mod_0.1	0.305	0	0.151	0.643	1.080	1.405	1.080
mod_0.2	0.000	-0.151	0	0.643	1.175	1.555	1.282
stimulus k mod_0.4	-0.524	-0.643	-0.643	0	0.772	1.080	1.751
mod_0.6	-1.080	-1.080	-1.175	-0.772	0	0.305	0.706
mod_0.8	-1.282	-1.405	-1.555	-1.080	-0.305	0	0.583
mod_1.0	-1.555	-1.080	-1.282	-1.751	-0.706	-0.583	0

Table 7.9   Matrix **Z** of normal deviates corresponding to the observed proportion element $p_{j>k}$ of matrix **P** in experiment II.

		stimulus j					
Matrix Z	mod_0.0	mod_0.1	mod_0.2	mod_0.4	mod_0.6	mod_0.8	mod_1.0
mod_0.0	0	-0.050	0.305	1.405	1.751	2.054	1.751
mod_0.1	0.050	0	0.305	1.080	1.751	2.054	1.751
mod_0.2	-0.305	-0.305	0	0.994	2.054	6.000	1.751
stimulus k mod_0.4	-1.405	-1.080	-0.994	0	1.175	1.080	1.555
mod_0.6	-1.751	-1.751	-2.054	-1.175	0	0.358	0.915
mod_0.8	-2.054	-2.054	-6.000	-1.080	-0.358	0	0.202
mod_1.0	-1.751	-1.751	-1.751	-1.555	-0.915	-0.202	0

From the average test results for each test group of 25 subjects, an interval scale was constructed from experiments I and II. The mean scale values obtained for each value of modulation depth in each of the two experiments is provided in Table 7.10, along with the standard deviation (SD) values. The psychological continua are here referred to as "relative unpleasantness" for experiment I and "relative roughness" for experiment II. The term "relative" expresses the condition that the Thurstone's method produced as output a scale difference between the means of the stimulus responses, locating the stimuli on an interval scale with respect to one another, with a zero point which is set arbitrarily at the scale value of the first stimulus.

Table 7.10 Mean subjective response scale values and, in parentheses, the one standard deviation values for the seven test stimuli obtained using Thurstone's method.

Stimuli			Thurstone scale values			
Modulation depth m	$a_{r.m.s.}$ [m/s^2]	VDV [m/s$^{1.75}$]	Experiment I: Relative unpleasantness		Experiment II: Relative roughness	
m = 0.0	0.41	0.640	0	(0.338)	0	(0.982)
m = 0.1	0.41	0.644	-0.302	(0.288)	-0.054	(0.913)
m = 0.2	0.41	0.658	-0.077	(0.386)	0.287	(1.098)
m = 0.4	0.41	0.707	0.300	(0.414)	1.113	(1.419)
m = 0.6	0.41	0.773	0.895	(0.343)	1.853	(1.256)
m = 0.8	0.41	0.847	1.16	(0.357)	2.588	(0.795)
m = 1.0	0.41	0.925	2.302	(0.182)	3.555	(0.587)

In order to test the internal consistency of the Thurstone scale values, a Chi-square χ^2 test of independence (Hinton, 1999) was performed to verify if each of the pattern of frequencies of responses observed for each modulation condition was statistically different from each other. For experiment I, a value of $\chi^2 = 64.54$ was found, while for experiment II, a value of $\chi^2 = 129.36$ was found. Since the calculated values were greater than the critical value at a p = 0.01 level of significance, the difference in the responses provided by the test subjects for the different test stimuli should be considered significant.

The subjective response scale values obtained for each of the two experiments by means of Thurstone's method of the paired-comparisons are presented in Figure 7.6. For modulation depth m ranging from 0.0 to 0.2 the scale values are nearly constant, while a monotonic increase is evident for modulation depths greater than m = 0.2. This would suggest that the nature of the human perception of amplitude-modulated stimuli depends critically on the value of the modulation depth that is considered. Below a certain critical value of modulation depth, the test subjects seem to be relatively insensitive to small differences in modulation depth. Above the critical value, the test subjects are sensitive to the differences in amplitude modulation.
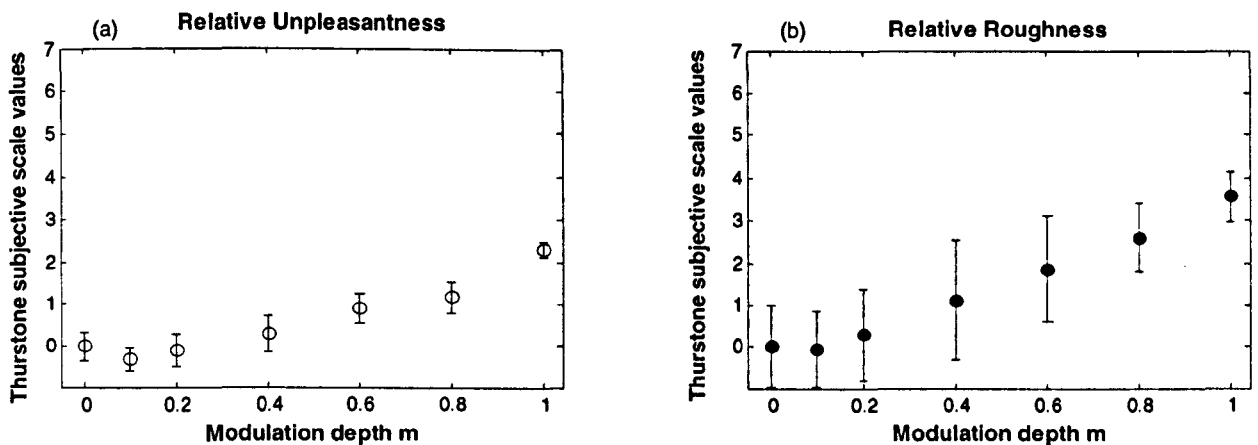
Figure 7.6 Mean subjective response scale values as a function of modulation depth m obtained using Thurstone's method. Data are shown as mean value plus or minus one standard deviation.

(a) relative unpleasantness values obtained from experiment I.
(b) relative roughness values obtained from experiment II.

7.5   Study 2: Procedure of the Borg CR-10 Scale Method

7.5.1 Test Methodology for Experiments III and IV

Experiments III and IV used the direct psychophysical protocol of the category-ratio Borg CR-10 scale under the same semantic descriptors of unpleasantness and roughness used in the paired-comparison tests. Perceived unpleasantness and perceived roughness of the vibration were assessed using the Borg CR-10 scale following the instructions provided by Borg (1998) for the scale's administration. Subjects were instructed to use the Borg CR-10 scale (refer to Figure 3.7) by first finding the verbal label which best fits the perceived sensation, and then choosing a number to express the rating. Subjects were allowed to use any number on the scale, including decimals values. If subjects experienced the perceived unpleasantness or roughness to be stronger than their own personal experience, they were allowed to give any number above 10 in order to avoid ceiling effects. The test subjects were further asked to judge each test stimuli on its own merits, independent of preceding stimuli, in order to avoid possible bias due to the order of presentation of the stimuli (Gescheider, 1997). The test subjects were encouraged to focus their

eyes on a board which was placed about 1 meter ahead at eye level, which presented the Borg rating scale.

The same seven signals used in experiments I and II for the paired-comparisons protocol were again employed in experiments III and IV for the Borg CR-10 scaling method. All the stimuli had the same time duration of 4 seconds as in the pair-comparison tests. In order to assess the individual's ability to rate stimuli using the Borg's scale, each of the seven exposures was repeated four times giving a total of 28 assessment trials. In order to minimize any possible bias resulting from learning or fatigue effects, the order of presentation of the test signals was randomized for each subject. A break of 10 seconds after the presentation of each set of seven stimuli was used to avoid annoyance effects. Total testing time for a single test subject amounted to 15 minutes. An example of a complete test run of 28 stimuli, and the associated answer table used to collect the subjective responses is presented in Appendix B.

7.5.2 Test Subjects for Experiment III and IV

For each of the two test conditions of experiment III and IV, an independent group of 25 individuals was tested. The test groups consisted of Sheffield University staff and students, whose age, height and weight characteristics are summarised in Table 7.11. On average, 96% of the subjects drove 2 to 10 hours per week, and all declared that they were in good physical and mental health.

Table 7.11   Physical characteristics of the two groups of test subjects used in the Borg CR-10 scale procedure of study 2.

		Age [years]	Height [cm]	Mass [kg]
Experiment III (n=25)				
Perceived	Mean (SD)	28.5 (5.04)	1.7 (0.08)	75.8 (14.30)
unpleasantness	Minimum	22.0	160.0	53.0
(Borg CR-10 Scale)	Maximum	42.0	185.0	107.0
Experiment IV (n=25)				
Perceived	Mean (SD)	29.4 (6.55)	1.8 (0.107)	76.0 (15.69)
roughness	Minimum	22.0	160.0	50.0
(Borg CR-10 scale)	Maximum	48.0	201.0	115.8.0

(SD) Standard deviation

7.5.3 Test Protocol of Experiment III and IV

For each test subject, a strict test protocol was adhered to in which a predetermined sequence of events, each of fixed time duration, was performed. Upon arrival in the laboratory, each participant was given an information sheet and a consent form describing the purpose, procedure, risks and time commitment of their participation. After providing written consent, a short questionnaire regarding their physical characteristics, health, driving experience and history of previous vibration exposure was presented. The information describing the experiment was then presented to the test subject by the experimenter using a set of fixed verbal instructions. The test procedure adhered to the fixed phases and mean time durations outlined in Table 7.12. The information sheet, which contained the consent form, questionnaire and fixed verbal instructions used for the Borg CR-10 scale procedure is presented in Appendix B.

Table 7.12   Steering wheel vibration testing protocol used for all subjects in the Borg CR-10 scale procedure of Experiment III and IV.

Phase	Tasks performed and information obtained
Questionnaire and Instruction Sheet (~2 minutes)	The subject was asked to read the intended purpose of the experiments and to sign a consent agreement form. Each subject provided personal details and completed a short questionnaire.
Adjustment of Driving Posture (~1 minute)	The subject was asked to remove heavy clothing, watches, or jewellers. They were then asked to adjust the seat position and backrest angle so as to simulate a driving task as realistically as possible.
Preparation for Test (~2 minutes)	The subject was required to maintain a constant palm grip on the steering wheel using both hands, as when driving on a winding country road. Subjects were also asked to wear ear protectors to avoid audio cues, and to focus their eyes on the Borg scale so as to avoid any visual distractions.
Familiarization with test procedure (~3 minutes)	A familiarization period was used to acquaint the subject with the use of the Borg CR-10 scale by means of practice ratings using a non-vibrational stimuli (acidity rating of common foods) and a dummy test involving two vibrational stimuli selected from the test set.
Borg CR-10 scale tests (28 stimuli x 4 seconds)	A 4 second vibration stimulus was presented to the test subject. Seven amplitude-modulated stimuli were scaled to the same reference energy of 0.41 r.m.s. m/s^2. Each of the seven exposures was repeated four times in order to assess the individual's ability to rate stimuli using the Borg's scale. Each run consisted therefore of 28 assessment trials presented in four sets of seven stimuli each.
Breaks (3 x 5 seconds)	A short break of 5 sec was made after finishing every set of seven assessment trials to avoid annoyance effects.

7.5.4 Results Obtained from Experiments III and IV

For experiments III and IV, a ratio scale was constructed from the Borg CR-10 responses provided by each group of 25 test subjects. A total of 100 (25 subjects x 4 presentations) CR-10 scale estimates were collected for each amplitude-modulated vibration stimulus. A mean CR-10 scale estimate for each modulation depth was then computed. The mean scale values obtained for each value of modulation depth in each of the two experiments is provided in Table 7.13, along with the one standard deviation values. Direct rating by means of the Borg CR-10 scale produces a subjective response value for each stimulus which is claimed to have ratio scale properties. The two psychophysical response continua are here referred to as "perceived unpleasantness" for experiment III and "perceived roughness" for experiment IV. The mean scale values and the one standard deviation values are presented for each of the two experiments in Figure 7.7

Table 7.13 Mean subjective response scale values and, in parentheses, the one standard deviation values for the seven test stimuli obtained using the Borg CR-10 scale procedure.

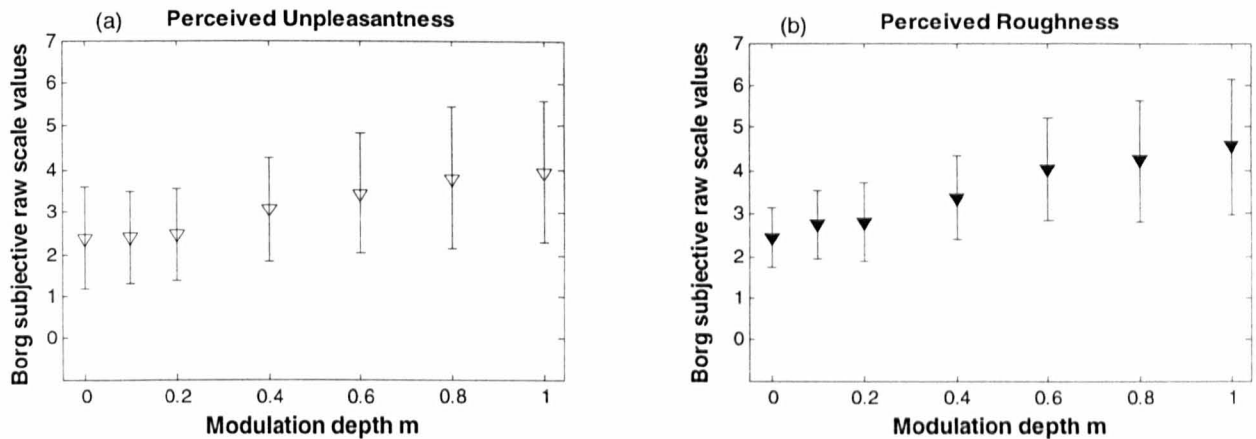| Stimuli			Borg scale values			
Modulation depth m	$a_{r.m.s.}$ [m/s^2]	VDV [m/s$^{1.75}$]	Experiment III: Perceived unpleasantness		Experiment IV: Perceived roughness	
m = 0.0	0.41	0.640	2.38	(1.212)	2.45	(0.708)
m = 0.1	0.41	0.644	2.42	(1.087)	2.75	(0.792)
m = 0.2	0.41	0.658	2.48	(1.080)	2.78	(0.915)
m = 0.4	0.41	0.707	3.06	(1.225)	3.37	(0.973)
m = 0.6	0.41	0.773	3.44	(1.398)	4.03	(1.186)
m = 0.8	0.41	0.847	3.79	(1.638)	4.22	(1.412)
m = 1.0	0.41	0.925	3.93	(1.628)	4.55	(1.582)

Figure 7.7   Mean subjective response scale values as a function of modulation depth m obtained using the Borg CR-10 scale. Data are shown as mean value plus or minus one standard deviation.

(a) perceived unpleasantness values obtained from experiment III.
(b) perceived roughness values obtained from experiment IV.

In order to identify any statistically significant differences among the Borg scale values, a one-factor ANOVA (Hinton, 1999) test was performed using the modulation depth parameter m as the independent variable. In the case of the paired-comparisons procedure (refer to section 7.4.4), a Chi-square test of independence was considered best since the nature of the results obtained using the Thurstone's method are in the form of frequency data, expressing the proportion of times any stimulus is judged greater than any other stimulus. When the nature of the data collected are in the form of numerical ratings, as it is the case of the Borg CR-10 scale, an ANOVA test is more appropriate (Hinton, 1999). Statistically significant differences between the Borg scale values were found at a $p = 0.01$ level of significance. Therefore, the modulation depth parameter m did have a significant effect on the subjective judgement of the steering wheel idle vibration when the Borg CR-10 scale procedure was used.

The subjective scale values obtained by means of the Borg CR-10 scale procedure corroborated the hypothesis of a critical transition value in the human subjective response as a function of the modulation depth. For values of modulation depth m ranging from 0.0 to 0.2, the subjective scale

values were nearly constant, suggesting that below a certain value of modulation depth, the test subjects were relatively insensitive to differences in amplitude modulation. Above the critical value of modulation depth, the test subjects were sensitive to these differences.

7.6   Model of the Human Hand-Arm Perception of Amplitude-Modulated Stimuli

The results obtained from Thurstone's method provided an interval scale with the zero point of the scale set arbitrarily. The results obtained from the Borg CR-10 scale, instead, provided a true zero, since it is a ratio scale (refer to Table 3.1). Since the unit of measurement of the Thurstone and Borg scales are not the same, a common scale was required to facilitate comparisons. For single-ended continua, it is common practice to equate the absolute zero point with the absolute threshold of perception of the physical quantity being evaluated during the subjective tests (Torgerson, 1958). In the case of amplitude-modulated stimuli, studies of the temporal sensitivity of the tactile system performed by Weisemberger (1986) have shown that the depth of modulation at threshold (m_{th}) necessary to just allow discrimination between a modulated and an unmodulated sinusoidal carrier waveform of 25 Hz was 0.2 for modulation frequencies ranging from 5 to 10 Hz. Based on Weisemberger's studies, and on the current experimental condition of a sinusoidal carrier frequency of f_c = 26 Hz and modulation frequency f_m = 6.5 Hz, the Thurstone and Borg scales were therefore compared by equating the zero point of the scale with the stimulus condition of threshold modulation depth m = 0.2.

Based on this observation, and on the current test results shown in Figures 7.6 and 7.7, it can be assumed that a threshold modulation depth of approximately 0.2 represents a critical point of separation between two different human response characteristics. Below the point m = 0.2 subjects do not perceive differences in amplitude modulation, and the sensation magnitude can be interpreted as sensory noise relative to the energy of the unmodulated waveform m = 0.0.

Above the point m = 0.2 the sensation magnitude grows monotonically as a function of the modulation depth m. A schematic representation of the proposed model of human perception of amplitude-modulated vibration delivered to the hand is shown in Figure 7.8.
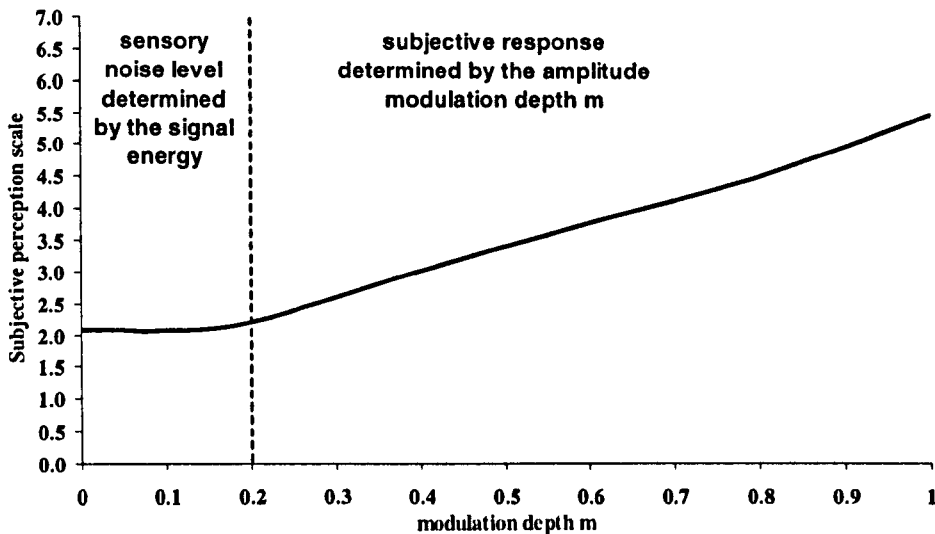

Figure. 7.8   Model of human hand-arm perception of amplitude-modulated vibrational stimuli.

Psychophysical relations of the type occurring for modulation depths greater than 0.2 were compactly expressed by means of the well-known Stevens' Power Law which in its most general form is expressed as:

$$\Psi = \Psi_o + k(X - X_{th})^\beta \tag{7.10}$$

where Ψ is the subjective perceived magnitude, X is the stimulus magnitude (expressed here as modulation depth m), k is a constant determined from the measurement units, β is the exponent of the power law, and the two constants Ψ_o and X_{th} indicate the starting point of the growth function at threshold on the response axis (y-axis) and on the stimulus axis (x-axis), respectively. In the current analysis, the constant Ψ_o represents the sensory response to the harmonic stimuli when no actual modulation is present, and X_{th} is the value of the modulation

depth at threshold m_{th}. The use of expression (7.10) implies that the sensation magnitude Ψ is a power function of the effective stimulation above the threshold of amplitude modulation m_{th}. The value X_{th} to which the physical stimuli on the x-axis were rescaled was chosen equal to the threshold level $m_{th} = 0.2$, whereas the value Ψ_o to which the subjective response scales on the y-axis were rescaled, was taken to be equal to mean value of the Borg response scales associated with the stimuli conditions $m = 0.0$, $m = 0.1$ and $m = 0.2$. It was decided to determine a mean value from the subjective responses associated with these three modulation depths since these three stimuli are all in the region of sensory noise where the human discrimination of signal modulation does not appear possible. The mean of the three response values therefore provided an estimate of the sensory noise. After translating the raw data along both axes, the growth functions of the human perceived unpleasantness and roughness were determined as a function of the difference in modulation depth with respect to threshold, $m^* = m - m_{th}$.

For this purpose, a regression analysis (Montgomery and Runger, 1999) was performed on the translated mean scale values as a function of the modulation index $m^* = m - m_{th}$ for each of the four experiments. In order to determine the Stevens' power law parameter values that best fit the translated subjective scale, the regression analysis used a least-squares fit, which minimises the sum of the squares of the deviations of the experimental data from the fitted model. A Stevens' power law exponent β and a coefficient of determination r^2 were obtained. The exponent β provided a metric which translates the measurable physical objective quantities (in this case the modulation index m^* of the steering wheel vibration stimuli) into perceived subjective quantities (in this case the subjective response of unpleasantness or roughness of the vibration). The coefficient of determination r^2 provided a measure of how much of the variability of the subjective values can be explained by the variability of the modulation index when correlating the subjective responses to the relative modulation index m^*.

Figure 7.9a presents the experimentally obtained unpleasantness scale values, and the fitted Stevens' power law, obtained using Thurstone's method ($\beta = 1.38$) and obtained using the Borg CR-10 scale ($\beta = 0.61$). Figure 7.9b presents the roughness scale values, and the fitted Stevens' power law obtained using Thurstone's method ($\beta = 0.92$) and obtained using the Borg CR-10 scale ($\beta = 0.63$). Also presented are the results of the regression analysis performed on the data, indicated by the power exponent β and the associated coefficient of determination (r^2).
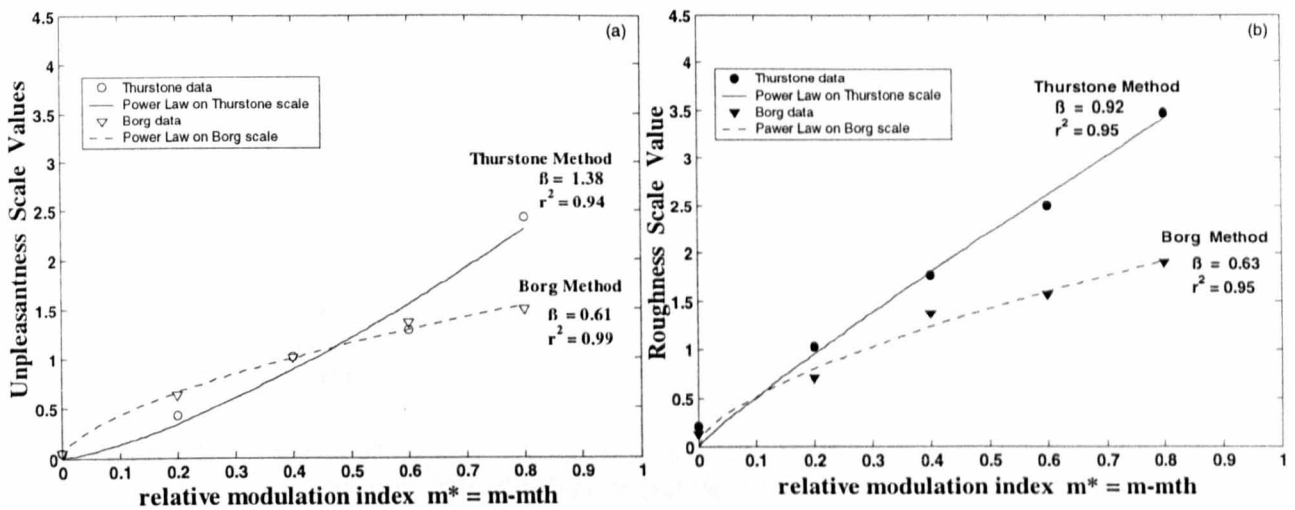

Figure 7.9   Growth functions of the human perceived disturbance of amplitude-modulated steering wheel idle vibration obtained by means of the Thurstone paired comparison method and by using the Borg CR-10 scale.

(a) perceived unpleasantness.
(b) perceived roughness.

As can be seen from Figure 7.9, the growth exponent β describing the human subjective response obtained by means of Thurstone's method of paired comparison was greater than unity for the perceived unpleasantness dimension, and nearly equal to unity for the perceived roughness, whereas the exponents from the Borg CR-10 experiments was found to be less than unity in both cases. This result suggests that the perceived unpleasantness and roughness of amplitude-modulated steering wheel stimuli was dependent on the psychophysical protocol used. From the results, it is not possible to definitively state whether the growth of the human subjective response to steering wheel vibration obtained is either positively accelerating (with an exponent

greater than unity) or negatively accelerating (with an exponent less than unity) as a function of the relative modulation index.

7.7   Discussion of the Psychophysical Test Results

The sensory attributes of vibration unpleasantness and vibration roughness belong to a group of perceptual dimensions which are based on the quality, rather than on the intensity, of the stimulus. Such dimensions are generally thought to depend on more than a single sense modality (Stevens, 1986). In the present work, the perceived unpleasantness and roughness of amplitude modulated steering wheel acceleration stimuli were found to depend on the psychophysical protocol used. Table 7.14 presents a summary of the Stevens' power law exponent (β) and the coefficients of determination (r^2) obtained from experiments I and II by means of Thurstone's method of paired comparison and from experiments III and IV by means of the category-ratio Borg CR-10 scale procedure.

Table 7.14   Stevens' power exponents β and coefficients of determination r^2 determined from the data of experiments I, II, III, and IV.

Experiment	Scaling Method	Semantic attribute	Stevens' Power Exponent β	Coefficent of determination r^2 *
Experiment I	Thurstone (indirect method)	Unpleasantness	1.38	0.94
Experiment II	Thurstone (indirect method)	Roughness	0.92	0.95
Experiment III	Borg CR-10 scale (direct method)	Unpleasantness	0.61	0.99
Experiment IV	Borg CR-10 scale (direct method)	Roughness	0.63	0.95

* $p < 0.01$

As can be seen from Table 7.14, the results found using the Borg CR-10 scale procedure do not fully support the results obtained using the Thurstone's method since the Stevens' power exponent β is different when using one or the other method. In particular, the Stevens' power exponent β describing the human subjective response obtained by means of Thurstone's method was greater than unity for the perceived unpleasantness dimension, and nearly equal to unity for the perceived roughness, whereas the exponents from the Borg CR-10 experiments remained

nearly constant with a average value of 0.62 for the two dimensions. In this research study the use of the Borg CR-10 scale has lead to smaller Stevens' exponents than paired comparison methods. Similar results have been also found in a series of research studies (De Baene *et al.*, 2004; De Baene *et al.*, 2004b) on the effect of the modulation depth m on the perception of the unpleasantness character of the sound caused by the amplitude fluctuation of amplitude-modulated tones delivered to the human ear. These studies used a direct method of magnitude estimation and an indirect method of paired-comparisons. They found that when a direct method of magnitude estimation was used, the curve of perceived unpleasantness was flat for modulation depth greater than m = 0.8. Whereas, when a paired-comparison procedure was used, the perceived unpleasantness of amplitude modulated tones was found to increases with the modulation depth. These results would suggest that the paired-comparisons procedure is more sensitive to detect small differences in the amplitude modulation parameter m than when a direct method of magnitude estimation is used.

A recent study on the subjective response to seated whole-body vibration (Giacomin and Hacaambwa, 2005) has shown that when calculating the growth of human subjective response as a function of the r.m.s. value by means of the Borg CR-10 scale procedure and by means of a magnitude estimation procedure, the Borg CR-10 scale procedure produced smaller exponents than did magnitude estimation. In this case the authors suggested that the result was due to a 'ceiling effect' which occurred when using the Borg CR-10 scale. The 'ceiling effect" may have been caused by a psychological fear of the test subject regarding the need to estimate rating values greater than the number 10 of the Borg CR-10 scale, as opposed to the possibility of choosing from among convenient existing values below this scale point.

In the research presented in this thesis, while difficult to demonstrate analytically (Laming, 1997), the lower exponent seems to be a reflection of an artifact in the Borg scale which occurs when only a portion of the dynamic range of the scale is used. In the experiments described here, the mean subjective response of the test group was never greater than 5.0 (refer to Table 7.13), thus accounting for less than half the dynamic range of the Borg CR-10 scale. This might explain the

lower Stevens' power exponent values obtained using the Borg CR-10 scale, suggesting that the Thurstone's method of the paired comparisons leads to more accurate estimates in subjective difference.

Given the differences in the experimental results obtained using the two psychophysical protocols, related metrics were calculated and used to lend support to one or the other of the data sets. An obvious metric for comparison is the vibration dose value (VDV), which is commonly used for quantifying the perceived intensity of the human response to vibration (Howarth and Griffin, 1991). Figure 7.10 presents the VDV values of the test stimuli as a function of the relative modulation depth $m* = m - m_{th}$. The VDV values (y-axis) have been translated for comparison purposes by removing the sensory noise associated with the unmodulated sinusoidal signal (m = 0.0). From figure 7.10 it can be seen that the perceived intensity predicted by means of the VDV value increases with relative modulation index $m*$ with a Stevens' power exponent of β = 1.32. Since the VDV value has found widespread acceptance in the human vibration and human testing communities (Howarth and Griffin, 1991), it is reasonable to assume that the power exponents obtained by means of Thurstone's paired comparison method provide a closer measure of human response to amplitude modulated steering wheel vibration than the results obtained using the Borg CR-10 scale.
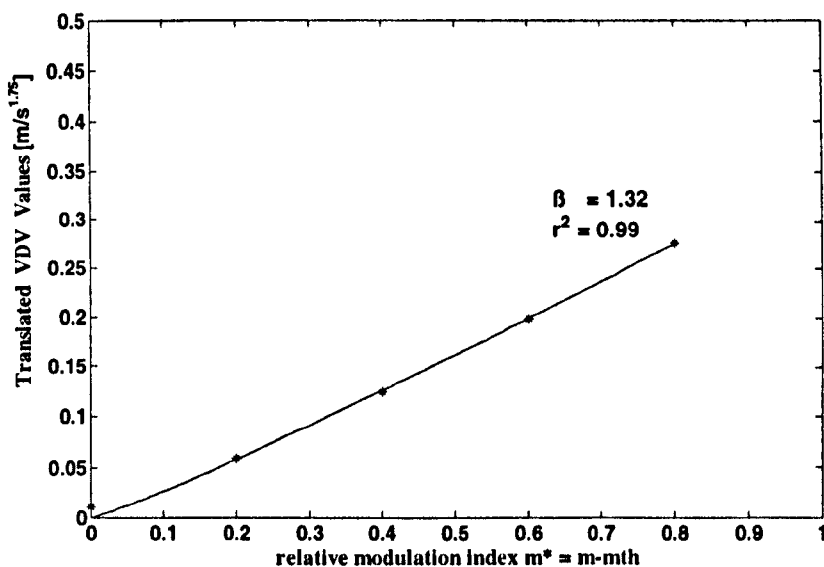

Figure 7.10 Vibration dose value (VDV) as function of relative the modulation index $m* = m - m_{th}$ after subtracting from each data point the VDV value of the unmodulated sinusoidal stimulus of the same r.m.s. amplitude as the test stimuli.

7.8   Summary

The experimental tests described in this chapter investigated the growth in the human subjective response to amplitude-modulated vibration stimuli of the type caused by a four-cylinder diesel engine idle in passenger cars. Based on the signal processing of the idle vibration data acquired as described in Chapter 5 and Chapter 6, it was decided to model the diesel idle vibration which occurs at the steering wheel using analytically defined sinusoidal amplitude-modulated stimuli having a carrier frequency equal to the second-order engine harmonic H_2 (26 Hz) and a modulation frequency equal to the half-order engine harmonic $H_{1/2}$ (6.5 Hz). Subjective evaluations of seven values of modulation depth parameter m were performed in order to define the growth function of the human perceived disturbance as a function of the modulation depth m. All stimuli were scaled to the same r.m.s. energy level (0.41 m/s^2) such that the modulation depth m was the only parameter which varied among them. Due to the bias which is introduced by the choice of the psychophysical test protocol, four experimental conditions, determined by the combination of two semantic descriptors and two psychophysical test methods, were performed so as to compare the resulting human responses. The psychophysical protocols chosen for measuring the human subjective response were Thurstone's method of paired-comparisons (Case III) and the category-ratio Borg CR-10 scale. The semantic attributes of unpleasantness and roughness were chosen as descriptors of the human response.

The subjective response scale values of perceived unpleasantness and roughness were found to depend on the psychophysical protocol used. In this research, the use of the Borg CR-10 scale has lead to smaller Stevens' exponents than paired comparison methods. The lower exponent seems to be a reflection of an artefact in the Borg scale which occurs when only a portion of the dynamic range of the scale is used. The mean subjective response of the test group was never found to be greater than 5.0, thus accounting for less than half the dynamic range of the Borg CR-10 scale. This would suggest that the Thurstone's method of the paired comparisons provides

more accurate estimates in subjective difference for test stimuli which do not vary over the complete extent of their dynamic range.

A model of the human perception of amplitude-modulated vibrational stimuli has been proposed based on the existing biomedical research, and on the experimental findings presented in this study. All data suggests that there is a critical value of modulation depth ($m = 0.2$) below which human subjects do not perceive differences in amplitude modulation. Below the value $m = 0.2$, the sensation can be interpreted as sensory noise relative to the energy of the unmodulated waveform. Above the value $m = 0.2$, the sensation grows monotonically as a power function of the modulation depth m. The Stevens' power exponents determined from the test data suggest that the perceived unpleasantness is dependent on modulation depth m with an exponent greater than 1, and that the perceived roughness is dependent with an exponent close to unity.

Chapter 8

Conclusions and Recommendations for Future Research

8.1 Summary of the Research Findings

The experimental activities described in Chapters 5 to 7 of this thesis were performed in order to answer questions about the nature of diesel idle vibration in automobiles under varying fuel conditions and under different engine technologies, and to model the growth in the human subjective response to the idle vibration stimuli occurring at the steering wheel. This chapter summaries the main findings and attempts to provide an answer to the questions posed in the introductory Chapter 1 in light of the experimental results.

- What vibrational signatures occur at the steering wheel of diesel-engined automobiles when at idle? And how much are these related to the vibration signature measured at the engine?

A set of vibration recordings were performed on the engine block and on the steering wheel using two automobiles which had different injection systems, under different diesel fuel conditions. The measured acceleration time histories were analysed using a combination of time domain, frequency domain and time-frequency domain analysis in order to identify the typical characteristics of diesel idle vibration.

From the signal processing analysis of Chapter 5 the steering wheel idle vibration time histories were found to be highest in level along the vertical direction. This finding is in agreement with previous research (Peruzzetto, 1988; Schröder and Zhang, 1997; Amman et al., 2001; Giacomin et al., 2004) which suggests that acceleration magnitudes measured at the steering wheel along the vertical direction are normally greater than those along either the fore-and-aft or the lateral direction.

From the power spectral densities and transmissibility functions determined for the engine block and for the steering wheel measurement points, it was concluded that the transmission of the diesel idle vibration from the engine to the wheel reduced the frequency bandwidth of the vibration to only the low-order harmonics of the engine rotational frequency. In particular, the energy conveyed to the steering wheel covered only the low frequency range up to 200 Hz. The second-order engine harmonic H_2 was found to account for most of the energy of the steering wheel idle vibration. The dominant role of harmonic H_2 in the case of a 4-cylinder engine corroborates the analytical results of Rahnejat (1998) and the experimental measurements performed by Dixon et. al. (1994).

The presence of sideband components in the power spectral densities of the steering wheel vibration at frequencies above and below the second-order engine harmonic H_2 suggested that the steering wheel idle vibration is characterized by amplitude modulation. Amplitude modulation of the second-order engine harmonic H_2 by the half-order engine harmonic $H_{1/2}$ has been identified as the main characteristic of the steering wheel signature of automobiles at idle. Diesel

idle vibration occurring at the steering wheel can therefore be considered a mixture of a periodic component determined by the engine firing frequency and its even-order harmonics, and of an aperiodic component whose amplitude changes over time due to the combustion event repeating every engine working cycle at the half-order engine rotational frequency $H_{1/2}$.

The time-frequency wavelet-based analysis of Chapter 6 have confirmed that the diesel idle vibration occurring at the steering wheel is better described in terms of amplitude variation than in terms of frequency variation. The periodicity of the amplitude fluctuation was found to be that of the half-order engine harmonic $H_{1/2}$. The coefficients of variation describing the changes in the amplitude were found to be greater (a mean value of 12.54 percent between the two methods) than those describing the changes in the frequency (a mean value of 1.01 percent between the two methods) for all fuels and both automobiles tested.

Partial confirmation of the research findings presented in this thesis can be found in the literature relative to diesel engine idle noise. Amplitude modulation of the type caused by a low frequency modulation at the half-order engine rotational frequency has been found to be the main characteristic of the noise signature produced by a 4-cylinder common-rail diesel engine operating at idle at 810 rpm. (Lèclere et al., 2005). Time-frequency analysis performed by Lèclere et al. has shown that the periodic fluctuation of diesel engine noise is best described by a dominant frequency of approximately 27 Hz (the firing frequency), and by a modulation frequency of approximately 7 Hz (the half-order engine harmonic). Amplitude modulation has also been observed in studies of engine crankshaft rumble noise at varying engine speeds from idle to a maximum of 2700 rpm (Lim and Witer, 2000). From their studies Lim and Witer suggested that the periodicity of the amplitude modulation of engine rumble noise is directly related to the half-order engine rotational frequency $H_{1/2}$.

- How do the vibration signatures change when changing from one fuel to another ? And how much can the signatures vary from one engine to another ?

The fuel-related changes in the vibration signatures at the engine block were quantified by means of the index of *inter-fuel* variability $S_2\%$. Both the global signal statistics and the cycle-to-cycle statistical variations were determined for all ten reference fuels. The results suggested that the indirect-injection (IDI) engine of the Renault 19 was the most affected by fuel quality. For the Renault 19, the global *inter-fuel* variability $S_2\%$ calculated for the transverse direction at the engine block, and calculated across all fuels, was 23.15 percent. The result of the same calculation for the Ford Focus was only 2.09 percent. For the Renault 19, the cycle-to-cycle *inter-fuel* variability $S_2\%$ calculated for the transverse direction at the engine block, and calculated across all fuels, was 32.65 percent. The result of the same calculation for the Ford Focus was as only 17.17 percent. Despite the fact that the Renault 19 was an IDI-engined automobile, and thus was potentially capable of using fuels of poorer ignition quality due to the higher turbulence and higher mixing of fuel and air achieved in the combustion prechamber, the engine block analysis suggested that the action of the electronic controller of the common rail system of the Ford Focus was better able to compensate fuel differences.

The fuel-related changes in the vibration signatures at the steering wheel were quantified by means of the index of *inter-fuel* variability $S_2\%$. Both the global signal statistics and the cycle-to-cycle statistical variations in the vibration signatures were determined. The global *inter-fuel* statistical variation values $S_2\%$ were all found to be less than 13 percent across all ten fuels for both automobiles. On the other hand, the cycle-to-cycle *inter-fuel* variation values $S_2\%$ were all found to be greater than 13 percent across all ten fuels for both automobiles. The fact that $S_2\%$ was found to be higher when determined from cycle-to-cycle than when determined using the complete two minute vibration signal confirms that the half-order engine harmonic $H_{1/2}$ has the effect of making steering wheel idle vibration best described on a cycle-to-cycle basis. Being

characterised by $S_2\%$ values which are greater than 13 percent, which is the human just-noticeable-difference value for hand-arm vibrational stimuli, the differences between fuels are likely to be perceived by the driver when holding a steering wheel at idle.

Regarding the effect of engine technology, the engine related changes in the vibration signatures at the engine block were analysed by means of the cycle-to-cycle statistical variation. In this thesis a coefficient of cycle-to-cycle *intra-fuel* variability $S_1\%$ was defined, which for each fuel type permitted a comparison of the variability in the acceleration signal of the Renault 19 to that found in the vibration signal of the Ford Focus. When averaged across all ten reference fuels, the overall indices of the cycle-to-cycle *intra-fuel* variability $S_1\%$ were found to be similar for the Renault 19 and for the Ford Focus. In the case of the Renault 19, $S_1\%$ for the engine block in the transverse direction was 4.05 percent when averaged across all ten fuels, whereas the same quantity was 3.14 percent for the Ford Focus. Although the analysis of the fuel-related changes suggested that the indirect-injection (IDI) engine of the Renault 19 was more affected by fuel quality, the overall response of the engine block was found not to be affected by the type of engine tested.

Also regarding the effect of engine technology, comparison of the engine block power spectral densities suggested that the vibrations measured for the two engines differed in terms of amplitude only in the frequency range from 200 to 800 Hz, which coincides with the frequency range where the response of the engine structure is greatest. In the frequency range from 200 to 800 Hz, the spectrum of the IDI engine differed from the DI engine due to an increased bandwidth of the vibrational energy associated with the bending frequencies of the engine structure and with the cylinder combustion processes. The DI engine of the Ford Focus had vibrational energy mostly at frequencies in the range from 200 to 400 Hz, whereas for the IDI engine of the Renault 19 the range was mostly from 200 to 800 Hz. In the lower frequency range, up to 200 Hz, no evident differences were found in terms of the amplitudes of the engine harmonics.

- What is the most appropriate wavelet-based signal processing method to use for quantifying the statistical variation of diesel idle vibration signals ?

The time-frequency wavelet-based analysis of Chapter 6 used both the continuous wavelet transform and the orthogonal wavelet transform to identify which of the two wavelet methods provided the most sensitive tool for analysing steering wheel idle vibration. The wavelet analysis was performed in order to establish whether the variation in the diesel steering wheel idle vibration could be best characterized as due to changes in the instantaneous signal character caused by the rapid variation in the combustion peaks, or due instead to more slowly developing differences which occur across complete thermodynamic engine cycles. Orthogonal wavelet analysis, combined with time-varying auto-covariance (TVA) analysis performed across a complete engine thermodynamic cycle, was identified as the most sensitive method for analysing the statistical variation in the steering wheel vibration signals. The higher *intra-fuel* variability values (a mean value of 22.61 percent determined across both automobiles) obtained using the OWT and TVA suggested that the variation in the steering wheel vibration was best quantified in terms of cycle-to-cycle combustion energy rather than by an unequal instantaneous distribution of combustion peaks (a mean value of *intra-fuel* variability of 2.41 percent determined across both vehicles).

- What is the most appropriate psychophysical method to use for quantifying the human subjective response to the diesel engine idle vibration which arrives at the driver through the steering wheel ?

The experimental tests described in Chapter 7 investigated the growth in the human subjective response to amplitude-modulated vibration stimuli of the type caused by a four-cylinder diesel engine idle in passenger cars. The psychophysical protocols chosen for measuring the human

subjective response were Thurstone's method of paired comparison (Case III) and the category-ratio Borg CR-10 scale.

The subjective response scale values of perceived unpleasantness and roughness were found to depend on the psychophysical protocol used. In this research, the use of the Borg CR-10 scale has lead to smaller Stevens' exponents than paired comparison methods. The lower exponent seems to be a reflection of an artefact in the Borg scale which occurs when only a portion of the dynamic range of the scale is used (Laming, 1997). The mean subjective response of the test group was never found to be greater than 5.0, thus accounting for less than half the dynamic range of the Borg CR-10 scale. This would suggest that the Thurstone's method of the paired comparisons provides more accurate estimates in subjective difference.

- How can the human subjective response to idle vibration stimuli, which are perceived through the steering wheel, be modelled ? And how might this be used in practice by the producers of fuels, engines and of complete automobiles ?

The objective of the testing activities described in Chapter 7 was to develop a model of human hand-arm perception of the diesel idle vibration as perceived through the automotive steering wheel. Based on the signal processing described in Chapter 5 and Chapter 6, it was decided to model the diesel engine vibration which occurs at the steering wheel when at idle as sinusoidal amplitude-modulated signals having a carrier frequency equal to the second-order engine harmonic H_2 and a modulation frequency equal to the half-order engine harmonic $H_{1/2}$. Subjective evaluations of seven values of modulation depth parameter m were performed in order to define the growth function of the human perceived disturbance as a function of the modulation depth m.

A model of the human perception of amplitude-modulated vibrational stimuli has been proposed based on the existing biomedical research, and on the experimental findings presented in this thesis. All data suggests that there is a critical value of modulation depth ($m = 0.2$) below which human subjects do not perceive differences in amplitude modulation. Below the value $m = 0.2$,

the sensation can be interpreted as sensory noise relative to the energy of the unmodulated waveform. Above the value $m = 0.2$, the sensation grows monotonically as a power function of the modulation depth m. The Stevens' power exponents determined from the test data suggest that the perceived unpleasantness is dependent on modulation depth m with an exponent greater than 1, and that the perceived roughness is dependent with an exponent close to unity.

For producers of fuels, engines and of complete automobiles the proposed model of human hand-arm perception of vibrotactile amplitude-modulated stimuli can be used in order to perform a more accurate evaluation of customer's perception of vehicle idle quality. Different engines and different fuels can be described in terms of the modulation depth m that is produced for that specific vehicle, and the human subjective response to the various values of modulation depth m can be predicted based on the current findings. However, further experimental tests are necessary in order to achieve a complete characterisation which is representative of the widest possible number of operating condition encountered in automobiles when at idle. This last point is discussed in more detail in the next section.

8.2 Suggested Future Research

8.2.1 Comparison of Current Findings to the Properties of Real Fuels

The experimental testing described in Chapter 7 used analytically defined sinusoidal amplitude-modulated stimuli, which were scaled to have equal r.m.s. acceleration amplitude, in order to investigate the effect of only the single parameter of modulation depth m. However, real operating conditions may lead to different r.m.s. values depending on the type of fuel, engine and automobile in question. A general knowledge of psychophysics and of the human nervous system suggests that vibration level would be the first order parameter separating idle stimuli, while waveform would be a second order parameter. Standardised methods for evaluating the human

response to hand-arm vibrations of different level are widely available, and thus do not currently constitute a research challenge. It can therefore be hypothesised that the effect of the steering wheel r.m.s. vibration level can be easily quantified using standard methods, and that the r.m.s. level should serve as the first step in the steering wheel idle evaluation problem before passing to the difficult questions addressed in the research described in this thesis. In order to test this hypothesis, two additional laboratory experiments were performed in order to compare the current findings to the properties of vibration signatures associated with real fuel conditions.

A first experiment (referred to as experiment V) used the original steering wheel vibration stimuli as measured for the steering wheel of the Ford Focus. A second experiment (referred to as experiment VI) used the same original steering wheel vibration stimuli of experiment V, but scaled to a single r.m.s. acceleration amplitude. As a result of the experiments of Chapter 7, Thurstone's paired-comparison method was found to provide more accurate estimates of the human response to vibration stimuli than the Borg CR-10 scale procedure. Therefore, in the present experiments V and VI, Thurstone's method was chosen to quantify the human subjective response to the original diesel steering wheel idle vibration stimuli using the semantic descriptor of unpleasantness. All the stimuli used in experiments V and VI had the same time duration of 4 seconds as in the paired-comparison tests performed in section 7.4. The values of the modulation depth parameter m of the steering wheel idle vibration for all 10 fuel conditions for the Ford Focus 1.8 are presented in Table 8.1, along with the global r.m.s. values. The modulation values were determined by analysing each experimental waveform, and represented the mean modulation value acting over the complete time history.

For the application of Thurstone's paired-comparison method, five stimuli were selected from the set of the ten original steering wheel acceleration time histories. The selection was made such that the five test signals each had different values of modulation depth. The stimuli chosen were those of Fuel 1, Fuel 2, Fuel 4, Fuel 6, and Fuel 7.

Table 8.1   Modulation depth m of the steering wheel idle vibration stimuli measured for the Ford Focus 1.8 for each of the 10 diesel fuels.

Fuel type	Steering wheel idle Modulation depth (m)	Global r.m.s. [m/s²]
Fuel 1 (C.N. 77)	0.24	0.54
Fuel 2 (C.N. 52.9)	0.16	0.58
Fuel 3 (C.N. 63.3)	0.20	0.56
Fuel 4 (C.N. 69.3)	0.22	0.52
Fuel 5 (C.N. 52.4)	0.24	0.56
Fuel 6 (C.N. 50.7)	0.31	0.41
Fuel 7 (C.N. 54.5)	0.23	0.57
Fuel 8 (C.N. 54.9)	0.21	0.57
Fuel 9 (C.N. 56.5)	0.22	0.55
Fuel 10 (C.N. 44.7)	0.24	0.56

Figure 8.1 presents the mean subjective scale values along with the standard deviation values as a function of the modulation depth m of the original steering wheel signals. Figure 8.1a presents the scale values obtained from experiment V, while Figure 8.1b presents the scale values obtained from experiment VI.
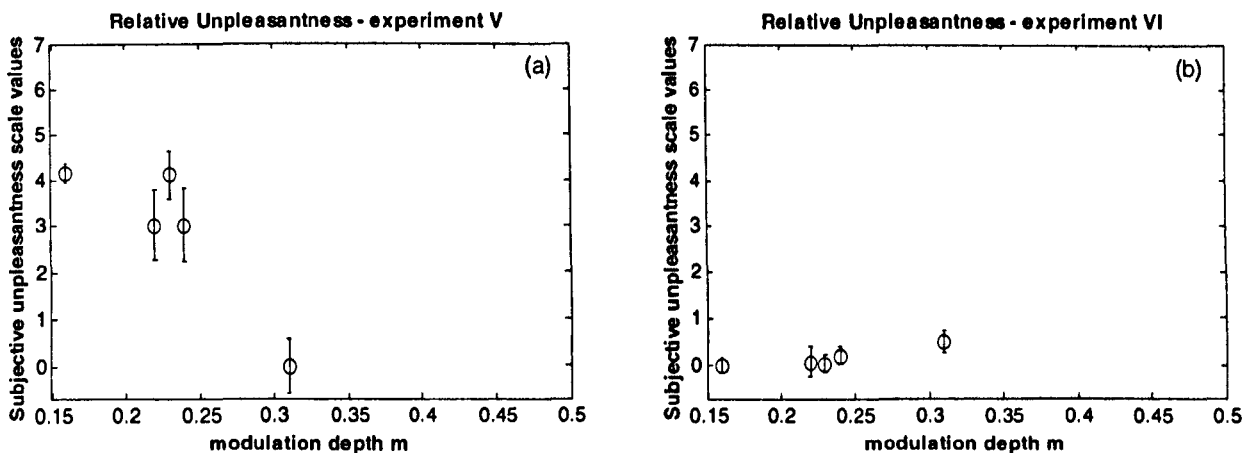
Figure 8.1   Mean subjective scale values as a function of modulation depth m, obtained using Thurstone's method. Data are shown as mean value plus or minus one standard deviation.

(a) relative unpleasantness values obtained from experiment V.
(b) relative unpleasantness values obtained from experiment VI.

The results from experiment V suggest that, when stimuli conditions differ in their intensity, the differences between the subjective scale values may be attributable to the difference in the signal

energy rather than to the differences in the modulation depth. On the other hand, the results from the experiments VI suggest that, when stimuli conditions are similar in their intensity, the human discrimination of different fuel conditions is based on the amplitude modulation of the vibration signature. Further, the results of experiment VI confirm the general model developed in this thesis.

Figure 8.2 presents the mean subjective response values obtained from experiment V, plotted as a function of the root mean square acceleration values of the test stimuli. As can be noted from this figure, the differences in the subjective scale values are a relatively linear function of the r.m.s. acceleration values.

Relative unpleasantness
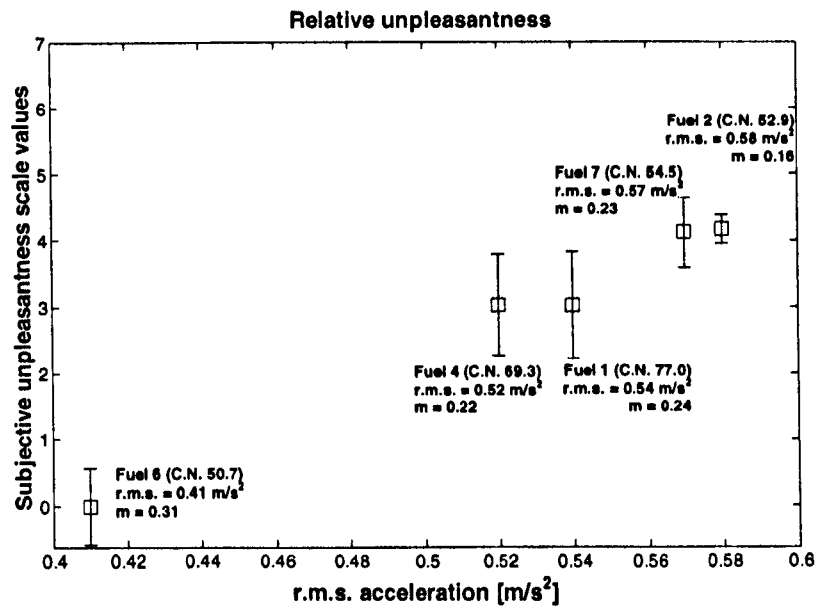
Figure 8.2   Mean subjective scale values as a function of the r.m.s. acceleration value of the test stimuli. Data are shown as mean value plus or minus one standard deviation.

For diesel idle vibration occurring at the steering wheel, with modulation depth greater than m = 0.2, the human perception of steering wheel idle vibration can therefore be described as a two-stage process. The first stage is a judgement of vibration intensity. The second stage is a judgement of the waveform modulation.

8.2.2 Further Research

Further psychophysical tests are required to validate the predictive model and to extend the measure to information other than the modulation depth parameter m. A few important areas in which further research would be beneficial are listed below.

Psychophysical testing using more original steering wheel idle vibration stimuli which differ in their intensity: The suggested two-stage model of the process of human discrimination for modulation depths greater than 0.2 was based on only five stimuli conditions. In order to have an accurate validation of the proposed model, further psychophysical tests, using more stimuli, are needed.

Psychophysical testing using steering wheel idle vibration stimuli form 6, 8 or 12-cylinder automobiles: The signal processing and the subjective responses described in this thesis were obtained from the study of the vibration signature measured from only two automobiles, which both had a 4-cylinder engine. A different number of cylinders, and different automobile design change the harmonic content of the steering wheel signal being measured. For example, a higher number of cylinders would change the firing frequency to a higher value than for a 4-cylinder engine. Also an increased number of cylinders would lead to a more balanced engine at idle. In order to guarantee the generality of the method, research needs to be performed using steering wheel vibrations from automobiles having 6, 8 and 12-cylinder engines. Also, further experimental tests are required to evaluate if the approach is applicable to gasoline engined automobiles.

Modelling the growth function of the human subjective response to amplitude-modulated stimuli using analytically defined signals of different energy level: The model of human perception of amplitude-modulated vibrational stimuli, proposed in section 7.6, was obtained using only one reference value of r.m.s. for all stimuli. Further psychophysical tests are required to investigate how the growth of the subjective response to amplitude-modulated stimuli changes when using higher or lower reference r.m.s. acceleration values than those used in the study described in this thesis.

References

Abry, P. (1997). *Ondelettes et turbulence. Multirésolutions, algorithmes de décomposition, invariance d'échelles*. Paris: Diderot Editeur.

Algom, D. and Marks, L.E. (1984). *Individual differences in loudness processing and loudness scales*. Journal of Experimental Psychology: General. 113: p. 571-593.

Allan, L.G. (1975). *The relationship between judgments of successiveness and judgments of order*. Perception & Psychophysics. 18 (1): p. 29-36.

Amman, S., Pielemeier, B., Snyder, D. and Toting, F. (2001). *Road vibration investigation using the Ford vehicle vibration simulator*. SAE Paper 2001-01-1572.

Anderton, D., Grover, E.C., Lalor, N. and Priede, T. (1970). *Origins of Reciprocating Engine Noise - Its characteristics, prediction and control*. Paper 70-WA/DGP-3 presented at ASME Winter Meeting.: p. 1-9.

Ando, H. and Motomochi, M. (1987). *Contribution of fuel transport lag and statistical perturbation in combustion to oscillation of SI engine speed at idle*. SAE Paper 870545.

American Society for Testing and Materials (1996). *Standard test methods for distillation of petroleum products*. ASTM D 86-96.

Baird, J.C. (1997). *Sensation and judgement. Complementarity Theory of Psychophysics*. Mahwah, New Jersey: Lawrence Erlbaum Associate, Inc.

Ball, J.K., Raine, R.R. and Stone, C.R. (1998). *Combustion analysis and cycle-by-cycle variations in spark ignition engine combustion Part 2: a new parameter for completeness of combustion and its use in modelling cycle-by-cycle variations in combustion*. Proceedings of the Institution of Mechanical Engineers Part D - Journal of Automobile Engineering. 212: p. 507-523.

Baret, C., Guglielmetto, L. and Storer, D. (2001). *Vehicle NVH target definition and the role of testing in the process*. In *Associazione Tecnica dell'Automobile (ATA) 7th International Conference. The role of experimentation in the automotive product development process*. Firenze, Italy,

Békésy, G.v. (1940). *The neural terminations responding to stimulation of pressure and vibration*. J. Exp. Psychol. 26: p. 514-519.

Békésy, G.v. (1957). *Neural volleys and the similarity between some sensations produced by tones and by skin vibrations*. J. Acoust. Soc. Am. 29 (10): p. 1059-1069.

Bellizzi, S., Guillemain, P. and Kronland-Martinet, R. (2001). *Identification of coupled non-linear modes from free vibration using time-frequency representations.* Journal of Sound and Vibration. 243 (2): p. 191-213.

Bellmann, M.A., Weber, R., Baumann, I., Hillebrand, P. and Mellert, V. (2000). *Methods for improving the objective description of subjective car vibration quality assessments.* ISMA 25.

Bendat, J.S. and Piersol, A.G. (1986). *Random data. Analysis and Measurement procedures.* 2nd ed. New York: John Wiley & Sons, Inc.

Bertrand, P. and Bertrand, J. (1985). *Representation temps-frequence des signaux a large bande.* La Recherche Aerospatiale (in French). 5: p. 277-283.

Bidan, P., Kouadio, L.K., Valentin, M. and Montseny, G. (1998). *Electrical assistance for S.I. engine idle-speed control.* Control Engineering Practice. 6: p. 829-836.

Biermayer, W., Thomann, S. and Brandl, F. (2001). *A software tool for noise quality and brand sound development.* SAE Paper 2001-01-1573.

Bolanowski Jr, S.J. and Gescheider, G.A. (1988). *Four channels mediate the mechanical aspects of touch.* J. Acoust. Soc. Am. 84 (5): p. 1680-1694.

Borg, G. and Borg, E. (1992). *Intelligence and rating behaviour in a psychophysical study of size. Report from the department of Psychology, no. 758.* Stockholm University: Stockholm.

Borg, G. (1998). *Borg's perceived exertion and pain scales.* Champaign, IL: Human Kinetics.

Brammer, A.J. and Muster, D. (1975). *Noise radiated by internal-combustion engines.* J. Acoust. Soc. Am. 58 (1): p. 11-21.

Brammer, A.J. and Verrillo, R.T. (1988). *Tactile sensory changes in hands occupationally exposed to vibration.* J. Acoust. Soc. Am. 84 (5): p. 1940-1941.

Brunt, M.F. and Emtage, A.L. (1997). *Evaluation of burn rate routines and analysis errors.* SAE Paper 970037.

British Standards Institution (1987). *British Standards Institution. Guide to measurement and evaluation of human exposure to whole-body mechanical vibration and shock.* BS 6841. London.

British Standards Institution (1987). *Measurement and evaluation of human exposure to vibration transmitted to the hand.* BS 6842. London.

British Standards Institution (1989). *Safety aspects of experiments in which people are exposed to mechanical vibration and shock.* BS 7085. London.

British Standards Institution (1993). *Sound system equipment - glossary of general terms and calculation methods.* BS 6840-2. London.

British Standards Institution (1997). *Specification for Automotive Diesel Fuel.* BS EN 590. London.

British Standards Institution (1997). *Sound system equipment - loudspeakers.* BS-EN 60268-5. London.

British Standards Institution (2005). *Human response to vibration - Measurement instrumentation.* BS EN 590. London.

Burros, R.H. (1951). *The application of the method of paired comparisons to the study of reaction potential.* Psychological Review. 58: p. 60-66.

Burros, R.H. and Gibson, W.A. (1954). *A solution for case III of the law of comparative judgment.* Psychometrika. 19 (1): p. 57-64.

Burrus, C.S., Gopinath, R.A. and Guo, H. (1998). *Introduction to wavelets and wavelet transforms. A primer.* New Jersey, U.S.A.: Prentice-Hall, Inc.

Carmona, R.A., Hwang, W.L. and Torresani, B. (1997). *Characterization of signals by the ridges of their wavelet transforms.* IEEE Trans. Signal Processing. 45 (10): p. 2586-2590.

Checkosky, C.M. and Bolanowski Jr, S.J. (1992). *The effects of stimulus duration on the response properties of Pacinian corpuscles: implications for the neural code.* J. Acoust. Soc. Am. 91: p. 3372-3380.

Chiollaz, M. and Favre, B. (1993). *Engine noise characterization with Wigner-Ville time-frequency analysis.* Mechanical System and Signal Processing. 7: p. 375-400.

Chui, C.K. (1992). *An Introduction to Wavelets. Wavelets Analysis and its Applications.* Vol. 1. Boston: Academic Press, Inc.

Cole, R.D., Taylor, M.G. and Rossi, F. (1986). *Additive solutions to diesel combustion problems. Paper No. C310/86.* Institution of Mechanical Engineers Conference on Petroleum Based Fuels and Automotive Applications, London, U.K.

Coren, S. and Ward, L.M. (1989). *Sensation and perception.* 3rd ed. Fort Worth: Harcourt Brace Jovanovich College Publishers.

Craig, J.C. (1972). *Difference threshold for intensity of tactile stimuli.* Perception & Psychophysics. 11 (2): p. 150-152.

Cross, D.V. (1973). *Sequential dependencies and regression in psychophysical judgments.* Perception & Psychophysics. 14: p. 547-552.

Dalpiaz, G. and Rivola, A. (1997). *Condition monitoring and diagnostics in automatic machines: comparison of vibration analysis techniques.* Mechanical System and Signal Processing. 11 (1): p. 53-73.

Dalpiaz, G., Rivola, A. and Rubini, R. (2000). *Effectiveness and sensitivity of vibration processing techniques for local fault detection in gears.* Mechanical System and Signal Processing. 14 (3): p. 387-412.

Daubechies, I. (1992). *Ten Lectures on Wavelets.* Pennsylvania: SIAM.

David, H.A. (1988). *The method of paired-comparison.* Ed. Charles Griffin, & Company Ltd. New York: Oxford University Press.

De Baene, W., Vandierendonck, A. and Leman, M. (2004). *Which method to choose when studying roughness: Magnitude estimation vs. Paired comparison.* Poster presented at the "Annual Meeting of the Belgian Psychological Society" in Brussels (Belgium).

De Baene, W., Vandierendonck, A., Leman, M., Widmann, A. and Tervaniemi, M. (2004b). *Roughness perception in sounds: behavioral and ERP evidence.* Biological Psychology. 67: p. 319-330.

De Nicalao, G., Rossi, C., Scattolini, R. and Suffritti, M. (1999). *Identification and idle speed control of internal combustion engines.* Control Engineering Practice. 7: p. 1061-1069.

DeBotton, G., Ben-Ari, J. and Sher, E. (2000). *Vibration monitoring as a predictive maintenance tool for reciprocating engines.* Proc. Instn. Mech. Engrs Part D. 214: p. 895-903.

Delprat, N., Escudie, B., Guillemain, P., Kronland-Martinet, R., Tchamitchian, P., and Torresani, B. (1992). *Asymptotic wavelet and Gabor analysis: extraction of instantaneous frequencies.* IEEE Transactions on Information Theory. 38 (2): p. 644-664.

Demers, M.A. (2001). *Steering wheel vibration diagnosis.* SAE paper 011607.

Dixon, J., Rhodes, D.M. and Phillips, A.V. (1994). *The generation of engine half orders by structural deformation.* Proceedings of IMechE Conference on Vehicle NVH and Refinement, paper C487/032/94: p. 9-17.

Ekman, G. and Künnapas, T. (1963). *A further study of direct and indirect scaling methods.* Scand. J. Psychol. 4: p. 77-80.

Entran Devices Limited (1991). *MSC Series Multi-channel Conditioning Unit.* Instruction Manual. Watford.

Erdreich, J. (1986). *A distribution based definition of impulse noise.* J. Acoust. Soc. Am. 79 (4): p. 990-998.

Farge, M., Hunt, J.C.R. and Vassilicos, J.C. (1994). *Wavelets, Fractals and Fourier Transforms.* Oxford: Clarendon Press.

Feldman, M. (1994a). Non-linear system vibration analysis using Hilbert Transform - I. Free vibration analysis method "FREEVIB". Mechanical System and Signal Processing. 8: p. 119-127.

Feldman, M. (1994b). Non-linear system vibration analysis using Hilbert Transform - II. Forced vibration analysis method "FORCEVIB". Mechanical System and Signal Processing. 8: p. 309-318.

Feldman, M. (1995). *Identification of non-linear system parameters via instantaneous frequency: application of the Hilbert transform and Wigner-Ville techniques.* Proceedings of 13th IMAC, Nashville, TN: p. 637-642.

Franzén, O. (1969). *The dependence of vibrotactile threshold and magnitude functions on stimulation frequency and signal level.* Scand. J. Psychol. 10: p. 289-297.

Fujikawa, K. (1988). *Analysis of steering column vibration.* Motion & Control. 4: p. 37-41.

Fullerton, G.S. and Cattel, J.M. (1892). *On the perception of small differences.* Philadelphia: University of Pennsylvania Press.

Gaberson, H.A. (2001). *Wavelet use for transient event detection in machinery vibration signals.* Proc. Imac. XIX Conf on Structural Dynamics: p. 998 -1004.

Gade, S. and Gram-Hansen, G.M. (1996). *Non-stationary signal analysis using wavelet transform, short-time Fourier transform and Wigner-Ville distribution.* Brüel & Kjær Technical Reviews No.2.

Gescheider, G.A. (1967). *Auditory and cutaneous temporal resolution of successive brief stimuli.* Journal of Experimental Psychology. 75 (4): p. 570-572.

Gescheider, G.A. (1976). *Evidence in support of the duplex theory of mechanoreception.* Sensory Process. 1: p. 68-76.

Gescheider, G.A., Verrillo, R.T., Capraro, A.J. and Hamer, R.D. (1977). *Enhancement of vibrotactile sensation magnitude and predictions from the duplex model of mechanoreception.* Sensory Process. 1: p. 187-203.

Gescheider, G.A. and Joelson, J.M. (1983). *Vibrotactile temporal summation for threshold and suprathreshold levels of stimulation.* Perception & Psychophysics. 33: p. 156-162.

Gescheider, G.A., Sklar, B.F., Van Doren, C.L. and Verrillo, R.T. (1985). *Vibrotactile forward masking: psychophysical evidence for a triplex theory of cutaneous mechanoreception.* J. Acoust. Soc. Am. 78: p. 534-543.

Gescheider, G.A., Bolanowski Jr, S.J., Verrillo, R.T., Arpajian, D.J. and Ryan, T.F. (1990). *Vibrotactile intensity discrimination measured by three methods.* J. Acoust. Soc. Am. 87 (1): p. 330-338.

Gescheider, G.A., Hoffman, K.E., Harrison, M.A., Travis, M.L. and Bolanowski, S.J. (1994). *The effects of masking on vibrotactile temporal summation in the detection of sinusoidal and noise signals.* J. Acoust. Soc. Am. 95 (2): p. 1006-1016.

Gescheider, G.A., Hoffman, K.E., Harrison, M.A., Travis, M.L. and Bolanowski, S.J. (1994b). *The effects of masking on vibrotactile temporal summation in the detection of sinusoidal and noise signals.* J. Acoust. Soc. Am. 95 (2): p. 1006-1016.

Gescheider, G.A., Zwislocki, J.J. and Rasmussen, A. (1996). *Effects of stimulus duration on the amplitude difference limen for vibrotaction.* J. Acoust. Soc. Am. 100 (4): p. 2312-2319.

Gescheider, G.A. (1997). *Psychophysics. The fundamentals.* 3rd ed: Lawrence Erlbaum Associates, Inc.

Gescheider, G.A., Berryhill, M.E. and Verrilo, R.T. (1999). *Vibrotactile temporal summation: probability summation or neural integration?* Somatosensory and Motor Research. 16: p. 229-242.

Gescheider, G.A., Bolanowski, S.J. and Hardick, K.R. (2001). *The frequency selectivity of information-processing channels in the tactile sensory system.* Somatosensory and Motor Research. 18: p. 191-201.

Giacomin, J. and Onesti, C. (1999). *Effect of frequency and grip force on the perception of steering wheel rotational vibration.* In *The new role of experimentation in the modern automotive product development process. ATA 6th Int. Conf.* Firenze, Italy, 17-19 November,

Giacomin, J., Steinwolf, A. and Staszewski, W.J. (1999). *A vibration mission synthesis algorithm for mildly nonstationary road data.* In *The new role of experimentation in the*

modern automotive product development process. ATA 6th Int. Conf. Firenze, Italy, 17-19 November,

Giacomin, J. and Abrahams, O. (2000). *Human fatigue due to automobile steering wheel vibration.* In *SIA Conference on car and train comfort.* Le Mans, France, 15-16 November, p. 1-11.

Giacomin, J., Steinwolf, A. and Staszewski, W.J. (2000). *An algorithm for mildly nonstationary mission synthesis [MNMS].* Engineering Integrity. 7: p. 44-56.

Giacomin, J., Shayaa, M.S., Dormegnie, E. and Richard, L. (2001). *Human perception of sinusoidal steering wheel rotational vibration.* In *36th United Kingdom Group Meeting on Human Responses to Vibration.* Centre for Human Sciences, Farnborough, UK, 12-14 September,

Giacomin, J., Shayaa, M.S., Dormegnie, E. and Richard, L. (2004). *A frequency weighting for the evaluation of steering wheel rotational vibration.* International Journal of Industrial Ergonomics. 33: p. 527-541.

Giacomin, J. and Fustes, F. (2005). *Subjective equivalence of steering wheel vibration and sound.* International Journal of Industrial Ergonomics. Vol. 35, Issue 6, p 517-526.

Giacomin, J. and Gnanasekaran, S. (2005). *Driver estimation of steering wheel vibration intensity: questionnaire-based survey.* Journal of the Engineering Integrity Society. 18: p. 23-29.

Giacomin, J. and Hacaambwa, T.M. (2005). *Subjective response to seated fore-and-aft direction whole-body vibration.* Submitted to International Journal of Industrial Ergonomics.

Gilson, E.Q. and Baddeley, A.D. (1969). *Tactile short-term memory.* Quartely Journal of Experimental Psychology. 21: p. 180-184.

Gonzalez, A., Ferrer, M., De Diego, M., Piñero, G. and Garcia-Bonito, J.J. (2003). *Sound quality of low-frequency and car engine noises after active noise control.* Journal of Sound and Vibration. 265: p. 663-679.

Griffin, M.J. and Whitham, E.M. (1976). *Duration of whole-body vibration exposure: its effect on comfort.* Journal of Sound and Vibration. 48: p. 333-339.

Griffin, M.J. (1981). *Dose-effect relationships for vibration-induced white finger.* In *Proceedings of the United Kingdom Informal Group Meeting on Human Response to Vibration.* HeriotWatt University, Edinburgh, 9-11 September, p. 112-127.

Griffin, M.J. (1982). *The effect of vibration on health*, in *Memorandum No. 632*. Institute of Sound and Vibration Research, University of Southampton.

Griffin, M.J. (1990). *Handbook of Human Vibration*. London: Academic Press.

Griffin, M.J. (1995). *The ergonomics of vehicle comfort*. In *Vehicle comfort and ergonomics. ATA 3rd International Conference*. Firenze, Italy, p. 213-221.

Grigg, H.C., Renowden, P.S. and Bodo, L. (1986). *The properties of diesel fuel as they relate to the operation of fuel injection equipment. Paper No. C305/86*. Institution of Mechanical Engineers Symposium on Petroleum Based Fuels, Lomdon.

Gu, F., Ball, A.D. and Rao, K.K. (1996). *Diesel injector dynamic modelling and estimation of injection parameters from impact response. Part 2: Prediction of injection parameters from monitored vibration*. Proceedings of the Institution of Mechanical Engineers Part D - Journal of Automobile Engineering. 210 (4): p. 303-312.

Guilford, J.F. (1954). *Psychometric Methods*. 2nd ed. New York: McGraw-Hill Publishing Cmpany Ltd.

Gurram, R., Rakheja, S. and Brammer, A.J. (1995b). *Driving point mechanical impedance of the human hand-arm system:synthesis and model development subject to sinusoidal and stochastic excitations*. J. Sound. Vibr. 180: p. 437.

Gutter, S. and Kantz (2001). *The auto-synchronized wavelet transform analysis for automatic acoustic quality control*. Journal of Sound and Vibration. 243 (1): p. 3-22.

Haasnoot, R.A. and Mansfield, N.J. (2003). *Effect of vibration envelope on relative sensation of vibration on a steering wheel*. In *38th United Kingdom Group Meeting on Human Responses to Vibration*. Institute of Naval Medicine, Alverstoke, Gosport, PO12 2DL, England, 17-19 September,

Hamer, R.D., Verrillo, R.T. and Zwislocki, J.J. (1983). *Vibrotactile masking of Pacinian and non-Pacinian channels*. J. Acoust. Soc. Am. 73 (4): p. 1293-1303.

Hanes, R.M. (1970). *Human sensitivity to whole-body vibration in urban transportation systems: a literature review. Transportation Programs Report APL/JHU TPR 004*. Applied Physics Laboratory, The Johns Hopkins University: Maryland.

Harrison, M. (2004). *Vehicle Refinement. Controlling noise and vibration in road vehicles*. Oxford: Elsevier Butterworth-Heinemann.

Hartmann, W.M. (2000). *Signals, sound and sensation*, ed. R.T. Beyer. New York: Springer-Verlag.

Heinze, P. (1986). *Engine performance and emissions with future type diesel fuels. Paper No. C306/86.* Institution of Mechanical Engineers Conference on Petroleum Based Fuels and Automotive Applications, Lomdon, U.K.

Hellman, R.P. (1981). *Stablity of individual loudness functions obtained by magnitude estimation and production.* Perception & Psychophysics. 29: p. 63-70.

Hertzberg, H.T.E. (1972). *The human buttock in sitting: pressures, patterns, and palliatives.* American Automobile Transactions. 72: p. 39-47.

Heywood, J.B. (1988). *Internal Combustion Engine Fundamentals:* McGraw-Hill Book Co.

Hickling, R., Feldmaier, D.A. and DSung, S.H. (1979). *Knock-induced cavity resonances in open chamber diesel engines.* J. Acoust. Soc. Am. 65 (6): p. 1474-1479.

Hills, F.J. and Schleyerbach, C.G. (1977). *Diesel fuel properties and engine performance.* SAE Paper 770316.

Hinton, P.R. (1999). *Statistics explained.* London: Routledge.

Hinze, P.C. and Cheng, W.K. (1998). *Assessing the factors affecting SI engine cycle-to-cycle variations at idle.* 27th Symposium (International) on Combustion / The Combustion Institute. 1-2: p. 2119-2125.

HMSO (1907). *Department Committee on Compensation for Industrial Diseases. Report of the department committee on compensation for industrial diseases.* Cd 3495. London.

Hoard, J. and Rehagen, L. (1997). *Relating subjective idle quality to engine combustion.* SAE paper 970035: p. 1-5.

Hoard, J. and Rehagen, L. (1997). *Relating subjective idle quality to engine combustion.* SAE Paper 970035.

Hodges, C.H., Power, J. and Woodhouse, J. (1985). *The use of sonogram in structural acoustics and an application to the vibrations of cylindrical shells.* Jornal of Sound and Vibration. 101: p. 203-218.

Hollins, M. and Roy, E.A. (1996). *Perceived intensity of vibrotactile stimuli: the role of mechanoreceptive channels.* Somatosensory and Motor Research. 13 (3-4): p. 273-286.

Hong, G.S., Rahman, M. and Zhou, Q. (1996). *Using neural network for tool condition monitoring based on wavelet decomposition.* Int. J. Mach. Tools Manufact. 36 (5): p. 551-566.

Howarth, H.V.C. and Griffin, M.J. (1991). *Subjective reaction to vertical mechanical shocks of various waveforms.* Journal of Sound and Vibration. 147 (3): p. 395-408.

International Organization for Standardization (1983). *Acoustics-Preferred reference quantities for acoustic levels.* ISO 5349. Geneva.

International Organization for Standardization (2001). *Mechanical Vibration - Measurement and assessment of human exposure to hand-transmitted vibration - Part 1: General guidelines.* ISO 5349-1. Geneva.

International Organization for Standardization (2001). *Mechanical Vibration - Vibrotactile perception thresholds for the assessment of nerve dysfunction, Part 1: Methods of measurement at the fingertips.* ISO 13091-1. Geneva.

Isomura, A., Hara, T. and Kmiya, K. (1995). *Human Factors on driver's steering wheel operation: three parameters evaluating characteristics of driver's steering wheel operations.* JSAE Review. 16: p. 388-410.

Ivaldi, D., Cortassa, C. and Tonetti, M. (2004). *Control strategies role in diesel engine: from the past to the future.* Associazione Tecnica dell'Automobile (ATA). 57 (5/6): p. 38-43.

Iwata, H. (1968). *Effects of rock drills on operators, Part 3. Joint and muscle pain, and deformity of bone and joint.* Industrial Health. 6: p. 47-58.

Iwata, H., Dupuis, H. and Hartung, E. (1972). *Ubertragung von horizontalen Sinusschwingungen auf die oberen Extremitaten bei Halbpronationsstellung und Reaktion des M. biceps.* Int. Arch. Arbeitsmed. 30: p. 313-328.

Johansson, R.S., Landstrom, U. and Lundstrom, R. (1982). *Responses of mechanoreceptive afferent units in the glabrous skin of the human hand to sinusoidal skin displacements.* Brain Research. 244: p. 17-25.

Jurden, R. (1995). *Automotive Electronics HandBook.* New York, U.S.A.: McGraw-Hill, Inc.

Kidoguchi, Y., Yang, C., Kato, R. and Miwa, K. (2000). *Effects of fuel cetane number and aromatics on combustion process and emissions of a direct-injection diesel engine.* JSAE Review. 21: p. 469-475.

Kim, J.H., jung, S.G. and Kim, K.S. (1985). *An investigation of the steering wheel vibration and its reduction in passenger cars.* SAE paper 852267.

Knibestol, M. and Vallbo, A.B. (1970). *Single unit analysis of mechanoreceptor activity from the human glabrous skin.* Acta Physiol. Scand. 80: p. 178-195.

Knudson, V. (1928). *Hearing with the sense of touch.* Journal of General Psychology. 1: p. 320-352.

Kouremenos, D.A., Rakopoulos, C.D. and Hountalas, D.T. (1996). *Experimental investigation of the performance and exhaust emissions of a swirl chamber diesel engine using JP-8 aviation fuel.* International Journal of Energy Research. 21: p. 1173-1185.

Krist, R. (1994). *Modellierung des sitzkomforts. Eine experimentelle studie.* Widen: Schuch.

Kronland-Martinet, R. and Morlet, J. (1987). *Analysis of sound through wavelet transforms.* International Journal of Pattern Recognition and Artificial Intelligence. 1 (2): p. 273-302.

Labs, S.M., Gescheider, G.A., Fray, R.R. and Lyons, C.H. (1978). *Psychophysical tuning curves in vibrotaction.* Sensory Process. 2: p. 231-247.

Ladommatos, N., Parsi, M. and Knowles, A. (1996). *The effect of fuel cetane improver on diesel pollutant emissions.* Fuel. 75 (1): p. 8-14.

Laming, D. (1997). *The Measurement of Sensation.* Oxford: Oxford University Press.

Lamoré, P.J.J. (1986). *Envelope detection of amplitude-modulated high-frequency sinusoidal signals by skin mechanoreceptors.* J. Acoust. Soc. Am. 79 (4): p. 1082-1085.

Lamoré, P.J.J. and Keemink, C.J. (1988). *Evidence for different types of mechanoreceptors from measurements of the psychophysical threshold for vibrations under different stimulation conditions.* J. Acoust. Soc. Am. 83 (6): p. 2339-2351.

Lèclere, Q., Pézerat, C., Laulagnet, B. and Polac, L. (2005). *Application of multi-channel spectral analysis to identify the source of a noise amplitude modulation in a diesel engine operating at idle.* Applied Acoustics. 66: p. 779-798.

Lee, S., Park, S. and Daisho, Y. (2004). *An experimental study of the effects of combustion systems and fuel properties on the performance of a diesel engine.* Proceedings of the Institution of Mechanical Engineers Part D - Journal of Automobile Engineering. 218: p. 1317-1323.

Lee, S.K. and White, P.R. (2000). *Application of wavelet analysis to the impact harshness of a vehicle.* Proc. Instn.Mech. Engrs Part C. 214: p. 1331-1338.

Li, D., Magnuson, D.S.K. and Jung, R. (2000). *Non-stationary analysis of extracellular neural activity.* Neurocomputing. 32-33: p. 1083-1093.

Li, D. and Jung, R. (2002). *Tracking rhythmicity in nonstationary quasi-periodic biomedical signals using adaptive time-varying covariance.* Computers in Biology and Medicine. 32 (4): p. 261-282.

Li, W., Gu, F., Ball, A.D. and Leung, A.Y.T. (1999). *The representation of engine acoustic signal using continuous wavelet transform.* Proc, of 1st Int. Conf. on the interpretation of dynamics monitoring & Control: p. 433-438.

Lichty, L.C. (1967). *Combustion engine processes.* New York: McGraw-Hill Book Company.

Lim, T.C. and Witer, A.J. (2000). *Experimental characterization of engine crankshaft rumble noise signatures.* Applied acoustics. 60: p. 45-62.

Lin, J. and Qu, L. (2000). *Feature extraction based on Morlet wavelet and its application for mechanical fault diagnosis.* Journal of Sound and Vibration. 234 (1): p. 135-148.

Liu, S., Gu, F. and Ball, A. (2002). *The on-line detection of engine misfire at low speed using multiple feature fusion with fuzzy pattern recognition.* Proceedings of the Institution of Mechanical Engineers Part D - Journal of Automobile Engineering. 216: p. 391-402.

Ljungberg, J., G, N. and Lundström, R. (2004). *Cognitive performance and subjective experience during combined exposures to whole-body vibration and noise.* Internatinal Arch. Occup. Environ. Health. 77: p. 217-221.

LMS International (1996). *LMS Cada X Fourier Monitor manual.* Revision 3.5 B. Leuvan.

LMS International (2002). *LMS Cada-X Fourier Monitor Manual.* Revision 3.5.E. Leuvan.

Logue, A.W. (1976). *Individual differences in magnitude estimation of loudness.* Perception & Psychophysics. 19: p. 279-280.

Lowet, G., Van de Ponseele, P., Pauwels, S., Van Wayenberge, T. and Sas, P. (1998). *Development of a metric to quantify diesel engine irregularities.* ISMA 23.

Lundström, R. and Burström, L. (1989). *Mechanical impedance of the human hand-arm system.* International Journal of Industrial Ergonomics. 3: p. 235-242.

Mallat, S. (1998). *A Wavelet Tour of Signal Processing.* San Diego, California: Academic Press.

Mansfield, N.J. and Marshall, J.M. (2001). *Symptoms of musculoskeletal disorders in stage rally drivers and co-drivers.* British Journal of Sports Medicine. 35: p. 314-320.

Marks, L.E. and Stevens, J.C. (1965). *Individual brightness functions.* Perception & Psychophysics. 1: p. 17-24.

Marks, L.E. (1974a). *Sensory process. The new psychophysics.* New York: Academic press.

Marks, L.E. (1974b). *On scales of sensation: Prolegomena to any future psychophysics that will come forth as sciences.* Perception & Psychophysics. 16: p. 358-376.

Marks, L.E. (1991). *Reliability of magnitude matching.* Perception & Psychophysics. 49: p. 31-37.

Martin, J.H. and Jessell, T.M. (1999). *Modality coding in the somatic sensory system,* in *Principles of neural science,* E.R. Kandel, J.H. Schwartz, and T.M. Jessell, Editors. Appleton and Lange. V, p. 341-352.

Maslow, A.H. (1954). *Motivation and personality.* New York: Harper.

Matekunas, F.A. (1983). *Modes and measures of cyclic combustion variability.* SAE Paper 830337.

Mathworks Inc (Version 6, September 2000a). *Signal Processing Toolbox for use with Matlab.*

Mathworks Inc (Version 6, September 2000b). *Wavelet Toolbox for use with Matlab.*

McAulay, R.J. and Quatieri, T.F. (1986). *Speech analysis/synthesis based on a sinusoidal representation.* IEEE Trans. Acoust. Speech Signal Processing (ASSP). 34 (4): p. 744-754.

McFadden, P.D. (1986). *Detecting fatigue cracks in gear by amplitude and phase demodulation of the meshing vibration.* ASME journal of Vibration, Acoustics, Stress, and Reliability in Design. 108: p. 165-170.

Meier, R., Otto, N., Pielemeier, W. and Jeyabalan, V. (1998). *The Ford vehicle vibration simulator for subjective testing.* Sound and Vibration. 32 (5): p. XX??

Messiah, A. (1961). *Quantum Mechanics.* North-Holland: Amsterdam.

Metzger, P. (1994). *Komfortverstandis bei Kraftfahrern.* Diplomarbeit an der Freien Universitat Berlin.

Miller, G.A. (1956). *The magical number seven, lus or minus two: Some limits on capacity for processing information.* Psychological Review. 63: p. 81-97.

Mishoe, J.W. and Suggs, C.W. (1977). *Hand arm vibration Part II: Vibrational responses of the human hand.* J. Sound. Vibr. 53: p. 545-558.

Miura, T., Morioka, M., Kimura, K. and Isida, N. (1957). *On the occupational hazards by vibrating tools (Report III).* Reports of the Institute for the Science of Labour. 52: p. 12-23.

Miura, T., Morioka, M., Kimura, K. and Akuta, A. (1959). *On the occupational hazards by vibrating tools (Report IV) - On the vibration of vibrating tools and the tentative threshold limit value of vibration.* Journal of Science of Labour. 35: p. 760-767.

Miwa, T. (1967). *Evaluation methods for vibration effect. Part 3:Measurements of threshold and equal sensation contours on hand for vertical and horizontal sinusoidal vibrations.* Industrial Health. 5: p. 213-220.

Miwa, T. (1968). *Evaluation methods for vibration effect. Part 7. The vibration greatness of the pulses.* Industrial Health. 7: p. 143-164.

Monaghan, M.L. (1981). *The high speed direct injection diesel for passenger cars.* SAE Paper 810477.

Montgomery, D.C. (1996). *Introduction to Statistical Quality Control.* 3rd ed: John Wiley & Sons.

Montgomery, D.C. and Runger, G.C. (1999). *Applied Statistics and Probability for Engineers.* 2nd ed, ed. W. Anderson. New York: John Wiley & Sons, Inc.

Moore, B.C.J. (2003). *An Introduction to the Psychology of Hearing.* 5th ed. London: Academic Press.

Morioka, M. (1999). *Effect of contact location on vibration perception threshold in the glabrous skin of the human hand.* In *34th United Kingdom Group Meeting on Human Responses to Vibration.* Ford Motor Company, Dunton, Essex, England, 22-24 September, p. 27-36.

Morioka, M. (2001). *Sensitivity of Pacinian and non-Pacinian receptors: effect of surround and contact location.* In *36th United Kingdom Group Meeting on Human Responses to Vibration.* Centre for Human Science, QinetiQ, Farnborough, UK, 12-14 September, p. 266-276.

Mountcastle, V.B., LaMotte, R.H. and Carli, G. (1972). *Detection thresholds for stimuli in humans and monkeys: comparison with threshold events in mechanoreceptive afferent fibres innervating the monkey hand.* Journal of Neurophysiology. 35: p. 122-136.

Neely, G., Ljunggren, G., Sylven, C. and Borg, G. (1992). *Comparison between the visual analogue scale (VAS) and the category ratio scale (CR) for the evaluation of leg exertion.* International Journal of Sports Medicine. 13: p. 133-136.

Newland, D.E. (1994). *An Introduction to Random vibration, spectral and Wavelet Analysis.* 3rd ed: Longman.

Nishimura, Y. and Ishii, K. (1986). *Engine idle stability analysis and control.* SAE paper 860412.

Nishiyama, K. and Watanabe, S. (1981). *Temporary threshold shift of vibratory sensation after clasping a vibrating handle.* International Arch. Occup. Environ. Health. 49: p. 21-33.

Nunnally, J.C. and Bernstein, I.H. (1994). *Psychometric Theory.* New York: McGraw-Hill.

Nylund, N., et al. (1997). *Effects of physical and chemical properties of diesel fuel on NOx emissions of heavy-duty diesel engines.* SAE Paper 972997.

Oakland, J.S. (1996). *Statistical Process Control.* 3rd Edition ed. Oxford: Butterworth-Heinemann.

Oppenheim, A.V. and Schafer, R.W. (1975). *Digital signal processing.* London: Prentice-Hal.

Owen, K. and Coley, T. (1995). *Automotive Fuels Reference Book.* 2nd Edition ed. Warrendale, Pennsylvania: Society of Automotive Engineers.

Oxford Dictionary (2000). *Oxford Advanced Learner's Dictionary Sixth edition.* Oxford: Oxford University Press.

Ozdor, N., Dulger, M. and Sher, E. (1994). *Cyclic Variability in Spark Ignition Engines: A literature Survey.* SAE paper 940987: p. 1514-1552.

Pak, C.H., Lee, U.S., Hong, S.C., Song, S.K., Kim, J.H., and Kim, K.S. (1991). *A study on the tangential vibration of the steering wheel of passenger car.* SAE Paper 912565: p. 961-968.

Parsons, K.C., Griffin, M.J. and Whitham, E.M. (1982). *Vibration and comfort. Part III. Translational vibration of the feet and back.* Ergonomics. 25: p. 705-719.

Pasti, L., Walczak, B., Massart, D.L. and Reschiglian, P. (1999). *Optimization of signal denoising in discrete wavelet transform.* Chemometrics and Intelligent Laboratory Systems. 48: p. 21-34.

Pavletic, R., Sinyavskiy, V.V., Bizjan, F. and Leskovšek, D. (1990). *I.C. engine having performance parameters preferential for automotive operating conditions.* The forth International Symposium COMODIA90: p. 185-191.

Pelmear, P.L., Taylor, W. and Wasserman, D.E. (1992). *Hand-arm Vibration.* New York: Van Nostrand Reinhold.

Peng, Z., Chu, F. and He, Y. (2002). *Vibration signal analysis and feature extraction based on reassigned wavelet scalogram.* Journal of Sound and Vibration. 253 (5): p. 1087-1100.

Peruzzetto, P. (1988). *Assessing the relative importance of hand vibration with respect to whole-body vibration.* In *United Kingdom and French joint Meeting on Human Response to Vibration.* I.N.R.S., Vandoeuvre, France, 26-28 September, p. 1-11.

Pflueger, M. and Stuecklschwaiger, W. (2001). *Sound and Vibration Quality map for Commercial Vehicles.* Sae Paper 2001-01-1570.

Phillips, J.R., Johansson, R.S. and Johansson, O. (1992). *Responses oh human mechanoreceptive afferents to embossed dot array scanned across fingerpad skin.* Journal of Neuroscience. 12: p. 827-839.

Pielemeier, W., Greenberg, J., Meier, R., Jeyabalan, V. and Otto, N. (2001). *Some factors in the subjective evaluation of laboratory simulated ride.* SAE Paper 2001-01-1569.

Piersol, A.G. (1992). *Data Analysis,* in *Noise and Vibration Control Engineering: Principles and Applications,* L.L.a.V. Bernarek, I.L., Editor. John Wiley & Sons, Inc.: New York. chapter 3, p. 45-73.

Pineau, C. (1982). *The psychological meaning of comfort.* Internatinal Review of Applied Psychology. 31: p. 271-283.

Pischinger, F.F., Schmillen, K.P. and Leipold, F.W. (1979). *A new measuring method for the direct determination of diesel engine combustion noise.* SAE Paper 790267: p. 39-48.

Pollack, I. (1952). *The information of elementary auditory displays.* J. Acoust. Soc. Am. 24: p. 745-749.

Pottinger, M.G. and Marshall, K.D. (1986). *A Review of Tire / Pavement Interaction Induced Noise and Vibration,* in *The Tire Pavement Interface, ASTP STP 929,* M.G. Pottinger and T.J. Yager, Editors. American Society for Testing and Materials: Philadelphia. p. 183-287.

Poulton, E.C. (1989). *Bias in quantifying judgments.* London: Erlbaum.

Priede, T., Grover, E.C. and Lalor, N. (1969). *Relation between noise and basic structural vibration of diesel engines.* SAE Paper 690450.

Priede, T. (1992). *Noise and Vibration Control of the Internal Combustion Reciprocating Engine,* in *Noise and Vibration Control Engineering: Principles and Applications,* L.L.a.V. Bernarek, I.L., Editor. John Wiley & Sons, Inc.: New York. chapter 19, p. 665-707.

Pyykkö, I., Färkkilä, M., Toivanen, J., Korhonen, O. and Hyvärien, J. (1976). *Transmission of vibration in the hand-arm system with special reference to changes in compression force and acceleration.* Scandinavian Journal of Work, Environment and Health. 2: p. 87-95.

Qatu, M., Sirafi, M. and Johns, F. (2002). *Robustness of powertrain mount system for noise, vibration and harshness at idle.* Proc. Instn. Mech. Engrs Part D. 216: p. 805-810.

Rahnejat, H. (1998). *Multi-body Dynamics: Vehicles, Machines and mechanisms.* Bury St Edmunds, UK: Professional Engineering Publishing Limited.

Randall, S.B. (2001). *Roll-down considerations in idle quality.* SAE Paper. 2001-01-1501.

Ren, Y., Randall, R.B. and Milton, B.E. (1999). *Influence of the resonant frequency on the control of knock in diesel engines.* Proc. Instn. Mech. Engrs Part D. 213: p. 127-133.

Reynolds, D.D. and Soedel, W. (1972). *Dynamic response of the hand-arm system to a sinusoidal input.* Journal of Sound and Vibration. 21: p. 339-353.

Reynolds, D.D. and Angevine, E.N. (1977). *Hand-arm vibration, Part II: Vibration transmission characteristics of the hand and arm.* Journal of Sound and Vibration. 51 (2): p. 255-265.

Reynolds, D.D. and Keith, R.H. (1977). *Hand-arm vibration, Part 1: Analytical model of the vibration response characteristics of the hand.* journal of Sound and Vibration. 51 (2): p. 237-253.

Reynolds, D.D., Standlee, K.G. and Angevine, E.N. (1977). *Hand-arm vibration, Part III: Subjective response characteristics of individuals to hand-induced vibration.* Journal of Sound and Vibration. 51 (2): p. 267-282.

Riesenberg, K.O. and Faupel, W. (1999). *Diesel-engine management.* 2nd ed, ed. H. Bauer. Stuttgart: Bosch, R.

Rubini, R. and Meneghetti, U. (2001). *Application of the envelope and wavelet transform analysis for the diagnosis of incipient faults in ball bearings.* Mechanical System and Signal Processing. 15 (2): p. 287-302.

Society of Automobile Engineers (1974). *Vehicle Dynamics Terminology.* SAE J670e. Warrendale, PA.

Sakakibara, H., Kondo, T., Miyao, M., Yamada, S., Nakagawa, T., Kobayashi, F., and Ono, Y. (1986). *Transmission of hand-arm vibration to the head.* Scandinavian Journal of Work, Environment and Health. 12: p. 359-361.

Satgé de Caro, P., Mouloungui, Z., Vaitilingom, G. and Berge, J.C. (2001). *Interest of combining an additive with diesel-ethanol blends for use in diesel engines.* Fuel. 80: p. 565-574.

Schoeggl, P. and Ramschak, E. (1997). *Vehicle driveability assessment using Neural Network for development calibration and quality test.* SAE Paper 2000-01-0702.

Schröder, F. and Zhang, T. (1997). *Objective and subjective evaluation of suspension harshness. Paper 97A2I05.* In *6th European Automobile Cooperation: International Congress, Cernobbio, Italy,* p. 63-72.

Scott, W.M. (1973). *Noise of small indirect injection Diesel Engines.* SAE paper 730242.

Shafiquzzaman, K., Trapenskas, D. and Johansson, O. (2000). *Effects of different fuels on annoyance from diesel engine sounds.* Noise Control Eng. J. 48 (3): p. 102-106.

Shim, D., Park, J., Khargonekar, P.P. and Ribbens, W.B. (1996). *Reducing automotive engine speed fluctuation at idle.* IEEE Transactions on Control System Technology. 4 (4): p. 404-410.

Shundoh, S., Kakegawa, T., Tsujimura, K. and Kobayashi, S. (1991). *The effect of injection parameters and swirl on diesel combustion with high pressure fuel injection.* SAE paper 910489.

Slater, K. (1985). *Human Comfort.* Springfield, IL: Charles C. Thomas.

Smallwood, D.O. (1998). *Characterization and simulation of gunfire with wavelets.* Sandia national Laboratories SAND 98-0670C: p. 1-9.

Sony (1994). *Digital Sony PC216A.* Instrumentation-cassette recorder/channel expansion unit manual.

Sörensson, A. and Lundström, R. (1992). *Transmission of vibration to the hand.* Journal of low frequency noise and vibration. 11 (1): p. 14-22.

Sörensson, A. and Burström, L. (1997). *Transmission of vibration energy to different parts of the human hand-arm system.* International Arch. Occup. Environ. Health. 70: p. 199-204.

Stankovic, L. and Bohme, J.F. (1998). *Time-frequency analysis of multiple resonances in combustion engine signals.* Signal processing. 79: p. 15-28.

Staszewski, W.J. and Tomlinson, G.R. (1994). *Application of the wavelet transform to fault detection in a spur gear.* Mechanical System and Signal Processing. 8 (3): p. 289-307.

Staszewski, W.J., Worden, K. and Tomlinson, G.R. (1997). *Time-frequency analysis in gearbox fault detection using the Wigner-Ville distribution and pattern recognition.* Mechanical System and Signal Processing. 11 (5): p. 673-692.

Staszewski, W.J. (1998a). *Identification of nonlinear system using multiscale ridges and skeletons of the wavelet transform.* J. Sound. Vibr. 214 (4): p. 639-658.

Staszewski, W.J. (1998b). *Wavelet based compression and feature selection for vibration analysis.* Journal of Sound and Vibration. 211 (5): p. 735-760.

Stelling, J. and Dupuis, H. (1996). *Different acute effects of single-axis and multi-axis hand-arm vibration.* International Arch. Occup. Environ. Health. 68: p. 236-242.

Stevens, J.C. and Stevens, S.S. (1963). *Brightness function: effects of adaptation.* Journal of the Optical Society of America. 53: p. 375-385.

Stevens, S.S. (1946). *On the theory of scales of measurement.* Science. 103 (2684): p. 677-680.

Stevens, S.S. (1955). *The measurement of loudness.* J. Acoust. Soc. Am. 27: p. 815-820.

Stevens, S.S. and Galanter, E.H. (1957). *Ratio scales and category scales for a dozen perceptual continua.* Journal of Experimental Psychology. 54: p. 377-411.

Stevens, S.S., Carton, A.S. and Shickman, G.M. (1958). *A scale of apparent intensity of electric shock.* Journal of Experimental Psychology. 56: p. 328-334.

Stevens, S.S. (1959). *Tactile vibration: dynamics of sensory intensity.* Journal of Experimental Psychology. 57 (4): p. 210-218.

Stevens, S.S. (1960). *Ratio scales, partition scales and confusion scales.*, in *Psychological scaling: Theory and applications*, H. Gulliksen and S. Messick, Editors. Wiley: New York.

Stevens, S.S. and Harris, J.R. (1962). *The scaling of subjective roughness and smoothness.* Journal of Experimental Psychology. 64 (5): p. 489-494.

Stevens, S.S. (1966). *A metric for the social consensus.* Science. 151: p. 530-541.

Stevens, S.S. and Greenbaum, H. (1966). *Regression effect in psychophysical judgment.* Perception & Psychophysics. 1: p. 439-446.

Stevens, S.S. (1968). *Tactile vibration: Change of exponent with frequency.* Perception & Psychophysics. 3: p. 223-228.

Stevens, S.S. (1986). *Psychophysics: introduction to its perceptual, neural and social prospects,* ed. G. Stevens. New Brunswick, U.S.A.: Transaction Books.

Stout, J.L., Mancini, M., Host, R. and Hancock, K. (2003). *Combustion uniformity as a measure for engine idle NVH.* SAE Paper 2003-01-1429.

Takeda, N., et al. (1982). *Improvement on steering column shake.* Journal of JSAE. 36 (12).

Talbot, W.H., Darien-Smith, I., Kornhuber, H.H. and Mountcastle, V.B. (1968). *The sense of flutter-vibration: comparison of the human capacity with response patterns of mechanoreceptive afferents from the monkey hand.* Journal of Neurophysiology. 31: p. 301-304.

Taylor, W., Pelmear, P.L. and Pearson, J.C.G. (1975). *A longitudinal study of Raynaud's phenomenon in chain saw operators,* in *Vibration white finger in industry,* W. Taylor and P.L. Pelmear, Editors. Academic Press: London. Chap. 2, p. 15-20.

Teghtsoonian, M. and Teghtsoonian, R. (1983). *Consistency of individual exponents in cross-modal matching.* Perception & Psychophysics. 33: p. 203-214.

Teghtsoonian, R. (1971). *On the exponents in Stevens' law and the constant in Ekman's law.* Psychological Review. 78 (1): p. 71-80.

Teghtsoonian, R. and Teghtsoonian, M. (1978). *Range and regression effects in magnitude scaling.* Perception & Psychophysics. 24 (4): p. 305-314.

Tektronix Inc. (1999). *TDS 210/220 digital real-time oscilloscope.* User manual.

Thorndike, E.L. (1910). *Handwriting.* Teachers College Record. 11 (2).

Thurstone, L.L. (1959). *The measurement of values.* Chicago: The University of Chicago Press.

Torgerson, W.S. (1958). *Theory and method of scaling.* New York: John Wiley & Sons, Inc.

Verrillo, R.T. (1965). *Temporal summation in vibrotactile sensitivity.* J. Acoust. Soc. Am. 37 (5): p. 843-846.

Verrillo, R.T. (1966a). *Effect of spatial parameters on the vibrotactile threshold.* J. Exp. Psychol. 71: p. 570-575.

Verrillo, R.T. (1966b). *Vibrotactile sensitivity and the frequency response of the Pacinian corpuscle.* Psychon. Sci. 4: p. 135-136.

Verrillo, R.T., Fraioli, A.J. and Smith, R.L. (1969). *Sensation magnitude of vibrotactile stimuli.* Perception & Psychophysics. 6: p. 366-372.

Verrillo, R.T. and Gescheider, G.A. (1977). *Effect of prior stimulation on vibrotactile thresholds.* Sensory Process. 1: p. 292-300.

Verrillo, R.T. (1985). *Psychophysics of vibrotactile stimulation.* J. Acoust. Soc. Am. 77 (1): p. 225-232.

Verrillo, R.T. and Gescheider, G.A. (1992). *Perception via the sense of touch,* in *Tactile Aids for the Hearing Impaired,* I.R. Summers, Editor. Whurr: London. p. 1-36.

Viemeister, N.F. (1979). *Temporal modulation transfer functions based upon modulation thresholds.* J. Acoust. Soc. Am. 66 (5): p. 1364-1380.

Wang, H. and Jung, R. (2002). *Variability analyses suggest that supraspino-spinal interactions provide dynamic stability in motor control.* Brain Research. 930: p. 83-100.

Wang, W.Q. and McFadden, P.D. (1995). *Application of orthogonal wavelets to early gear damage detection.* Mechanical System and Signal Processing. 9 (5): p. 497-507.

Wang, W.Q. and McFadden, P.D. (1996). *Application of wavelets to gearbox vibration signals for fault detection.* Journal of Sound and Vibration. 192 (5): p. 927-939.

Wang, W.Q., Ismail, F. and Golnaraghi, M.F. (2001). *Assessment of gear damage monitoring techniques using vibration measurements.* Mechanical System and Signal Processing. 15 (5): p. 905-922.

Wanschura, R.G. and Dawson, W.E. (1974). *Regression effect and individual power functions over sessions.* Journal of Experimental Psychology. 102: p. 806-812.

Ward, L.M. (1973). *Repeated magnitude estimation with a variable standard: sequential effects and other properties.* Perception & Psychophysics. 13: p. 193-200.

Ward, L.M., Armstrong, J. and Golestani, N. (1996). *Intensity resolution and subjective magnitude in psychophysical scaling.* Perception & Psychophysics. 58 (5): p. 793-801.

Watanabe, H. and Tahara, T. (1998). *Study of the effects on exhaust emissions in direct injection diesel engines: Effects of fuel injection system, distillation properties and cetane number.* JSAE Review. 19 (21-26).

Webster's Dictionary (2004). *Webster's Eleventh New Collegiate Dictionary.* Springfield, MA: Merriam-Webster, Inc.

Weisenberger, J.M. (1986). *Sensitivity to amplitude-modulated vibrotactile signals.* J. Acoust. Soc. Am. 80 (6): p. 1707-1715.

Wolf, A. and Portal, E. (2001). *Engine roughness: analysis and reduction considering air and structural borne noise paths, interfaces and innovative NVH-parts.* Sae Paper 2001-01-1575.

Wong, C.L. and Steere, D.E. (1982). *The effects of diesel fuel properties and engine operating conditions on ignition delay.* SAE Paper 821231, SAE Transaction. Vol. 91.

Wos, H., Marek, T., Noworol, C. and Borg, G. (1988). *The reliability of self-ratings based on Borg's scale for hand-arm vibrations of short duration (Part II).* International Journal of Industrial Ergonomics. 2: p. 151-156.

Wos, H., Wangenheim, M., Borg, G. and Samuelson, B. (1988). *Perceptual rating of local vibration: a psychophysical study of hand-arm vibration of short duration (Part I).* International Journal of Industrial Ergonomics. 2: p. 143-150.

Yang, C., Kidoguchi, Y. and Miwa, K. (1998). *Effect of rich and high turbulence combustion on NO x and particulate emissions from a high speed direct-injection diesel engine.* The forth International Symposium COMODIA98: p. 63-68.

Zheng, H., Li, Z. and Chen, X. (2002). *Gear fault diagnosis based on continuous wavelet transform.* Mechanical System and Signal Processing. 16 (2-3): p. 447-457.

Zwislocki, J.J. (1960). *Theory of temporal summation.* J. Acoust. Soc. Am. 32: p. 1046-1060.

Zwislocki, J.J. (1991). *Natural measurement,* in *Ratio scaling of psychological magnitude: In honour of the memory of S. S. Stevens,* S.J. Bolanowski and G.A. Gescheider, Editors. Erlbaum: Hillsdale, NJ. p. 18-26.

Appendix A

Technical Specifications of Equipment

A.1 Accelerometers Specifications for Vibration Measurement

A.1.1 Triaxial EGAS3 Accelerometer used the Experimental Idle Vibration Tests

The technical specifications of the triaxial accelerometers are presented in Figure A.1 and A.2. Certificate of calibration and properties for each single axis of measurement direction are presented in Figure A.3 for the engine block measurements, while in Figure A.4 are presented those for the steering wheel measurements.

Serial number: W00521 used for the engine block idle vibration measurements.

Serial number: N98121 used for the steering wheel idle vibration measurements.

Model: EGAS3-CM-25-/L2M

Specifications

TRIAXIAL EGAS3

EGAS3-C & EGAS3-CM

1m (3.3 ft) x 3 Shielded Teflon cables

15 (.59")

15 (.59")

7.5 (.29")

4 (.18")

EGAS3-C : 10-32UNF x 0.16" Deep
EGAS3-CM : M5 x 0.8 x 4 Deep
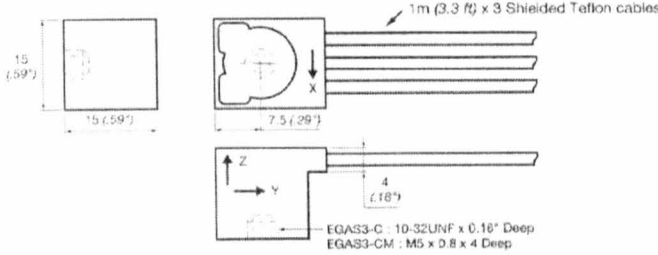
Dim: mm (inches)

Triaxial Mounting Blocks for up to 3 Single Axis EGAS

MTG-F2 (Purchase Accelerometers separately from mounting blocks)   MTG-F3 (Purchase Accelerometers separately from mounting blocks)

EGAS-FS & FT
16.3 (.64")
21 (.83")
21 (.83")
Ø 2.8 (.11")
2 mounting holes
Central mounting hole
21 (.83")
For sensor mounting screw

Central mounting hole
Ø 6.2 (.24")
8 (.31")
Ø 4.2 (.16")

EGAS-F
17 (.67")
17 (.67")
Central mounting hole
17 (.67")
For sensor mounting screw
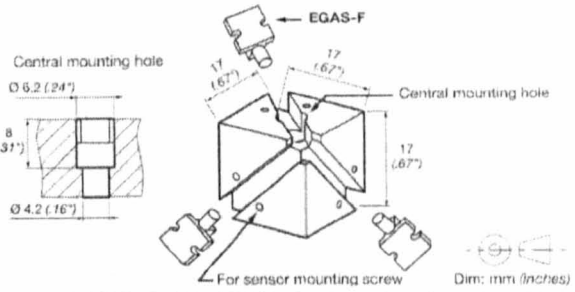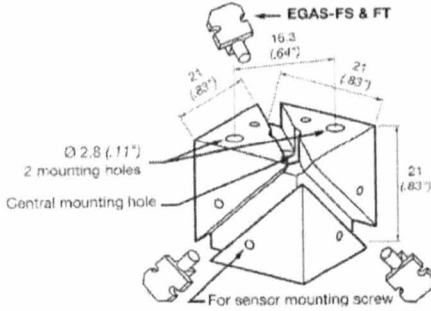
Dim: mm (inches)

EGAS3 Multiaxial Series - Specifications for each individual axis

g RANGES "FS"	g OVERRANGE LIMIT	FREQUENCY RESPONSE ±1/2dB nom./min.	NATURAL FREQUENCY nom.	SENSITIVITY mV/g nom.	OUTPUT "FSO" mV nom.
± 5	± 500	0 to 150/80 Hz	300 Hz	20	± 100
± 10	± 1000	0 to 200/120 Hz	400 Hz	10	± 100
± 25	± 2500	0 to 400/240 Hz	800 Hz	4	± 100
± 50	± 5000	0 to 600/350 Hz	1200 Hz	2	± 100
± 100	± 10000	0 to 900/500 Hz	1800 Hz	1	± 100
± 250	± 10000	0 to 1300/750 Hz	2600 Hz	0.4	± 100
± 500	± 10000	0 to 1750/1000 Hz	3500 Hz	0.2	± 100
± 1000	± 10000	0 to 2500/1500 Hz	5000 Hz	0.1	± 100
± 2500	± 10000	0 to 3500/2000 Hz	7000 Hz	0.04	± 100

EXCITATION: 15VDC
IMPEDANCE IN: 1300 Ω nom. typ.
IMPEDANCE OUT: 1500 Ω nom.
COMB. NON-LINEARITY& HYSTERESIS: ± 1%
TRANSVERSE SENSITIVITY: 2% max
DAMPING RATIO AT 20°C (70°F):   0.7 nom. (0.5 to 0.9)
OVERRANGE STOPS: Integral
THERMAL ZERO SHIFT: ± 1mV/50°C (± 1mV/100°F)
THERMAL SENSITIVITY SHIFT (TSS):   ± 2.5%/50°C (± 2.5%/100°F)
OPERATING TEMPERATURE: -40°C to 120°C (-40°F to 250°F)
COMPENSATED TEMPERATURE: 20°C to 80°C (70°F to 170°F)
ZERO OFFSET AT 20°C (70°F):   ± 15mV typ.

E G A S3 E9	**Entran**®	TITLE **EGAS3 ACCELEROMETERS** Triaxial Miniature Rugged	Entran® ENGLAND Garston, Watford, Herts EUROPEAN HEADQTRS Les Clayes-sous-Bois, FRANCE
			SPECIFICATION NUMBER / ISSUE / PAGE
			EGAS3S01E / A / 1 of 2

Figure A.1   Technical specifications for the triaxial EGAS3 accelerometer used for the experimental idle vibration measurements. Part I.

Options and Accessories:

COMPENSATED TEMPERATURE RANGES:	STANDARD	= 20°C to 80°C (70°F to 170°F)
	Z1	= -20°C to 40°C (0°F to 100°F)
	Z2	= 0°C to 60°C (32°F to 140°F)
	Z4	= 40°C to 90°C (100°F to 200°F)
	Z*	= Non-standard, contact Entran.
5 WIRE BRIDGE WIRING FOR ADJUSTABLE ZERO OFFSET ON EGAS & EGAS-F ONLY:	5	= 5 Wire
EXCITATION VOLTAGE:	STANDARD	= 15VDC
	V00	= Replace "00" with Excitation between 1 and 15 If less than 15, Sensitivity (FSO) will decrease accordingly.
	V*	= Non-standard Excitation with standard FSO and non-standard TSS, contact Entran.
SPECIAL LEAD LENGTH:	L00F	= Replace "00" with total length in feet.
	L00M	= Replace "00" with total length in meters.
SPECIAL MODULE LOCATION:	M00F	= Replace "00" with distance between sensor and module in feet.
	M00M	= Replace "00" with distance between sensor and module in meters.
WATERPROOFING LEAD EXIT ON EGAS-FS & EGAS-FT:	X	= Short term waterproofing. Limited to 105°C (220°F).
CONNECTOR WIRED TO LEADS OR CABLE:	C	= Microtech type male (w/o mate)
	R	= RJ Telephone type male (w/o mate) for EGAS & -F
	RS	= RJ Telephone type male for cable (w/o mate) for -FS & -FT
MATING CONNECTORS FOR CONNECTOR OPTIONS:	See Cable and Connector Bulletins	
TRIAXIAL MOUNTING BLOCKS:	MTG-F2 for mounting 3 EGAS-FS & -FT (see EG Accessories)	
	MTG-F3 for mounting 3 EGAS-F (see EG Accessories)	

Model Number construction:

EGAS Series	-	F Housings	-	100 Range	-	/Z1/L2M/R Options
		- -				C, R or RS
		-F				L00F or L00M
		-FS				M00F or M00M
		-FT				V1 thru V15 or V*
						X
						Z1,Z2,Z4, or Z*
						5

Wiring:

Figure A.2 Technical specifications for the triaxial EGAS3 accelerometer used for the experimental idle vibration measurements. Part II.

(a)

(b)

(c)

Figure A.3 ENTRAN Certificate of calibration and specifications for the triaxial EGAS3 accelerometer used to record the engine block idle vibration along the (a) X-axis, (b) Y-axis, (c) Z-axis.

(a)

(b)

(c)

Figure A.4 ENTRAN Certificate of calibration and specifications for the triaxial EGAS3 accelerometer used to record the steering wheel idle vibration along the (a) x'-axis, (b) y'-axis, (c) z'-axis.

A.1.2 Monoaxial EGAS Accelerometer used in the Experimental Laboratory Tests

The monoaxial accelerometer, which was placed on the rotational steering wheel test rig, is presented Figure A.5. The technical specifications of the monoaxial accelerometer are presented in Figure A.6.

Model: EGAS-FT-25-/L02M
Serial number: S99329 used for the steering wheel vibration measurements for the test rig in the laboratory.

Certificate of calibration and properties for the single axis of measurement direction are presented in Figure A.7.
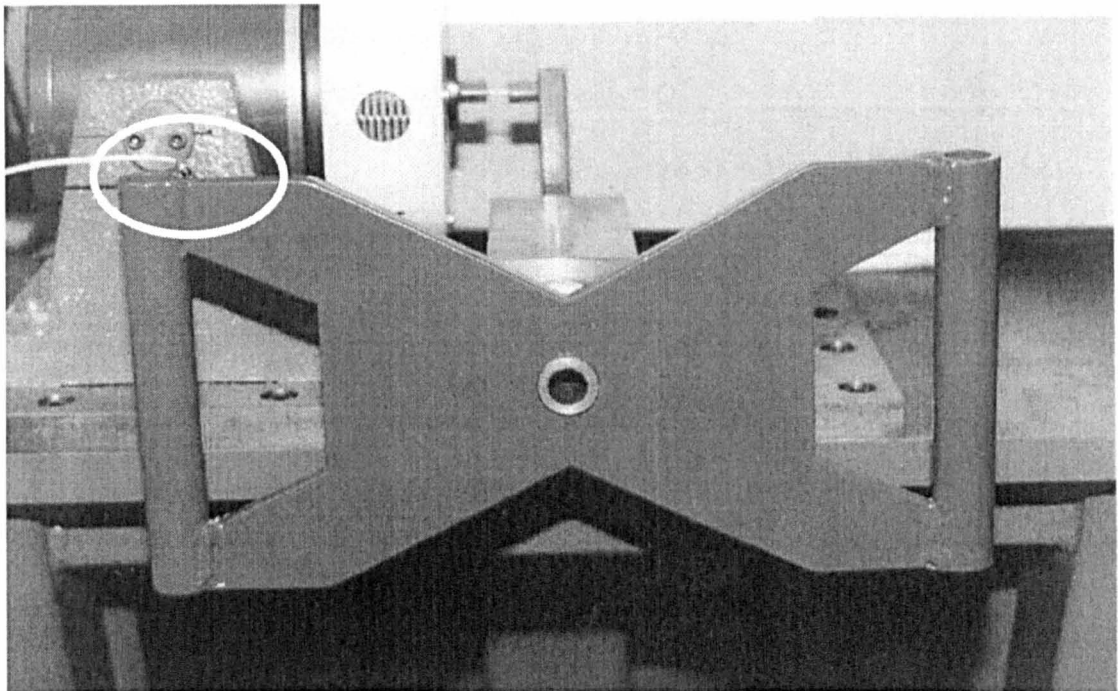
Figure A.5 Accelerometer position at the rotational steering wheel test rig, located on the top left side of the wheel.

Specifications

EGAS, EGAS-F, EGAS-FS & EGAS-FT
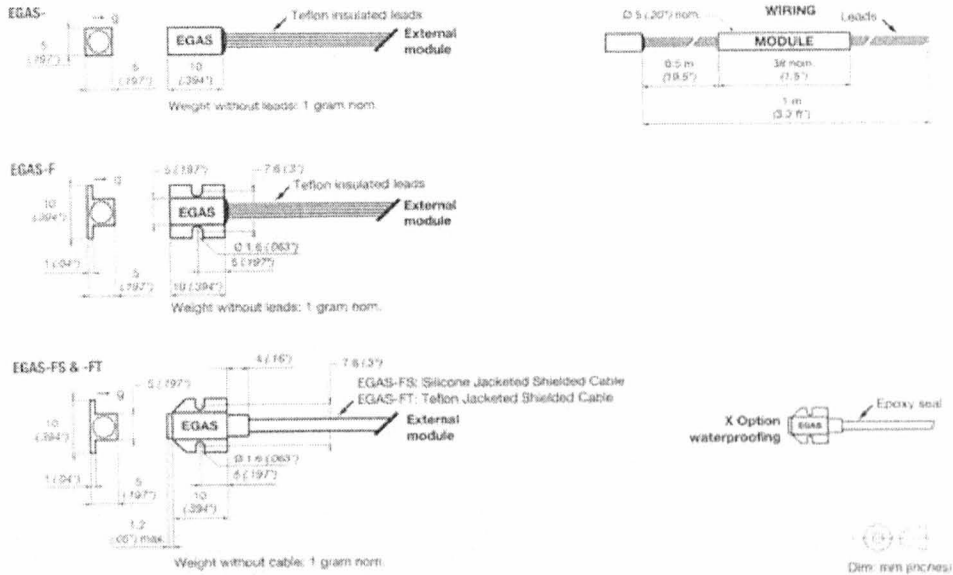
EGAS Series

g RANGES "FS"	g OVERRANGE LIMIT	FREQUENCY RESPONSE ±1/2dB nom./min.	NATURAL FREQUENCY nom.	SENSITIVITY mV/g nom.	OUTPUT "FSO" mV nom.
± 5	± 500	0 to 150/80 Hz	300 Hz	20	± 100
± 10	± 1000	0 to 200/120 Hz	400 Hz	10	± 100
± 25	± 2500	0 to 400/240 Hz	800 Hz	4	± 100
± 50	± 5000	0 to 600/350 Hz	1200 Hz	2	± 100
± 100	± 10000	0 to 900/500 Hz	1800 Hz	1	± 100
± 250	± 10000	0 to 1300/750 Hz	2600 Hz	0.4	± 100
± 500	± 10000	0 to 1750/1000 Hz	3500 Hz	0.2	± 100
± 1000	± 10000	0 to 2500/1500 Hz	5000 Hz	0.1	± 100
± 2500	± 10000	0 to 3500/2000 Hz	7000 Hz	0.04	± 100

EXCITATION:	15VDC
IMPEDANCE IN:	1300 Ω nom. typ.
IMPEDANCE OUT:	1500 Ω nom.
COMB. NON-LINEARITY& HYSTERESIS:	± 1%
TRANSVERSE SENSITIVITY:	2% max
DAMPING RATIO AT 20°C (70°F):	0.7 nom. (0.5 to 0.9)
OVERRANGE STOPS:	Integral
THERMAL ZERO SHIFT:	± 1mV/50°C (± 1mV/100°F)
THERMAL SENSITIVITY SHIFT (TSS):	± 2.5%/50°C (± 2.5%/100°F)
OPERATING TEMPERATURE:	-40°C to 120°C (-40°F to 250°F)
COMPENSATED TEMPERATURE:	20°C to 80°C (70°F to 170°F)
ZERO OFFSET AT 20°C (70°F):	± 15mV typ.

	TITLE	Entran		
Entran®	EGAS ACCELEROMETERS Miniature Rugged	ENGLAND Garston, Watford, Herts	EUROPEAN HEADQTRS Les Clayes-sous-Bois, FRANCE	
		SPECIFICATION NUMBER	ISSUE	PAGE
		EGASS001E	A	1 of 2

Figure A.6 Technical specifications for the monoaxial EGAS accelerometer used for the experimental laboratory tests.

Entran®

CERTIFICATE OF CALIBRATION

Property of :   P.O. :   Entran FO : 21138

PLEASE READ OPERATING INSTRUCTIONS BEFORE POWERING UNIT

Model : EGAS-FT*-25-/L02M   Axis :   S/N   : S99329
Type : ACCELEROMETER
Range : 25 g   Do Not Exceed   : 2500 g
Compensated Range : 20 to 80 °C   Operating Range : -40 to 120 °C
Specifications : *: DIN type 7 pin connector to be wired to sensor for MSC.

Other characteristics according to : EGASS001E-A

CALIBRATION DATA

¹Non linearity :±   ¹Hysteresis :±   ¹CNL&H :± 1.00 %FSO
¹Th. zero shift :± 1.00 mV/50°C   ²Thermal Sens. Shift :± 2.50 %/50°C
¹Zero (typ.)   : ± 15 mV
Ref. Temp.   : 22 °C (72°F)
Shunt Cal   :   with :   KΩ   across :
Sensitivity   : 3.681 mV/g with Excitation : 15.0 V   Max. : 18.0 V
Natural frequency : 740 Hz   Damping : 0.66
Input ohms   : 1368   Ω   Output ohms : 1562   Ω
Cal Equip.   : M65
Notes   : ELECTROMAGNETIC COMPATIBILITY,
                  RESIDENTIAL, COMMERCIAL AND LIGHT INDUSTRY.

WIRING

Connector : DIN 7b.   Transducer to Comp. Module :   Total length :
+In. : 1   +Out. : 5   Common mode : V output
-In. : 2   -Out. : 4   referenced to -Input =

¹The calibrated values do not exceed the data sheet specifications, value shown is the data sheet value.
²Value given by manufacturing design.

The above instrument has been calibrated against a working standard which is directly traceable to a
National standard.
All data interpreted per Entran Instruction Manuals unless otherwise indicated.

Control : S. COSTE (ENT QC1)   Date : 08/11/99

                                                              DGQ018D

Figure A.7   ENTRAN Certificate of calibration and specifications for the monoaxial EGAS accelerometer used to record the steering wheel test rig vibration along the z-axis.

A.2   Signal Conditioning Amplifier for Vibration Measurement

Specifications   C E
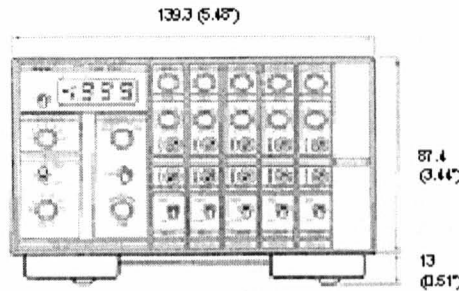
MSC6

Chassis with Power Supply

	MSC6
FOR A1 AMPLIFIERS:	Not Available
FOR A2 AMPLIFIERS (Also accepts A1 amplifiers):	
NUMBER OF CHANNELS:	6
POWER:	115/220VAC (± 10%, 45-440Hz) Switch Selectable (Optional 12/24 VDC)
DISPLAY:	3 1/2 DIGIT LED, 1.999V or 19.99V Switchable
EXCITATION TO SENSOR (Common to all Channels):	Switchable: 5V, 6V, 8V, 10V, 12V and 15V
INTERNAL CALIBRATION:	±1mV through ±10V continuously adjustable

Signal Conditioning Channels A1 & A2

	A1	A2
OUTPUT:	±10V or ±2V	4-20mA and ±10V or ±2V
AMPLIFIER GAIN (Switchable with fine control):	1 to 2000	10 to 10000
AMPLIFIER BANDWIDTH (-1dB):	0 to 50KHz	0 to 1.5KHz
ZERO OFFSET:	±40mV at input	± 10mV at input

INPUT RANGE:	5mV to 1.0V
INPUT MODE:	Full, Half or 1 Arm Bridge, Internal Bridge Completion
INPUT IMPEDANCE:	1MΩ Differential
OUTPUT TYPES:	Tape and Galvo
OUTPUT IMPEDANCE FOR TAPE:	0.5Ω
OUTPUT FOR GALVOS:	±10mA into 120Ω
OUTPUT LINEARITY:	0.05%
OPERATING TEMPERATURE:	0°C to 40°C (32°F to 104°F)
INPUT CONNECTORS:	DIN Type 7 Pin, with unwired mate
OUTPUT CONNECTORS:	D Type with unwired mate
CE CONFORMANCE:	EN61010-1, EN 50081-1, EN 50082-1

Entran®	TITLE **MSC INSTRUMENTATION** Multi-Channel Signal Conditioning	Entran® ENGLAND EUROPEAN HEADQTRS Bareliot, Watford, Herts Les Clayes-sous-Bois, FRANCE			M S C
		SPECIFICATION NUMBER	ISSUE	PAGE	
		MSCS0001E	01	1 of 2	E48

Figure A.8   Technical specification for the multi-channel signal conditioning MSC6.

A.3   Tape Recorder for Vibration Measurement

SPECIFICATIONS

| Item / Model	PC204Ax	PC208Ax	PC216Ax
Tape Transport			
	DG60Ms	DG90Ms	DGD120MB
	120	180	360
Usable tape and record/playback time	DT-16	DT-60	DT-90	DT-120
	48	60	90	120
	* The figures show the time in min for normal tape speed. In the double speed mode, the figures are half of those given here. * Tape width: 3.81 mm, tape speed: 8.15 mm/s (normal speed), 16.30 mm/s (double speed)		
Head Configuration	Rotary heads (2 for recording, 2 for playback) Drum dia. 30 mm, Wrapping angle: 90°, Drum rotation: 2000r/min (normal speed), 4000r/min (double speed)		
Writing speed	3.133 m/s (normal speed), 6.266 m/s (double speed)		
Start-up/stopping time	1 s or less (from PAUSE, normal speed)/0.5 s or less (normal speed)		
Servo	Capstan: Phase control (in REC·FWD) and ATF control (in FWD) Drum: Phase control, speed control Reel: Tension control (in FWD/REC·FWD)		
Motors	Drum (1), capstan (1), reels (2), control (1)		
FF/REW time	60 s or less (DG60Ms)		
Record/playback			
Channels (main data)	2 (normal speed only) 4	2 (normal speed only) 4/8	2 (normal speed only) 4/8/16/32with PCD32Ax)
Sampling frequency	3 kHz (with 1.25 kHz bandwidth), 6 kHz (with 2.5 kHz bandwidth), 12 kHz (with 5 kHz bandwidth), 24 kHz (with 10 kHz bandwidth), 48 kHz (with 20 kHz bandwidth) (64-times oversampling in both record and playback)		
Quantization	16 bit, linear (15 bit for main channel, LSB I/O 1 bit)		
Error correction	Double Reed Solomon		
Subcode channel	Announcement, address, time, ID, B/C mode, recording tape speed, input range setting (analog mode), event", memo (max. 12 characters) "External input only		
Frequency response 2ch mode: 4ch mode: 8ch mode: 16ch mode: 32ch mode:	DC to 20 kHz (normal speed), +0.5 to –1.0 dB, 0 dB @200 Hz DC to 10 kHz (normal speed), +0.5 to –1.0 dB, 0 dB @200 Hz DC to 20 kHz (double speed), +0.5 to –1.0 dB, 0 dB @200 Hz DC to 5 kHz (normal speed), +0.5 to –1.0 dB, 0 dB @200 Hz DC to 10 kHz (double speed), +0.5 to –1.0 dB, 0 dB @200 Hz DC to 2.5 kHz (normal speed), +0.5 to –1.0 dB, 0 dB @200 Hz DC to 5 kHz (double speed), +0.5 to –1.0 dB, 0 dB @200 Hz DC to 1.25 kHz (normal speed), +0.5 to –1.0 dB, 0 dB @200 Hz DC to 2.5 kHz (double speed), +0.5 to –1.0 dB, 0 dB @200 Hz		
Dynamic range	80 dB or more (within the bandwidth)		
S/N ratio	78 dB or more (within the bandwidth)		
Interchannel phase difference	1° or less (within the bandwidth)		2° or less
Cross talk	–80 dB or less (within the bandwidth)		
Distortion	0.02% or less (within the bandwidth)		
DC linearity	±0.1% or less (within the bandwidth)		
Drift	±0.1% or less each in recording and playback blocks (for 2 hours from 15 minutes after power-on)		
Input	Input range: ±20 Vp, ±10 Vp, ±5 Vp, ±2 Vp, ±1 Vp, ±0.5 Vp, Coupling: DC, Input impedance: 100 kΩ, unbalanced		
Output	Output level: ±1 Vp to ±5Vp, continuously variable, Output current: 10 mA max. Output impedance: 50Ω, unbalanced Test signal: ±100% sine wave (500 Hz for normal speed/1 kHz for double speed)/+100% DC/ –100% DC/ 0 V, 4 types selectable		
Input/output zero point adjustment	Auto calibration: Gain, offset (at power-on or selfcheck)		
USB digital input/output (analog mode)	Input/output signal: TTL, 1 bit, Sampling frequency: 96 kHz (normal speed), 192 kHz (double speed)		
Parallel digital output (analog mode)	Output signal: TTL, 16 bit parallel data (main channel data: 15 bit, LSB: 1 bit) Data transfer rate: 96 kword/s (normal speed), 192 kword/s (double speed) Word clock: 96 kHz (normal speed), 192 kHz (double speed)		
Serial digital input/output (digital mode)	Input/output signal: Bit serial (balanced RS-422A) Bit rate (synchronous): 1.536 Mbps (normal speed), 3.072 Mbps (double speed) Bit rate (asynchronous): less than 0.768 Mbps (normal speed), less than 1.536 Mbps (double speed)		

PCHB244 Hybrid Data Recorder
- Same dimensions and weight as PC204Ax/208Ax
- Simultaneous 4-channel record/replay of analog and digital signal
- Wide-band analog recording of DC to 100 kHz (1 channel mode)
- Bit serial data of up to 3.072 Mbps (1 channel mode)
- Channel provided for IRIG-B time code
- Selectable 1/2/4 channel mode.

Item / Model	PC204Ax	PC208Ax	PC216Ax
Function			
Search speed	Max. 200 times normal speed		
Search target	Mark 1, Mark 2, ID, Start ID, END (front panel) ID, Start ID, END, counter, address, time (RS-232C)		
Manual search	16 times normal speed by pressing FF/REW in FWD mode		
Remote control (option)	PCRM21Ax		PCRM22Ax
	Connects to REMOTE, RS-232C or EXT		
RS-232C control	Refer to system application chart		
EXT control	External relay contact input		
Fan control mode	Stops the ventilation fan until the unit's internal temperature reaches a given temperature level.		
Monitor ID:	000 to 999, with "A" display for auto increment indication (switchable between On and OFF)		
Tape counter:	±h, min, s		
Tap remainder counter:	±h, min (in recording and playback)		
Address:	±h, min, s		
Time:	Year-month-day/h-min-s display switchable		
Caution:	LCD Display: Low DC voltage, mechanical trouble, condensation, error check message LED: Over range input (analog mode)		
Monitor output	Data signal of a selected channel (analog mode)		
Sound monitor	Switchable between memo announce and data signal of a selected channel (analog mode): built-in speaker or earphone (jack)		
Synchronous record/playback	Synchronous record/playback with two units (PC216Ax only): 10kHz each for 16 channels or 5kHz each for 32 ch mode 1/ playback at double speed		
Self check	Power, servo, heads (recording/playback function) and amplifiers		
Power requirements and other specifications			
DC Voltage:	12 to 28 V (rated), 11 to 30 V (allowable range) via DC IN connector		
Current consumption: (double speed + power save mode)	Approx. 1.4 A @12 V	Approx. 1.5 A @12 V	Approx. 2.0A @12 V
(double speed + normal mode)	Approx. 2.0 A @12 V	Approx. 2.4 A @12 V	Approx. 3.0A @12 V
AC Voltage:	100 to 240 V (rated), 90 to 250 V (allowable range), 47 to 440 Hz (supplied AC power pack)		
Current consumption, 120 V @ 60 Hz (double speed + power save mode)	0.3A	0.35A	0.45A
(double speed + normal mode)	0.4A	0.5A	0.6A
Battery (Built-in)	12 V 2.3 Ah (NP-1B, option)		
Dimensions (excl. projection)	297 (W) × 70 (H) × 220 (D) mm 11.7" (W) × 2.8" (H) × 8.7" (D)		297 (W) × 100 (H) × 220 (D) mm 11.7" (W) × 3.9" (H) × 8.7" (D)
Weights	Approx. 3.5 kg / 7.8 lbs (net)		Approx. 4.5 kg / 10 lbs (net)
Performance temperature/humidity	+5°C to 40°C, 40% to 80% RH (no condensation)		
Operation temperature/humidity	0 to +45°C, 20 to 90% RH (no condensation)		
Storage temperature/humidity	–10°C to 50°C, 10% to 90% RH (no condensation)		
Performance pressure	800 hPa to 1060 hPa		
Operating position	Horizontal (normal position), vertical (front panel facing upwards)		
Vibration resistance	MIL-STD-810C, Method 514.2 Curve V (±15 m/s² (equivalent of ±1.5 G)), normal operation in horizontal position		
Shock resistance	400 m/s² (equivalent of 40 G) 11 ms (in storage)		
Safety regulation compliance	UL, EN61010-1		
EMI/EMS regulations compliance	EMI: EN55011-A, FCC Part 15, Class A EMS: EN50082-1		
Supplied accessories	AC power pack, Microphone, Operation manual, DC power cord, cassette tape, spare DC fuse, DG5CL cleaning cassette, screw driver, spare EXT connector, carrying belt.		

● **Dimensions**

PC216Ax   unit: mm
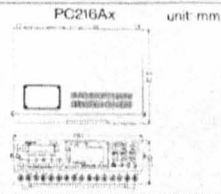
Design and specifications are subject to change without prior notice.

Figure A.9   Technical specification for the Sony tape recorder model PC216Ax.

A.4   Power Amplifier PA 100E and Vibrator V20 for Laboratory Tests

Specifications

Parameter	Units	V2	V4	V20	V20
Power Amplifier		PA30E	PA30E	PA30E	PA100E
Sine force peak	N	9	17.8	53	100
Random force rms	N	3	5.9	17.6	33
Acceleration peak	g	91	91	32	60
Velocity peak	m/s	1.05	1.49	1.14	1.51
Displacement p-p	mm	2.5	5	10	10
Armature mass	kg	0.01	0.02	0.17	0.17
Armature diameter	mm	Spigot	Spigot	38	38
Suspension stiffness	kgf/mm	0.32	0.45	1.14	1.14
Cooling		Natural	Natural	Natural	Natural
System power utility	VA	100	100	100	200

Parameter	Units	V20	V55	V55	V55
Power Amplifier		PA300E	PA100E	PA300E	DSA1-1K
Sine force peak	N	155	142	310	444
Random force rms	N	58	50	110	160
Acceleration peak	g	90	28.9	63	90
Velocity peak	m/s	1.78	0.81	1.14	1.52
Displacement p-p	mm	10	12.7	12.7	12.7
Armature mass	kg	0.17	0.5	0.5	0.5
Armature diameter	mm	38	76.2	76.2	76.2
Suspension stiffness	kgf/mm	1.14	1.79	1.79	1.79
Cooling		Forced air	Natural	Forced air	Forced air
System power utility	VA	600	200	600	1000

Options
  Berryllium copper spiders for V2 and V4 shakers to reduce axial stiffness.
  Trunnions for models V4, V20 and V55.
  Constant current drive for modal applications.
  Three axis testing configurations for models V20 and V55.
  Metric/Imperial/American table threads.

Three Axis Testing with Small Shakers
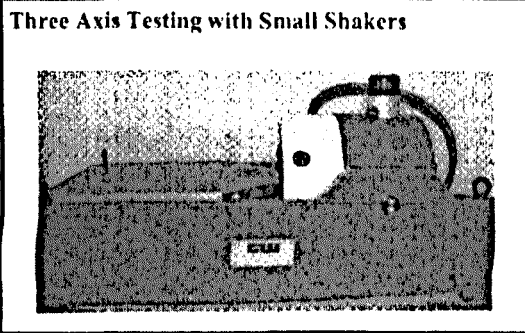
Gearing & Watson Electronics Ltd

South Road, Hailsham, East Sussex, BN27 3JJ, United Kingdom
Tel +44 (0)1323 846464   Fax +44 (0)1323 847550
E mail: sales@gearing-watson.com   Web: www.gearing-watson.com

Figure A.10   Technical specification for the power amplifier PA100E and the shaker V20 used during the experimental laboratory tests.

A.5   Geometrical Dimension of Mounting Blocks and Clamp for Vibration Measurement

The geometrical dimensions of the engine mounting blocks and mounting plates are presented in Figure A. 11 and Figure A.12, respectively.

The geometrical dimensions of the steering wheel mounting clamp are presented in Figure A. 13 to Figure A.15.
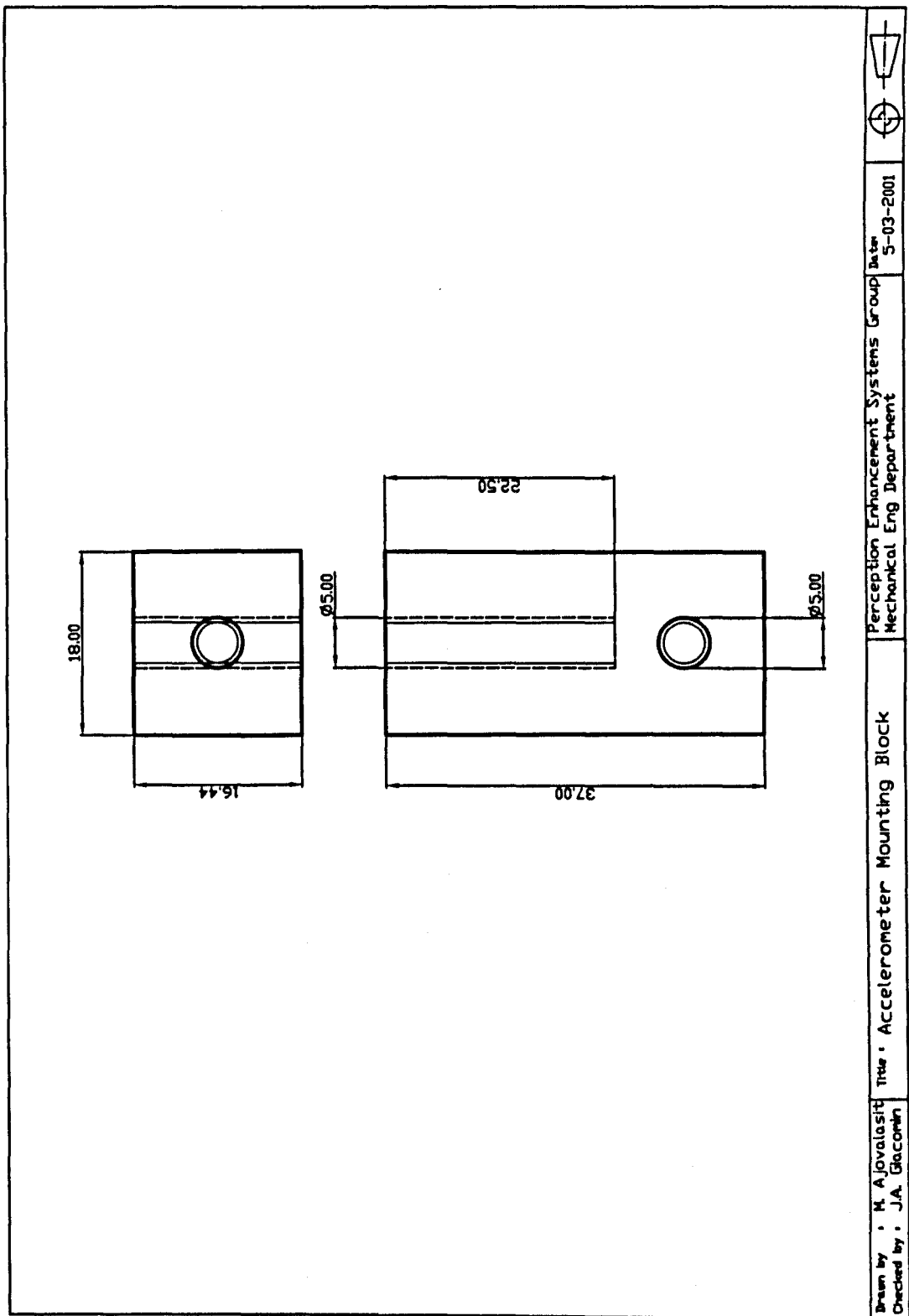
Figure A.11 Geometrical dimensional of the engine mounting blocks used to record the engine idle vibration on the test automobiles.
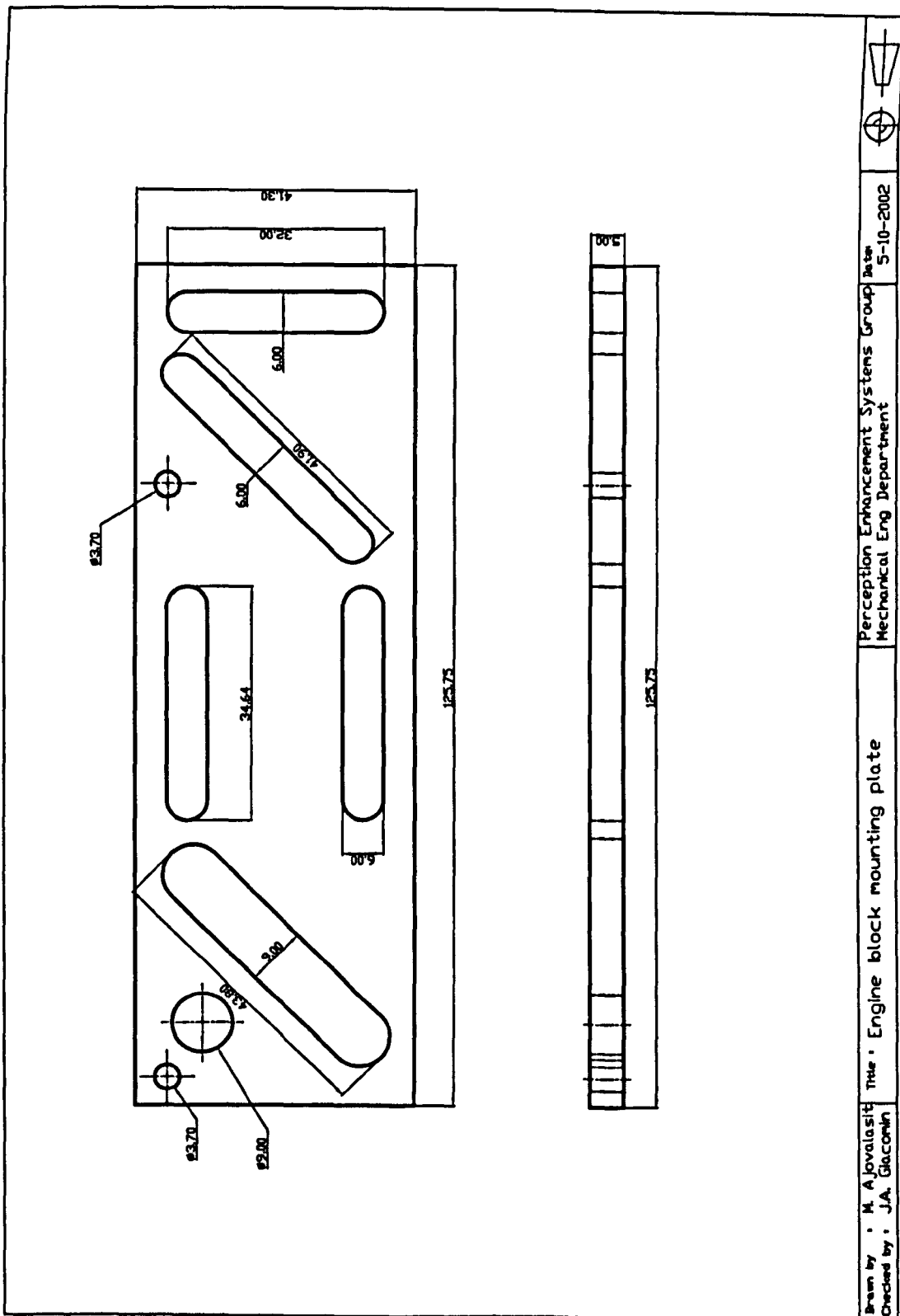
Figure A.12 Geometrical dimensional of the engine mounting plates used to record the engine idle vibration on the test automobiles.

Number	Part Name	Observations
1	Steering Wheel Clamp (Upper part)	
2	Steering Wheel Clamp (Lower part)	
3	Stainless Hexagon Socket Set Screw	Mounting Screw for accelerometer
4	Bolt M6x60	VM DIN 125
5	Plain Flat Washers M6	
6	Nut M6	Aburdun DIN 934

Drawn by : M. Ajovalasit   Title : Ensamble Drawing
Checked by : J.A. Giacomin

Perception Enhancement Systems Group   Date: 5-03-2001
Mechanical Eng Department

Figure A.13   Geometrical dimensional of the assembly of the steering wheel clamp used to record the steering wheel idle vibration on the test automobiles.

Figure A.14 Geometrical dimensional of the upper part of the steering wheel clamp used to record the steering wheel idle vibration on the test automobiles.
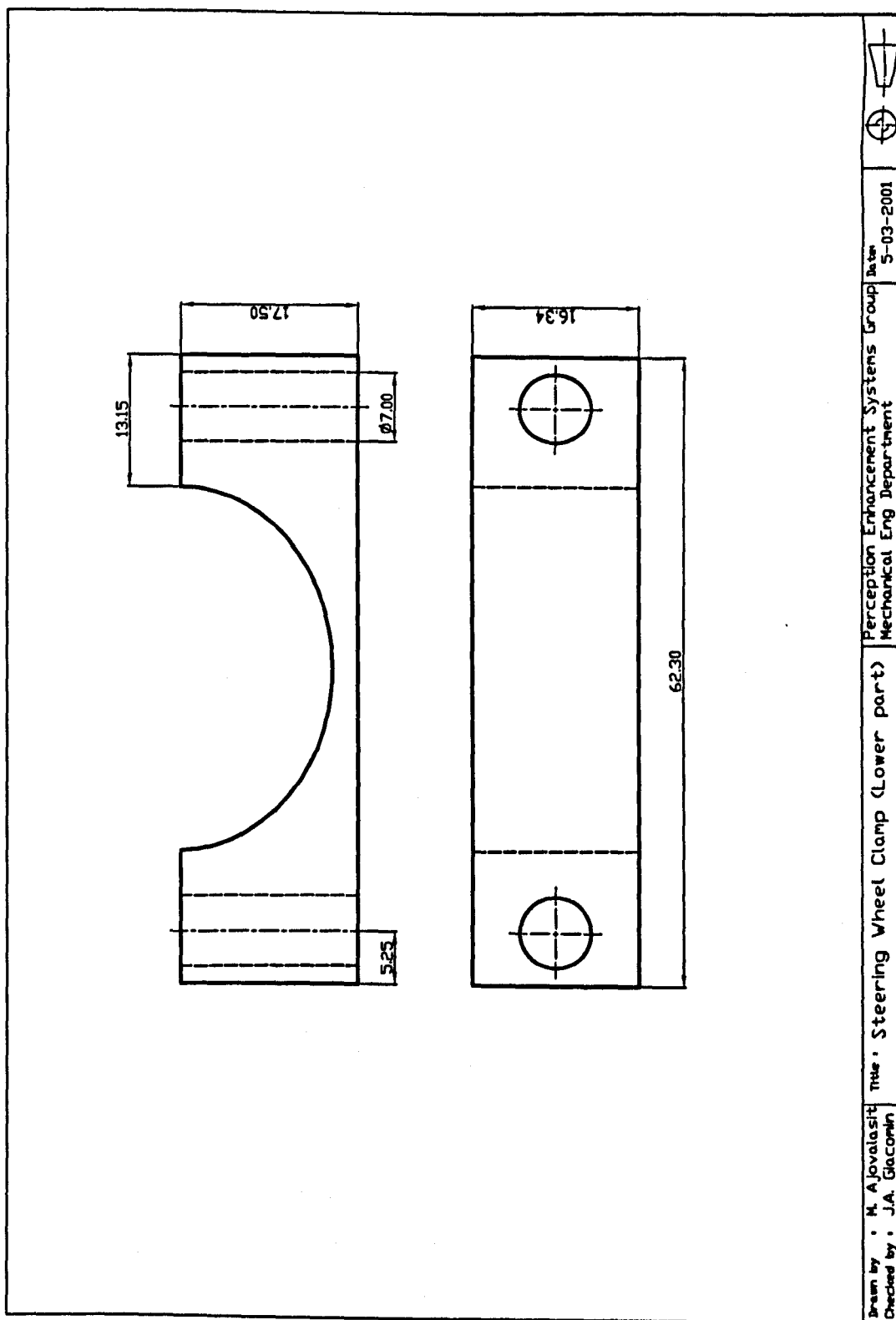
Figure A.15 Geometrical dimensional of the lower part of the steering wheel clamp used to record the steering wheel idle vibration on the test automobiles.
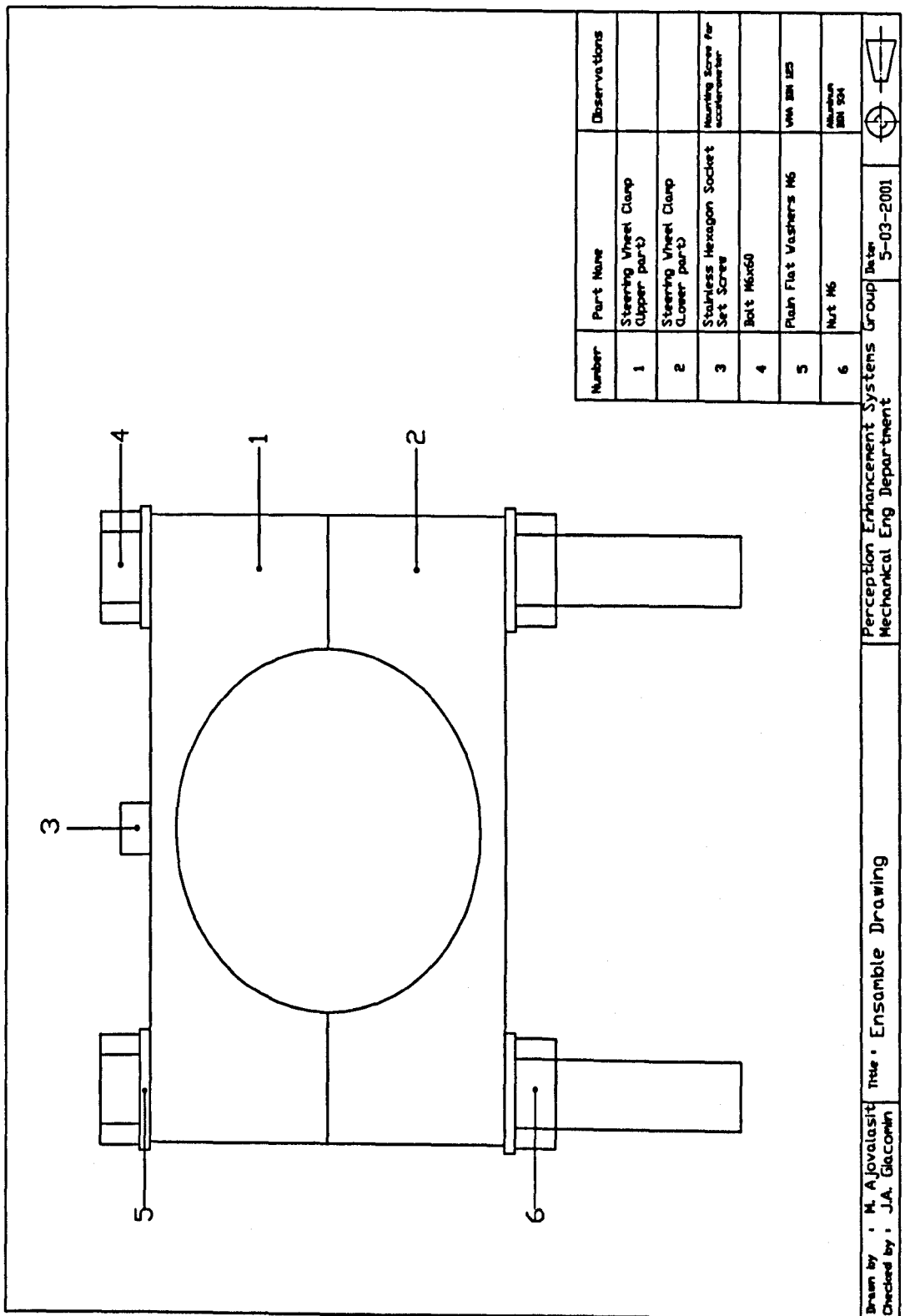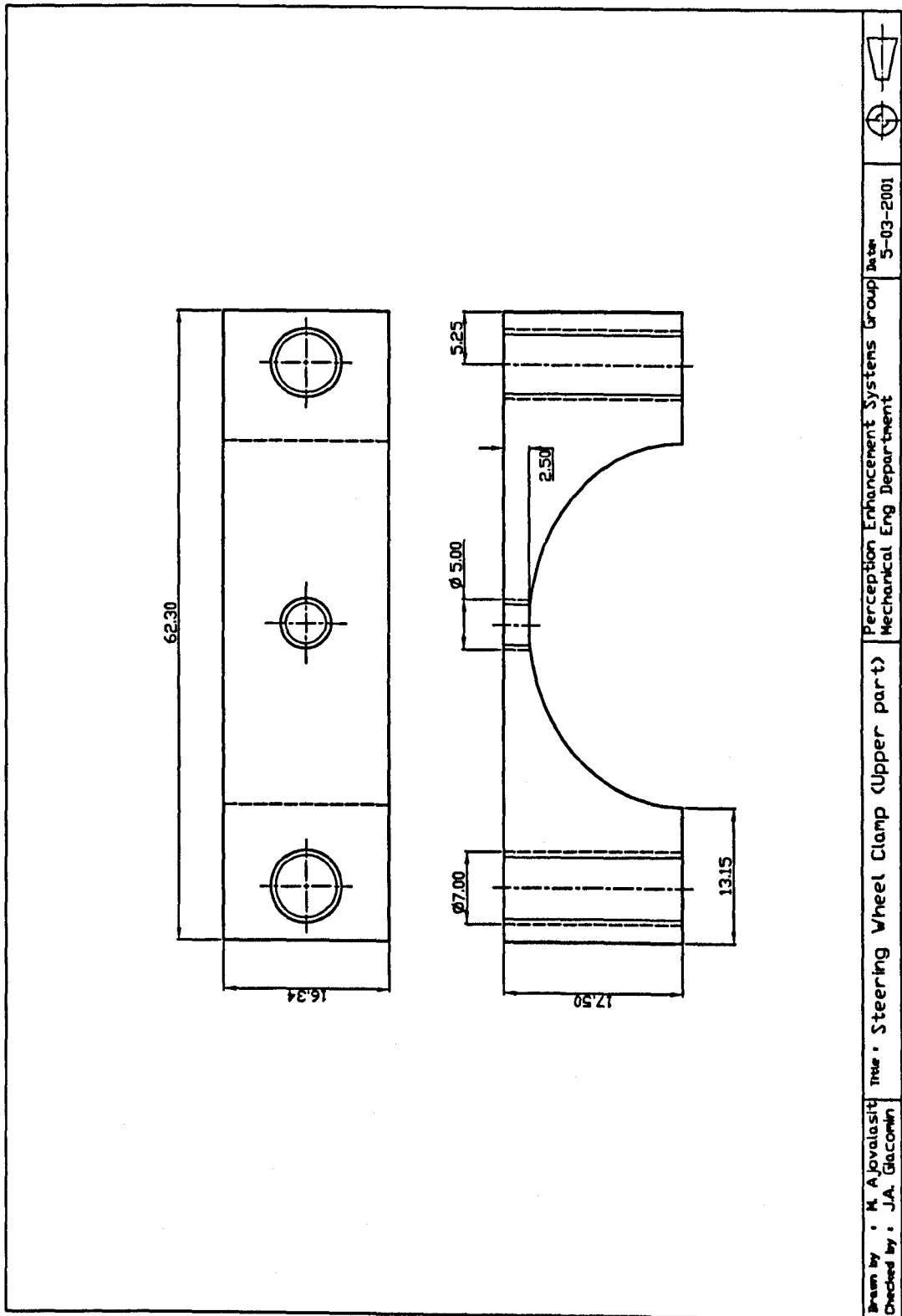
Appendix B

Laboratory Test Sheets

B.1 Paired-Comparison Procedure

B.1.1 Test Subject Consent Form and Questionnaire used for the Paired-Comparison Procedure

Dept. of Mechanical Engineering
The University of Sheffield

Test of Human Perception of Steering Wheel Idle Vibration

Please read carefully the information below which briefly summarises the experiment which you are being requested to perform, and please indicate your agreement to participate by completing and signing the sections below.

The purpose of this experiment is to investigate the human perception of hand-arm vibration. You will be asked to sit in a specially-designed simulator where you will be exposed to rotational steering wheel vibrations similar in level to those experienced in automobiles. The simulator is equipped with hardware and software systems which limit the vibration producing potential of the equipment in accordance with the health and safety guidelines specified by *British Standard 7085 Safety aspects of experiments in which people are exposed to mechanical vibration and shock.*

Each trial consists of two intervals of 4-second vibration signals separated by a 2-second time gap. You will be asked to compare the two signals such that you can indicate which of the two stimuli you consider to be *the most unpleasant*.
A complete series of 42 trials will last for approximately 16 minutes.

Experimenter's details:
Mr. Marco Ajovalasit (Room MD66)
Human Dynamics Group (HDG)
Dept. of Mechanical Engineering
Tel.: 0114 22 27833
Fax.: 0114 22 27890
E-mail: m.ajovalasit@sheffield.ac.uk

Please provide the following details: Date: /   /

Section A - Personal Details

Full Name: _____   Signature: _____

Sex: Male ☐   Female ☐

Occupation: _____   Age (years): _____

Height (m): _____   Weight (kg): _____

Section B – Driving Experience

1. What type of vehicle do you normally drive?

   Car ☐   Van ☐   Lorry/ Truck/Bus   ☐   4x4 Off-Roader ☐

   Other vehicles, please specify: _____

2. Do you drive a vehicle on a regular basis?

   Yes ☐   No ☐

   If yes, how many hours per week do you drive?

   < 2 ☐   2-10 ☐   10-30 ☐   > 30 ☐

Section C – Information About You...

1. Are you often exposed to vibrations, or do you regularly use vibration-producing tools as part of work or hobbies (i.e. tractors, drills)?

   Yes ☐   No ☐

   If Yes, please specify:_____

2. Do you have any physical condition which you feel may affect your vibration test responses?

   Yes ☐   No ☐

   If Yes, please specify:_____

3. Did you consume alcohol or coffee in the last hour before the experiment?

   Yes ☐   No ☐

   If Yes, please specify:_____

Thank you for participating in this research study. All information will be used for statistical analyses only and will remain strictly confidential. If you would be prepared to participate in future research, your contact details would be greatly appreciated:

Email address: _____

B.1.2 Verbal Instructions to the Test Subject used for the Paired-Comparison Procedure

☐ **Welcome**, thank you for taking part in this study

☐ The **purpose** of this experiment is to investigate the human perception of hand-arm steering wheel vibration in automobiles. The experiment will be performed using the steering wheel **simulator** that you see in front of you.

☐ I would like now to ask if you could please read **carefully** and complete a **consent form** and the **personal data form** for the experiment. It's particularly important that you provide a signature to authorize your participation in my research study.

☐ Please now remove any articles of **heavy clothing**, any **watches** and any **jewellery**, **glasses** or other items such as mobile phones which might effect your perception of hand arm vibration.

☐ The simulator has **numerous features which guarantee your safety**. The control software has built-in safely limits which restrict the maximum vibration output to safe values. The power amplifier has similar limiting circuits, and the vibrator is incapable of physically exceeding health and safety limits.

☐ Please now sit in the simulator and adjust the **sitting posture** to a comfortable position, reproducing as closely as possible **a realistic driving posture**.

☐ Please **hold the steering wheel in the centre** avoiding touching the lower or upper arms. You will be also asked to **maintain for all the experiments a constant palm grip** on the steering wheel using both hands, as when driving on a winding country road.

☐ Please position the **ear protectors until completely close your ears**, and please put the **dark blind glasses and close your eyes**. These measures are taken to ensure that neither sight nor noise affect your responses to the stimuli..

☐ We can now begin the tests. You are about to be exposed to **two vibration signals in pairs** (having a length of 4 seconds each) applied to the steering wheel simulator, separated by a 2-second time gap. The whole test contains 42 pairs of vibration signals. **After presenting each pair**, you are asked to indicate which of the two stimuli you consider to **be "more unpleasant"**.

☐ I will indicate to you the test signal by pronouncing the word "first" or " second", respectively. Please say **by the word "first"** if you find more unpleasant the first stimulus or **by the word "second"** if you find more unpleasant the second stimulus

☐ You are reminded that the total test duration is approximately 16 minutes. **After every 6 pairs** you will have a little pause of **5 seconds** to relax your hands

☐ If at any time before or during the experiment you should decide that you wish to **stop**, please state this and the procedure will be brought to a halt.

☐ Finally, I will signal to you the start of the test. You will be required to signal back that you are ready.

☐ Do you have any questions before the test starts?

☐ Ok, now the **testing is complete**. Thank you very much for having taken part in this experiment.

B.1.3 Example of Answer Table for Collecting the Subjective Responses used for the Paired-Comparison Procedure

Name test subject:

Date of the experiment:

Stimulus label	Modulation depth
Stimulus 1	A	m = 0.0
Stimulus 2	B	m = 0.1
Stimulus 3	C	m = 0.2
Stimulus 4	D	m = 0.4
Stimulus 5	E	m = 0.6
Stimulus 6	F	m = 0.8
Stimulus 7	H	m = 1.0

Pref. Set	Playlist 1 1st	2nd	Preference
I	A	C	
	B	H	
	D	A	
	E	D	
	F	B	
	D	E	
PAUSE (5 sec)			
II	H	A	
	D	B	
	E	H	
	C	D	
	A	F	
	H	E	
PAUSE (5 sec)			
III	C	F	
	A	H	
	B	D	
	F	E	
	B	A	
	H	D	
PAUSE (5 sec)			
IV	F	A	
	D	C	
	H	B	
	C	E	
	E	F	
	B	C	
PAUSE (5 sec)			
V	D	F	
	E	A	
	F	C	
	A	B	
	C	H	
	B	E	
PAUSE (5 sec)			
VI	C	B	
	H	F	
	E	C	
	F	D	
	D	H	
	A	E	
PAUSE (5 sec)			
VII	F	H	
	E	B	
	A	D	
	H	C	
	B	F	
	C	A	

B.2   Borg CR-10 Scale Procedure

B.2.1 Test Subject Consent Form and Questionnaire used for the Borg CR-10 Scale Procedure

Dept. of Mechanical Engineering
The University of Sheffield

Test of Human Perception of
Steering Wheel Idle Vibration

Please read carefully the information below which briefly summarises the experiment which you are being requested to perform, and please indicate your agreement to participate by completing and signing the sections below.

The purpose of this experiment is to investigate the human perception of hand-arm vibration. You will be asked to sit in a specially-designed simulator where you will be exposed to rotational steering wheel vibrations similar in level to those experienced in automobiles. The simulator is equipped with hardware and software systems which limit the vibration producing potential of the equipment in accordance with the health and safety guidelines specified by *British Standard 7085 Safety aspects of experiments in which people are exposed to mechanical vibration and shock.*

The experiment will last a total of approximately 15 minutes, in which time you will be asked to perform 28 individual trials. Each trial will consist of a vibration exposure lasting 4 seconds, after which you will be asked to state your opinion regarding the *unpleasantness* of the vibration using an appropriate subjective scale. It is important that you answer what you actually perceive, and not what you believe you might be expected to answer.

Experimenter's details:
Mr. Marco Ajovalasit (Room MD66)
Human Dynamics Group (HDG)
Dept. of Mechanical Engineering Department
Tel.: 0114 22 27833
Fax.: 0114 22 27890
E-mail: m.ajovalasit@sheffield.ac.uk

Please provide the following details: Date: /   / 2003

Section A - Personal Details

Full Name: _____   Signature: _____

Sex: Male ☐   Female ☐

Occupation: _____   Age (years): _____

Height (m): _____   Weight (kg): _____

Please turn over

Section B – Driving Experience

1. What type of vehicle do you normally drive?

Car ☐   Van ☐   Lorry/ Truck/Bus ☐   4x4 Off-Roader ☐

Other vehicles, please specify: _____

2. Do you drive a vehicle on a regular basis?

Yes ☐   No ☐

3. On average how many hours per week do you drive?

< 2 ☐   2-10 ☐   10-30 ☐   > 30 ☐

Section C – Information About You...

1. Are you often exposed to vibrations, or do you regularly use vibration-producing tools as part of work or hobbies (i.e. tractors, drills)?

Yes ☐   No ☐

If Yes, please specify:_____

2. Do you have any physical condition which you feel may affect your vibration test responses?

Yes ☐   No ☐

If Yes, please specify:_____

3. Did you consume alcohol or coffee in the last hour before the experiment?

Yes ☐   No ☐

If Yes, please specify:_____

Thank you for participating in this research study. All information will be used for statistical analyses only and will remain strictly confidential. If you would be prepared to participate in future research, your contact details would be greatly appreciated:

Email address: _____

B.2.2 Verbal Instructions to the Test Subject used for the Borg CR-10 Scale Procedure

☐ **Welcome**, thank you for taking part in this study

☐ The **purpose** of this experiment is to investigate the human perception of hand-arm steering wheel vibration in automobiles. The experiment will be performed using the steering wheel **simulator** that you see in front of you.

☐ I would like now to ask if you could please read **carefully** and complete a **consent form** and the **personal data form** for the experiment. It's particularly important that you provide a signature to authorize your participation in my research study.

☐ Please now remove any articles of **heavy clothing**, any **watches** and any **jewellery**, **glasses** or other items such as mobile phones which might effect your perception of hand arm vibration.

☐ The simulator has **numerous features which guarantee your safety**. The control software has built-in safety limits which restrict the maximum vibration output to safe values. The power amplifier has similar limiting circuits, and the vibrator is incapable of physically exceeding health and safety limits.

☐ Please now sit in the simulator and adjust the **sitting posture** to a comfortable position, reproducing as closely as possible **a realistic driving posture**.

☐ Please **hold the steering wheel in the centre** avoiding touching the lower or upper arms. You will be also asked to **maintain for all the experiments a constant palm grip** on the steering wheel using both hands, as when driving on a winding country road.

☐ During the whole period of testing **it is very important that you do not shift your eyes around the room**. Keep your eyes on the scale in front of you. Additionally, you will be asked to position the ear protectors until completely close your ears. This measure is taken to ensure that the noise doesn't affect your responses to the stimuli.

☐ You will use this scale to rate your perception of unpleasantness of the vibration, that is how unpleasant the vibration feels to you.

☐ As you can see, the scale stretches from "nothing at all" (0) to "absolute maximum".

- *"Extremely strong—Max P" (10)* is such an extremely strong perception of unpleasantness that is the most unpleasant vibration you have ever experienced in your life. Use that as your 10 point rate it is Your "Max P", P is for perception.

- *"Absolute maximum"*: It may be possible, however, to experience or to imagine a sensation even *more unpleasant* than what yourself have previously experienced in your life. Therefore "Absolute maximum", the highest possible level is placed somewhat further down the scale without a fixed number and marked with a dot " ". If you perceive a stimulus *more unpleasant* than 10 ("Extremely strong—Max P"), you may use any number above 10, such 11, 12 or even higher.

- *"Extremely weak"* corresponding to 0.5 on the scale is something just noticeable, i.e., something that is on the boundary of what is possible to perceive.

☐ You will use the scale in the following way:

1. Always start by looking at the verbal expressions.
2. Then choose a number.
3. If your perception corresponds to "very weak", you say 1. If it is "moderate", you say 3, and so on.
4. You may use whatever numbers you want, also half values, such as 1.5 or 2.5, or decimals, e.g., 0.3, 0.8, 1.7, 2.3, 5.6, or 11.5.
5. It is very important that you answer what you perceive and not what you believe you ought to answer.
6. Be honest as possible and try not to overestimate or underestimate the perceived vibration. It is your own feeling of unpleasantness that is important, not how it compares to other people's. What other people think is not important either.
7. Remember to start by looking at the verbal expressions before every rating, and then give a number.

☐ Do you have any questions before the test starts?

☐ We can now begin the tests. On each trial a 4 second vibrational signal will be presented at the steering wheel simulator. The whole test contains 28 stimuli of vibration signals. After presenting each pair, you are asked to express your judgement of perceived unpleasantness by using the Borg CR-10 scale.

☐ You are reminded that the total test duration is approximately 16 minutes. **After every 7 stimuli** you will have a little pause of **5 seconds** to relax your hands.

☐ If at any time before or during the experiment you should decide that you wish to **stop**, please state this and the procedure will be brought to a halt.

☐ Finally, I will signal to you the start of the test. You will be required to signal back that you are ready.

☐ Ok, now the **testing is complete**. Thank you very much for having taken part in this experiment.

B.2.3 Example of Answer Table for Collecting the Subjective Responses used for the Borg CR-10 Scale Procedure

Name test subject:
Date of the experiment:

Playlist 1

Rating score

Set	Signal
I	G (1.0)
	D (0.4)
	A (0.0)
	C (0.2)
	E (0.6)
	F (0.8)
	B (0.1)

Pause (5 sec)

Set	Signal
II	A (0.0)
	E (0.6)
	D (0.4)
	G (1.0)
	C (0.2)
	B (0.1)
	F (0.8)

Pause (5 sec)

Set	Signal
III	B (0.1)
	E (0.6)
	G (1.0)
	D (0.4)
	F (0.8)
	A (0.0)
	C (0.2)

Pause (5 sec)

Set	Signal
IV	A (0.0)
	F (0.8)
	B (0.1)
	G (1.0)
	D (0.4)
	C (0.2)
	E (0.6)

	Stimulus label	Modulation depth
Stimulus 1	A	$m = 0.0$
Stimulus 2	B	$m = 0.1$
Stimulus 3	C	$m = 0.2$
Stimulus 4	D	$m = 0.4$
Stimulus 5	E	$m = 0.6$
Stimulus 6	F	$m = 0.8$
Stimulus 7	H	$m = 1.0$